Achieving Efficient Control of Hydraulic Systems Using On/Off Valves

A DISSERTATION
SUBMITTED TO THE FACULTY OF THE GRADUATE SCHOOL
OF THE UNIVERSITY OF MINNESOTA
BY

Michael Berne Rannow

IN PARTIAL FULFILLMENT OF THE REQUIREMENTS
FOR THE DEGREE OF
Doctor of Philosophy

Dr. Perry Li and Dr. Thomas Chase

May, 2016

Acknowledgements

There are many people that have earned my gratitude for their contribution to my time in graduate school. I would like to thank my advisers, Dr. Perry Li and Dr. Thomas Chase for their guidance and advice. I would like to acknowledge the National Science Foundation (NSF) for supporting my research through grants EEC-0540834 and ENG/CMS-0409832. I would also like to thank the Center for Compact and Efficient Fluid Power (CCEFP) for supporting my research. Finally, I would like to thank my wife, Jody, and my kids, Emily and Benjamin, for putting up with me as I worked to complete my dissertation.

Abstract

Hydraulic systems offer a range of benefits, such as high power density, ruggedness, linear actuation, and low cost, which have led to the use of hydraulic actuation systems throughout a wide range of industries. However, they also typically suffer from lower efficiency than competing methods of actuation, which limits their appeal in some applications, and presents a threat to their continued prevalence as energy efficiency becomes increasingly important. The relatively low efficiency of hydraulic systems is due in part to inefficient components, such as pumps and motors, and partially due to the typical method of control, which uses throttling valves to place restrictions in the flow path to dissipate excess power as heat. Several approaches to reducing throttling losses have been studied, such as using pumps, motors, or transformers to control individual actuators, or creating circuits with multiple pressure levels to reduce the pressure drop across individual valves. However, these approaches often suffer from high cost and size requirements, or experience reduced control performance, which can limit their appeal. An alternative approach is to use high-speed on/off valves to charge and discharge energy storage elements to transform the power flow rather than restricting it. Different configurations of switching hydraulic circuits can be used to create variable pumps, motors, actuators, or transformers. This approach can significantly reduce the power loss that is typically associated with controlling hydraulic systems using conventional valves.

However, control using high speed switching valves presents several challenges. The most significant drawback is the power ripple that results from the discontinuous nature of the control valves. While this can be mitigated using energy storage elements, such as inertias and accumulators, it cannot be completely eliminated. Furthermore, there is a fundamental trade off between the degree of smoothing and the speed of response of the system. In chapter 2 the system dynamics of a switching system are studied in the context of a specific switching circuit, the Virtually Variable Displacement Pump (VVDP), and it is demonstrated that the trade off between ripple and response time can be improved by increasing the Pulse-Width-Modulation (PWM) frequency and through the use of feedback control.

An example of the VVDP circuit, which uses an on/off valve to load and unload a fixed displacement pump with an accumulator to smooth the output flow, is shown experimentally to improve the efficiency of the control system by up to 43% over a throttling valve system when operating at $2.5Hz$. However, this efficiency benefit is reduced to 24% when the switching frequency is increased to $10Hz$. This highlights another challenge with designing switching circuits: the power loss mechanisms that occur in on/off valve controlled systems, particularly transition throttling and compressibility losses which occur every switch, can reduce the potential efficiency benefits and must be taken into account as PWM frequencies are increased.

The throttling loss that occurs as the valve transitions between states is often the largest source of power loss in on/off valve systems operating at moderate to high PWM frequencies. The long transition time of many conventional switching valves places an upper limit on the PWM frequencies that can be achieved while still providing an efficiency benefit. To reduce the effect of the transition loss, the concept of hydraulic soft switching is introduced in chapter 3 which, in simulation, reduced the transition loss by 81%. This technique, which mimics a concept from switching electrical converters, provides temporary flow paths for the hydraulic fluid to bypass the transitioning on/off valve, thus avoiding most of the transition throttling.

Another power loss that must be considered, particularly at high PWM frequencies, is the power needed to actuate the on/off valve. While increasing the PWM frequency can be effective at reducing the output ripple and the size of the energy storage elements, the energy needed to accelerate the switching elements in conventional on/off valves at high PWM frequencies is not insignificant. If the kinetic energy of the switching element is not re-captured, the power needed to actuate the valve increases with the PWM frequency cubed. To address this problem, a novel type of rotary valve that spins at a constant speed is presented in chapter 4. This rotary valve achieves high PWM frequencies by alternately connecting a fixed port in the housing to supply or tank as the spool rotates. The duty ratio, which describes the fraction of the rotation that the valve is "on," is adjusted by moving the valve spool axially. The fact that the valve rotates with a constant speed eliminates the need to accelerate the valve element, meaning the valve must only overcome viscous friction. This has the potential to enable much higher switching speeds than conventional valves. However, with this novel

valve architecture, there are a number of design trade offs that must be negotiated. In chapter 4, the design of the rotary valve, in the context of both a VVDP and a Virtually Variable Displacement Pump/Motor (VVDPM), is formulated as a constrained power loss minimization problem to determine the optimal design parameters. For the VVDPM, this optimization is done for a device that is operating as the wheel motor in a Hydraulic Hybrid Passenger Vehicle.

In addition to losses due to throttling across control valves, hydraulic system efficiency is degraded by power losses within hydraulic components, such as pumps and motors. The majority of these losses stem from leakage and friction caused by high pressure applied to elements that move relative to each other. In conventional piston type devices, which are common in the hydraulics industry, the displacement of the unit, and thus its power output, is varied by changing the stroke length of the pistons as they are rotated. This method maintains high pressure on the same number of pistons, regardless of the power output, resulting in leakage and friction losses that do not decrease with the power output and a sharp drop in efficiency at low displacements. In order to address this problem, a different form of on/off control can be used: direct control of individual pistons in a pump/motor. Using this method, pressure is removed from pistons to reduce the pump/motor displacement, which allows the power losses in the system to decrease with displacement. In chapter 5, the power loss mechanisms in both a conventional and discrete piston device are compared, and the potential efficiency benefit is highlighted.

One challenge with creating discrete piston controlled pump/motors is designing the control valves to operate quickly and efficiently enough to provide effective control of the pressure in the piston chambers. Designs have been proposed that use two fast-acting electrohydraulic valves to connect the piston to supply or tank. This approach provides flexibility in selecting the disabling strategy and valve timing, but it also leads to designs that are expensive and complicated to control. The requirements for a discrete piston control valve are that it must switch quickly, especially as the pump/motor shaft speed increases, require little actuation power, and have repeatable timing with respect to the pump/motor shaft position. These characteristics match well with the two degree of freedom rotary valve described in chapter 4. In chapter 6 several valve designs based on the rotary valve concept are proposed, and a mechanism using the rotary valve as a

pilot stage driving three-way spool valves is selected, analyzed, and designed as a part of a discrete piston controlled pump/motor. The detailed design of a discrete piston prototype, which uses hydromechanical rather than electrohydraulic control valves is described, and experimental results are presented in chapter 7. While high internal leakage caused by manufacturing challenges limited the experimentally demonstrated efficiency, estimates of the power loss without the internal leakage, analytical equations, and simulation results demonstrate the potential of the discrete piston control approach.

Whether they are used to create switching circuits that avoid the losses associated with conventional throttling valves, or if they are used to reduce the leakage and friction losses in a discrete piston controlled pump motor, on/off valves can be used to improve the efficiency of hydraulic control systems. However, the design of switching valve controlled systems is not without challenges, and this thesis examines many of the potential benefits, as well as difficulties in creating efficient and effective solutions using on/off valves.

Contents

List of Tables

List of Figures

Chapter 1

Introduction

Hydraulic systems, which use a pressurized liquid to transmit or transform power, are used in a wide variety of applications. They are ubiquitous throughout numerous industries, such as manufacturing, transportation, mining, construction, agriculture, and many others. Hydraulic systems are widely used due to the numerous advantages they provide, such as: high power density, ability to operate in rugged environments, capability of simple linear actuation, flexible installation, tolerance to shock loading, and relatively low cost, among other benefits. However, hydraulic systems typically suffer from low energy efficiency when compared with competing methods of power transmission. In a study prepared by Oak Ridge National Laboratory in 2012[1], the average fluid power system efficiency throughout all industries was about 22%. The same study estimated that hydraulic systems in the United States consume between 1.5 and 2.4 Quads (quadrillion BTUs) of energy per year, with an additonal 0.5 Quads consumed by pneumatic systems. Thus, even a modest increase in the average efficiency of hydraulic systems would result in a substantial reduction in the national energy comsumption.

The inefficiency of hydraulic systems stems from multiple sources. Hydraulic components with moving parts, such as pumps, motors, valves, and cylinders, experience friction and leakage of high pressure oil, which reduce their efficiencies. Energy is also lost to pressure drops as oil passes through hoses and fittings. Finally, a significant amount of energy is lost due to the conventional methods of controlling hydraulic systems. Typically, power in hydraulic systems is controlled via throttling valves, which

restrict the flow of hydraulic oil to only allow the desired power to flow to the application. This method of control is analogous to resistive control in electronic systems, and it results in a significant amount of potentially useful energy being converted into heat. In addition to wasting fuel, in many systems the heat generated by inefficiencies in the system requires a large cooling system to maintain tolerable operating temperatures. Thus any energy saved will have the added benefit of reducing the cooling demands for the system.

This thesis will examine several approaches to improving the energy efficiency of hydraulic systems by employing the use of high-speed on/off valves. One way that using on/off valves to control a hydraulic system, an approach that has been labeled "Digital Hydraulics," can improve efficiency is to eliminate the throttling that occurs across conventional control valves. An ideal on/off valve has two states: it will either be fully open, resulting in little throttling across it, or fully closed, resulting in zero flow losses. By quickly switching between these two efficient states, the average power flow across the valve can be controlled, often with the addition of energy storage devices for smoothing. A second way that on/off valves can be used to improve hydraulic system efficiency is to provide discrete control of individual pumping/motoring chambers within a pump or motor. This approach has the potential to create more efficient pumps and motors by reducing the leakage and friction losses that occur in conventional devices. Both of these approaches for improving hydraulic system efficiency will be studied in this thesis.

An example of the inefficient methods of control employed in typical hydraulic systems is shown in Fig. 1.1. In each example circuit, there are three loads, each with a different pressure and flow requirement, as shown in the graph to the right of each system. In system A, a fixed displacement pump generates a fixed amount of flow, and a relief valve regulates the pressure to a fixed high value. For each actuator, a control valve is used to throttle the desired amount of flow from the high pressure line to the load. This circuit is the simplest method of control, but it also results in the highest amount of energy lost as heat across the valves, which is shown in red. In the second circuit, a proportional bleed-off valve is placed in parallel with the loads to divert excess flow from the fixed displacement pump. Using this circuit, the system pressure can be reduced to be only slightly above the highest load, but the flow generated by the pump

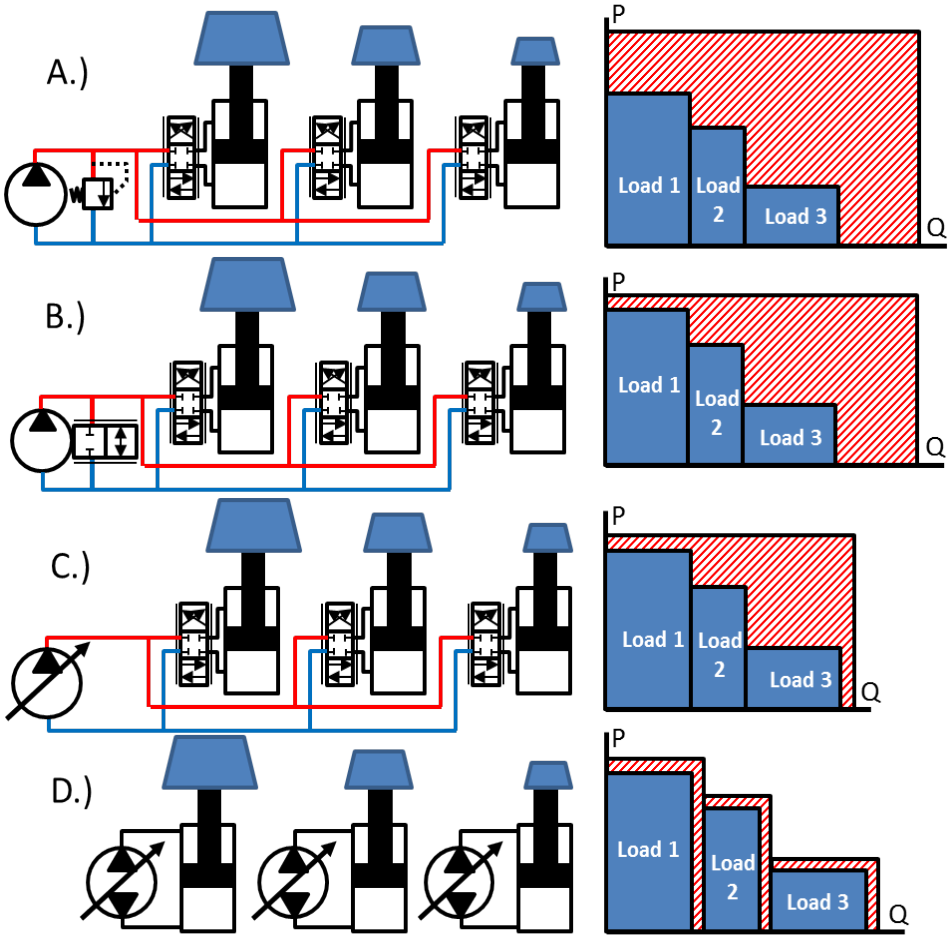

Figure 1.1: Four conventional methods for controlling hydraulic circuits

is still fixed. In system C, a variable displacement pump is used to reduce the flow to match the sum of the flow demands. A control device, such as a loadsense compensator, can be used to maintain the pump outlet pressure at a small margin above the highest load. This configuration reduces the wasted energy considerably, but there is still energy lost when driving loads 2 and 3, as the difference between the pump outlet pressure and the load pressure is made up by throttling across the control valves. Finally, system D uses a separate variable displacement pump to control each load without any throttling losses. While this approach avoids throttling, some energy will be lost to leakage and friction in each pump. This system will also typically be larger and much more expensive than systems A-C, and the control bandwidth may be lower than the valve controlled approaches. While this approach has been studied as a way to reduce power losses [2], it has not been widely adopted.

Disregarding system D, the control methods used in the vast majority of hydraulic systems (A-C) use throttling valves to meter flow and control pressure. Any pressure drop that occurs across a valve results in wasted energy. In electrical systems, a similar control problem exists, when a voltage lower than the supplied voltage is required. This problem can be solved, as it is in hydraulic systems, by dissipating excess power across a resistive device. However, in electrical systems, a different approach is typically used: instead of using resistors to make up the difference in voltage levels, the power can be transformed through the use of high-speed switching elements. In this approach, transistors are used to quickly transition between providing energy to the load and storing excess power in energy storage elements, such as inductors and capacitors. This approach can be used to efficiently increase or decrease voltage to meet a demand. Switching DC-DC converters result in much more efficient control of power, and they are ubiquitous throughout a wide variety of electrical systems.

Many of the concepts from switching electronic converters can be applied to hydraulics. High-speed on/off valves can be used, along with capacitances, such as accumulators, and/or inertias, such as flywheels or long tubes, to create hydraulic switching circuits. Rather than dissipating excess power, switching converters transform power by charging and discharging energy storage elements.

As with electronic converters, there are many different configurations of on/off control circuits. A hydraulic buck converter can be used to efficiently transform a higher

pressure into a lower one, while putting out more flow than is put in. A boost converter can be used to transform power in the opposite direction, boosting the pressure while reducing the flow. A third configuration of hydraulic transformer called a buck-boost converter can be used to transform power in either direction. By including mechanical circuit elements, such as pumps and actuators, along with hydraulic components, circuits can be developed that transform mechanical input power into hydraulic output power, or vice versa. An example of this is a Virtually Variable Displacement Pump (VVDP), which uses an on/off valve, an accumulator, and a fixed displacement pump to create a device that sends less than the full pump flow to the load, but also unloads the pump from the load pressure for a fraction of the switching period. This is essentially a boost converter that boosts the effort variable (shaft torque input, pressure output), and reduces the flow variable (shaft speed input, flow rate output). A similar approach can be used to create a Virtually Variable Displacement Motor/actuator (VVDM) or the combination Virtually Variable Displacement Pump/Motor (VVDPM). This thesis will look in depth at the VVDP circuit and analyze its performance and efficiency characteristics. The results will also be extended to a VVDPM circuit.

While on/off control circuits have the potential to significantly improve hydraulic system efficiency when compared with systems controlled via throttling valves, there are a number of potential sources of energy loss that must be considered in their design. For example, while on/off valves are efficient in the on/off states, energy can be lost when the valve transitions between them. Throttling and leakage through components, fluid/line compressibility, and valve actuation power also can reduce the efficiency of on/off controlled circuits. The discontinuous nature of on/off control also generates a ripple on the power flowing through the hydraulic circuit, which is affected by the selection of circuit components and the switching frequency. In order to determine the potential benefit of an on/off control circuit as well as to create an efficient and effective design, the power ripple and sources of energy loss must be considered. In this thesis, several methods of improving the VVDP and VVDPM circuits will be explored, including a new circuit element, called a soft switch, that can drastically reduce transition losses, and a novel type of switching valve that can achieve high switching frequencies without requiring significant input power.

A second approach for improving hydraulic system efficiency is to integrate on/off

valves into hydraulic pumps and motors. By using fast switching valves to enable/disable individual chambers within a pump or a motor, the effective displacement of the device can be varied. This approach is in contrast to conventional designs, which vary displacement by changing the stroke length of the pumping pistons. Conventional pumps and motors exhibit low efficiency when operating in partial displacement conditions, which is primarily due to the fact that most of the loss mechanisms do not decrease as the output power is decreased. By changing the stroke length to vary the displacement, high pressure is maintained on all of the pistons, resulting in leakage and friction forces on all pistons, regardless of the pump/motor displacement. By using on/off valves to remove pressure from pistons as they are not needed, the leakage and friction losses in pumps and motors can be reduced. This can reduce the losses shown in Fig. 1.1 D.

While many of the leakage and friction losses will decrease with discrete piston control, other losses, such as throttling and actuation power, may increase. Thus, a study will be done to examine the different losses in pumps and motors, and estimate the potential benefit of discrete piston control.

Discrete piston control can be achieved with independently electronically-controlled on/off valves for each piston, but this can lead to designs that are larger, more expensive, less robust, and more complex to package and control than conventional devices. These factors can be a barrier to the adoption of discrete piston controlled devices. A different approach that is taken in this thesis is to use a hydro-mechanical mechanism to achieve discrete piston control. This approach will create a device that is simpler to control and potentially more compact and less expensive than a device using fully independent electronic valves. To accomplish this, the novel rotary on/off valve that was developed for creating a VVDP and VVDPM is adapted for use inside a piston pump/motor.

While on/off valve control is not used in most conventional hydraulic systems, it is an active area of interest by a number of different researchers. The next section presents an overview of the existing state of the art around on/off hydraulic control.

1.1 Literature Review

In 2011, Linjama [3] published a paper describing the current state of the art in the broad field of Digital Hydraulics, which he defined as “hydraulic and pneumatic systems

having discrete valued component(s) actively controlling system output." One area of research described in that paper which is studied in [4] and [5] is to connect on/off valves in parallel. By combining valves with different area combinations (i.e. binary coding), a number of on/off valves can approximate a proportional valve. While this is still fundamentally a dissipative method of control, it does highlight some benefits of using on/off valves for control. While more valves are needed, on/off valves require less precise manufacturing and fewer control electronics, making them much less expensive. The authors also state increased contamination resistance and improved system reliability due to redundancy. The primary drawbacks of this approach are the increased complexity, and the fact that it controls the system by turning unwanted energy into heat. While this approach of using on/off valves connected in parallel can provide benefits in some situations, it is not focused on improving the efficiency of hydraulic systems, and thus, it is not a focus of the work presented in this thesis.

1.1.1 On/Off Valve Based Hydraulic Circuits

Another broad area of Digital Hydraulics described in [3] is the concept of using on/off valves as high speed switches to control the power flow in a hydraulic circuit. By combining switching valves with energy storage elements, such as inertias and accumulators, the average power flow can be controlled or transformed. The inspiration for using switches and energy storage elements for control comes from power electronics. Merrill [6] compared electronic and hydraulic switching circuits and found that hydraulic switching converters must overcome a number of challenges. First, the ratio of capacitance to inductance in hydraulic fluid and components is typically much higher, which can degrade performance and efficiency. The ratio of switching speed to control bandwidth is also significantly lower in hydraulic circuits than electrical circuits. It was also found that the ripple on the output from switching valves tends to have a larger effect on the output. Despite these challenges, many researchers have studied the design and effectiveness of hydraulic switching circuits.

There are two primary configurations of switching converters: the buck converter and the boost converter. These two fundamental designs can be created using different types of components, act in different power domains, or be combined to create more complex circuits. The buck converter, also described as a step-down or flow-boost circuit, will

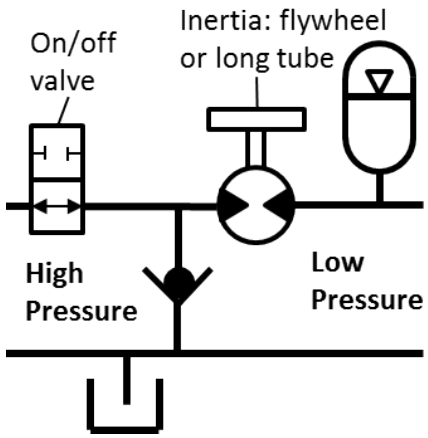

Figure 1.2: Hydraulic buck converter circuit

transform a high pressure and low flow into a lower pressure and higher flow by charging and discharging an inertia element, which is typically either a flywheel or a long tube of hydraulic oil. Figure 1.2 depicts an example of a hydraulic buck converter circuit. In this figure, the inertia element is a hydraulic motor with a flywheel. The on/off valve switches between applying high pressure to the inertia causing it to accelerate, and blocking high pressure, which causes the inertia to pull fluid from the tank and decelerate. The check valve can be replaced with a second on/off valve that allows power to flow back from the low pressure side to the high pressure side.

In contrast, a boost converter, also known as a step-up or pressure-boost circuit, can transform a lower pressure and high flow into a higher pressure and lower flow by using a charged-up inertia to boost pressures higher than the input. Figure 1.3 shows a boost converter circuit that is essentially the reverse of the buck converter shown in Fig. 1.2 with the on/off valve and the check valve switched. In this circuit, the back side of the inertia, which can be either a motor and flywheel or a long tube of fluid, is connected to either tank or a high output pressure. Thus the inertia alternates from accelerating when connected to tank, and decelerating when connecting to high pressure. The accumulator smooths the output power and provides flow when the inertia is connected to tank.

The authors in [7] presented the concept of switch-mode hydraulic converters and derived the ideal equations relating pressure, flow, and duty ratio for both buck and boost type transformers. They have some discussion on efficiency and have experimental

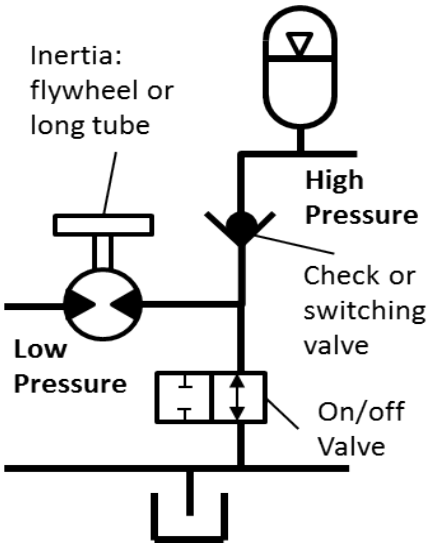

Figure 1.3: Hydraulic boost converter circuit

results showing the operation of the system. Their system used conventional solenoid valves at less than 10 Hz frequencies with large accumulators and flywheels. In [8], this work was extended to a combined buck-boost converter. This circuit, which uses the output of a buck converter as the input to a boost converter is better at controlling low-pressure loads. Wang et al. [9] looked at the pressure ripple in a boost converter that results from the on/off valve switching. They used an oil volume as a capacitance and simulated the effect of different volumes. In experiments, they demonstrated boosting a $50bar$ input pressure to up to $120bar$ with a system operating at $5Hz$. Work described in [10] also presented idealized buck and boost equations, but replaced the flywheel with a long fluid hose to generate the necessary inductance. This reduces the cost and complexity of the system, but adds a coupling between inductance and capacitance, as each length of hose/fluid will have both. With long inductance tubes, the effects of pressure wave propagation becomes important and must be taken into account. The paper presented some simulation results and preliminary experimental results with some degree of correlation to simulations for efficiency and flow modulation. Negri [11] applied the inductance tube concept to a boost converter and developed a model that looked at the inductance and resistance of the long tube but did not include compressibility or valve switching losses. Their model predicted higher efficiency at higher switching

frequencies and a limited feasible operating range at higher flows. They presented experimental results of a system running at 8 and $16Hz$. Pan [12] added a more detailed model for both buck and boost configurations that was used to simulate the system over a wider range of flows and frequencies. They computed an optimal switching frequency of $337Hz$ for the system studied and presented experimental results (at lower frequencies) showing an efficiency of $> 70\%$ in some low flow operating regions. The authors in [13], [14], [15], [16], and [17] also used a long tube as an inductance to create different switching converters. Brown et al. [13] used two inductance tubes and modulated the in-flow and out-flow to create a 4-port transformer. To achieve high switching frequencies, they designed a high-speed motor-driven rotary valve that varies the duty ratio by adjusting the relative position of two stators with a spinning rotor in between. In this paper they present ideal transformer equations and pressure-flow maps, study a number of power loss mechanisms, and present some simulated efficiency maps. For their valve, the losses were dominated by leakage in the larger than desired clearances, and it had problems with cavitation in the inlet ports. However, they demonstrated the feasibility of the concept and proposed solutions to the observed short-comings. The authors in [16] and [17] studied a similar system, but focused on creating a buck converter. They used a conventional under-lapped spool valve, which led to some leakage loss. The proposed application was robotics, to provide the power density benefit of hydraulics without the severe efficiency penalty of throttling valves. The papers compared the efficiency of the on/off system to a proportional system and found a 75% improvement over a walking cycle in simulation. Scheidl et al. [14] created an analytical model of an idealized inductance tube in the frequency domain as well as a numerical model and presented experimental results for a buck converter. They also described how using two switching valves, instead of one switching valve and one check valve, can allow bi-directional power flow and enable capturing of energy from a load. For a system switching at $70Hz$, they measured a peak efficiency of 76%, which was 16% better than a throttling valve system. However, the efficiency dropped below the throttling valve efficiency in some operating conditions due to the components used. Kogler and Scheidl [15] used a similar model and experimental apparatus, but added a description of a Cuk converter, which is essentially a boost and a buck converter in series. This circuit can allow transforming an input pressure either up or down,

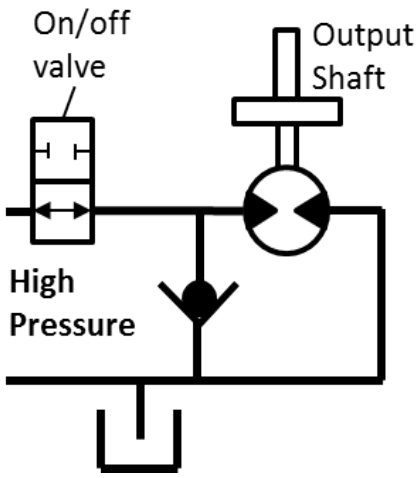

Figure 1.4: Virtually variable displacement motor

depending on the need of the load. They simulated buck conversion efficiency up to 30% better than throttling at low duty ratios and high flow rates, and experiments measured a 20% efficiency improvement. While the circuits studied in this thesis are not hydraulic pressure transformers, but rather hydraulic-mechanical transformers, many of the characteristics studied by these authors, such as the pressure ripple, component selection, and efficiency of switching circuits are similar to work presented in chapter 2.

Another way to create a hydro-mechanical buck converter is to take power directly out of the inductance, which is in the form of a motor and rotary inertia. In this configuration, the output power is converted by a hydraulic motor into the mechanical domain, and power is not transformed from a higher input pressure to a lower output pressure, but instead to a lower output torque. This circuit can also be described as a Virtually Variable Displacement Motor (VVDM), which is shown in Fig. 1.4. This circuit is very similar to the buck converter shown in Fig. 1.2, except rather than a low pressure hydraulic output, an output shaft is added to the hydraulic motor. In [18] and [19] the authors looked at the output speed ripple of such a device and demonstrated that higher switching frequencies and higher inertias reduce the speed fluctuations. The PWM duty ratio had a smaller effect on the ripple, especially in experiments, and changing the modeled viscous friction had little effect on the ripple. Zhu et al. [20] used a VVDM for driving a propeller for an underwater vehicle. Rather than using PWM, the

authors proposed using quasi pulse frequency modulation, which lowers the frequency at lower duty ratios. This allows for valves with long transition times to achieve low duty ratios without spending the entire "on" time in transition. Their system used conventional 2-stage valves. The dynamic response and the torque ripple on the motor were studied experimentally, but efficiency was not. The system as proposed used a pump with a relief valve to generate the constant input pressure to the system. This would cause the system to have similar efficiency to a throttling valve system. However, if a more efficient pressure source was used, the system could be more efficient than a throttling valve system. The VVDM circuit can also be thought of as a torque or pressure control device, which is the topic in [21]. This paper derived detailed equations for describing the ripple in an on/off valve pressure control application.

The boost converter analog to the VVDM is the Virtually Variable Displacement Pump (VVDP), which converts a mechanical input power on the shaft of a pump into a hydraulic output power. This circuit is studied in detail in chapter 2 and is depicted in Fig. 2.1(b). Tomlinson and Burrows [22] studied a VVDP system that set a desired output pressure and bounds on the output ripple to load/unload the pump, rather than the more typical approach of using PWM. This study demonstrated the concept and presented experimental results. The valve used was a conventional valve that did not achieve high frequencies. The effect of the pressure ripple bound on the switching frequency was demonstrated, but efficiency was not a focus of the paper. Li et al. [23] looked at the trade off between the size of the pressure ripple and the speed of response, and how that can be manipulated by sizing the accumulator and adding closed-loop control. This analysis is also clarified in chapter 2 of this thesis. Batdorff and Lumkes [24] developed a model of the VVDP that included power losses due to throttling in the transitioning valve and the compressibility of the oil. Lumkes et al. [25] added to that work by modeling and testing the system with a custom high-speed 3-way valve. They tested the VVDP at switching speeds up to $60Hz$ and reported efficiencies that were higher than a throttling valve circuit at low frequencies and low duty ratios, but similar or lower in other conditions. A similar model that used a pressure-dependent bulk modulus was described in [26], which is the basis for chapter 2 of this thesis. The experimental results from a system switching between 2.5 and $10Hz$ showed efficiencies exceeding those in a throttling valve system across the operating range. In [27], a

VVDP was created using a latching valve, which is described in [45]. That paper focused on developing a control algorithm that could achieve a desired repeated pressure profile. They used an adaptive controller with several different adaptation algorithms to estimate the derivative of the pressure, and then used a state machine and knowledge of the upcoming pressure demand to achieve the desired control. Finally, [28] described a circuit that combines a VVDP and a VVDM, which was used to drive a hybrid flywheel rail car.

Modeling of the losses in a VVDP done in [24], [25], and [26] indicate that throttling losses through the switching valve as it is transitioning can have a significant detrimental effect on the system efficiency, particularly at high frequencies. To address this problem, a soft-switching approach was proposed in [29], which is the basis for chapter 3 of this thesis. In this approach, fluid is temporarily routed away from the transitioning valve to be stored in a small softswitching chamber. Van de Ven [30] builds on this work by proposing a hydraulic locking mechanism that enables the softswitching approach.

A modified version of the VVDP is presented in [31] and [32], which uses a single fixed-displacement pump to drive multiple hydraulic circuits by apportioning the full pump flow to each branch for a variable fraction of the switching period. This has the advantage of allowing each branch to be driven at the specific pressure and flow rate that it requires, but can introduce output ripples that vary with the flow demands of the other branches. The authors in [31] studied the effect of switching frequency and accumulator size on the ripple size, and used conventional valves operating at relatively low PWM frequencies. In [32], the authors used a valve prototype that was similar to the phase-shift rotary valve in [13], but it was designed as a proof of concept and was limited in its ability to vary the duty ratio.

1.1.2 PWM Control

The use of switching valves to regulate the power flow in a hydraulic system presents challenges in controlling the system to achieve the desired output. A common approach is to use Pulse-Width-Modulation (PWM) duty ratio to approximate continuous values, with the addition of a ripple on the power flow. Lehman and Bass [33] look at the effect of using PWM to control a closed-loop system. The effect of feeding back a system with ripple can lead to a steady-state error or instability when the switching frequency

is low. They proposed a frequency-dependent averaging method to improve closed-loop performance. In [34], the authors derive a similar correction term for using PWM to control electromechanical systems. In the area of pneumatics, several researchers have investigated PWM control. In [35] and [36], the states-space averaging technique is used to derive an averaged system model that can be used with conventional linear [36] or non-linear [35] control design techniques. This averaging technique is also used in chapter 2 to study the dynamics of a VVDP. Jeronymo et al. [37] used an averaged system and performed a linear system identification. They also added a predictive term to improve the control performance. Royston and Singh [38] also investigated PWM control of a pneumatic cylinder, but focused their research on the design of a high-speed rotary valve that uses a phase shifting input along with a stator and a rotor to generate a variable pulse-width signal. The control approach in this paper is to use simple PID control along with a high switching frequency to achieve acceptable performance. In [39], a control approach was proposed that uses an on/off valve to provide the flow required to drive an actuator and then a throttling valve to cancel out the pressure ripples arising from the on/off control. This approach avoids the typical trade off between output ripple and response time that occurs in switching hydraulic circuits. While the design of feedback control algorithms using switching circuits is not studied in this thesis, the on/off valve systems studied make use of PWM to control the system output, and the work done by these authors could be applied design controllers for the circuits in chapters 2 and 4.

1.1.3 High Speed On/Off Valves

Many researchers have recognized that designing an effective on/off controlled system relies on a well-designed on/off valve. The ideal valve is fast, has a low pressure drop and leakage, and uses little actuation power. In [40], a two degree of freedom valve is used to achieve high speed, 2-stage-like performance from a simple component. An electric motor is used to rotate the spool to open up a pilot orifice. The pressure differential created by the pilot orifice then quickly moves the valve axially. This valve can achieve a 2-3 ms transition time and a flow of 18 lpm at 9 bar. Chapter 4 also presents a two degree of freedom valve, although it uses the rotation to achieve the on/of switching of the valve, rather than to create a force imbalance that actuates the spool. Another

approach is to perform a detailed design of a solenoid to improve its performance. This is done in [41], where a detailed model was created to predict the forces available for actuation. The authors in [42] designed a fast acting pneumatic valve for PWM control of a hydraulic cylinder. The strategy in this valve is to use a large plate as the moving element to improve the magnetic circuit and create a large flow area for a small displacement. Yamada et al. [43] and Yokota and Akutu [44] presented similar studies on the design of piezo-electric (PZT) driven hydraulic valves. These valves can transition quickly, in less than $1ms$, but the displacement available from a PZT actuator is typically too small for common hydraulic systems. These papers discuss the use of their valves as the pilot for multi-stage valves, which would change the trade off between speed and flow area. A different approach to creating a high-speed switching valve that also allows high flows is to use multiple poppet valves driven by a single pilot stage, as was described in [53]. Citing the fact that poppet volume increases faster than flow area as the diameter increases, the authors describe a valve with 14 small-diameter poppets driven by a single pilot valve to achieve $100lpm$ flow with a switching time of around $1ms$. For conventional size hydraulic valves, it is difficult to achieve high speeds without significant actuation power. This is due to the fact that linear switching elements, typically driven by electromagnetic actuators, must accelerate and decelerate a moving mass each time the valve is switched. A different approach for creating a high speed on/off valve based on continuous rotary motion is taken in chapters 4-7 of this thesis.

The strategy to mitigate the problem of high actuation power that is taken in this thesis and by other investigators is to use continuous rotary motion to generate the PWM signal. The advantage of this approach is that there is no acceleration of components; the valve element operates at a constant speed. A simple application of this approach is given in [46] and [47]. These papers detail a method of generating square pneumatic pressure waves for testing the dynamic response of different components. These valves consist of a spinning plate with grooves that pass between openings in the stator. If an application requires a variable duty ratio, this concept can be extended to have one fixed stator and one adjustable, to vary the phase between them. This is the approach taken in [13], [32], and [38]. A similar approach is taken in [48], which describes a phase-shift valve. This valve has multiple spinning plates that can rotate

with respect to each other. This paper presents the valve concept and detailed modeling of the losses that occur in the valve. In [49], a 2-way motor driven rotary spool valve is described that is a simpler version the valve studied in this thesis. The valve spool spins at a constant speed, and translates axially to adjust the duty ratio. The PWM duty ratio is coded into the profile of the valve spool. This paper presents experimental results for component and system efficiency but does not contain many analytical equations. In chapter 4, this concept is extended to 3-way and 4-way valves that are used to create a VVDP or a Virtually Variable Displacement Pump/Motor (VVDPM). An analysis of the power losses in such a valve are also described in this thesis. The rotary valve, which is the basis for chapter 4 of this thesis, is described in [50] and [51]. This valve has a helical land profile and operates with two degrees of freedom; it can rotate and translate axially. This design allows the repeated on/off action to be achieved by the constant rotary motion, while the adjustment of the duty ratio, which is typically much slower than the switching frequency, is controlled by changing the axial position.

The reason linear valves typically require significant actuation power to achieve high switching speeds is that the kinetic energy of the valve element is not recaptured, and thus it is lost. Rather than using constant rotary motion to solve this problem, as is done in chapter 4, Manhartsgruber [52] created a linear 3-way spool valve that resonates at the desired switching frequency of $400Hz$. The resonance allows the kinetic energy to be re-captured and is excited by an electromagnetic or piezoelectric actuator acting on a plate, which creates a pressure pulse on one end of the valve spool. The duty ratio of the valve is adjusted by changing the bias position of the sinusoidal resonance with respect to the valve ports.

A different way to reduce electrical actuation power in switching valves is to use bi-stable valves, which are held with open or closed without any holding current in the solenoid. Johnson et al. [45] describes a switching valve that uses permanent magnets to hold the valve spool in either state until it is acted on by a pulse of force from the solenoid. This valve is typically used in fuel injection systems and can open a $10mm^2$ flow area in $0.45ms$. A different type of bi-stable valve is described in [54] for use in parallel valve digital hydraulic systems. This valve uses a permanent magnet, but also uses an accelerated mass to act as a "hammer" on the metering element. This arrangement allows the actuator to build up kinetic energy in the hammer before contact

is made with the switching element. The collision provides a high starting force to move the valve out of its stable operating point.

1.1.4 Discrete Piston Control

Another area of significant research into the use of on/off valves is to use them to control individual chambers in a hydraulic device, such as a pump, motor, or transformer. This can be referred to as discrete piston control and has been studied by a number of researchers. This approach will be investigated in this thesis.

One area of development for discrete piston control is the use of mechanical mechanisms to disable pistons for a variable part of their pumping stroke in order to create a variable displacement pump. In this approach, pistons are disabled by connecting them to tank through a mechanically controlled mechanism. In [55] and [56], the pumping chamber is connected to tank through a poppet valve that is driven by an eccentric cam. By varying the cam eccentricity, the fraction of the pumping stroke that is enabled can be varied. In an alternate design [57], pistons can be enabled/disabled by covering/uncovering a hole in the side of the piston. In this design, an adjustable sleeve is used to cover a hole drilled in the side of the piston for a variable fraction of the pumping stroke. Both of these approaches achieve discrete piston control through purely mechanical means, but, in contrast to the design presented in chapter 6, they are only able to create variable displacement pumps, not motors.

Another approach to discrete piston control that uses mechanical control methods that can be applied to a hydraulic motor is described in [58]. In the design described in this paper, a piston motor is made to be variable displacement by using 2 2-stage poppet valves for each chamber. The poppet valves are controlled by a pilot stage that is driven by an adjustable cam-ring around the outside of the motor. Unlike other discrete piston designs, such as the design presented in chapter 6, this motor uses a rotating piston barrel, which requires the use of some type of port plate to communicate the high and low pressures from rotating piston barrel to the stationary input/output ports.

A different approach is to use electronically controlled valves on each piston chamber to create a discrete piston variable displacement device. Artemis Intelligent Power [59] has been a pioneer in this field and a number of papers have been written about their technology. In 1990 [60], the concept of the Digital Displacement pump using actively

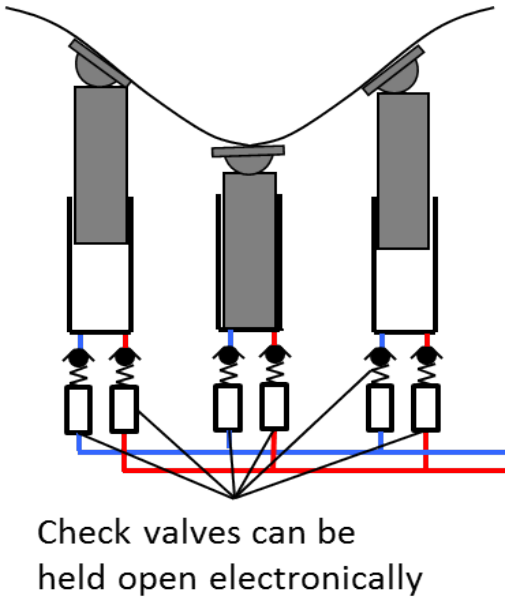

Figure 1.5: Sketch of Digital Displacement control concept

controlled poppet valves was introduced. In this design, a fixed displacement pump is fitted with two latching check valves for each piston to connect each chamber to either supply or tank pressure. Figure 1.5 presents a sketch of this concept, with two electrically latching valves for each piston. The latching check valves used are useful for pre-compressing and de-compressing the oil in the piston chamber, but they cannot open against pressure, which places some restrictions on when they are operated. A model and control concept for the device are described in [61]. In this paper, a choice between disabling individual pistons for their entire stroke or turning them off mid-stroke is made. Their choice was to disable pistons for their entire stroke, which they measured to have roughly 5dB lower noise output. However, this approach creates a larger ripple in the output flow, which can necessitate adding flow smoothing devices (i.e. accumulators). While their design allows the flexibility to switch between control modes, their published work only includes a description of the whole-stroke disabling approach. In [62], the dynamic performance of the device was predicted, and in [63], the concept was extended to a motor. This paper outlines the primary benefit of discrete piston control, which is that power losses, such as leakage, friction, and compressibility, can be reduced for

pistons that are disabled, enabling higher efficiencies at low displacements. The control of Digital Displacement pumps and motors is described in [64]. This paper presents a simulation model and control strategies for deciding when to enable/disable pistons in either a pressure or flow control mode. Simulations demonstrate the controllability of the device as well as the drawback of flow ripple that is associated with discrete piston control. In [65], control of Digital Displacement pumps and motors is described in the context of a tidal energy harvester, with a hydrostatic transmission composed of a large displacement ring-cam pump, and a small radial piston motor. The radial piston design was selected to minimize the friction at the piston-cam interface. The paper presents estimated power losses due to various mechanisms as a function of displacement. Wadsley [66] described the advantages of using the Digital Displacement Pump/motor in mobile equipment, citing improved efficiency, control flexibility, and fast response. Finally, [59] described the current focus on wind power applications and outlined an efficiency map that maintains 90% efficiency over a wide operating range. This was shown to be 10-20% higher than conventional swash plate devices.

Discrete piston control using electrohydraulic valves on each piston has also been investigated by a number of other researchers. In [67], discrete piston control was proposed as a way to create compact pump/motors for hydraulic hybrid vehicles. They proposed using one 3-way valve to select pressure or tank and another 2-way valve to enable/block each piston. This arrangement allows control strategies described as Partial Flow Diverting and Partial Flow Limiting. Partial Flow Diverting connects the piston chamber to tank for part or all of the power stroke, whereas Partial Flow Limiting closes off the piston chamber for part of the down-stroke, allowing the piston to draw a void in the chamber. The piston chamber is not opened again until the piston has moved up enough to fill the void again. The advantage of Flow Limiting is that it reduces the throttling loss across the tank valve. However, it does require drawing air into the hydraulic oil, which may cause cavitation or system compressibility problems. The paper states that more investigation of this approach is needed. Beyond describing the piston control strategies, the paper models the throttling loss across the valves, and describes the requirements of a fast, large valve for discrete piston control.

The authors in [68], [69], [70], [71], and [72] continued research into the Flow Diverting and Flow Limiting strategies, with a model and experimental apparatus to examine

the different approaches. The architecture in these papers was to use either 2 2-way valves or a bi-directional check valve. The design of the bi-directional check valve, which is a two-stage poppet valve, was described in [68], which presents a model and measured results of the valve. Merrill et al. [69] described the Flow Limiting and Flow Diverting (either partial or whole stroke) control strategies and presented results of simulated losses in each case. They found that the Partial Stroke Flow Diverting had the highest losses due to throttling across the on/off valves. In [70], a single-piston test rig was described for testing the Flow Limiting and Flow Diverting strategies, as well as the bi-directional check valve. This paper presents traces showing the operation of the pump operating with different control strategies. In his Ph.D thesis [71], Merrill further investigated the different control strategies, and he presented the simulation model used to study the system along with simulation results in a number of operating conditions. He found that the partial flow diverting strategy was the least efficient in high-speed, low pressure conditions, but that there was little difference between the strategies in other conditions. He pointed out that the electrical energy needed to control the valves is not insignificant, and can be $> 15\%$ of the total output power in high-speed, low-displacement conditions. That paper also correlated experimental and simulation results for a 3-piston inline pump using off-the-shelf on/off valves. He highlighted that a large, fast valve with repeatable timing is crucial for the efficient operation of the system. Holland [72] further described the different piston control strategies and presented the details of experimental results from both a single piston and a 3 piston test set-up.

In [73], a 3-piston inline pump was converted from being controlled by passive check valves to being controlled by actively controlled switching valves. The volumetric and mechanical efficiencies were measured in the baseline and modified states. Due to the valves selected, the efficiency in the modified case was lower than the baseline, but the modified system was able to provide variable displacement capability. The electrical power to the valves was found to reduce the efficiency in the range of $8-15\%$. Efficiencies measured in the partial displacement cases were lower than in the full displacement case. Heikkila et al. [74] used a similar 6-piston inline device, but added 3 switching valves to each piston instead of 2. This allowed the device to act as a hydraulic transformer with a mechanical shaft input. Each piston was connected to tank and two different output ports, while the shaft was driven by a motor. This configuration allows for

multiple loads to be driven, for power to be put back on the motor shaft from either load, or for power transfer between the two loads. The control approach used was to enable/disable pistons for their entire stroke, which lead to significant ripple on the output. An accumulator was used to smooth the output. The efficiency of the device reached a maximum in the low 80s at 100% displacement, and decreased for lower displacements. Experimental results showed the pressure ripple, pressure response time, the reaction to flow disturbances, and power sharing between two loads.

Armstrong and Yuan [75] applied the concept of controlling discrete pumping elements to a geroter-type pump/motor. Instead of controlling individual pistons, the authors applied 2 2-way valves to each pocket in the star of a geroter. By selecting which chambers were active, they showed that, for example, a 7-chamber device could have 2^7 different configurations that provide a wide range of output torques in the motoring case. The paper described control logic for selecting the ideal configuration and presented simulation results.

Finally, a different type of discrete chamber control was described in [76]. In this research, actively controlled valves were used to connect discrete chambers in a multi-chamber hydraulic cylinder to pressure or tank. The individual chambers have different areas so that different combinations of chambers create different output forces. By applying this approach to two sides of a double-acting cylinder, a digital hydraulic transformer can be created that allows for a variable transformation ratio based on the chambers selected.

The results presented in this thesis are different from the existing research in a number of ways. In contrast to many of the discrete piston designs, the approach taken in this thesis is to use a hydro-mechanical control mechanism to enable/disable individual pistons, which has advantages and disadvantages. The primary disadvantage is reduced flexibility when compared with electrical valve control; only one control mode can be used, and the timing of the valves cannot easily be adjusted for varying input conditions. However, using a mechanical control design can greatly simplify the packaging and control of the device, and it can result in a more robust system than a device that utilizes multiple actively controlled valves per piston. The actuation power for a mechanical control system is strictly mechanical and hydraulic, which are readily available in a hydraulic pump/motor. With mechanical or hydraulic actuation, there is

no holding power required, as there is in many actively controlled valves. By using a control device that is mechanically coupled to the pump/motor shaft, reliable timing can be ensured. Finally modeling of the losses in the pump/motor shows that the primary efficiency benefits of the discrete piston approach can be achieved using a mechanically controlled device. In chapter 5, a detailed investigation of the way that power losses scale in both a discrete piston device and a conventional swashplate type device is presented. This comparison, which outlines the primary benefit of discrete piston control, is first presented in this thesis. An investigation of the flow ripple characteristics of different piston disabling strategies is also introduced in chapter 5.

The mechanical control approach taken in this thesis is a similar direction to the one taken in [57], [55], and [58], although there are a number of differences. Unlike [57] and [55], the work presented in this thesis will apply to a motor as well as a pump, and in contrast to [58], the design will utilize stationary piston cylinders, which removes the need for a port plate to communicate oil to rotating pistons. Instead of an adjustable cam, the control of the effective pump/motor displacement will be achieved using a two degree-of-freedom valve that can translate and rotate. By coupling the rotary movement to the pump/motor shaft, only the axial position of the single rotary valve must be adjusted to control the displacement of each piston.

1.2 Overview

In this thesis, a number of different aspects of on/off valve controlled hydraulic circuits are considered, such as circuit design, power loss reduction, on/off valve design, and a combination of on/off valves and a pump/motor. In chapter 2, one type of on/off valve circuit is considered: a Virtually Variable Displacement Pump (VVDP). A system model is developed that is used to describe a trade-off between the speed of response of the system and the ripple on the output pressure. Sources of energy loss are also predicted, and then compared with experimental measurements of the circuit. In chapter 3, a novel concept for reducing the power loss in an on/off valve controlled circuit is described. This soft switching approach borrows from designs developed for electronic switching converters that use small capacitances to temporarily route fluid away from a transitioning switch. The model of the soft switching device is integrated into a VVDP,

but it can also be applied to many different on/off valve controlled systems. This concept is shown through simulation to have significant potential for reducing power loss in a hydraulic switching circuit. In chapter 4, a design for a new type of rotary on/off valve is presented, and its design is formulated as an optimization problem. The rotary valve that is described has the potential to efficiently achieve very high switching frequencies, due to the fact that it rotates continuously in one direction and does not require the acceleration/deceleration of a valve element that is typical in conventional linear valves. However, the rotary valve structure creates a number of constraints that create tradeoffs between different mechanisms of power loss and performance. The optimal design of the valve is presented as a way to minimize the power loss while still meeting specified performance constraints. This approach is described for both a VVDP and a VVDPM.

In chapters 5, 6, and 7, a different approach for using on/off valves to improve hydraulic system efficiency is explored. The two-degree of freedom rotary valve described in the previous chapter is used to control individual pistons of a hydraulic pump/motor. Controlling individual pistons in a pump has the potential to improve efficiency, particularly at low displacements, by removing pressure from pistons when they are not needed. This is in contrast to conventional pumps and motors that maintain pressure, and thus leakage and friction, on all pistons regardless of the displacement. There are several advantages to integrating the rotary valve with a pump/motor. First, by using the valve to control the flow from individual pistons, less power flows through the valve, which benefits some of the design tradeoffs described in chapter 4. Second, by controlling individual pistons, the on/off valve can reduce losses that are present in a conventional piston pump/motor. Finally, by using a rotary valve, the large number of electronically controlled valves that are used in competing discrete piston pumps are avoided. Chapter 5 presents an analysis of the losses in a conventional and discrete piston pump/motor, demonstrating the potential efficiency improvement that can be achieved through the use of discrete piston control. Several different strategies for achieving discrete piston control, such as whole piston disabling and partial stroke disabling are described and compared. In chapter 6, the detailed design of the discrete piston prototype is presented. Several design concepts for creating a mechanically controlled discrete piston pump/motor are compared, and a design is selected. A dynamic model of the selected concept is presented, and the detailed mechanical design of the full

pump/motor prototype is described. Finally, in chapter 7, experimental results of the discrete piston controlled pump/motor are presented, showing the dynamic operation of the device along with measured efficiency results.

Chapter 2

Virtually Variable Displacement Pump

In conventional hydraulic systems, control of the power in the system is often achieved through the use of throttling valves. Much like how the power in electrical systems can be controlled inefficiently by dissipating power across resistors, hydraulic control using throttling valves operates by converting excess power into heat. This dissipative form of control is a significant source of wasted energy in hydraulic systems.

A different approach has been proposed that achieves control by transforming power rather than dissipating it. In an analog to an electrical switching DC-DC converter, control of hydraulic systems can be achieved through the use of switching valves and energy storage elements. In contrast to throttling valves, which are typically only partially open, resulting in a large pressure drop across them, switching valves are held in either the fully-open or fully-closed state. Control is then achieved by adjusting the ratio of the time spent in the open state to the time spent in the closed state with energy storage elements used to smooth the input and output power.

There are numerous architectures for on/off valve control that can be implemented in hydraulic systems to achieve different control objectives, such as controlling the power out of a pump, the power out to an actuator, distributing power to multiple actuators, or transforming power between two different pressures. In this chapter, a circuit that

uses an on/off valve to control the power out of a pump will be studied.[1] However, many of the equations and conclusions derived in this chapter can be easily adapted to other circuit architectures.

In many hydraulic systems, the speed of the pump that generates the hydraulic power cannot be manipulated to control the power output of the pump, since pumps are often driven by constant-speed electric motors or internal combustion engines that power multiple systems simultaneously. For systems with a fixed displacement pump, that means the flow out of the pump is typically not matched to the flow required by the rest of the hydraulic system. In this case, the excess flow must be diverted away from the load, which, in a conventional throttling valve case, is done at the load pressure. The bleed off of the excess flow at high pressure results in a significant energy loss. The on/off valve circuit described in this chapter is designed to prevent this energy loss.

There is another method of controlling the power out of a pump that makes use of variable displacement pumps. In this case, the displacement of the pump is varied so that, regardless the speed of pump, the flow out to the hydraulic system is equal to the flow that is required by the load. This approach is significantly more efficient than throttling valve control, but it requires the use of variable displacement pumps and circuit elements to control them. Variable displacement pumps are typically larger and more expensive than fixed displacement pumps, and many low-cost applications do not use them.

In this chapter, an on/off valve circuit is studied which uses an on/off valve, a check valve, a fixed displacement pump, and an accumulator to create a hydraulic power source with a variable output flow, which can be referred to as a Virtually Variable Displacement Pump (VVDP). In the next section, the concept and system equations of the VVDP are described. In section 2.2, the trade-off that exists between the output ripple and the response time is discussed, and section 2.3 describes the mechanisms of power loss in a VVDP. Section 2.4 contains experimental results of a VVDP system, and concluding remarks are presented in section 2.5.

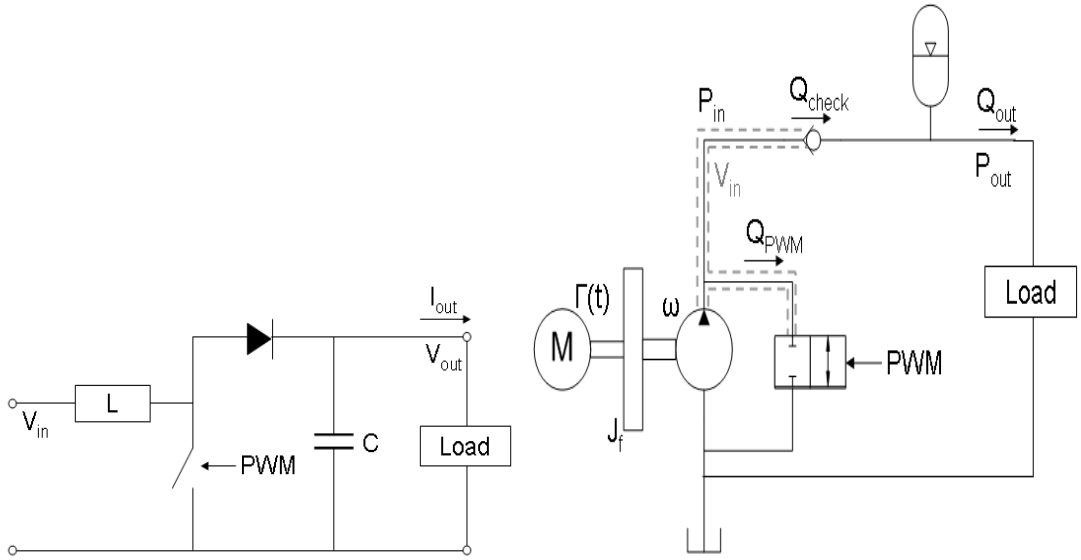

(a) DC-DC boost converter

(b) PWM variable displacement pump

Figure 2.1: Electrical DC-DC boost converter and its hydro-mechanical analog. The electrical DC-DC boost converter is a transformer between input (V_{in}) and output voltages (V_{out}). In the hydro-mechanical analog, it is a transformer between prime mover torque input (Γ) and pressure output (P_{out}).

2.1 Concept and System Model

The concept of a PWM based virtually variable displacement pump comes from the DC-DC switched mode boost converter found in power electronics. Figure 2.1 shows a comparison between the two systems.

In the hydraulic case, the high speed on/off valve mimics the transistor in the electrical case, switching the circuit between two different states. The inertia of the fixed displacement pump and the prime mover (and optionally a flywheel) is the functional equivalent of the inductor; it serves to smooth the torque load on the prime mover driving the pump. The check valve acts as a diode and ensures that there is no back flow from the load when the PWM valve is open. The accumulator, the analog of a capacitor, provides smoothing of the output power.

The system cycles between two modes of operation. When the on/off valve is closed, the check valve opens, and the full flow of the pump is directed to the load and accumulator. Flow not used by the load fills the accumulator. Once the on/off valve opens, the full flow of the pump is diverted to tank. This causes the pressure on the inlet side of the on/off valve to drop below the accumulator pressure, which causes the check valve to close. The accumulator then provides the flow to the load until the on/off valve closes again. The engine torque is used to store energy in the rotating inertia. As such, the circuit in Figure 2.1 boosts the prime mover torque input Γ to the output pressure P_{out} when Γ and P_{out} are seen as effort variables in a transformer.

The following equations describe the dynamic behavior of a VVDP circuit and can be used to study its characteristics. In developing a model of the system, several simplifying assumptions are made. The driving pump is assumed to be an ideal flow source, the check valve is assumed to open instantaneously, fluid friction and leakage are assumed to be negligible, the accumulator is assumed to operate adiabatically, and the fluid inertia effects are assumed to be insignificant. With these assumptions, the system is modeled as a three state system with the inertia of the pump rotor and flywheel, the compressed oil on the inlet side of the system, and the compressed gas in the accumulator as the energy storage elements.

Summing the engine torque $\Gamma(t)$ and the torque induced by the inlet volume pressure

[1] Some of the material in this chapter was originally published by ASME in [26].

P_{in} on the drive shaft yields:

$$J_f\dot{\omega} = -\frac{D}{2\pi}P_{in} + \Gamma(t) \tag{2.1}$$

where J_f is the rotary moment of inertia of the pump, motor, and flywheel, ω is the rotational velocity of the pump, and D is the displacement of the pump. P_{in} is the pressure in the inlet volume, V_{in}, which extends from the pump outlet to the check valve and the PWM valve (see Fig. 2.1(b)). The dynamic equation for the compressible oil volume is:

$$\dot{P}_{in} = \frac{\beta(P_{in})}{V_{in}}\left(\frac{D\omega}{2\pi} - Q_{pwm} - Q_{check}\right) \tag{2.2}$$

where $\beta(P_{in})$ is the pressure dependent bulk modulus of the fluid, Q_{pwm} is the flow through the on/off valve, and Q_{check} is the flow through the check valve.

The bulk modulus of the oil relates to its stiffness and is defined by the following equation:

$$\beta = -V\frac{dP}{dV} \tag{2.3}$$

where V is the volume of the fluid being compressed/decompressed, and dP/dV is the rate of change of pressure with respect to the change in volume. For typical air-free hydraulic oils, values in the range of $10000 - 18000bar$ are typically used.

When air is introduced into a hydraulic system, the stiffness of the oil can decrease dramatically, particularly at low pressures. Several authors have developed equations for the effective bulk modulus when air is present in the oil, such as [77, 78]. In [79], the stiffness of the container is also taken into account. The container stiffness can be a significant issue when flexible hydraulic hoses are used, however, the fluid chambers studied here can (and should) be designed to be inside a solid manifold, so the container stiffness is neglected. The equation for the bulk modulus derived in [77] is:

$$\beta_{Yu} = \frac{\beta_{oil}\left(1 + 10^{-5}P\right)^{1+1/\gamma}}{\left(1 + 10^{-5}P\right)^{1+1/\gamma} + 10^{-5}R\left(1 - cP\right)\left(\beta_{oil}/\gamma - 10^5 - P\right)} \tag{2.4}$$

where β_{oil} is the bulk modulus of air-free oil, P is the gauge pressure of the oil in Pa, γ is the ratio of specific heats for the gas (typically 1.4 for air), R is the fraction of the volume that is air at atmospheric pressure, which is typically between 0 and 0.1, and c is the coefficient of air bubble variation due to air being dissolved into the oil at

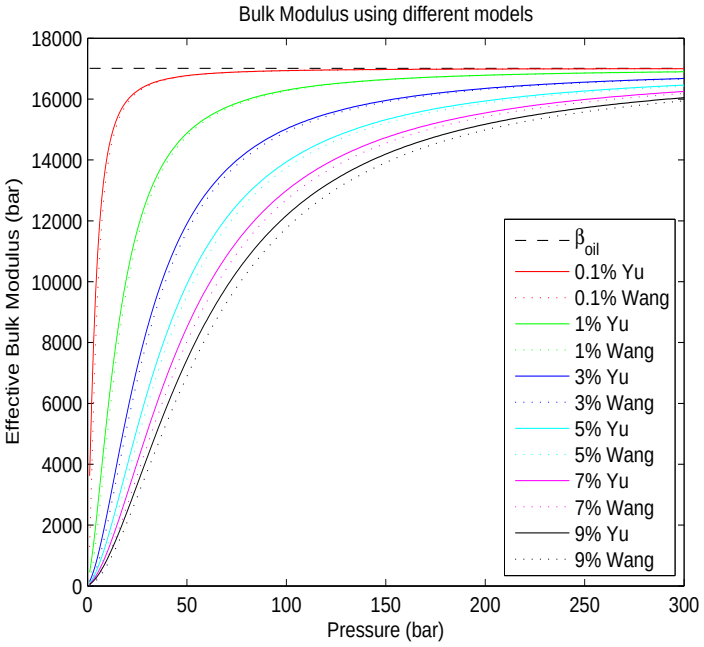

Figure 2.2: Effective bulk modulus for different models and amounts of entrained air

high pressures. This value must be non-negative, and $cP < 1$ over the pressure range of interest.

A similar equation was derived in [78]:

$$\beta_{Wang} = \frac{1 + \left(\frac{V_{a0} - V_{ad}}{V_{f0}}\right)\left(\frac{P_0}{P}\right)^{1/\gamma}}{1 + \left(\frac{\beta_{oil}}{\gamma P}\right)\left(\frac{V_{a0} - V_{ad}}{V_{f0}}\right)\left(\frac{P_0}{P}\right)^{1/\gamma}}\beta_{oil} \tag{2.5}$$

where V_{a0} is the volume of air at atmospheric pressure, V_{ad} is the volume of oil dissolved in the oil, V_{f0} is the volume of fluid, and P_0 is atmospheric pressure.

Figure 2.2 shows the results of the two bulk modulus equations, Eq. (2.4) and Eq. (2.5), for different amounts of entrained air. For both models, it is assumed that no air is absorbed into the fluid as the pressure is increased. The amount of air entrained with the oil is very difficult to know for a given system, and depends on the design of the hydraulic components and circuit, as well as the quality of the seals and the amount of churning and mixing the oil goes through when in contact with air. In Fig. 2.2 it is clear that both models produced similar results, and only differ appreciably for high

amounts of air entrainment. While the bulk modulus does converge to the constant value of β_{oil} at high pressures, at low pressures, the bulk modulus is only a fraction of the high-pressure value. For fluid volumes that experience repeated transitions between high and low pressures, this effect must be taken into account. Using a simplified model with a constant bulk modulus can significantly under estimate the compliance of the oil at low pressures, which occur regularly in an on/off valve controlled system.

The PWM valve is modeled as an orifice with a time varying area $a(t)$:

$$Q_{pwm} = a(t)K\sqrt{P_{in}} \tag{2.6}$$

where $K = C_d\sqrt{\frac{2}{\rho}}$ with C_d being the discharge coefficient, and ρ being the oil density. The orifice area, $a(t)$, is the control input to the system.

The check valve is assumed to exhibit a fixed pressure drop, ΔP_{check}, when it is open. Thus, $Q_{check}(t)$ is given by:

$$Q_{check} = \begin{cases} 0 & \text{if } P_{in} < P_{out} + \Delta P_{check} \\ \frac{D}{2\pi}\omega - Q_{pwm} & \text{if } P_{in} \geq P_{out} + \Delta P_{check} \end{cases} \tag{2.7}$$

where P_{out} is the pressure in the accumulator. This equation includes a quasi-static assumption on the inlet pressure when the check valve is open. This is reasonable since the pressure dynamics for both P_{in} and P_{out} are governed by the relatively slow accumulator when the check valve is open.

Since the accumulator volume changes at a high frequency, it is assumed that the dynamics of the gas in the accumulator are defined by the equation for the adiabatic compression of an ideal gas:

$$P_{out}\left(t\right)V^{\gamma}\left(t\right) = P_0 V_0^{\gamma} \tag{2.8}$$

where V is the volume of the gas in the accumulator and P_o and V_o are the initial pressure and volume of the gas in the accumulator. The adiabatic assumption is valid since the charging/discharging cycles of the accumulator in an on/off valve controlled system are typically too fast to allow for significant heat transfer between the gas in the accumulator and the environment.

Differentiating Eq. (2.8) with respect to time and defining $-\dot{V}$ as the net flow into

the accumulator gives the following equation for the outlet pressure of the system:

$$\dot{P}_{out} = \gamma \frac{P_{out}}{V} \underbrace{[Q_{check} - Q_{out}(t)]}_{-\dot{V}} \tag{2.9}$$

where Q_{out} is the output flow rate and depends on the characteristics of the load. In summary, the system state equations are:

$$J_f \dot{\omega} = -\frac{D}{2\pi} P_{in} + \Gamma(t) \tag{2.10}$$

$$\dot{P}_{in} = \frac{\beta(P_{in})}{V_{in}} \left(\frac{D}{2\pi} \omega - Q_{pwm} - Q_{check} \right) \tag{2.11}$$

$$\dot{P}_{out} = K_{acc}(P_{out})(Q_{check}(t) - Q_{out}(t)) \tag{2.12}$$

where $K_{acc}(P_{out})$ is the volumetric stiffness, in units of Pa/m^3, of the accumulator, given by:

$$K_{acc}(P_{out}) = \gamma \frac{P_{out}^{(1+1/\gamma)}}{{P_0}^{1/\gamma} V_0} \tag{2.13}$$

In the next section, this model will be used to study the trade off between the dynamic response of the system and the on/off valve induced pressure ripple in a virtually variable displacement pump.

2.2 System Dynamics

The primary dynamic response is studied under the assumption that the dynamics of the inlet oil volume do not play a significant role[2]. This assumption is based on the fact that a hydraulic oil volume is typically many times stiffer than an accumulator. It is further assumed that the PWM valve opens and closes instantaneously. While this is an approximation, the valve transition time must be small in comparison to the PWM period for any PWM system to operate efficiently. With these two assumptions, the system reduces to:

$$J_f \dot{\omega} = -u(t) \frac{D}{2\pi} \left(P_{out} + \Delta P_{check} \right) + \Gamma(t) \tag{2.14}$$

$$\dot{P}_{out} = K_{acc}(P_{out}) \left[u(t) \frac{D}{2\pi} \omega - Q_{out}(t) \right] \tag{2.15}$$

[2] The inlet volume does have an effect on the efficiency, which is studied in Section 2.3.2.

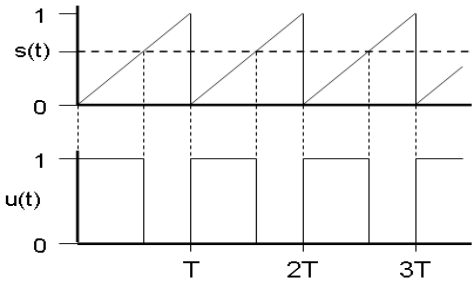

Figure 2.3: Pulse-width-modulated Input Signal

$u(t) \in \{0, 1\}$ is the input to the reduced system and represents the state of the on/off valve. For control via pulse-width-modulation, $u(t)$ is generated by comparing the desired duty ratio, $s(t) \in [0, 1]$, to a periodic sawtooth wave (Fig. 2.3):

$$u(t) = \begin{cases} 1 & \text{if } s(t) \geq (t/T) \bmod 1 \\ 0 & \text{if } s(t) < (t/T) \bmod 1 \end{cases} \tag{2.16}$$

where T is the period of the PWM cycle.

State-space averaging, which consists of using the duty ratio to average the system dynamics in the on and off states, can be used in the analysis of switch-mode systems [80]. The design rule-of-thumb is that if the switching frequency is at least on the order of 4-10 times faster than the control bandwidth, the method is accurate [33]. At lower frequencies, this technique may introduce inaccuracy leading to instability or steady-state bias when a feedback controller is designed based on the averaged system.

Applying state-space averaging, the average system dynamics can be written as:

$$J_f \dot{\bar{\omega}} = -s(t)\frac{D}{2\pi}(\bar{P}_{out} + \Delta P_{check}) + \Gamma(t) \tag{2.17}$$

$$\dot{\bar{P}}_{out} = K_{acc}(\bar{P}_{out}) \left[s(t)\frac{D}{2\pi}\bar{\omega} - Q_{out}(t) \right] \tag{2.18}$$

where $\bar{P}_{out}$ and $\bar{\omega}$ correspond to the averaged state variables.

Equations (2.17)-(2.18) are valid under the assumption that all the dynamic states are slowly varying in comparison to the control input, $s(t) \in [0, 1]$.

In steady-state, the equations become:

$$Q_{out}(t) = \frac{s(t)D}{2\pi}\bar{\omega}; \qquad \Gamma(t) = \frac{s(t)D}{2\pi}(\bar{P}_{out}(t) + \Delta P_{check}) \tag{2.19}$$

These equations show that the flow out of the system and the torque on the prime mover are modified by the duty ratio $s(t)$, representing a pump with an effective displacement of $s(t)D$.

In the next section, these average dynamic equations are used to describe the pressure ripples on the system output, which are an inevitable feature of on/off controlled systems. In section 2.2.2, the dynamic response of the system is discussed for a system with a simple loading condition.

2.2.1 Pressure Ripples

Consider first the pressure ripples when $\bar{P}_{out}$ is constant, corresponding to a constant duty ratio s. Since the prime mover speed typically varies much slower than the PWM frequency, this analysis is restricted to when $\bar{\omega}$ is constant. If the pressure ripple is small such that $K_{acc}(P_{out}) \approx K_{acc}(\bar{P}_{out})$, then from Eqs. (2.15), (2.16) and (2.19), the instantaneous (not average) pressure dynamics are given by:

$$\dot{P}_{out} \approx \begin{cases} K_{acc}(\bar{P}_{out})\frac{D\bar{\omega}}{2\pi}(1-s) & \text{if } t \bmod T \leq s \cdot T \\ -K_{acc}(\bar{P}_{out})\frac{D\bar{\omega}}{2\pi}s & \text{if } t \bmod T > s \cdot T \end{cases} \tag{2.20}$$

Integrating this equation over T yields a sawtooth ripple waveform with its amplitude given by:

$$\begin{aligned} P_{ripple} &= K_{acc}(\bar{P}_{out})\frac{D\bar{\omega}}{2\pi}T(1-s)s \\ &= 4P^{max}_{ripple}(1-s)s \end{aligned} \tag{2.21}$$

where P^{max}_{ripple} is the maximum ripple magnitude achieved when $s = 0.5$:

$$P^{max}_{ripple} = \frac{1}{4}\left[\frac{D\bar{\omega}}{2\pi}\right]K_{acc}(\bar{P}_{out})T \tag{2.22}$$

Equation (2.21) shows that, for a given operating pressure $\bar{P}_{out}$ and maximum pump flow, the ripple size can be reduced by increasing the PWM frequency or by decreasing the accumulator's volumetric stiffness $K_{acc}(\bar{P}_{out})$ in Eq. (2.13). The latter is in turn achieved by increasing the accumulator precharge volume V_0 or pressure P_0. Increasing the PWM frequency can often be a challenge due to the speed of response of conventional switching valves and power losses that increase with the switching frequency, as described in section 2.3.

2.2.2 Dynamic Response and Feedback

The dynamic response of the system cannot be determined without the load characteristic. For simplicity, consider a case of an orifice load:

$$Q_{out} = K_{load}\sqrt{P_{out}} \tag{2.23}$$

The average system becomes:

$$\dot{\bar{P}}_{out} = K_{acc}(\bar{P}_{out})\left[s\frac{D\bar{\omega}}{2\pi} - K_{load}\sqrt{\bar{P}_{out}}\right] \tag{2.24}$$

For a duty ratio s^*, let the corresponding equilibrium pressure be $\bar{P}^*_{out}$ such that $s^*\frac{D\bar{\omega}}{2\pi} = K_{load}\sqrt{\bar{P}^*_{out}}$. Then, assuming the pressure changes are small enough that $K_{acc}\left(\bar{P}^*\right)$ can be considered a constant, the linearized dynamic equation of the pressure error, $\bar{P}_e = \bar{P}_{out} - \bar{P}^*_{out}$, is:

$$\dot{\bar{P}}_e = -\underbrace{K_{acc}(\bar{P}^*_{out})\frac{K_{load}}{2\sqrt{\bar{P}^*_{out}}}}_{\lambda}\bar{P}_e + K_{acc}(\bar{P}^*_{out})\frac{D\omega}{2\pi}\tilde{s} \tag{2.25}$$

where $\tilde{s}(t) = s(t) - s^*$. The magnitude of the open loop system eigenvalue, λ, increases linearly with the accumulator's volumetric stiffness, $K_{acc}(\bar{P}^*_{out})$. This is achieved by decreasing the precharge volume V_0 or pressure P_0.

Note that a trade off exists between the ripple size in Eq. (2.21) and open loop system bandwidth (λ in Eq. (2.25)). In fact,

$$\frac{P^{max}_{ripple}}{\lambda} = \frac{T}{2}\left[\frac{D\bar{\omega}}{2\pi}\right]\frac{\sqrt{\bar{P}_{out}}}{K_{load}} \tag{2.26}$$

The ripple size (P^{max}_{ripple}) and the time constant ($1/\lambda$) are hyperbolically related (Fig. 2.4). Thus, if pressure ripple is decreased, the time constant of the system is also increased. This relationship is independent of the accumulator parameters. This equation highlights a fundamental trade off in the design of on/off controlled systems; the energy storage elements needed to smooth the discontinuous power output from the switching valves also have the effect of reducing the response speed of the system. This trade off can be alleviated by increasing PWM frequency or by reducing maximum pump flow.

Adding feedback control can significantly improve this trade off by decreasing response time with little effect on ripple size. For example, the feedback equation:

$$\tilde{s} = \frac{2\pi}{D\omega}K_{fb}(P^* - \bar{P}_{out}(t))$$

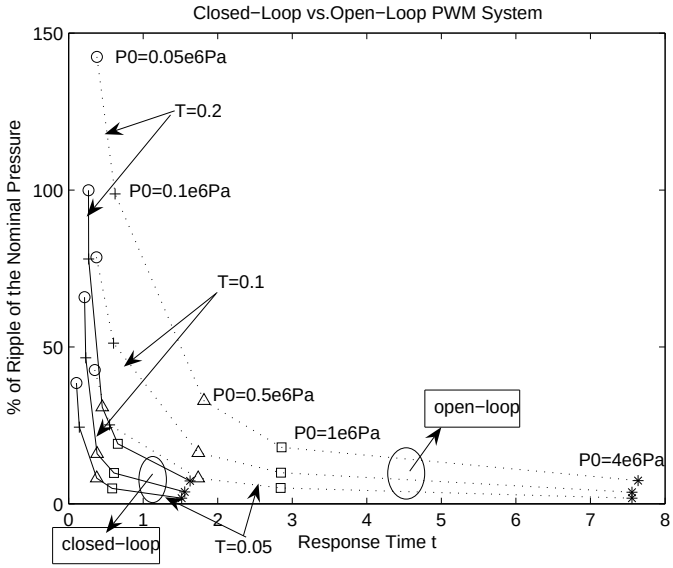

Figure 2.4: Simulated open loop trade-off between peak-to-peak ripple size and response time for different PWM periods, T, and accumulator pre-charge pressure, P_0 [23].

changes the closed loop eigenvalue from $-\lambda$ to $-(\lambda + K_{acc}(\bar{P}^*_{out})K_{fb})$. The feedback gain, K_{fb}, can be chosen arbitrarily large subject to saturation. Figure 2.4 demonstrates the improvement in the system dynamics that can be achieved using feedback control. By implementing closed-loop pressure control, both the response time and the ripple magnitude can be reduced without increasing the PWM frequency.

2.3 Power Loss Mechanisms

Identifying the sources of energy loss in a PWM controlled hydraulic system is critical to designing efficient virtually variable displacement pumps. Cao et al. [7] explain that the efficiency and performance of a real switch-mode hydraulic system may be degraded by transition time in the PWM valve, fluid compressibility in the inlet oil volume, pressure drops across the PWM and check valves, closing time for the check valve, hysteresis in the accumulator bladder, fluid friction, and leakage.

The goal in this section is to quantitatively examine three of these sources of power loss and develop guidelines for the design of efficient virtually variable displacement

pumps. The types of loss that are investigated are throttling through the fully open PWM and check valves, loss due to the compressibility of the hydraulic oil, and throttling through the PWM valve as it transitions between open and closed. These three effects are considered independently here as an approximation, although in reality, the different sources of loss are acting simultaneously and will have some interaction.

2.3.1 Full Open Valve Throttling

The primary reason for developing on/off controlled systems is to minimize loss due to valve throttling. However, as with any valve, a small throttling loss still occurs across the PWM and check valves, which is quantified here. The valve transition time is assumed to be negligible in comparison with the full open time in this analysis.

Let the pressure drops across the fully open PWM valve and the check valve be ΔP_{pwm} and ΔP_{check}. The power loss is then:

$$\begin{aligned} L_{open} &= \Delta P_{pwm}(1 - s(t))\frac{D\omega}{2\pi} + \Delta P_{check}s(t)\frac{D\omega}{2\pi} \\ &= \frac{D\omega}{2\pi}\left(\Delta P_{pwm} + (\Delta P_{check} - \Delta P_{pwm})s(t)\right) \end{aligned} \tag{2.27}$$

Eq. (2.27) reveals that L_{open} is a convex combination of losses in the check valve and the PWM valve, and it increases with pump flow. ΔP_{check} and ΔP_{pwm} combine to produce a loss that is dependent on the duty ratio, $s(t)$, whereas the constant loss term is a function of only ΔP_{pwm}. Clearly, reducing the full-open pressure drop through the PWM and check valves will reduce this source of power loss.

2.3.2 Compressibility Loss

Every time the inlet volume transitions from low to high pressure, energy must be used to compress the fluid, which is then lost when the PWM valve opens. The energy required to compress a unit of fluid from atmosphere to a given pressure is:

$$E = \int_{V_0}^{Vf} P(V)\ dV = \int_{P_0}^{P} V(p)\frac{p}{\beta(p)}\ dp \tag{2.28}$$

where the definition of the bulk modulus in Eq. (2.3) is used to change the variable of integration. In this equation, V_0 is the initial volume of the fluid being compressed, V_f

is the final volume, P_0 is the initial pressure of the fluid volume, and P is the pressure to which it is being compressed. Equation (2.3) can also be integrated to determine the compressed volume of the fluid at a given pressure:

$$V_f(P) = V_0 e^{-\int_{P_0}^{P} \frac{p}{\beta(p)}\, dp} \tag{2.29}$$

Combining Eqs. (2.28) and (2.29) gives the following equation for the energy stored in the fluid:

$$E(P, V_0) = \int_{P_0}^{P} V_0 e^{-\int_{P_0}^{p} \frac{\bar{p}}{\beta(\bar{p})}\, d\bar{p}} \frac{p}{\beta(p)}\, dp \tag{2.30}$$

This equation is similar to one derived in [81], which uses the energy stored in the fluid in defining a storage function for deriving passivity-based controllers for hydraulic actuators. Equation (2.30) can be numerically integrated using a model for the pressure dependent bulk modulus, such as Eq. (2.4) or (2.5). Figure 2.5 shows the result of such an integration using the Eq. (2.4). Clearly, more air in the fluid results in more energy being required to raise its pressure. The compressibility loss varies significantly at different pressure, which is determined by the load. However, the compressibility loss also varies linearly with the inlet volume, which can be reduced through proper system design.

2.3.3 Transition Loss

When an on/off valve transitions between open and closed states, the open area through the valve becomes small, resulting in a momentary rise in the energy lost to throttling across the valve. The energy loss per cycle due to this increased throttling is:

$$E_{trans} = \int_{t_{close}} P_{in}(t) Q_{pwm}(t)\, dt + \int_{t_{open}} P_{in}(t) Q_{pwm}(t)\, dt \tag{2.31}$$

where t_{close} and t_{open} are the intervals during one PWM period when the PWM valve is in transition, and Q_{pwm} is the flow through the PWM valve. It is assumed that the pressure-driven check valve transition is much faster than the PWM valve transition, and thus, the transition loss is dominated by throttling through the PWM valve.

Relationships are needed to describe $P_{in}(t)$ and $Q_{pwm}(t)$ while the PWM valve is in transition. We assume that P_{out} is constant for the purpose of estimating the transition

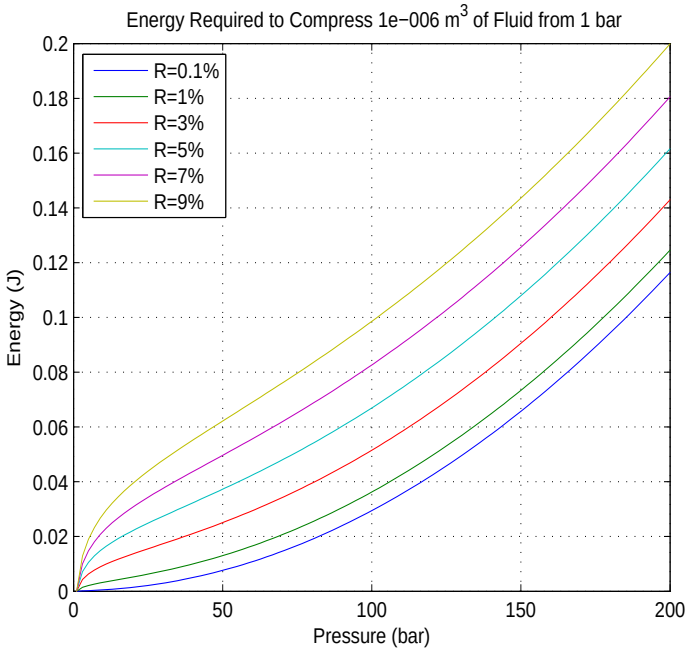

Figure 2.5: Energy required to compress $1cm^3$ of oil from atmosphere to a given pressure for different amounts of air entrained in the oil

loss. If $P_{in} < P_{out} + \Delta P_{check}$, the check valve is closed and all of the flow goes through the PWM valve:

$$P_{in}(t) = \left(\frac{D\omega}{2\pi a(t) K}\right)^2 \qquad Q_{pwm}(t) = \frac{D\omega}{2\pi} \tag{2.32}$$

where K contains the constant coefficients in the orifice equations, which can also be written as $c_d\sqrt{\frac{2}{\rho}}$ for a certain orifice coefficient c_d and oil density, ρ. If the inlet pressure is high enough to open the check valve, the pressure and flow rate are determined by:

$$P_{in}(t) = P_{out} + \Delta P_{check} \qquad Q_{pwm}(t) = K a(t)\sqrt{P_{out} + \Delta P_{check}} \tag{2.33}$$

Note that for effective on/off control, $a(t)$ must be large enough so that, when the on/off valve is fully open, $P_{in} < P_{out}$. Otherwise, the check valve will not close.

To solve for the transition loss, the integrals in Eq. (2.31) are split, corresponding to Eqs. (2.32) and (2.33):

$$E_{trans,close} = \frac{D^3\omega^3}{8\pi^3 K^2}\int_{t_0}^{t_c}\frac{dt}{a(t)^2} + \left(P_{out} + \Delta P_{check}\right)^{3/2} K \int_{t_c}^{t_{close}} a(t)\, dt \tag{2.34}$$

$$E_{trans,open} = \left(P_{out} + \Delta P_{check}\right)^{3/2} K \int_{t_0}^{t_c} a(t)\, dt + \frac{D^3\omega^3}{8\pi^3 K^2}\int_{t_c}^{t_{open}}\frac{dt}{a(t)^2} \tag{2.35}$$

where t_0 is the beginning of each transition and t_c is the time when the check valve opens. The first term of Eq. (2.34) and the second term of Eq. (2.35) represent the transition when the check valve is closed and Q_{pwm} is constant. The other terms represent the cases when the check valve is open and the pressure is constant. The value of t_c can be determined from the fact that at t_c, $a(t_c) = \frac{D\omega}{2\pi K\sqrt{P_{out}+\Delta P_{check}}}$, which follows from Eqs. (2.32) and (2.33).

In the ideal case, $a(t)$ is known, and the integrals in Eqs. (2.34) and (2.35) can be easily solved. For example, if the area follows a quadratic profile, $a(t) = ct^2$, where the constant c is determined from $c = a_{open}/t_{open}^2$, then the energy lost for opening is:

$$E_{trans,open} = \frac{t_{open} D\omega \Delta P_{pwm}^{1/4}}{6\pi}\left[2\left(P_{out} + \Delta P_{check}\right)^{3/4} - \Delta P_{pwm}^{3/4}\right] \tag{2.36}$$

In this quadratic case, which would result from a constant force being applied to the valve spool, it is evident that decreasing the valve transition time and ΔP_{pwm} will reduce the transition loss. Unfortunately, Eqs. (2.34) and (2.35) are not symmetric, and

the solution for the closing case with a quadratic area profile is complicated and does not provide the same design intuition. While Eq. (2.36) only represents a valve with a quadratic opening profile, the conclusion that reducing the transition time and fully open pressure drop reduces the transition loss is applicable to other valve trajectories.

The actual profile for $a(t)$ can be obtained though studying the valve geometry, matching observed pressure profiles, or estimating by applying simplifying assumptions. For comparison with the experiments described in section 2.4, valve geometry and observed profiles were used. The PWM valve that was used had a number of circular orifices with a diameter of $d = 3.5mm$. Using the equation for a partially covered circular port [82], the area was determined to be:

$$a(t) = 4\left[\frac{d^2}{2}\arctan\left(\sqrt{\frac{x(t)}{d-x(t)}}\right) - (d-x(t))\sqrt{x(t)(d-x(t))}\right] \tag{2.37}$$

where $x(t)$ is the effective spool displacement. Equation (2.37) assumes no overlap between the spool and orifice. It was found that a sinusoidal position profile produced a good match with the experimentally measured pressure profiles shown in Fig. 2.6:

$$x(t) = \begin{cases} \frac{d}{4}(1-\cos\left(\frac{2\pi t}{T_{open}}\right) & \text{opening} \\ \frac{d}{4}(\cos\left(\frac{2\pi t}{T_{closed}}+1\right) & \text{closing} \end{cases} \tag{2.38}$$

The opening and closing times, $T_{open} = 20ms$ and $T_{close} = 40ms$, were chosen to obtain the best fit for P_{in} during transition.

The equations that describe the different types of loss in a virtually variable displacement pump can be divided into constant losses, duty ratio dependent losses, and switching frequency dependent losses. This can be useful when designing a system and selecting the PWM frequency. The losses across the PWM and check valves are dependent on the amount of flow through them. Therefore, they are expected to be proportional to duty ratio. The throttling loss during transition and the loss due to compressibility in the inlet volume occur every PWM cycle and can be expected to be proportional to frequency. Combining these losses, the overall average power loss in the system can be written as:

$$Power_{loss} = a_0 + a_1 \cdot s(t) + a_2(P_{out}) \cdot f \tag{2.39}$$

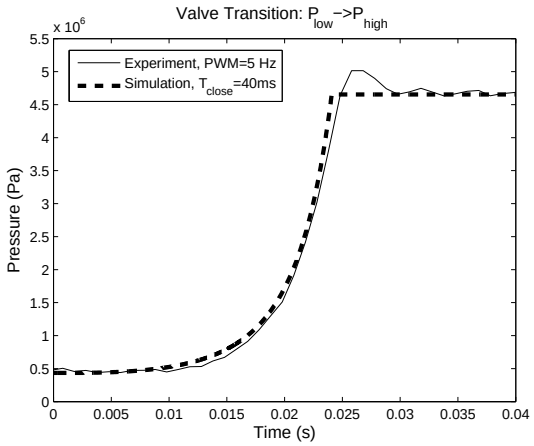

(a) PWM valve closing

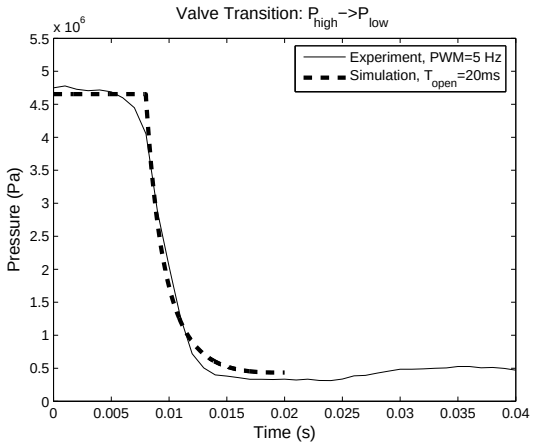

(b) PWM valve opening

Figure 2.6: Inlet pressure profile during PWM valve transition

where a_0, a_1 and a_2 are the constant, duty ratio, and frequency coefficients:

$$a_0 = \Delta P_{pwm} Q_{pump} \tag{2.40}$$

$$a_1 = (\Delta P_{check} - \Delta P_{pwm}) Q_{pump} \tag{2.41}$$

$$a_2(P_{out}) = E_{comp}(P_{out}) + E_{trans}(P_{out}) \tag{2.42}$$

Notice that in an actual system, constant effects such as leakage and fluid friction would also increase a_0, but these are assumed to be small and are not considered in this investigation.

Since the third term in Eq. (2.39) is proportional to frequency, minimizing a_2 is critical for the design of efficient PWM systems as the switching frequency is increased to improve the trade off described in Eq. (2.26). This is accomplished by minimizing the compressibility and transition losses. Equation (2.34) and (2.35) indicate that reducing the loss due to transition is achieved by minimizing the amount of time that the valve spends between the on and off states. However, there can be a trade-off between a short transition time and a large open area, which is desired for reducing ΔP_{pwm}. Knowing the magnitude of the coefficients in Eq. (2.39) is useful in designing the PWM valve and selecting the desired switching frequency.

2.4 Experimental Studies

Experimental measurements of the efficiency of a PWM hydraulic system are presented in this section and compared to a throttling valve system. In addition, the effect of PWM frequency on the output ripple and closed-loop pressure control are demonstrated.

The experimental apparatus used to create the VVDP circuit shown in Fig. 2.1(b) is shown in Fig. 2.7. The fixed displacement gear pump is integrated with the oil reservoir (G) and provides $5.68 l/min$, and components are sized for that flow. The PWM valve (C) is a linear proportional valve, which has a manufacturer specified transition time of $20 ms$ and a full-open pressure drop of $\Delta P_{pwm} = 4.3 bar$ at the full pump flow. The check valve has a fully open pressure drop of $\Delta P_{check} = 0.28 bar$.

A nitrogen-filled diaphragm accumulator (D) has an initial gas volume of $0.16 l$ and a pre-charge pressure of $41 bar$. Since the pump is driven by an AC induction motor, it is assumed that the pump speed is held constant, eliminating the need for a large

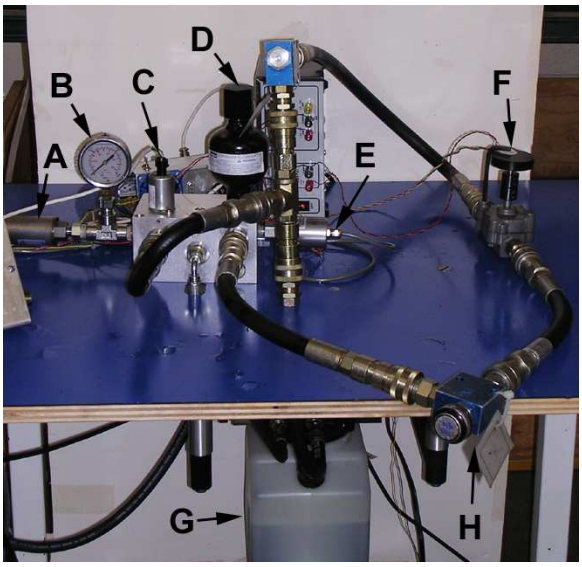

Figure 2.7: Experimental apparatus

inertia. The hydraulic load in the system is an adjustable needle valve (H). The hose and manifold making up the inlet volume is $V_{in} \approx 40cm^3$. The system also has pressure sensors (A, B, and E) on both sides of the check valve, and a flow meter (F) on the output line.

This experimental apparatus was not designed to be optimal, but to demonstrate the system performance with simple, readily available components. The PWM valve has a high full-open pressure drop across it and a long transition time. The inlet volume is also relatively large to facilitate simple connections. Improving these deficiencies would create a system with higher efficiency.

The next section presents experimental results showing details of the system operation over two PWM cycles as well as an experimental relationship between duty ratio and flow rate. Section 2.4.2 shows the effect of PWM frequency and closed-loop control on the system performance. Section 2.4.3 presents results that demonstrate the improvement in efficiency over a throttling valve controlled system, as well as a study of the sources of energy loss in the system.

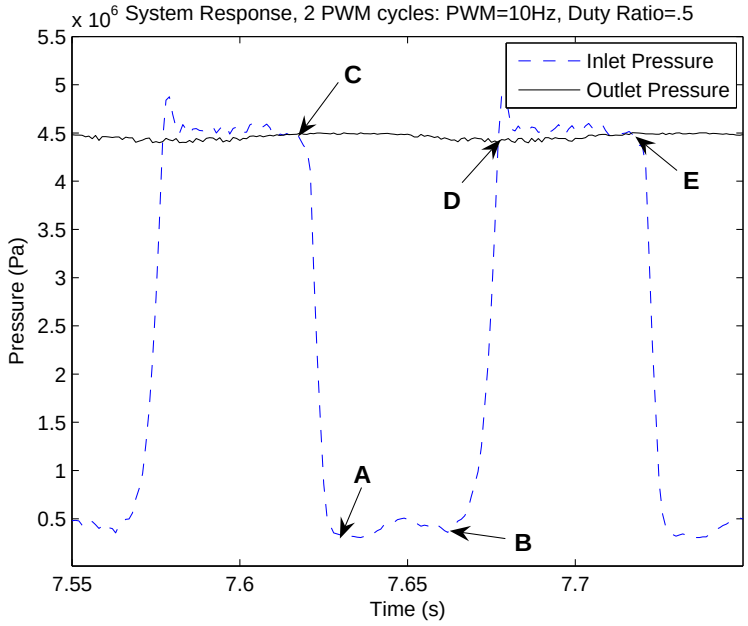

Figure 2.8: Inlet (P_{in}) and outlet (P_{out}) pressures over 2 PWM cycles for a $f = 10Hz$ system with duty ratio $s = 0.5$

2.4.1 System Operation

A close-up view of the inlet and outlet pressures over 2 PWM cycles at a switching frequency of $10Hz$ is shown in Fig. 2.8. Between points A and B, the inlet pressure is low. The only load on the pump during this time is the pressure drop across the fully open PWM valve. Between C and A (opening), and again between B and D (closing), the system is in transition. During these periods, the pressure drop across the valve is high and the full pump flow is going through the partially open PWM valve; this leads to a significant loss of energy.

The averaging effect of the accumulator can be seen on the plot of output pressure: between D and E, the accumulator is charging, and between C and D it is discharging. The difference between C and D (about $1.3bar$) is the output pressure ripple of the system.

The average output flow rate of the system as a function of the duty ratio is shown in Fig. 2.9. This plot confirms Eq. (2.19) by demonstrating a linear relationship between

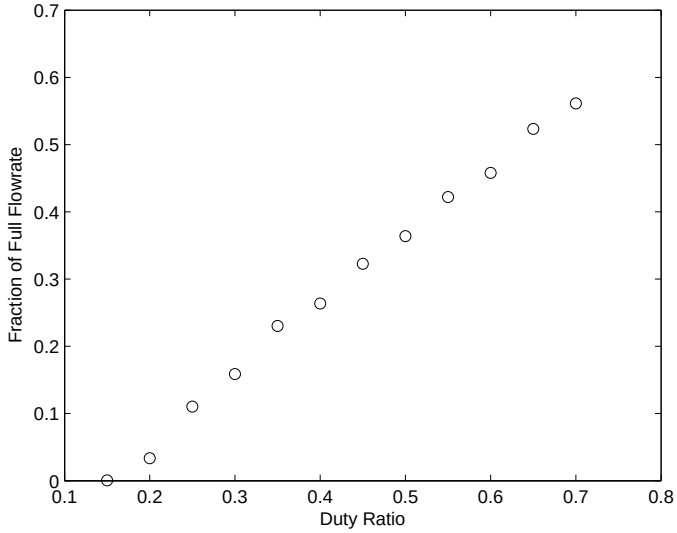

Figure 2.9: Output flow rate as a function of PWM duty ratio ($s(t)$) for a system operating at 5 Hz

the duty ratio and the flow rate. Note that, due to the transition time of the valve, 0 flow occurs at a duty ratio of about 0.15 for $5Hz$ operation. Below this value, there is not enough time to fully close the valve and compress the fluid before the valve is opened again. In this region, no flow is sent across the check valve to the load, but the PWM valve is still partially closed for part of each period, causing throttling. It is important to avoid this inefficient region of operation by taking the transition time of the valves into account when deriving the control signal.

2.4.2 System Dynamics

The open-loop step response of the system was observed by changing the duty ratio to step from 50% to 60% of the full output flow rate.

The experimentally measured response of the system using a PWM frequency of $5Hz$ is shown in Fig. 2.10(a). The average output pressure over each PWM cycle was calculated, and the rise time was defined as the time required for the averaged pressure to go from 10% to 90% of its final value. The pressure settles to its final value in $3.01s$, and the ripple magnitude (peak to peak) is 4.3% of the nominal output pressure.

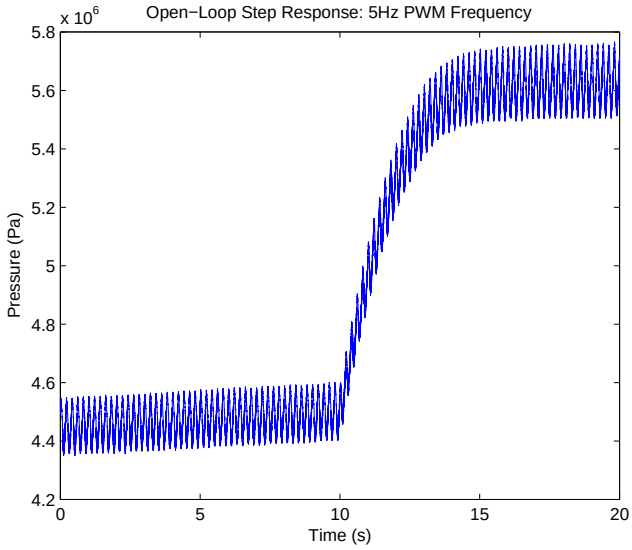

(a) $f = 5Hz$, $t_{rise} = 3.01s$, Ripple=4.3%

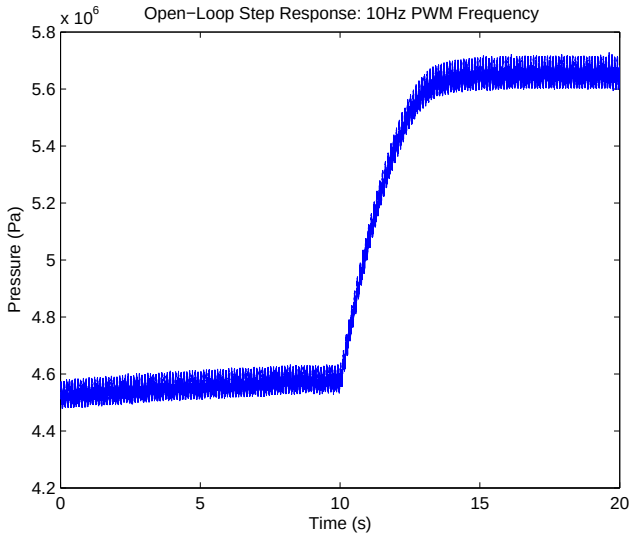

(b) $f = 10Hz$, $t_{rise} = 2.47s$,Ripple=2.0%

Figure 2.10: Experimental open-loop step responses as duty ratio is changed from $s = 0.5$ to $s = 0.6$.

Test	Rise Time (s)	Ripple (%)
Open-loop $5Hz$	3.01	4.3
Open-loop $10Hz$	2.47	2.0
Closed-loop $5Hz$	0.28	4.6

Table 2.1: Summary of rise time and ripple magnitude results for the steps depicted in Figs. 2.10(a), 2.10(b), and 2.11

Equation (2.21) and Fig. 2.4 predict that as PWM frequency is increased, the ripple magnitude is decreased without increasing the rise time. This effect is demonstrated by Fig. 2.10(b), where the step response is shown with a PWM frequency of $10Hz$. This experiment showed a rise time of $2.47s$ and a ripple magnitude of 2.0% of the output pressure. While the rise time decreased slightly, the output ripple was reduced by more than half, as predicted by Eq. (2.21). Clearly, increasing the PWM frequency leads to substantial improvement in the system performance.

Closed-loop control can also improve the trade off between ripple and response time, as explained in Section 2.2.2. An experiment was run to verify this by using a pressure control algorithm with the duty ratio computed from the following equation:

$$s(t) = s^*(P_{des}) + K_{fb}(P_{des} - P_{out}(t)) \tag{2.43}$$

where $s^*(P_{des})$ is the nominal duty ratio for the desired output pressure P_{des}, and $K_{fb} = 0.25$ is the feedback gain. P_{des} was chosen to be a step function with initial and final pressures corresponding to the values in the open-loop step response (Fig. 2.10(a)). Table 2.1 summarizes the step response time and the ripple magnitude for the open-loop and closed-loop steps.

The results of this experiment are shown in Fig. 2.11. The closed-loop step response for a system running at $5Hz$ had a rise time of $0.28s$ and a ripple of 4.6%. The rise time decreased by over 90% compared with the open-loop system illustrated in Fig. 2.10(a) with little increase in the ripple magnitude.

To demonstrate the ability of the system to track a pressure reference, a sinusoidal function was added to the nominal pressure. Fig. 2.12 shows the response of the system tracking a $0.5Hz$ reference pressure trajectory with little attenuation or phase shift. As the frequency of the reference was increased, the control signal began to saturate. The

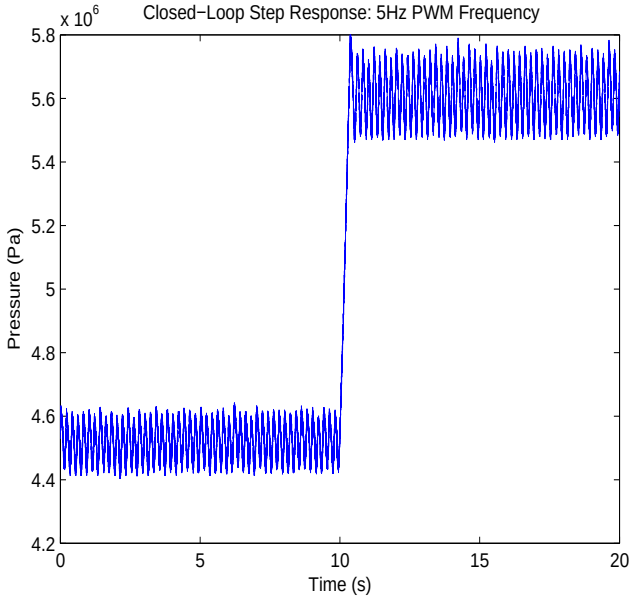

Figure 2.11: Closed-loop step response: $P_{des} = 4.52 \times 10^6 Pa \rightarrow 5.65 \times 10^6 Pa$, $f = 5Hz$, $t_{rise} = 0.28s$, Ripple=4.6%

saturation level is determined by the accumulator dynamics, and the capabilities of the pump and the load to fill and to discharge it.

While Eq. (2.43) implements pressure control of the system, feedback from a flow meter on the load line can easily be used to create a flow-controlled system.

2.4.3 Efficiency

The efficiency of the hydraulic system is defined as the power output to the load ($\bar{Q}_{out}\bar{P}_{out}$) divided by the power into the system from the pump ($\bar{Q}_{pump}\bar{P}_{in}$). The efficiencies stated here do not include the pump or driving motor. Note that the measured pressures and flow rates are averaged over 5 seconds to remove noise and any effect from the pressure and flow ripple from the measurements. Power and efficiency were calculated for various duty ratios and PWM frequencies of 1, 2.5, 5, and 10 Hz.

The system power was also measured with the system configured for throttling valve control. For this experiment, the PWM valve in Fig. 2.7 was instead utilized as a proportional valve in a bleed-off configuration.

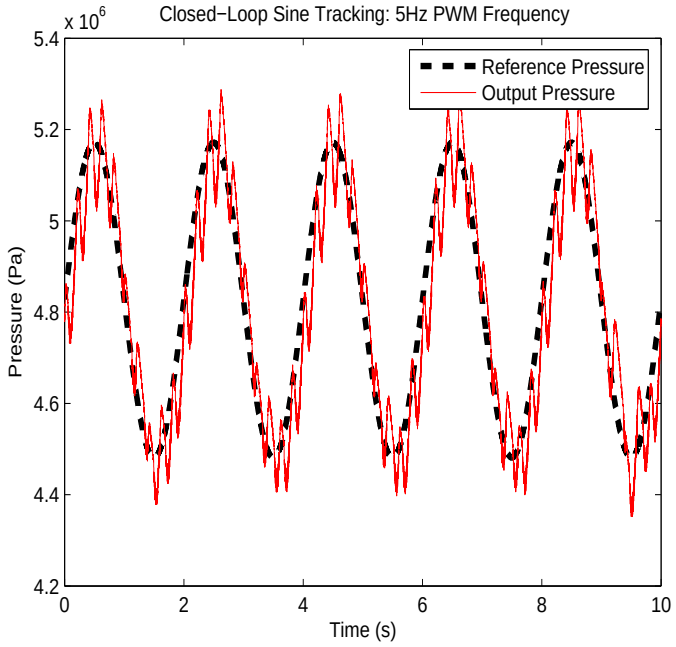

Figure 2.12: Closed-loop reference tracking: $f = 5Hz$

Figure 2.13 shows the results, with the power lost shown in Fig. 2.13(a), and the efficiency shown in Fig. 2.13(b). The PWM system is equivalent to the throttling valve system at high duty ratios, and significantly more efficient over the remaining range of operation. As the PWM frequency increases, the efficiency of the system decreases. For both the PWM and proportionally controlled valve, the efficiency decreases to zero at low duty ratios due to the fact that the power lost remains fairly constant with duty ratio while the power out to the load decreases. These results demonstrate the potential of PWM controlled systems in creating efficient hydraulic circuits to replace throttling valves.

The power lost in the PWM system is shown in Fig. 2.14 fitted to a plane in frequency and duty ratio. The plane is also rotated to show the quality of fit. The power loss and efficiency data measurements were taken from a system running at $4.8MPa$. Table 2.2 lists the values of the coefficients a_0, a_1 and a_2, as defined in Eq. (2.39), obtained by fitting this surface, as well as the coefficients determined from the predictive equations described in section 2.3.

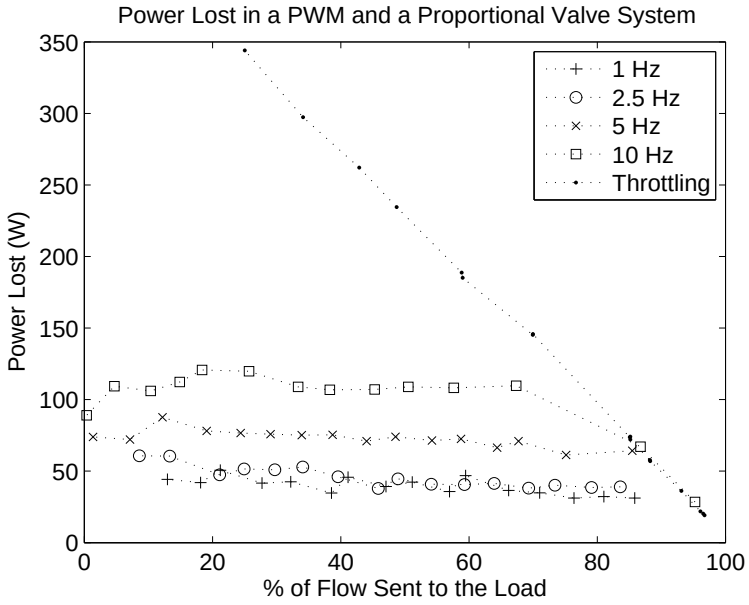

(a) Power loss

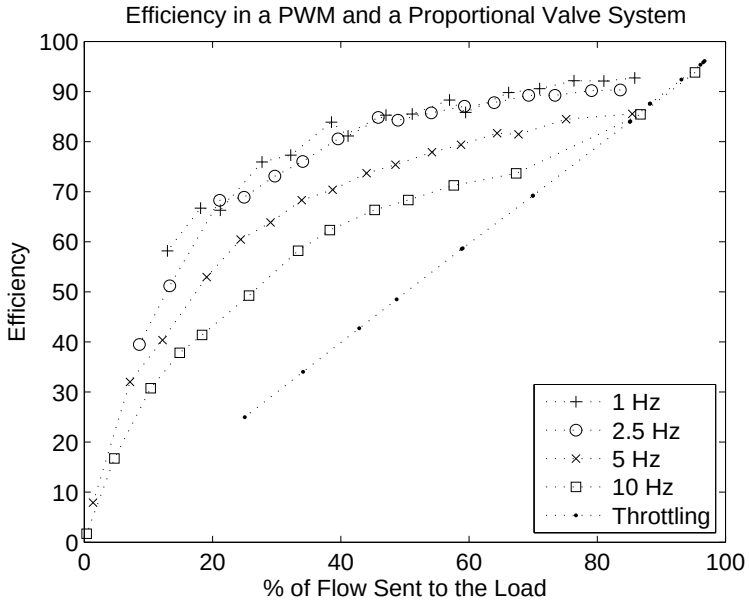

(b) Efficiency

Figure 2.13: Power loss and efficiency of a PWM system compared to a throttling valve controlled system at various PWM frequencies

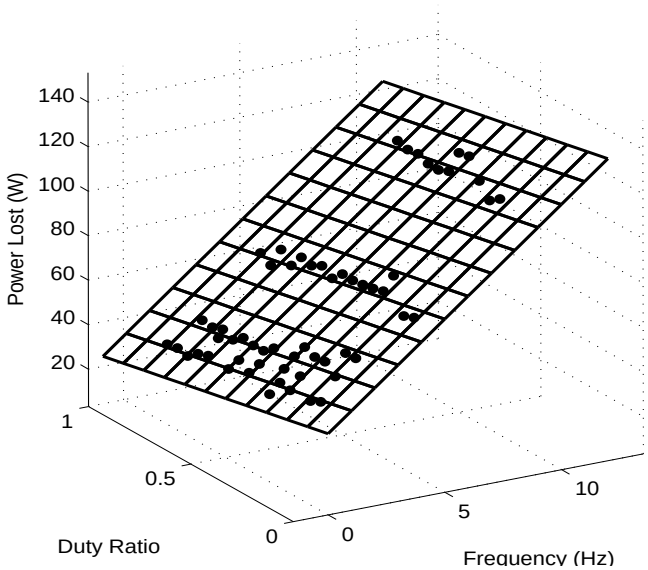

(a) Power lost surface

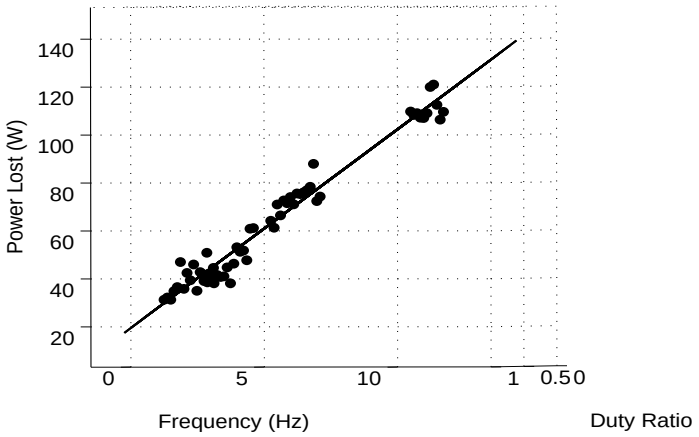

(b) Rotated power lost surface

Figure 2.14: Surface representing the power lost as a function of frequency and duty ratio for a system operating at $4.8MPa$

Coefficient	Predicted	Experiment
$a_0(W)$	41.1	39.7
$a_1(W)$	-38.5	-20.1
$a_2(W/Hz)$	6.5	8.3

Table 2.2: Coefficient values in the equation: $Power_{loss} = a_0 + a_1 \cdot s(t) + a_2(P_{out}) \cdot f$ from analysis (Eq. (2.40)-(2.42)), simulation and experiment.

2.5 Discussion

The study of the system dynamics in sections 2.2 and 2.4.2 described the trade off that exists between the ripple size and the response time. It was also demonstrated that this trade off can be improved by increasing the PWM frequency and adding feedback control. However, Eq. (2.39) shows that increasing the PWM frequency also increases the power loss. Thus, an additional trade off exists between the desired performance and the system efficiency.

The power loss results listed in the Predicted column of Table 2.2 were derived from the equations listed in section 2.3. In order to predict the frequency dependent loss coefficient, a_2, a value for the amount of entrained air in the oil must be used. The predicted value for a_2 given in Table 2.2 assumed 1.0% air in the oil, but in reality, this value is difficult to determine precisely. However, by combining the model equations for the transition loss and the experimental results, an estimate of the actual air entrainment can be obtained. Using Eqs. (2.31) through (2.38), the predicted energy loss due to the valve transition, E_{trans}, is $5.95J$. From table 2.2, a_2 was determined experimentally to be $8.3J$. Using the computed value of E_{trans}, Eq. (2.42) can then be applied to determine a loss due to fluid compressibility of $2.35J$. Solving Eq. (2.30) and Eq. (2.3) by iteration reveals that this energy loss corresponds to $R = 0.085$ air entrainment for the system load pressure, which was about $50bar$. While the exact ratio of air to oil in the actual system is not known, this estimated value seems high, but possible. In addition to a high degree of air entrainment, alternative explanations for this value for a_2 are a larger than expected inlet volume, more loss in transition throttling due to inaccuracy in modeling the transition profile, uncertainty in the oil parameters (such as β_{oil}), or unmodeled losses such as the flexibility of the hoses, which can cause the

effective compressibility of the system to increase. These results indicate that, in this system, throttling during the valve transition is responsible for the majority of the frequency-dependent losses.

The constant loss coefficient, a_0, was found to be nearly identical between the model and the experiment, which validates the assumption that losses due to fluid friction and leakage were negligible.

The duty ratio loss coefficient calculated using Eq. (2.41) is $a_1 = -38.5W$, whereas it was found to be $a_1 = -20.1W$ experimentally. From Eq. (2.41), a calculated result that is more negative than the experimental result suggests that either ΔP_{PWM} is too high or ΔP_{check} is too low in the model.

An attempt was made to explain the source of the discrepancy between the predicted and experimental values for a_1 by increasing the pressure drop across the check valve in simulation. Increasing ΔP_{check} by $2.07bar$ reproduces the experimentally obtained a_1 value. However, while some variation in the experimentally measured pressure drop across the check valve was observed, this additional pressure drop was 50% higher than the highest measured value. The discrepancy may also be attributable to inefficiencies in the accumulator, whether through fluid throttling, heat loss, or bladder hysteresis. This could potentially be due to throttling of the fluid entering and exiting the accumulator, which is diffitcult to model without knowing the details of the accumulator geometry.

This analysis can be used to determine the relative magnitude of the different sources of energy loss. Using the coefficients from Table 2.2, the loss is clearly dominated by the constant and duty ratio dependent losses ($a_0 + a_1 \cdot s$) at low PWM frequencies. This is equivalent to saying that the loss is dominated by the pressure drop across the PWM and check valves. However, the frequency dependent transition and compressibility losses quickly become the primary sources of power loss as the frequency is increased. This can be seen in Fig. 2.14 where it is clear that the slope of the surface in the direction of frequency is much greater than the slope in the direction of duty ratio. For this system, above $5Hz$, the majority of the losses can be attributed to frequency dependent losses associated with compressibility and transition throttling. This analysis demonstrates the need to minimize the frequency dependent losses, particularly the transition throttling losses, as the PWM frequency is increased.

While this system operated at a relatively low pressure of $4.8MPa$, it can easily be

scaled up to higher pressures. Typical hydraulic components are designed to operate at $25MPa$ or higher, so finding a pump, PWM valve, check valve, and accumulator that can withstand higher pressures should not be a problem. However, some types of accumulators, such as the diaphragm style used in these experiments are not intended to operate over a wide range of pressures with a single precharge pressure. However, piston type accumulators can be used if higher pressure operation is required.

While several simplifying assumptions are still included in the system model, for the frequency range studied here, the model appears to reasonably agree with the experimental data, indicating that the significant sources of energy loss have been captured in the proposed model.

The VVDP is only one of several on/off valve controlled architectures that can be used in hydraulic systems. One motivation for studying the VVDP is that it makes use of a constant flow source (the fixed-displacement pump), which has some benefit for certain high-speed valve designs that will be studied in chapter 4. However, the VVDP does have competition from conventional variable displacement pumps, which provide similar or better efficiency benefits to a VVDP without the large flow ripple, although the VVDP may have some benefits in regards to cost and controllability. In addition, the VVDP approach can be extended to a multi-circuit system that apportions flow from a single fixed-displacement pump to multiple hydraulic consumers in sequence [31]. This extension can have significant efficiency benefits when compared to a traditional variable displacement pump circuit.

Another on/off valve architecture is an inversion of the VVDP, which uses an on/off valve to apportion flow from a constant pressure source to an actuator. This can be called a Virtually Variable Displacement Motor or Actuator, an example of which is shown in Fig. 2.15. For this circuit, conventional analogs are less common (especially for linear actuators); traditional hydraulic systems typically use throttling valves to accomplish this task. This indicates a potential for significant efficiency improvements over conventional systems. However, this approach does create some challenges. In this configuration, the output power smoothing element is the inertia of the motor/actuator rather than an accumulator, which can often vary in size and speed depending on the load. The actuator typically interacts with the environment, and with only the inertia to smooth the output, pressure pulses could present a problem in some applications.

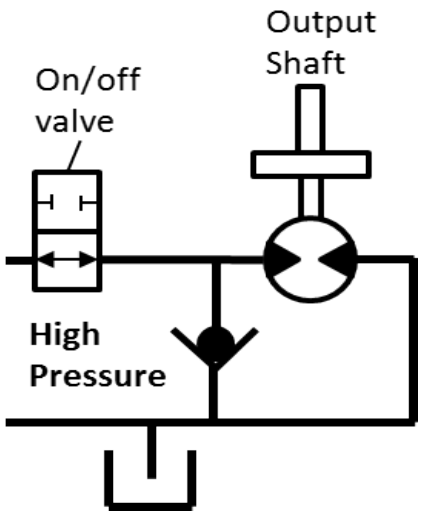

Figure 2.15: Hydraulic circuit for a Virtually Variable Displacement Motor (VVDM)

In addition, when an oil volume is compressed by connecting it to a constant pressure source instead of a constant flow source, there can be significantly higher compressibility losses; a phenomenon that is described in section 5.2.4.

Finally, on/off valves can be combined with an inertia and an accumulator to create a variable transformer [13, 7, 9, 10, 14, 16]. This combines characteristics of the VVDP and VVDM to create a system that transforms hydraulic power between power and flow. While there are hydraulic transformers that do not use on/off valves, they are not common in the hydraulics industry, and are a current area of research. Figure 2.16 shows the hydraulic circuits for a hydraulic boost converter, which can be used to increase the pressure while reducing the flow, and a hydraulic buck converter, which reduces the pressure while increasing the output flow.

The Virtually Variable Displacement Pump circuit presented in this chapter has a clear efficiency benefit over a fixed-displacement pump/proportional valve combination. With the addition of an accumulator and a check valve, a proportional bleed-off valve circuit can be converted to a VVDP. The utility of making this conversion can be judged by the dynamic requirements of the hydraulic system. The analysis done in this chapter shows a clear trade off between the responsiveness of the system and the output flow ripple. Increasing the PWM frequency improves the dynamic trade off, but has a

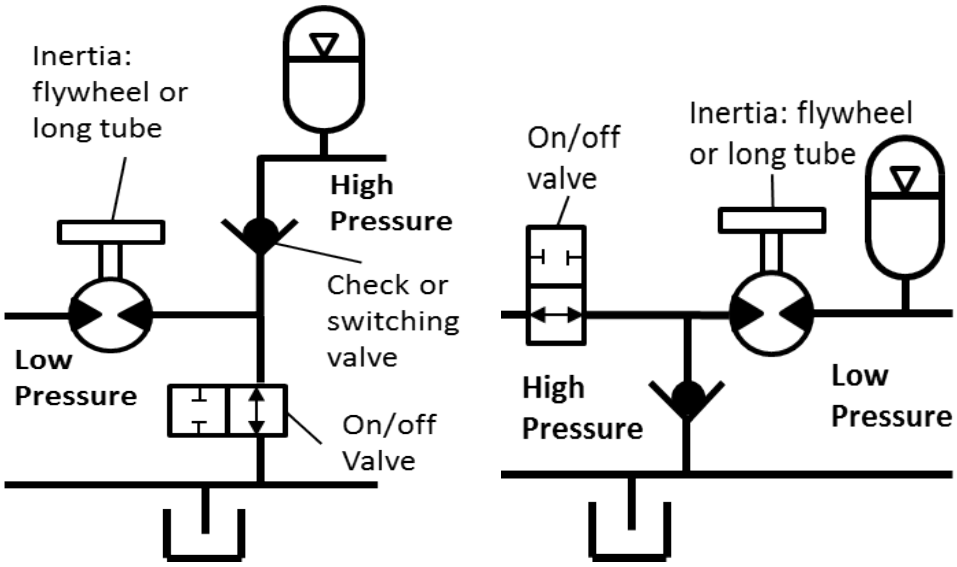

(a) Boost converter (b) Buck converter

Figure 2.16: Hydraulic transformer circuits using on/off valves

detrimental effect on the efficiency due to the compressibility and transition throttling losses. In the next chapter, a method is described that can reduce the transition losses, enabling higher switching frequencies and thus improved system dynamics.

Chapter 3

Softswitching Approach for Reducing Transition Losses

Control using high-speed on/off valves was proposed in chapter 2 as a way to significantly improve the efficiency of hydraulic systems over the traditional method of metering valve control. Control using on/off valves saves energy by eliminating high pressure throttling of hydraulic oil through metering or relief valves, since they are usually either fully open or fully closed.

However, while on/off control has the potential for significant energy savings over metering valve control, several effects contribute to inefficiencies in a pulse-width-modulation (PWM) controlled hydraulic system. Cao et. al. [7] suggest that energy can be lost in an on/off valve system as a result of valve transition times, fluid compressibility, pressure drops across the on/off valve(s), hysteresis in the accumulator bladder, fluid friction, and leakage. In chapter 2 and [50], a number of these energy losses were quantified and it was found that, for the systems studied, the valve transition time was the most significant source of energy loss, equating to roughly 60% of the total loss. The other significant losses in the system are due to compressibility (20%), full-open throttling (19%), and leakage (1%).

The valve transition loss arises from the fact that, as the on/off valve transitions between its two states, the open orifice area is decreased while a fixed flow rate of oil is flowing though it. This causes a high pressure drop across the valve and a significant

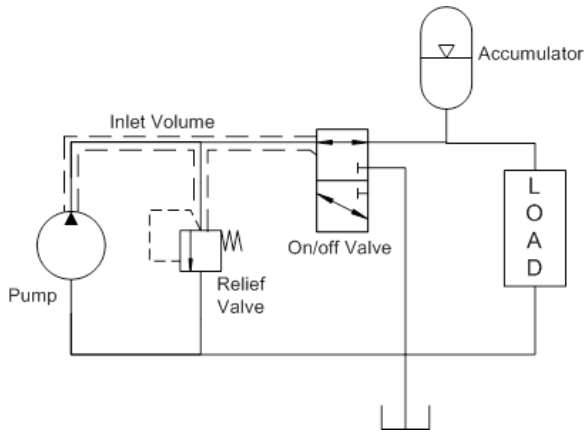

Figure 3.1: Virtual variable displacement pump using a 3-way on/off valve

amount of energy loss in throttling.

A current focus of development in on/off controlled systems is to develop valves that can achieve high PWM frequencies, which are desirable for minimizing the system ripple and improving control bandwidth, as described in chapter 2. Fast valves can also reduce the transition loss by reducing the amount of time spent throttling the flow. However, in conventional spool or poppet valves, the power required to accelerate and decelerate the valve spool increases proportionally to the switching speed cubed. Thus any reduction in transition losses by increasing the valve speed may be lost to increased valve actuation power.

An alternative valve design that avoids the requirement for a large amount of actuation power at high speeds is the unidirectional rotary on/off valve [50]. In this design, the valve spool rotates at a constant speed, and thus no power is required for spool acceleration. In this design, the transition time decreases proportionally to the PWM period. The details of this design are described in chapter 4.

In this chapter, an approach is proposed to significantly reduce the throttling loss during valve transition by providing a temporary alternate path for the fluid when the valve area is small.[1] This soft switching approach is similar to a technique in electronic switch-mode converters that uses small capacitors to temporarily absorb current when the transistors change state [83]. In an electronic system, soft switching is achieved by

[1] Some of the material in this chapter was originally published by ASME in [29].

sizing components to induce large current ripples, which create temporary periods of reverse current. This is impractical in a hydraulic system. In this chapter, a method is proposed in which an actively locked soft switch chamber is used in place of the traditional passive elements.

The reduction in transition loss can facilitate effective on/off control with slower valves which would normally have limited utility due to high transition losses. Since increasing the valve speed typically involves increasing the actuation power or decreasing the full open area, enabling efficient use of slower valves can significantly reduce the energy consumption in an on/off controlled system.

Section 3.1 outlines the soft switching concept, and section 3.2 describes the model equations used to describe the system. Section 3.3 presents simulation results, and section 3.4 contains a discussion of the results.

3.1 Soft Switching Concept

While the soft switching concept can be applied to different system architectures, in this chapter it is described in conjunction with the configuration depicted in Fig. 3.1. This configuration uses a 3-way on/off valve to vary the flow used from a fixed displacement pump. When considering the operation of the three-way valve with soft switching, it is easier to imagine the three-way valve as two mechanically coupled, two-way valves as shown in Fig. 3.2.

In a typical PWM cycle, beginning with the load valve fully open and the tank valve fully closed, the valve sequence is as follows: the load valve will close during time interval t_1, followed by the tank valve opening during t_2. After some dwell time specified by the duty ratio, the tank valve will close during t_3, which is followed by the load valve opening again over interval t_4. Thus, in each PWM cycle there are 4 transition events during which throttling can occur. Figure 3.3 depicts area profiles for the two valves following linear area trajectories, which is the characteristic of a rotary on/off valve [50].

In the simplest circuit, which uses a relief valve and is shown in Fig. 3.1, throttling will occur during each of these transition events. Figure 3.4 shows the pressure in the inlet volume for this circuit. Notice that significant pressure spikes will occur between t_1 and t_2, and again between t_3 and t_4 when both valves are closed. These pressure

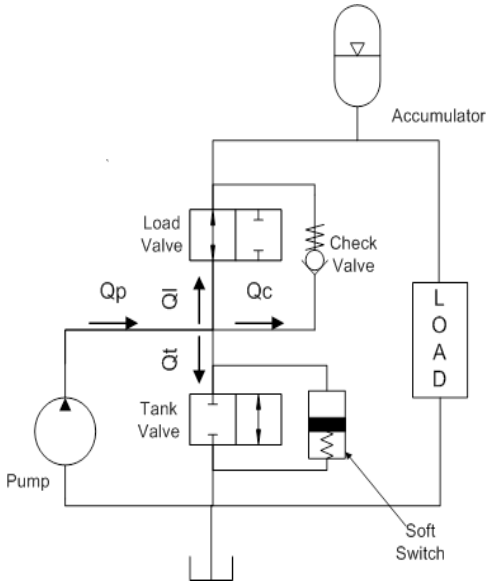

Figure 3.2: 3-way circuit with split tank and load valves, check valve, and soft switch

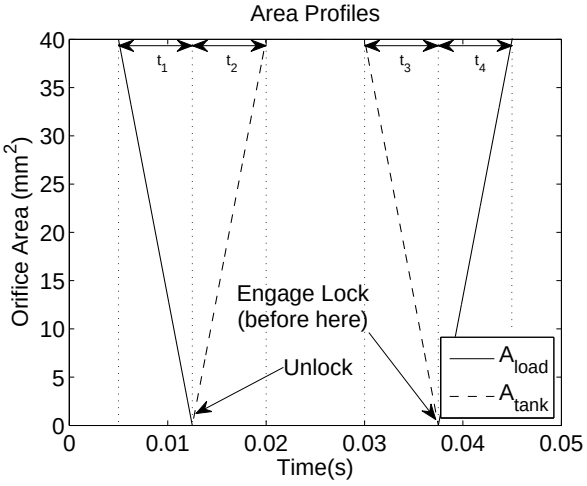

Figure 3.3: Area Profiles for 1 PWM Period

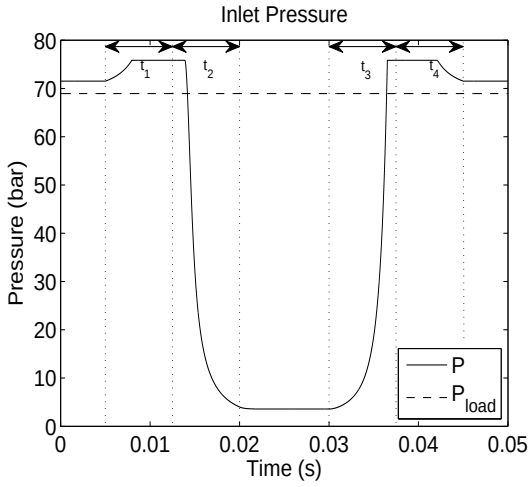

Figure 3.4: Inlet pressure profile for a 3-way circuit with a relief valve

spikes will be limited only by the compressibility of the oil in the inlet volume, and the pressure setting of the relief valve.

The soft switching approach can be applied to the load valve by simply adding a check valve in parallel instead of the relief valve, as shown in Fig. 3.2. With this addition, the transitions of the load valve will be eliminated by allowing oil to flow through the check valve rather than the partially open load valve. The pressure profile for a circuit with a relief valve in parallel with the load valve looks similar to the relief case in Fig. 3.4. However, note that in Fig. 3.4, the relief pressure is set to be just above the load pressure. This is possible when the load is at a constant pressure, but when the load pressure varies, the relief pressure must be set above the highest expected load. This could result in much higher pressure spikes during transition. The low relief setting in this example is to provide as conservative improvement results as possible. In addition, in the relief case, the oil flowing across the relief valve is lost to tank, whereas in the check valve case, the flow is sent to the load to do useful work.

In some cases, the load valve could be completely replaced by the check valve. However, the 3-way valve can be useful in some cases, such as in a valve that captures fluid momentum for actuation power [50]. Other on/off configurations, such as the multi-circuit approach described in [31], cannot use check valves to reduce the transition loss, and require more complicated techniques.

The addition of a check valve dramatically reduces the energy loss due to throttling. However, a significant loss still exists as a result of the two remaining transitions (t_2 and t_3). To eliminate these transition losses, the soft switch chamber shown in Fig. 3.5 can be used as a temporary storage mechanism.

The soft switch consists of a small chamber with a piston, a spring and an externally actuated locking mechanism. The locking mechanism holds the piston near the middle of the chamber. Once the tank valve begins to open, the lock is released, and the high pressure fluid fills the chamber. Thus, the fluid is able to flow into the soft switch instead of being forced through the closing valve. Once the tank valve is fully open, the spring in the soft switch chamber will force the piston back up to the top of the chamber. Then, once the tank valve begins to close and the pressure rises above the spring pressure, fluid will once again flow into the soft switch. Once the piston hits the lock mechanism, the tank valve should be mostly closed, and the pressure will quickly rise and open the check valve. Finally, once the load valve is fully open, the check valve will close and the fluid will flow through the full open load valve.

3.2 Modeling

To study the operation of the soft switch, a model of the pressure dynamics and soft switch chamber is developed. In defining this model it is assumed that the output pressure is constant over the switching period, there is no leakage, and fluid friction is negligible. Fluid inertia is also neglected due to the fact that it is highly dependent on the shape of the passages in the valve.

The area profiles for the transitioning valve were chosen to be linear as shown in Fig. 3.3, which matches the profile of a rotary on/off valve with rhombus shaped orifices in the bore (see section 7.2. The soft switching principle applies to any other type of valve trajectory, provided that the components are sized properly.

The pressure in the inlet volume of the circuit, which is depicted in Fig. 3.1, is given by the following equation:

$$\dot{P} = \frac{\beta(P)}{V_{in}} \left(Q_p - Q_t - Q_l - Q_c - A_s \dot{x}\right) \tag{3.1}$$

where V_{in} is the inlet volume, Q_p is the constant flow rate from the pump, Q_t, Q_l, Q_c are the flow rates through the tank, load, and check valves, A_s is the area of the soft

switch piston, and x is the position of the soft switch piston. The bulk modulus of the hydraulic oil, $\beta(P)$, is modeled using the pressure dependent equation, (2.5).

Flow rates through the check, tank and load valves are determined by the orifice equation:

$$Q_c = c_d a_c(t)\sqrt{\frac{2\left|P - P_{load}\right|}{\rho}}sign\left(P - P_{load}\right) \tag{3.2}$$

$$Q_t = c_d a_t(t)\sqrt{\frac{2\left|P - P_{atm}\right|}{\rho}}sign\left(P - P_{atm}\right) \tag{3.3}$$

$$Q_l = c_d a_l(t)\sqrt{\frac{2\left|P - P_{load}\right|}{\rho}}sign\left(P - P_{load}\right) \tag{3.4}$$

where c_d is the orifice coefficient, $a_c(t)$, $a_t(t)$, and $a_l(t)$ are the open areas for the check, tank, and load valves, and ρ is the density of the hydraulic oil. Note that the pressure drop across the fully open valve with full flow going through it is:

$$\Delta P_{open} = \frac{Q_p^2 \rho}{2a_0^2 c_d^2} \tag{3.5}$$

where a_0 is the full open area.

The check valve is modeled using the following equation:

$$\ddot{x}_c = \frac{1}{m_c}\left(\left(P - P_{load}\right)\pi\frac{d_c^2}{4} - k_c x_c - b_c \dot{x}_c - F_{c,preload}\right) \tag{3.6}$$

where x_c is the check valve position, m_c is its mass, b_c is the viscous damping coefficient, d_c is the diameter of the check ball, k_c is the spring stiffness, and $F_{c,preload}$ is the spring preload which is designed to be larger than the full open pressure drop. The open area of the check valve is:

$$a_c(t) = \pi d_c x_c \tag{3.7}$$

The soft switch chamber shown in Fig. 3.5 is modeled as a mass-spring-damper system with a pressure driving force:

$$\ddot{x} = \frac{1}{m_s}\left(PA_s - k_s x - F_{s,preload} - b_s \dot{x}\right) \tag{3.8}$$

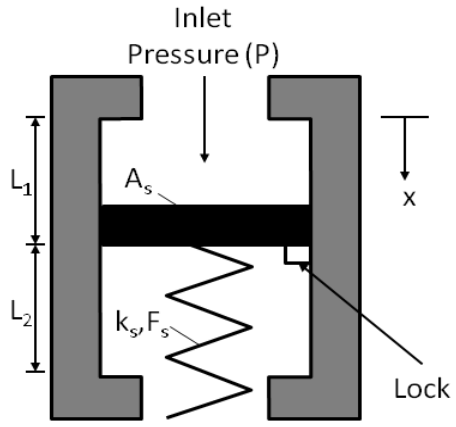

Figure 3.5: Diagram of the soft switch chamber

where m_s is the mass of the soft switch piston, b_s is the viscous damping coefficient, k_s is the spring stiffness, and $F_{s,preload}$ represents the spring preload.

In this analysis, the piston lock is treated as an instantaneously acting mechanism that can be arbitrarily disengaged. There are several approaches for developing an actual locking mechanism, and a discussion of these can be found in section 3.4. The overall length of the soft switch chamber is split into two sections, L_1 and L_2. When the piston lock is active, the piston is only allowed to travel between 0 and L_1. Once the lock is disengaged, the piston can travel throughout the entire chamber.

3.3 Simulations

Using the equations derived in Sec. 3.2, simulations of the three-way circuit with and without soft switching were conducted. The valve parameters were selected to approximate a three-way rotary on/off valve with a PWM frequency of $20Hz$. The time for each transition was specified to be $7.5ms$. The system was simulated with a flow rate of $37.9l/min$ and a load pressure of $69bar$. The fully open area of the valve was $40mm^2$. The inlet volume of the system was $30cm^3$, and the oil was assumed to have 3% entrained air. The check valve spring was set to have a $30N$ preload and a spring rate of $2N/mm$. The diameter of the pressure area on the check valve was $6.65mm$, the

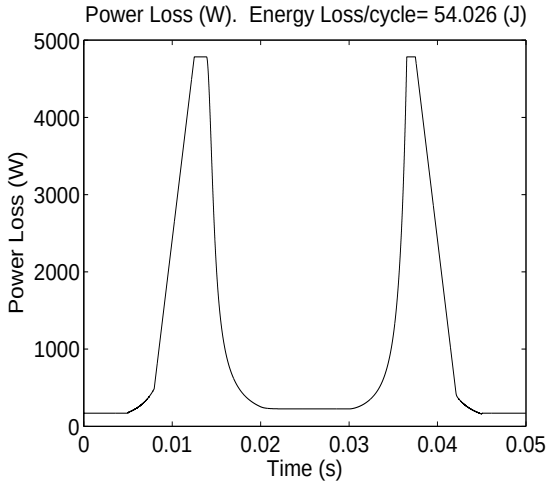

Figure 3.6: Power loss over 1 PWM period for a system with a relief valve

damping coefficient was $15Ns/m$, and the mass was $1.9g$. The system without a check valve or a soft switch chamber was simulated with a relief pressure $8.3bar$ higher than the load pressure. In an actual system, this would likely be set much higher, depending on the required variation in the load pressure. As the relief pressure is increased, the losses in the baseline system also increase.

Note that the fixed load pressure condition is not a requirement of the approach; soft switching works for dynamic loads as well as fixed. However, since most on/off systems require an accumulator to smooth pressure ripples, a load that is relatively constant over one PWM period is a typical load condition for moderate frequencies.

The pressure profile at 50% duty ratio for the relief valve system is shown in Fig. 3.4.

The power loss in the relief valve case is shown in Fig. 3.6, with a total loss of $54J$ for one cycle. In this figure, the large spikes in power loss due to the valve transitions are evident. Notice that there is a baseline loss of about $226W$, which is due to the full open pressure drop. This accounts for about $11.3J$ of energy lost each cycle and cannot be addressed by soft switching.

By adding a check valve across the load valve, the power loss can be dramatically reduced. Figure 3.7 shows the power loss in the check valve system, with a total loss of $25J$ for one cycle. In this figure, the two large loss spikes have been reduced by about

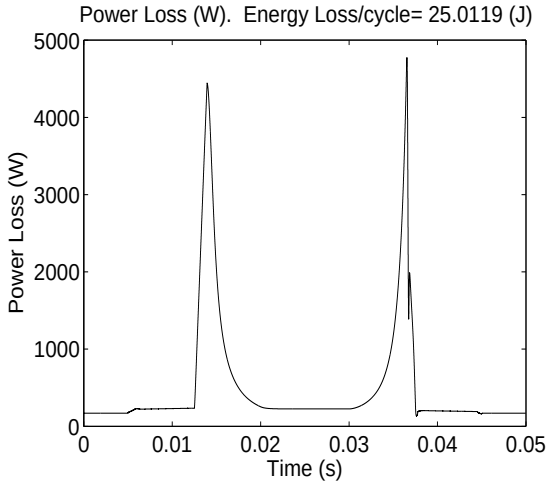

Figure 3.7: Power loss over 1 PWM period for a system with a check valve only

half as the check valve eliminates losses in 2 of the 4 transition events.

To further improve the system efficiency, a soft switching chamber was added with a piston area of $132mm^2$ and a piston mass of $2.6g$. The first segment of the chamber had a length of $L_1 = 6mm$, and the second had a length of $L_2 = 12mm$. The spring preload was set to be $110N$, and the spring rate was $1.5N/mm$. The damping of the piston was set at $8Ns/m$. The pressure profile for a system using these parameters is shown in Fig. 3.8.

Notice that the gradual transitions have been eliminated by the soft switch. The full open pressure between the two transitions is higher than in the case without soft switching for most of the low pressure period. This is due to the emptying and filling of the soft switch chamber, which maintains the higher pressure resulting from the spring force. Once the soft switch chamber is empty, the pressure drops down to ΔP_{open} before rising again as the chamber fills.

The flow rates through the three different valves are shown in Fig. 3.9, which demonstrates the operating principle of the soft switch concept. Initially, all of the flow is passing through the load valve. Then, as the load valve closes, flow transitions to the check valve. Then, from $0.0125s$ to $0.0162s$, the net flow through the three valves is less than the pump flow rate as the soft switch chamber fills and the tank valve opens. From $0.0162s$ to $0.0275s$, the flow is higher than the full pump flow as the soft switch

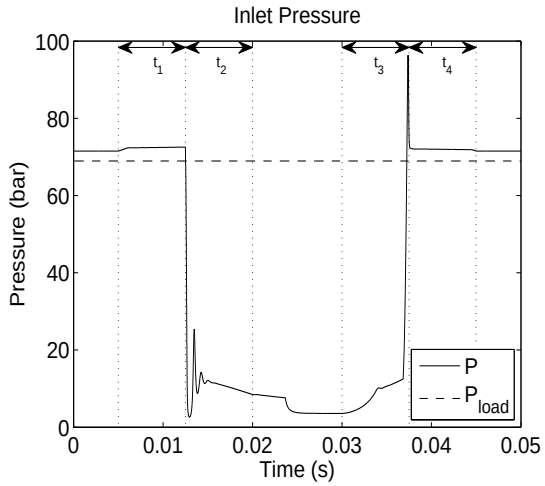

Figure 3.8: Pressure profile for a system with soft switching

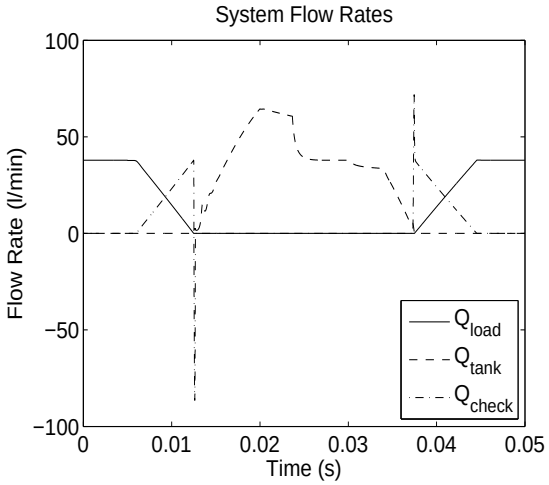

Figure 3.9: Flow rates in a soft switching system

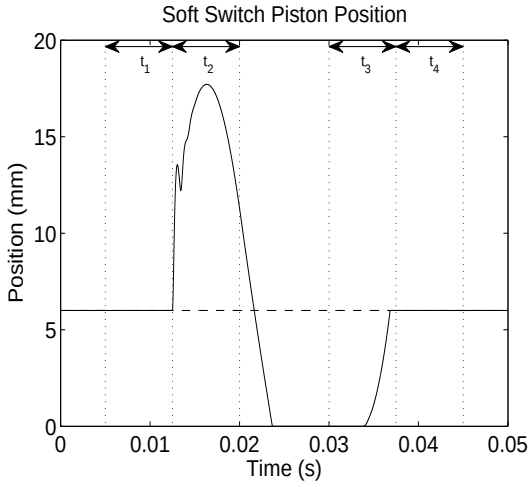

Figure 3.10: Position of the soft switch piston over 1 PWM period

chamber empties. Thus, the soft switch chamber temporarily stores fluid while the valve is transitioning and then releases it once the valves are fully open and the pressure drop is low.

The position of the soft switch piston is shown in Fig. 3.10. At the start of the simulation, the piston is pressed against the locking mechanism. When the lock is released, the piston leaves its initial position at l_1, and its displacement increases while the inlet pressure is higher than the spring pressure. Once the tank valve opens enough for the pressure to drop below the spring pressure, the soft switch chamber empties. The spring force must be high enough for the piston to return past l_1 before the tank valve begins to close again. Thus the system components must be sized to ensure that the soft switch will operate properly over the desired range of operation. Another constraint on the system is that the first half of the soft switch must fill and the inlet pressure must rise above load pressure before the load valve begins to open. Otherwise, high pressure fluid will flow back from the load, resulting in higher losses. This limits the length of l_1.

The power loss over one cycle in the soft switching system is shown in Fig. 3.11. From this figure it is clear that the majority of the large transition spikes have been eliminated by the soft switch. The remnant of the first spike is due to the fact that the soft switch piston requires some time and energy to move. The second remnant is due

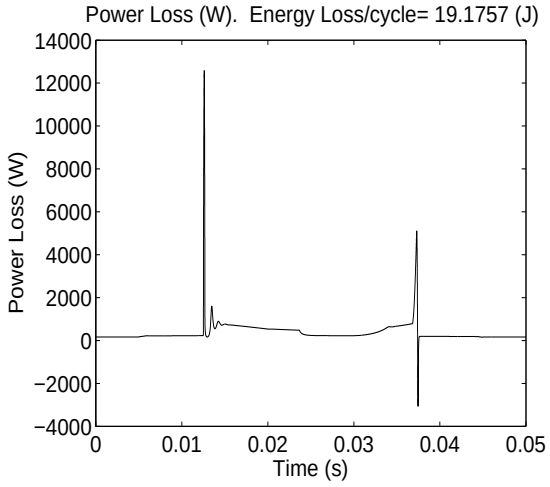

Figure 3.11: Power loss over 1 PWM period for a system with soft switching

System	Total Loss/cycle (J)
Relief	54.0
Check	25.0
Check and Soft Switch	19.2

Table 3.1: Loss per cycle for system with and without soft switching

to fluid compressibility and the dynamics of the check valve. The power loss between the two spikes is higher than in the system without soft switching due to the emptying soft switch chamber. However, it is evident from the fact that the total energy lost in one cycle is reduced to $19.2J$ that this additional loss is less than the energy that has been saved during transition, as shown in Table 3.1.

3.4 Discussion

Table 3.1 shows that adding a check valve in parallel with the load valve reduced the overall system loss by about 53% from a system using only a relief valve to limit pressure spikes. The addition of a soft switch chamber eliminated an additional 11% of the original losses, for a 64% reduction in the overall loss by applying the soft switching concept. Notice that the relief valve was set only slightly above the load pressure. In

many systems, the relief pressure must be set significantly higher to allow for varying load pressures. This would increase the losses in the relief valve system, making the soft switching approach even more beneficial.

The full open loss for the simulated system was about $11.3J$, which cannot be reduced by the soft switching approach. Thus, looking only at transition and compressibility losses, the relief, check and soft switch systems lose $42.7J$, $13.7J$, and $7.9J$ respectively. These numbers indicate that the soft switching approach can eliminate 81% of the transition and compressibility losses that exist in the base relief valve system.

A model that used an ideal check valve that opens and closes instantaneously was also used to study the system. A comparison between that simplified model and the equations in section 3.2 showed that the dynamics of the check valve contribute about $1.3J$ of extra energy loss per switch. This points to the need to have a check valve that open and closes as fast as possible to reduce power loss.

The simulations presented in this section were done with a duty ratio of 50%. With a properly timed locking mechanism, the soft switching approach is still valid for duty ratios that are lower. As the duty ratio is decreased, the amount of time that the load valve is open is decreased. However, by design, the soft switch piston is locked at l_1 any time the load valve is open, so no timing issues arise from decreasing the duty ratio.

As the duty ratio is increased, however, the time that the tank valve is open is decreased. During one cycle, the soft switch chamber must fill and empty while the tank valve is open in order for the system to operate properly. The speed at which the chamber empties is a function of the spring force, which forces the stored fluid through the tank valve. As the duty ratio is increased, there will be a point where there is not enough time for the chamber to fully empty before it must start filling again. Once this point is reached, the soft switching approach can no longer eliminate throttling during all 4 transitions. However, once proper operation is no longer possible, the locking mechanism can be disabled, and 3 of the 4 transition losses can still be eliminated (loss during t_2 will remain). To gain a greater range of feasible duty ratios, the system can be sized to empty faster. This is done by either storing less fluid (i.e. not completely eliminating the power loss during t_2) or using a stronger spring. Both of these options result in additional power loss. Thus a design choice must be made between efficiency and range of operation based on the expected operating conditions.

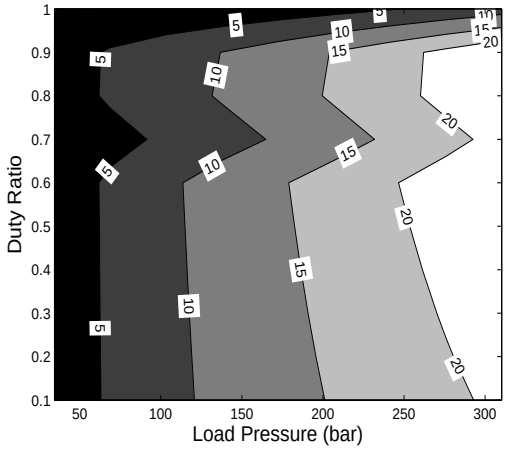

Figure 3.12: Reduction in energy lost/switch (J) from the check valve to the soft-switching case

As the PWM frequency is increased, there will be less time to empty the soft switch chamber. However, if the transition time is similarly scaled, then less fluid will have to be stored, and the timing will be similar to the slower system.

Despite the limited duty ratio range where the softswitch can properly operate, the approach provides a benefit across the full range of duty ratios. Figure 3.12 shows the improvement from the check-valve-only circuit to the soft switching circuit across a range of load pressures and duty ratios. Notice the discontinuity around 70% duty ratio. For the components sized in this simulation, that is the point where the soft switch did not have enough time to empty before filling again. However, notice that there is still substantial benefit beyond this point.

The system presented in this simulation was operated at $20Hz$ PWM frequency. The concept is valid at higher frequencies with the caveat that the timing issue described in the previous paragraph is taken into consideration. In addition, the compressibility of the oil in the inlet volume of the system can decrease the system effectiveness at higher PWM frequencies. This is a feature of all on/off controlled systems, with or without soft switching. Thus, a system with a sufficiently small inlet volume is a prerequisite for a properly functioning soft switch system. For example, in simulation the system was able to operate effectively at $80Hz$ with a $2.0ms$ transition time when the inlet volume

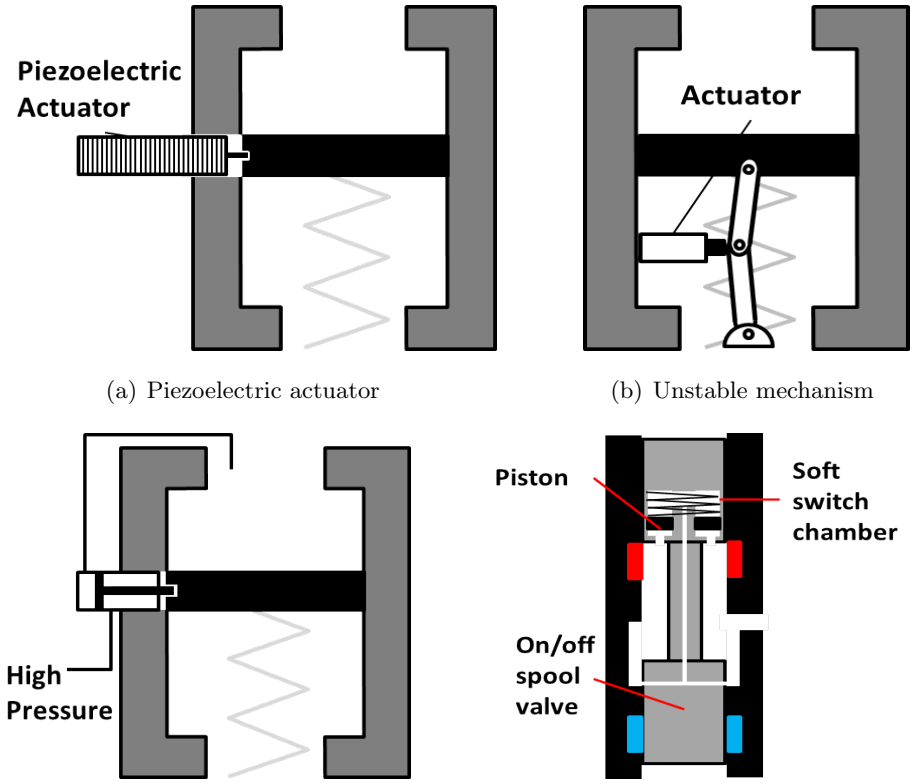

(a) Piezoelectric actuator

(b) Unstable mechanism

(c) Pressure triggered lock

(d) On/off valve triggered lock

Figure 3.13: Four concepts for creating a locking mechanism

was decreased to $8cm^3$ and l_1 was reduced to $3mm$.

The concept has thus far been described without discussion of the locking mechanism to be used. Several options exist for creating a lock with the required actuation speed, such as piezo electric actuators, pressure triggered latches, or mechanisms built into the on/off valve. Ideally, the locking mechanism will be triggered by a method with knowledge of the valve position. However, if this level of precision is not possible, a mechanism that is triggered by the pressure difference between the load and the inlet as the tank valve opens could also be used. This approach, while simpler, will result in some additional loss due to the time delay required for the tank valve to open enough for the pressure to fall below the load pressure. The locking mechanism that is selected must be capable of quickly releasing under a high load. The locking mechanism does not need to do much work, so if an approach can be designed to handle the large speeds

and forces, the overall power loss should not be affected. Figure 3.13 depicts sketches of four different concepts for creating a locking mechanism. In Fig. 3.13(a), a piezoelectric actuator is used to engage the soft switch piston and prevent it from moving. Piezoelectric actuators are capable of exerting large forces, but typically only for small displacements. The motion of the piezoelectric actuator could engage/disengage a pin from the piston, or possibly induce enough side-load or binding on the piston to create friction with the bore and prevent motion. In Fig. 3.13(b), a small actuator is used to nudge a mechanical linkage out of a stable resting state, allowing the pressure force to collapse the mechanism. In this concept, most of the load is held by the nearly vertical linkage, with only a small force needed to push the linkage to an unstable condition. Figure 3.13(c) depicts a lock that is triggered by the pressure difference between the load pressure and the pressure in the soft switch. This is probably the simplest method to implement, but it requires waiting until the tank valve is partially open to disengage the lock, which results in some additional loss. The fourth concept, depicted in Fig. 3.13(d), uses the motion of the on/off valve to trigger the release of the soft switch piston. In this example, a three-way spool valve is used as the on/off valve, and a blocked hydraulic chamber behind the soft switch piston holds it in place until the chamber is connected to low pressure by the motion of the spool. This approach can be designed to trigger at the ideal time, but in this concept the release speed of the fluid behind the soft switch piston is limited by the transition time of the valve. Using an unequal area piston could help mitigate this problem. A lock that is mechanically triggered by the on/off valve, as opposed to hydraulically triggered, could also be designed, but it would depend heavily on the design of the on/off valve. These examples are presented as concepts that have the potential to achieve the desired locking effect. The detailed design of this mechanism is relegated to future work. In [30], an example of a pressure-triggered locking mechanism is described.

The simulated valve had a transition time of $7.5ms$. In order to match the energy loss of the soft switching system with a faster valve, the transition time needs to be decreased to about $1.7ms$ for the relief valve case in simulation. Note that these are the times for one transition event. This represents a 4.4 times increase in speed, which will typically correspond to a significant increase in price and actuation power for the valve. Thus the soft switching approach has the potential to enable on/off control using lower

speed valves.

3.5 Conclusion

A method of significantly reducing the power lost in an on/off controlled hydraulic system has been introduced. The soft switching concept is a method for providing temporary alternative fluid paths around a transitioning valve, and thus avoiding the associated throttling losses. A check valve can be used to avoid two of the four transitions that occur in a three-way PWM controlled circuit; the remaining two transitions need an additional device to be eliminated. The soft switching chamber, which consists of a small piston with a spring and a lock, can be used to reduce the overall system loss. Simulations were performed based on a PWM valve operating at $20Hz$, and it was found that application of the soft switching concept resulted in an 81% reduction in transition losses, and a 64% reduction in overall system losses. This approach can make the efficient approach of on/off valve control even more attractive as an option for controlling hydraulic systems. In addition, soft switching can facilitate the use of slower valves for on/off control by significantly reducing the power loss resulting from slow transition times. In simulation, the soft switching system had the same efficiency as a system with a valve that was 4.4 times faster. This will allow simpler, lower power valves to achieve results similar to faster valves. This approach can be extended to other on/off valve controlled circuits, such as variable motors and transformers.

Chapter 4

Optimal Design of Rotary Valves for Creating On/Off Controlled Hydraulic Systems

A key element in developing hydraulic circuits controlled by on/off valves is the design of the on/off valve(s). In chapter 2, an analysis of the system dynamics of a Virtually Variable Displacement Pump (VVDP) circuit showed that switching at high frequency can improve the trade off between the output ripple and the speed of response. However, power losses caused by the compressibility of the fluid and throttling through the transitioning valve increase with the switching frequency. In this chapter, a new type of on/off valve is presented that can enable higher speed switching than conventional valves.[1] The design concept is to use a two degree-of-freedom spool valve that can both translate axially and rotate. This type of rotary valve can be used to create a VVDP circuit with a 3-way design, or it can be extended to a Virtually Variable Displacement Pump/Motor (VVDPM) using a 4-way architecture. In this chapter, the design of both of these valves is presented as an optimization problem to minimize the power loss in the valve.

In addition to transition throttling and compressibility losses, another type of power loss that increases with the switching frequency is the power needed to actuate the

[1] Some of the material in this chapter was originally published by ASME in [51].

switching valve. An ideal switching valve would have a very fast transition speed while also having a large full-open area to reduce throttling. These two conditions in conventional valves can result in a high power requirement to actuate the valve. As the switching frequency is increased, this power cannot be neglected. If it is assumed that the velocity of a conventional valve element scales proportionally with the PWM frequency, and there is no recuperation of the kinetic energy in the valve, then the power required to switch a conventional valve is given by:

$$L_{actuation} = fE_{switch} = f\frac{1}{2}m\left(k_v f\right)^2 \tag{4.1}$$

where f is the switching frequency, m is the valve element mass, and k_v is the proportionality coefficient between the switching frequency and the spool velocity. From this equation, it is clear that the actuation power increases proportionally to the frequency cubed.

In contrast, the rotary valves described in this chapter rotate at a relatively constant velocity and do not need to be accelerated/decelerated with each valve switch. Instead, the valve must only overcome the viscous friction that results from spinning the valve. Due to this fact, the power associated with actuating a rotary valve, which is given in Eq. (4.23), increases with the switching frequency squared. As PWM frequencies are increased to achieve better dynamic performance, a rotary valve can provide a significant benefit by reducing the actuation power requirement.

As described in chapter 2, there are a number of power loss mechanisms that occur in an on/off valve controlled system. Design choices made to reduce some losses can result in an increase in other losses. For example, a larger valve opening to reduce the full-open loss can increase the valve size and increase the inlet volume, which increases the compressibility loss. In addition, due to the architecture of the rotary valve, there are a number of design constraints that must be satisfied. Balancing the different power losses while satisfying the design constraints is not an intuitive process. By formulating the valve design as an optimization problem, the valve parameters can be selected in a way that minimizes the total power loss in the valve while satisfying all design constraints. In this chapter, this optimization approach is described for both the VVDP and the VVDPM. By presenting the optimal design for the valve, the full potential of the rotary valve approach can be judged and compared with other hydraulic control mechanisms.

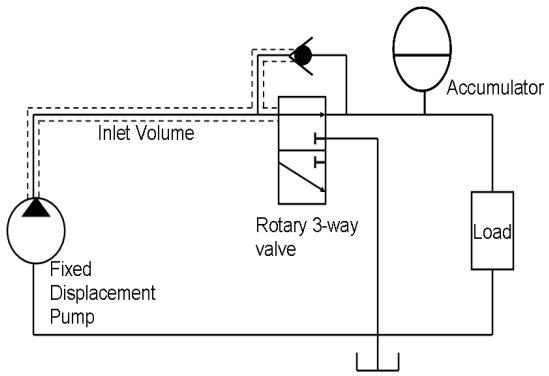

Figure 4.1: Virtually variable displacement pump circuit

In addition to facilitating the selection of design parameters for the valve, the constraint equations for the valve can be adjusted to test the power losses in designs with different features or configurations. For example, the rotary valve can be designed to capture the momentum of the oil flowing through it, which can reduce or eliminate the actuation power required. However, this requires a constraint on the valve that can increase other power losses. In this chapter a number of optimization studies are described that outline the effect of different design choices on the total power loss.

In the next section the 3-way rotary valve for creating a VVDP is described, which includes a formulation of the optimization problem, a description of the power loss equations and constraint equations, and a section describing the optimal power loss for a number of different design options. Following the VVDP section, a similar description of the 4-way valve that creates a VVDPM is presented.

4.1 Rotary Valve Enabled VVDP

The hydraulic circuit shown in Fig. 4.1 represents a VVDP. It is shown with the on/off valve as a 3-way valve instead of the 2-way valve and check valve shown in Fig. 2.1(b). While both configurations will create a VVDP, the rotary valve, shown in Fig. 4.2, is designed as a 3-way valve to enable the self-spinning feature, which will be described later. The valve spool shown in Fig. 4.2 has three sections: a central PWM section, and two outlet sections. The upper outlet section is connected to the load, and the lower outlet turbine is connected to tank. The central section contains a number of helical

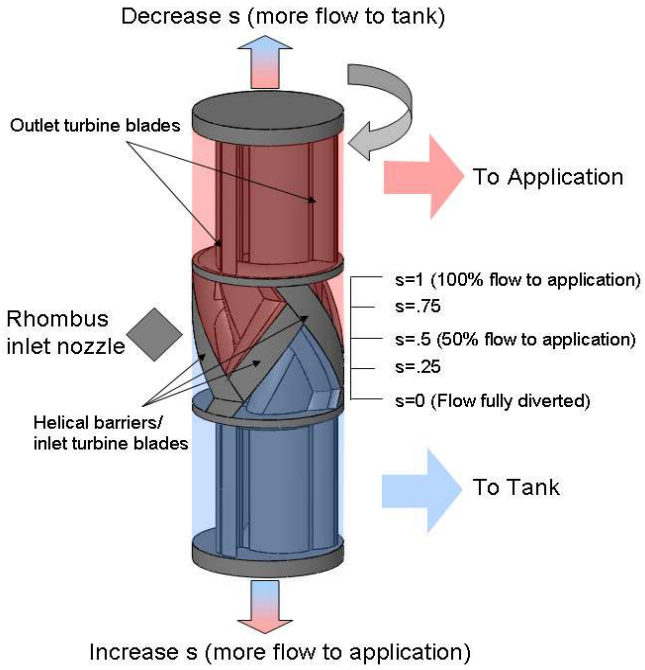

Figure 4.2: Diagram of 3-way rotary spool

lands that partition the central section into two regions. The open area above the helical lands (shown in red) is connected internally to the upper outlet section, and the area below the helical lands (shown in blue) is connected to the lower outlet section. As the valve spool rotates, the inlet orifices, which are stationary on the valve sleeve, will alternately connect the inlet to high pressure or to tank. By moving the valve axially with respect to the inlet orifices, the fraction of the rotation that the inlet (pump) is connected to the application is adjusted. Thus, the PWM frequency is controlled by the speed of the valve spool rotation, and the PWM duty ratio is adjusted by the axial position. Through this design, the repeated, high-speed switching of the on/off valve is encoded in the mechanical design of the valve and is accomplished without any acceleration/deceleration of the spool. The adjustment of the duty ratio, which is typically done at a much lower frequency, is left to the axial positioning mechanism.

Since the valve has two degrees of freedom, it requires an actuation method for both its rotary and axial motion. For the rotary actuation, two methods will be explored in

this chapter. The valve spool shown in Fig. 4.2 shows a spool that is designed for self-spinning. In this actuation method, the valve is designed to capture angular momentum from the oil that is entering and exiting the spool, and to use this momentum to provide the actuation power. In this design, both the center and outlet sections of the spool act as turbines: the inlet section is an impulse turbine, and the outlet sections are reaction turbines [84]. Since the valve is designed to capture energy from the fluid in order to rotate, there must be a constant flow of oil through the valve, which is accomplished with the 3-way design. In a 2-way design, the on/off valve either blocks or allows oil to flow to the tank. When the valve is blocking fluid, there is no oil passing through it, and with a self-spinning valve, the spool could stop rotating.

The self-spinning approach has a number of benefits. For example, it does not require any mechanical connection to the valve, allowing the valve to remain in a sealed chamber. It also does not require any external actuation power since it scavenges energy from the fluid flowing through it. However, there are also several drawback to this approach. In order to achieve a certain switching frequency, the valve must be designed to generate/capture enough momentum to overcome the viscous friction. The design choices that must be made to accomplish this can increase other losses in the valve. The speed of the valve is also dependent on the flow rate of the fluid that passes through it; if the flow rate is variable, then the PWM frequency will also vary. Finally, the self-spinning approach requires a 3-way design instead of the 2-way design, which can have an impact on the losses in the valve.

A different rotary actuation method is to use a shaft that connects to an external driving mechanism. This approach requires a sealed connection that can rotate and translate and an external driving mechanism. However, it also relaxes some of the design constraints on the system. In section 4.3, a comparison between the optimal design for both approaches is presented.

The axial actuation approach also has a number of options, which are related to the choice of the rotary actuation method. For a self-spinning valve that does not require an external connection to spin the spool, an axial positioning method that also does not need an external connection will simplify the packaging and sealing of the valve spool housing. Figure 4.3 shows a diagram of an axial positioning and sensing system that uses a small fixed-displacement pump to hydrostatically position the valve spool and

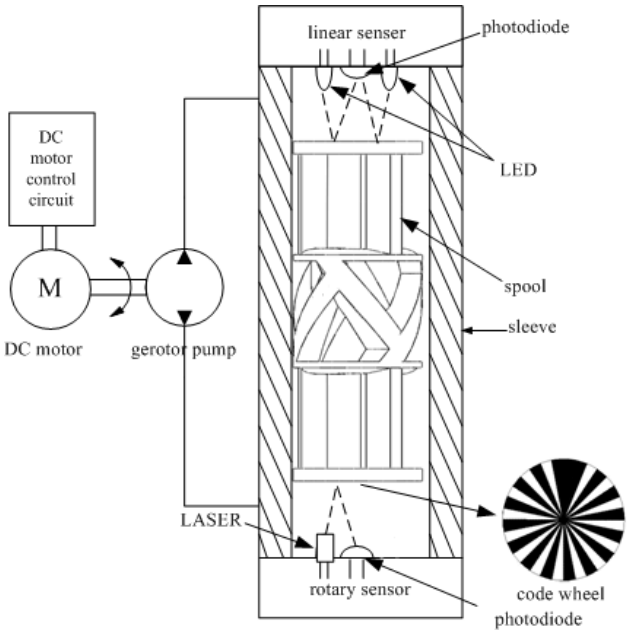

Figure 4.3: Diagram of linear actuation and rotary sensing system

optical sensors to detect the axial and rotary position of the spool. In [85], a technique is described for controlling the position of the spool using this architecture.

The valve spool is contained within a housing that provides connections from the pump to the inlet section, and from the outlet sections to either the load or to tank. Figure 4.4 shows a cutaway view of the valve housing containing the valve spool. The back of this housing is designed to mount directly on the outlet of a fixed displacement pump in order to minimize the inlet volume and the compressibility loss. On the front of the sleeve containing the spool, there are four hydraulic connection ports. The outer two ports connect to chambers at the ends of the spool, and are used for the hydrostatic axial positioning system. The inner two ports connect to the two outlet sections of the valve, and will be connected to either the load or to tank. In the middle of the cutaway, there is an inlet pressure rail, which encircles the center section of the valve and connects to three inlet orifices. There are three orifices to increase the PWM frequency (one rotation results in three PWM pulses) and help balance the spool. The number of inlet orifices (and corresponding number of PWM sections on the valve) is a design parameter that is studied in section 4.3.

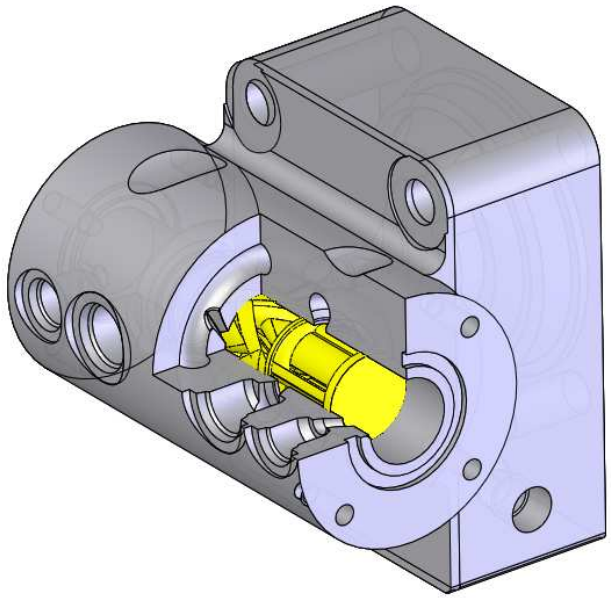

Figure 4.4: Cutaway rendering of rotary spool/sleeve assembly

In the next section the design of the VVDP valve spool is presented as an optimization problem, with the goal of minimizing the power loss in the valve. In section 4.3 the results of the optimization are presented, and several different design options are evaluated.

4.2 VVDP Design Optimization Formulation

In chapter 2, a number of losses were described that occur in a vvdp hydraulic circuit, such as full-open throttling, transition throttling, and compressibility loss. In addition, there are two valve-specific losses that can be significant: leakage in the valve, and valve actuation power. These five power losses are affected by the design parameters of the valve, and finding the set of parameters that results in the most efficient valve may not be an intuitive process. If equations for these losses can be derived that allow the valve design to be cast as an optimization problem, then the selection of the ideal valve parameters can be simplified. The following formulation describes the optimal design of the valve:

$$\min_{\mathbf{x}} \; L_{total} = L_{full-open} + L_{compress} + L_{leakage} + L_{transition} + L_{actuation}$$

$$\begin{aligned} \text{s.t. } & c_1(\mathbf{x}) \leq 0 \\ & c_2(\mathbf{x}) \leq 0 \\ & c_3(\mathbf{x}) = 0 \\ & x_{i,min} \leq x_i \leq x_{i,max} \text{ for } 1 \leq i \leq 8 \end{aligned} \tag{4.2}$$

where $c_1(\mathbf{x})$, $c_2(\mathbf{x})$, and $c_3(\mathbf{x})$ are constraint functions. The first constraint, $c_1(\mathbf{x})$, ensures that the valve achieves a minimum PWM frequency, $c_2(\mathbf{x})$ is a mechanical constraint that arises from the fact that the valve cannot be in transition for $> 100\%$ of the rotation, and $c_3(\mathbf{x})$ constrains the angle of the rhombus-shaped inlet orifice to match the angle of the helical lands and ensures closed-center operation, which means that there can be no connection between supply and tank pressure. The L terms represent the cycle-averaged power losses. The optimization parameter vector is given by $\mathbf{x} = [R_w,\ R_h,\ D,\ l,\ c,\ N,\ A_{out},\ l_{end}]$. In order, these represent the inlet orifice width (R_w), the inlet orifice height (R_h), the spool diameter (D), the spool length (l), the radial clearance between the spool and the sleeve (c), the number of helical sections on the valve (N), the flow area of the outlet turbine orifice (A_{out}), and the length of the sealing land on the ends of the spool (l_{end}). These variables represent the parameters that are incorporated in one or more trade offs between the different types of energy loss or the constraints. There are many other variables needed to define the rotary valve, but, for the most part, their effect on the energy loss is readily apparent, and they can be chosen to minimize the loss subject to unmodeled constraints (i.e. manufacturability, simplicity, etc.). Figure 4.5 shows the valve spool with the relevant design parameters.

For the VVDP design, the optimization is defined at a single operating condition with a constant inlet flow and load pressure. This is not the only way to formulate the problem, and for the VVDPM optimization, a different approach is taken. The inlet flow rate and load pressure are determined by the prime-mover speed and the applied load, which are external factors. In order to define an optimization for a varying set of flow rates and pressures, the desired duty cycle on the valve must be known. For a

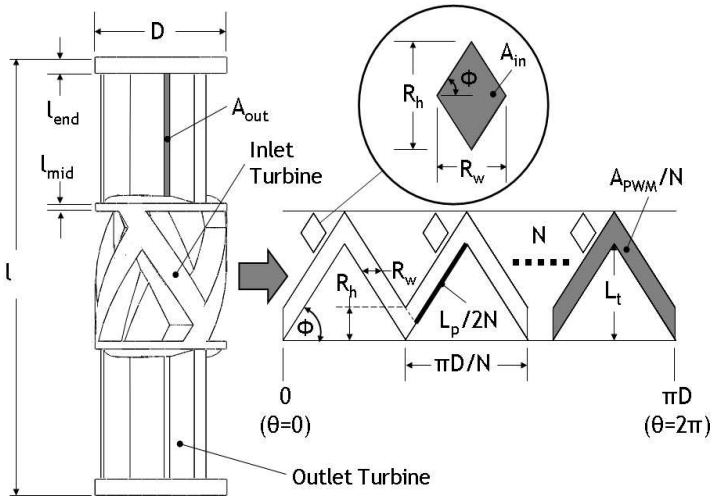

Figure 4.5: Spool geometry with unwrapped center section

VVDP, a constant flow rate and load pressure is a simple, but realistic duty cycle for the valve. In sections 4.2.1 through 4.2.5, the five different types of power loss are defined, and their dependence on the optimization parameters is derived. In section 4.2.6, the constraints on the design are described.

4.2.1 Full-Open Loss

The full open loss is caused by the pressure drop across the inlet nozzle, the valve spool, and the outlet turbine when the valve is fully open. The pressure drop across the inlet nozzle and the outlet turbine are calculated using the orifice equation:

$$P_{in} = \frac{\rho Q^2}{2\left(c_d N A_{in}\right)^2} \quad P_{out} = \frac{\rho Q^2}{2\left(c_d N A_{out}\right)^2} \tag{4.3}$$

where ρ is the density of the hydraulic fluid, c_d is the orifice coefficient, $A_{in} = 0.5 R_w R_h$ is the area of one inlet orifice, and Q is the constant flow rate from the pump. Notice that this equation is for a self-spinning design, so the full pump flow rate is always flowing through the valve, either through the tank branch or the load branch.

The pressure drop through the spool is difficult to model, as it is the result of a tortuous path through the turbine blades. In addition, the dependence of this path on the optimization parameters is not immediately clear. Two simple approximations are

to model the pressure drop as an orifice, with $\Delta P \propto Q^2$, or viscous pipe flow, with $\Delta P \propto Q$. Since the actual spool pressure drop will be result of both accelerating fluid (orifice) and viscous drag (pipe flow), a better model would be some combination of the two; $\Delta P \propto Q^{m_{spool}}$, with $m_{spool} \in [1, 2]$. If it is assumed that the equivalent flow path area is primarily dependent on the spool diameter and not the spool length, then the spool pressure drop can be modeled by the following equation:

$$P_{spool} = \frac{Q^{m_{spool}}}{k_{spool} D^{n_{spool}}} \tag{4.4}$$

where k_{spool} is a parameter containing all of the constant coefficients, and $n_{spool} \in [2, 4]$ is a parameter that defines the dependence of the pressure drop on the spool diameter. The values of m_{spool} and n_{spool} depend on the flow path geometry and can be found through a Computational Fluid Dynamics (CFD) analysis of the valve spool. In [86], a detailed description of the CFD approach for analyzing the valve spool is given. For the three-way valve geometry, Wang found that $n_{spool} = 2.75$ and $m_{spool} = 1.735$ provide a good match to CFD experiments. Note that $n_{spool} = 2$ would result from a flow area that is proportional to D, and $n_{spool} = 4$ would result from a flow area proportional to D^2.

With the pressure drops across different parts of the valve defined, the total full-open throttling loss can be computed from Eq.(4.5):

$$L_{full-open} = (1 - \kappa)\, QP_{in} + QP_{out} + QP_{spool} \tag{4.5}$$

where κ represents the fraction of the total rotation that the valve spends transitioning between states and is given by:

$$\kappa = \frac{4NR_w}{\pi D} \tag{4.6}$$

The $1-\kappa$ term in Eq. (4.5) is a result of the way the transition loss is computed; the transition loss equation (Eq. (4.19)) includes the pressure drop across the inlet orifice, which is omitted from Eq. (4.5) to avoid double counting.

4.2.2 Compressibility Loss

The compressibility loss equations capture the energy that is lost by compressing the fluid, and then connecting the compressed fluid to tank every PWM period. The energy

stored in the compressed fluid is given in chapter 2 by Eq. (2.30), which is repeated here:

$$E\left(P,V_0\right)=\int_{P_0}^{P}V_0e^{-\int_{P_0}^{p}\frac{\bar{p}}{\beta(\bar{p})}\,d\bar{p}}\frac{p}{\beta\left(p\right)}\,dp \tag{4.7}$$

where $\beta(P)$ is the pressure dependent bulk modulus of the fluid which is given by Eq. (2.5), and V_{in} is the inlet fluid volume, given by Eq. (4.8).

$$V_{comp}=\frac{N-1}{N}\left(D+2l_n+D_d\right)\frac{\pi^2D_d^2}{4}+NV_n+V_{in} \tag{4.8}$$

The inlet volume consists of the fluid volumes in the inlet pressure rail, the inlet nozzles ($V_n = A_{in}l_n$), and any volume between the pressure rail and the pump outlet (V_{in}). Notice that the inlet pressure rail is a function of the spool diameter, the number of PWM sections, the nozzle length (l_n), and the cross-sectional area of the pressure rail (D_d). The $\frac{N-1}{N}$ coefficient results from the fact that the inlet rail does not fully encircle the valve spool. It must extend long enough to connect all N of the inlet nozzles, but it is not needed for the last $\frac{1}{N}$ of the diameter.

These equations must be numerically integrated, but this can be done before the optimization procedure is run. The integral in Eq.(4.7) can be replaced by an equivalent term using a constant bulk modulus:

$$E_{comp}=\frac{V_{comp}P^2}{2\beta_{eq}} \tag{4.9}$$

where β_{eq} is computed by setting Eqs. (4.7) and (4.9) equal to each other. With this modification, the power loss due to the compressibility of the fluid is given by:

$$L_{compress}=\frac{V_{comp}P^2N\omega}{4\beta_{eq}\pi} \tag{4.10}$$

where ω is the angular velocity of the valve spool.

Notice that there is a trade off between the full-open loss and the compressibility loss through the selection of the spool diameter. A larger diameter will allow for larger flow paths and reduce the pressure drop, but it will also increase the diameter of the inlet rail and the compressibility loss.

4.2.3 Leakage Loss

The 3-way valve spool has 2 leakage paths where high pressure can leak to the tank rather than exiting to the load. The largest leakage path is across the helical barriers in the center section that separate the high pressure and low pressure halves of the valve, and the other is across the land at the high pressure end of the spool. The leakage across both of these paths is modeled as laminar flow between 2 plates [87].

The leakage across the center helical barriers is driven by a pressure difference between the load pressure, P, and the tank pressure, but the leakage across the end is not. The axial position of the valve is controlled hydrostatically, with a closed circuit connecting both ends of the valve with a small pump/motor. Assuming there is no external leakage from this circuit, the leakage from the high pressure end to the axial control loop must equal the leakage from the axial control loop to the low pressure end of the spool. If the two spool ends are identical, the mean pressure in the axial control circuit must be half of the load pressure. With these assumptions, the power loss across the two leakage paths is given by Eq. (4.11). This equation assumes that the valve is critically lapped, and the width of the inlet orifice is equal to the width of the helical land.

$$L_{leakage} = \frac{N\left(2l_t - R_h\right)c^3P^2}{12\mu R_w \sin^2(\phi)} + \frac{D\pi c^3\left(\frac{P}{2}\right)^2}{12\mu l_{end}} \tag{4.11}$$

where μ is the oil viscosity, ϕ is the angle of the helical barriers (see Fig. 4.5), and l_t is the travel length of the valve spool given by:

$$l_t = \frac{l - 2l_{mid} - 2l_{end}}{3} - R_h \tag{4.12}$$

where l_{mid} is the width of the mid lands between the center section and the two outlet sections, which is selected to be as small as the manufacturing process allows. Note that this equation suggests a larger orifice width, a shorter spool, a tighter clearance, and a longer end length are beneficial. These goals can conflict with other power losses or design constraints.

4.2.4 Transition Loss

Another source of power loss in the valve is throttling across the valve inlet when it is partially closed. The equation for this loss is derived by integrating the orifice equation for each of the 4 transitions that occur every PWM period (the closed-center 3-way valve requires 4 transitions: close supply, open tank, close tank, open supply). The approach for determining the transition loss is the same as was taken in section 2.3.3, where the pressure and flow across the valve are integrated across the transition. There is a critical point where the the equation transitions from a constant flow and a pressure determined by the orifice equation to a constant pressure set by the the load pressure plus the check valve pressure. Figure 4.6 shows the transition loss, along with the load pressure and the pressure drops across the spool and the outlet turbine. Some of the losses are exaggerated in this figure for demonstration purposes. Note that, by this partitioning of the throttling losses, the full-open pressure drop and the transition pressure drop occur over different parts of the valve rotation, while the spool and outlet pressure drops are active over the entire rotation. This is enforced in Eq. (4.5).

The inlet orifices are designed to have a rhombus shape, which creates orifices with the fastest possible area gain for all four transitions. The rhombus shape results in linear area profiles for the valve (see Fig. 4.6), which allows the transition loss in Eq. (2.31) to be simplified. The following derivation of the transition loss is very similar to one described in [51]. The pressure drop across the inlet orifice is given in Eq. (4.3). Since, during transition, the valve area is proportional to the valve rotation angle, the inlet pressure drop can also be written as:

$$P_{in}(\theta) = P_{open}\left(\frac{\theta_{tran}}{\theta}\right)^2 \quad \text{for } \theta_{crit} \leq \theta \leq \theta_{tran} \tag{4.13}$$

where P_{open} is the pressure drop across the inlet orifice when the valve is fully open, and θ_{crit} is the angle at which the pressure drop across the inlet is equal to the cracking pressure of the check valve that prevents pressure spikes. θ_{tran} is the rotation angle for a full transition (of a single orifice), which is defined by:

$$\theta_{tran} = \frac{2R_w}{D} \tag{4.14}$$

While there are 4 different transition events, due to the linear area profiles and the

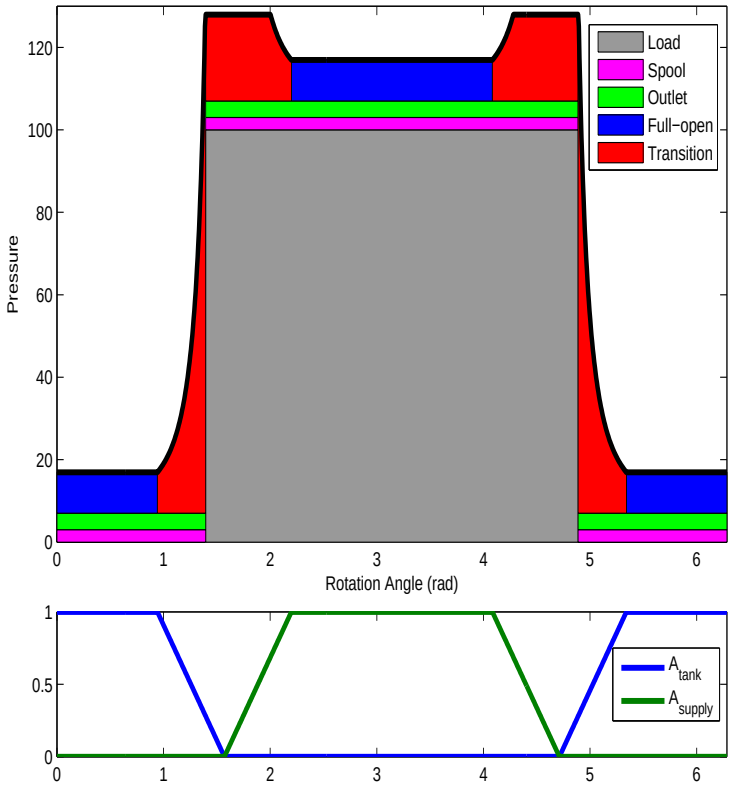

Figure 4.6: Inlet pressure profile with losses shown

symmetry of the valve, the power loss across an orifice while it is opening and closing is the same. When computing the power loss across a closing valve, the critical angle at which the check valve closes and all of the flow begins to flow across the inlet orifice is important. It can be computed from:

$$\frac{\theta_{crit}}{\theta_{tran}} = \frac{\sqrt{P_{open}}}{\sqrt{P_{load} + P_{check} - P_{spool} - P_{out}}} \tag{4.15}$$

where P_{check} is defined as the pressure drop needed to open the check valve shown in Fig. 4.1. The check valve in this circuit is simply to limit pressure spikes as the valve transitions. This function could also be accomplished by a relief valve, but that would result in higher transition losses. Note that in Fig. 4.6, $P_{check} > P_{open} + P_{spool} + P_{out}$, which is required to keep fluid flowing through the rotary valve in the "on" state and enable self-spinning. An externally rotated valve could use a lower check valve pressure, and use the check valve instead of the rotary valve to pass fluid in the "on" state, resulting in the rotary valve acting as more of a two-way valve. Allowing P_{check} to be less than the pressure drop across the spool would require a change in the structure of Eq. (4.5) and of the optimization problem for the externally rotated case, since the loss would be different in the "on" and "off" states, and a duty ratio profile for the valve would need to be specified. It is assumed that the difference between using the check valve only during transition, and using it for the full "on" state, is not enough to distort the comparison between a self-spinning and an externally rotated valve.

With the transition and critical angles defined, the energy loss across an opening (or closing) tank orifice is given by:

$$\begin{aligned} E_{trans,tank} &= \frac{Q}{\omega}\int_0^{\theta_{crit}} \left(P_{check} - P_{out} - P_{spool}\right) d\theta + \frac{Q}{\omega}\int_{\theta_{crit}}^{\theta_{tran}} P_{in} \\ &= \frac{Q}{\omega}\left(\left(P_{check} - P_{out} - P_{spool}\right)\theta_{crit} + P_{open}\theta_{tran}\left(\frac{\theta_{tran}}{\theta_{crit}} - 1\right)\right) \\ &= \frac{2QR_w}{\omega D}\sqrt{P_{open}}\left[\frac{P_{check} - P_{out} - P_{spool}}{\sqrt{P_{load} + P_{check} - P_{spool} - P_{out}}}\right. \\ &\left. + \sqrt{P_{load} + P_{check} - P_{spool} - P_{out}} - \sqrt{P_{open}}\right] \end{aligned} \tag{4.16}$$

The derivation for the energy lost across a transitioning supply orifice is the same as for the tank orifice except that the critical angle is found from:

$$\frac{\theta_{crit}}{\theta_{tran}} = \frac{\sqrt{P_{open}}}{\sqrt{P_{check} - P_{out} - P_{spool}}} \tag{4.17}$$

With that change, the energy lost across one supply orifice transition is:

$$E_{trans,supply} = \frac{2QR_w}{\omega D}\sqrt{P_{open}}\left[2\sqrt{P_{check} - P_{out} - P_{spool}} - \sqrt{P_{open}}\right] \tag{4.18}$$

Adding the losses for the four transitions and multiplying by the PWM frequency ($f_{PWM} = N\omega/(2\pi)$), and combining with the definition of the transition fraction given in Eq. (4.6) gives the equation for the transition power loss:

$$\begin{aligned} L_{transition} = \frac{\kappa\sqrt{P_{open}}Q}{2}\Bigg[&\frac{P_{check} - P_{out} - P_{spool}}{\sqrt{P_{load} + P_{check} - P_{spool} - P_{out}}} \\ &+\sqrt{P_{load} + P_{check} - P_{spool} - P_{out}} + 2\sqrt{P_{check} - P_{out} - P_{spool}} - 2\sqrt{P_{open}}\Bigg] \end{aligned} \tag{4.19}$$

Notice that κ, given by Eq. (4.6), contains the spool diameter, D, in the denominator. Thus, a larger valve should minimize the transition loss, which is in conflict with the compressibility loss.

4.2.5 Actuation Loss

The power required to drive the valve depends on whether it is designed to be self-spinning or externally rotated. For a self-spinning valve, the additional actuation power loss is zero; all of the energy needed to spin the valve is accounted for in the other losses already described. For an externally rotated valve, an additional power input is required to overcome the viscous drag on the spool. The viscous friction torque generated by the spool rotating in its bore can be derived from the equation for couette flow between two parallel plates [87] and is given by:

$$T_f = \frac{A_{eff}\mu D^2\omega}{4c} \tag{4.20}$$

where ω is the angular velocity of the valve spool and A_{eff} is the effective bearing area on the spool. The effective bearing area is the surface area that is at clearance c, plus

a term that takes into account the viscous drag due to fluid swirling in the enclosed pockets of the valve.

$$A_{eff} = A_{bearing} + \alpha(\pi D l - A_{bearing}) \tag{4.21}$$

where α is defined to be the ratio of non-bearing shear stress to bearing surface shear, or $\alpha = \frac{\tau_{non-bearing}}{\tau_{bearing}}$. In [51], a CFD analysis that provides an estimate of α is described. The bearing area, $A_{bearing}$ is defined as:

$$A_{bearing} = \pi D \left(R_h + 2l_{mid} + 2l_{end}\right) \tag{4.22}$$

With the friction torque and the effective bearing area defined, the power loss due to the actuation requirement is given by:

$$L_{actuation} = T_f \omega = \frac{A_{eff} \mu D^2 \omega^2}{4c} \tag{4.23}$$

If the efficiency of the actuator used to drive the shaft is known, this equation can be divided by that value to provide the power input needed to the actuator. From Eq. (4.23) it is clear that decreasing the size of the spool and increasing the valve clearance will help reduce the actuation loss. However this is in contrast to the transition and leakage equations, which call for a large spool and a small clearance. In addition to conflicts between the different power losses, design trade offs exist with the constraint equations, which are described in the next section.

4.2.6 Constraints

Equation (4.2) lists two inequality constraints and one equality constraint that the optimal valve design must satisfy. All three of these constraints are non-linear constraints. The optimization formulation also shows that the optimization variables are subject to upper and lower bounds, which are needed to ensure that the device can be manufactured and can be contained in a reasonable package size.

The first nonlinear inequality constraint is a minimum bound on the switching frequency. Since the compressibility and transition losses occur every PWM cycle, the optimal switching frequency from a power loss perspective is 0. However, as described

in chapter 2, a high switching frequency is often desired to provide good system dynamic performance. Since the design optimization is formulated to reduce the power loss, the desired switching frequency must be determined separately and specified as a constraint.

With a minimum frequency, f_{min}, specified, the constraint is:

$$c_1(\mathbf{x}) = f_{min} - \frac{\omega N}{2\pi} \tag{4.24}$$

For a self-spinning spool, the angular velocity is derived from a torque balance between the viscous friction on the spool (Eq. (4.20)) and the angular momentum captured by the inlet and outlet turbines. The inlet torque generated by the center section, which is designed to be an impulse turbine, is given by:

$$T_{in} = \frac{\rho R_{in}}{A_{in} N} Q^2 \tag{4.25}$$

In order to generate angular momentum that can be captured by the inlet section blades, the inlet nozzles are offset from the spool center line by a distance R_{in}. This offset distance can also be written as $R_{in} = r_{i,off} D/2$, where $r_{i,off}$ is the fraction of the spool radius by which the inlet is offset.

The outlet sections of the spool are designed to be reaction turbines, which provide the following torque:

$$T_{out} = R_{out} \rho Q \left(\frac{Q}{A_{out} N} - R_{out} \omega \right) \tag{4.26}$$

where $R_{out} = r_{o,off} D/2$ is the offset distance between the spool center axis and the velocity vector of the exiting fluid. The derivation of the turbine torque equations can be found in [51]. Note that the outlet turbine generates torque by increasing the angular momentum of the fluid as it passes through the outlet section of the valve. In order to increase the momentum of the fluid, the velocity can be increased by reducing the flow area of the exit orifice in the outlet turbine, A_{out}. However, Eq. (4.3) demonstrates that a smaller outlet orifice also generates a higher full-open loss. This creates a tradeoff between generating rotational torque to spin the valve or reduce the actuation loss, and minimizing the full-open throttling loss.

By setting the friction torque equal to the sum of the inlet turbine and outlet turbine

torques, an equation for the angular velocity of a self-spinning spool can be derived:

$$\omega = \frac{\rho Q^2 r_{i,off} \frac{D}{2}}{N\left(\frac{D}{2}\right)^2 \left(A_{eff}\frac{\mu}{c} + r_{o,off}^2 \rho Q\right)} \left(\frac{1}{A_{in}} + \frac{r_{o,off}}{r_{i,off} A_{out}}\right) \tag{4.27}$$

This equation is used in Eq. (4.24) to generate the first nonlinear constraint equation. Note that this constraint is only needed for a self-spinning valve. For an externally rotated valve, the angular velocity is simply specified to be $\omega = \frac{f_{min} 2\pi}{N}$.

The second inequality constraint, $c_2(\mathbf{x})$, states that largest fraction of the PWM period that the valve can spend in transition is 1.

$$c_2(\mathbf{x}) = \kappa - 1 \tag{4.28}$$

The final constraint, $c_3(\mathbf{x})$, is an equality constraint that arises from the fact that the rhombus inlet orifice must have the same angle as the helical land to provide a fast transitioning orifice and the desired closed-center characteristic of the valve. The geometry shown in Fig. 4.5 shows that the triangle under the helical land and half of the inlet rhombus orifice are similar, leading to the following constraint:

$$c_3(\mathbf{x}) = 2\frac{R_w}{R_h} - \frac{\pi D}{l_t N} \tag{4.29}$$

where $l_t = (l - 2l_{mid} - 2l_{end})/3 - R_h$ is the total length of axial travel for the valve spool.

While it is not explicitly stated in section 4.2, there is an additional equality constraint on the number of PWM sections, N. For this design parameter, only integer values are valid, which is in contrast to the rest of the optimization parameters, which can vary continuously. Since only a small set of values of N is realistically possible to manufacture, the value of N was constrained to a set of fixed values, and the optimal design was computed for each number of PWM sections.

These constraints interact with the loss equations in the previous section to restrict the optimal valve design parameters. In the following section, the numerical inputs and optimal results are presented for several design options.

4.3 VVDP Optimization Results and Design Studies

The optimization problem formulated in section 4.2 is a constrained nonlinear optimization problem which can be solved by many different commercially available optimization software packages. For the numerical results presented in this section, the Matlab Optimization Toolbox was used to compute the constrained optimal solutions. The software used the *fmincon* function to find the optimal design. Several of the solver algorithms were tried, and the Interior Point method was found to find the solution in the shortest time. The optimization was initialized with preliminary values for each of the seven active design variables.

The optimization was performed for a flow of $Q = 37.85lpm$ and a load pressure of $P = 200bar$, which corresponds to a small to medium hydraulic power demand and also matches a previously designed prototype. The oil density was set at $\rho = 876kg/m^3$, and the viscosity was $\mu = 0.0387m^3/s$, which match values for Mobil DTE 25 oil at $40C$. The equivalent bulk modulus, which is described in section 4.2.2, was $370MPa$. All of the orifice equations used the discharge coefficient of $c_d = 0.6$. The minimum inlet volume was $V_{in} = 5cm^3$, the length of the inlet nozzles was $l_n = 4.2mm$, and the cross-sectional diameter of the inlet pressure rail was $D_d = 6.8mm$. The width of the barriers between the three spool sections was $l_{mid} = 1.5mm$, and the factor defining the contribution to the fluid friction by the non-bearing area was $\alpha = 0.2$. The check valve opening pressure was set to be about $0.34bar$ higher than the pressure drop across the valve. The parameters for determining the pressure drop across the spool were derived from a CFD analysis (see [86]) and found to be: $k_{spool} = 1.45e-6$, $n_{spool} = 3.22$, and $m_{spool} = 1.91$. For the self-spinning case, the inlet offset fraction was $r_{i,off} = 0.79$, and the outlet offset fraction was $r_{o,off} = 0.9$, which were the largest offsets that could be reasonably manufactured.

While the goal of the optimization was to find the set of values for the design variables that minimizes the energy loss, some constraints needed to be placed on those values to ensure the final design could be manufactured. The orifice dimensions, R_w and R_h, had to be larger than $1mm$, and the spool diameter, D, needed to be larger than $17.8mm$. The length of the spool $l < 12.7cm$ and the spool/bore clearance $c > 12.7\mu m$ were also constrained. The spool outlet area, A_{out}, was constrained to be less than $200mm^2$, and

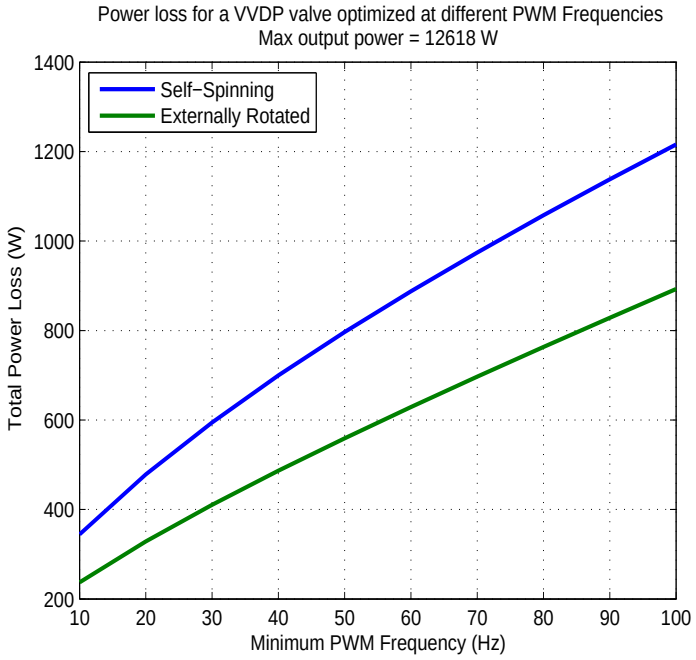

Figure 4.7: Total power loss for a self-spinning and an externally rotated 3-way valve at different PWM frequencies

the width of the land at the end of the spool, l_{end}, was constrained to be larger than $1.6mm$ to maintain structural strength.

With the numerical parameters and constraints defined, the design optimization for the valve could be performed. Figure 4.7 shows the optimal results for both the self-spinning and externally rotated designs with different minimum frequency bounds. For this study, there were $N = 3$ PWM sections on the valve, which is the desired value from a mechanical balancing perspective. From these results, it is clear that increasing the PWM frequency significantly increases the power loss, which agrees with the results in chapter 2. It is also clear that the externally rotated spool has a significant efficiency benefit over the self-spinning design. However, this does not account for any inefficiency in the external rotary actuator. Figure 4.8 provides some detail on why the externally rotated design has lower power losses.

In Fig. 4.8, the five different losses are shown for both the self-spinning and the externally rotated cases. Note that these results are for the valve optimized at each

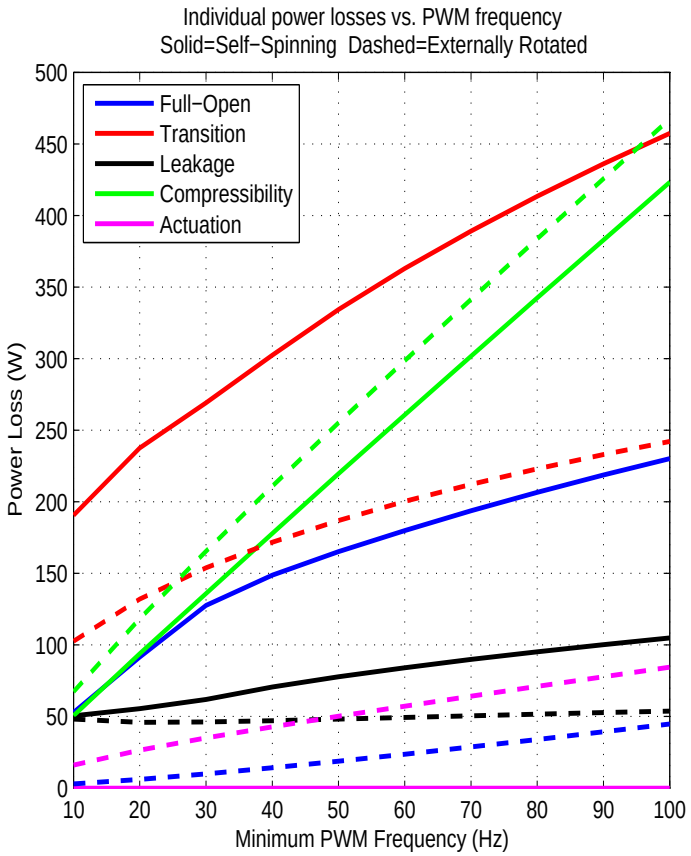

Figure 4.8: Individual power losses for a self-spinning (solid lines) and an externally rotated (dashed lines) 3-way valve at different PWM frequencies

PWM frequency, not a single design being driven across the frequency range. While all of the losses increase with the PWM frequency, the effect is particularly pronounced in the compressibility loss. The self-spinning design has a lower compressibility loss and no additional actuation power is required. However, the externally rotated case has much lower transition and full-open losses, and slightly lower leakage. To see what is causing the difference in the losses, the optimal design parameters are shown in Figs. 4.9 and 4.10.

Both the self-spinning and externally rotated designs have a decreasing optimal diameter as the frequency is increased, likely due to the fact that the compressibility loss increases with diameter. The length of the externally rotated spool is at the maximum allowed value across the frequency range, but this is not the case for the self-spinning case. In order to decrease the full-open and transition losses, a larger open area is desired, which can come from increasing the diameter or the length of the spool. However, increasing the diameter incurs a penalty in the compressibility loss. In the self-spinning case, increasing the length also increases the frictional torque that must be overcome, and at higher frequencies, a smaller length is needed to satisfy the self-spinning constraint (Eq. (4.24)). This constraint also drives an increase in the clearance, which results in an increase in leakage. The requirement to generate sufficient torque to spin the spool be capturing fluid momentum in the inlet and outlet turbines also drives the self-spinning design to have a small outlet area to generate actuation torque from the outlet turbine. In the externally rotated case, the optimal outlet area is at its maximum value, since that torque is not needed to spin the valve. Clearly, while it simplifies the packaging of the valve, the self-spinning feature drives an increase in the power loss in the three-way valve enabled VVDP. It is interesting to note that, in both cases, the constraint requiring $\kappa \leq 1$ (Eq. (4.28)) is always active, meaning that the optimal value of κ is one for both designs. Thus, the optimal valve is always in transition, which is achieved by having as large of an inlet orifice as possible.

Another design choice to study is the number of PWM sections arrayed around the valve spool. Increasing the number of sections decreases the angular frequency of the valve needed to achieve the specified PWM frequency requirement. However, it also tends to increase the size and leakage of the spool. Figure 4.11 shows the total power loss for optimal self-spinning and externally rotated valves with different numbers of

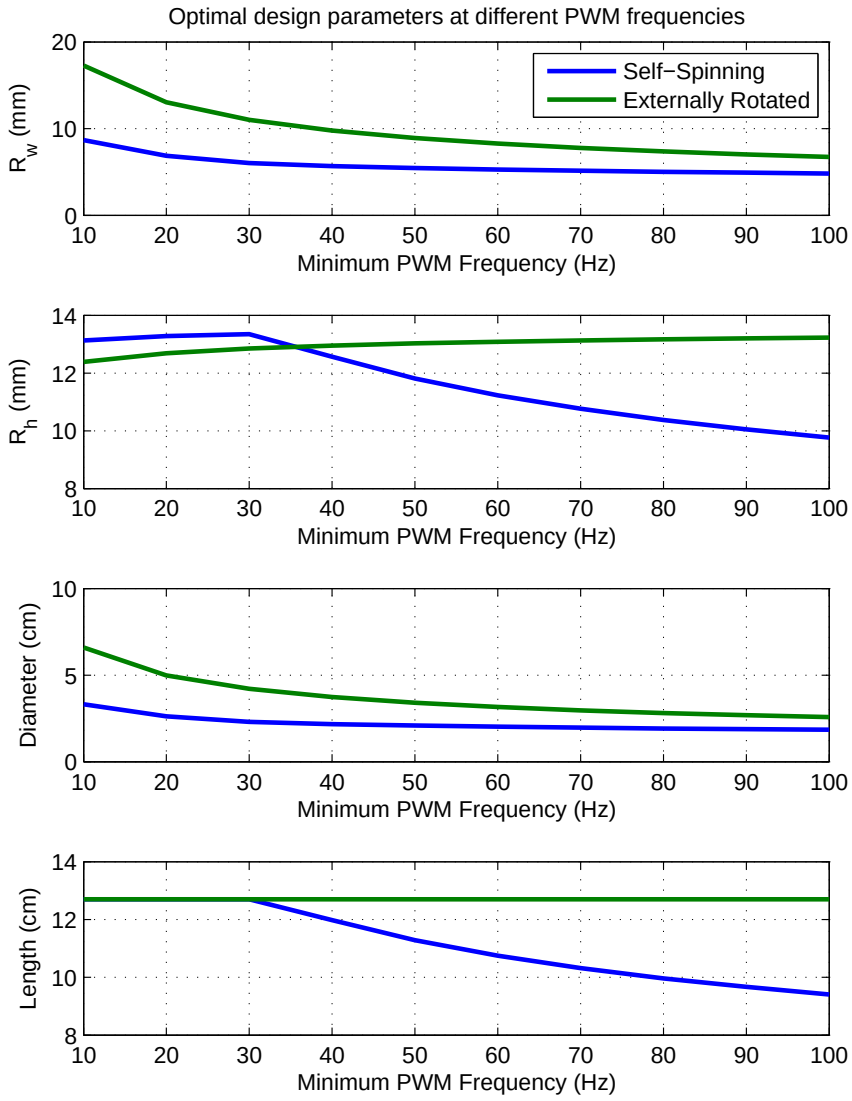

Figure 4.9: Optimal orifice width, height, spool diameter and length for a self-spinning and an externally rotated 3-way valve

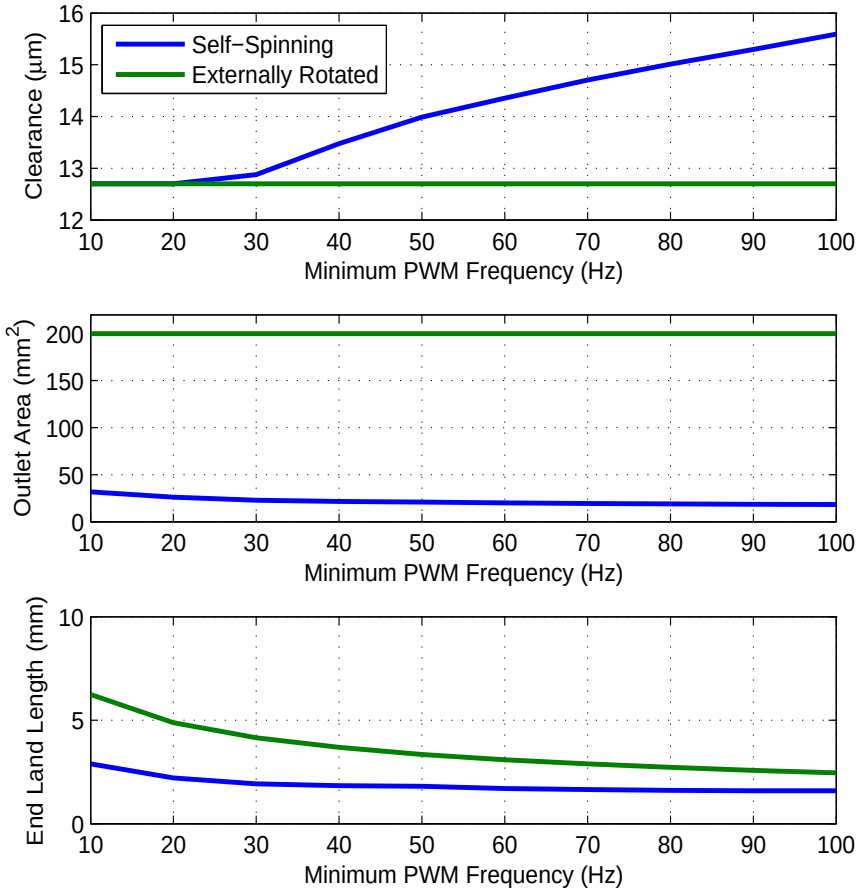

Figure 4.10: Optimal clearance, outlet area, and end land length for a self-spinning and an externally rotated 3-way valve

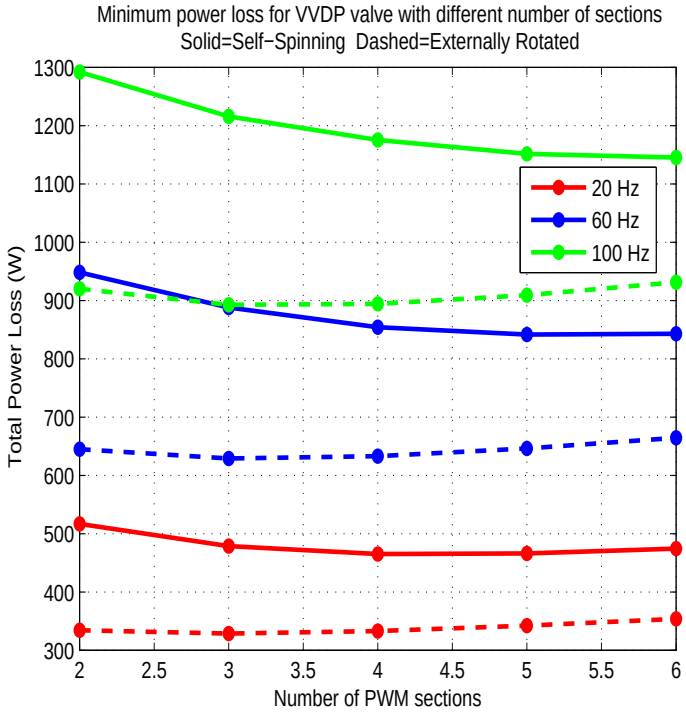

Figure 4.11: Total power losses for a self-spinning (solid lines) and an externally rotated (dashed lines) 3-way valve with different number of PWM sections

sections being driven at three different frequencies. From the figure, it is clear that the number of sections has little effect on the overall loss for the externally rotated case. For the self-spinning case, increasing the number of sections does reduce the overall loss, particularly at high frequencies. This makes some intuitive sense since increasing the number of sections decreases the angular frequency requirement on the valve spool, which helps relax the self-spinning constraint (Eq. (4.24)). When designing a self-spinning valve, a determination must be made whether the reduced power loss is worth the increased manufacturing complexity of adding additional PWM sections.

The previous figures were all generated for a VVDP running at a flow rate of $37.85 lpm$. Figure 4.12 shows the power loss in an optimal valve at different flow rates and frequencies. Clearly, as the flow rate increases, the power loss increases for both the externally rotated and the self-spinning designs. However, since the power flowing through the valve increases with flow, the efficiency of the device does not necessarily

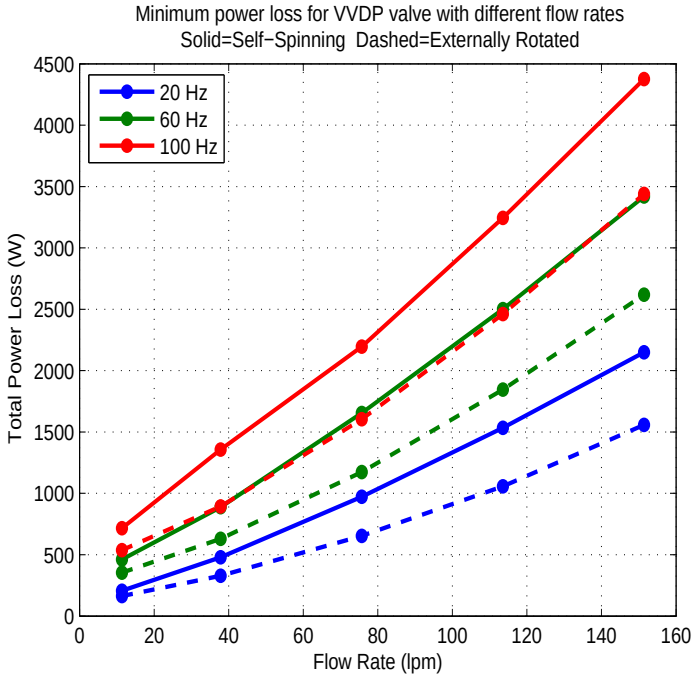

Figure 4.12: Total power losses for a self-spinning (solid lines) and an externally rotated (dashed lines) 3-way valve with different flow rates

decrease as the flow rate is increased.

In Fig. 4.13 the total power loss is normalized by the maximum output power through the valve. In this figure, it is clear that at medium to high flow rates, the power loss increases at roughly the same rate as the power through the valve. At lower flow rates, the power loss is a larger fraction of the total output power, especially at higher frequencies. It is important to note that these results are for valves optimized for every flow rate for which a data point is shown; they do not represent using the same valve design at different flow rates. To design a valve that is optimal for a range of flow rates would require a desired duty cycle to be specified. In a VVDP, the valve is coupled with a fixed displacement pump, which, if it is driven at a constant speed, is a constant flow source. For a VVDM or VVDPM, where the valve is coupled with a motor, the typical use case is for the flow rate through the valve to depend on a varying motor speed requirement. In the next section, the design of a VVDPM that is optimized for a

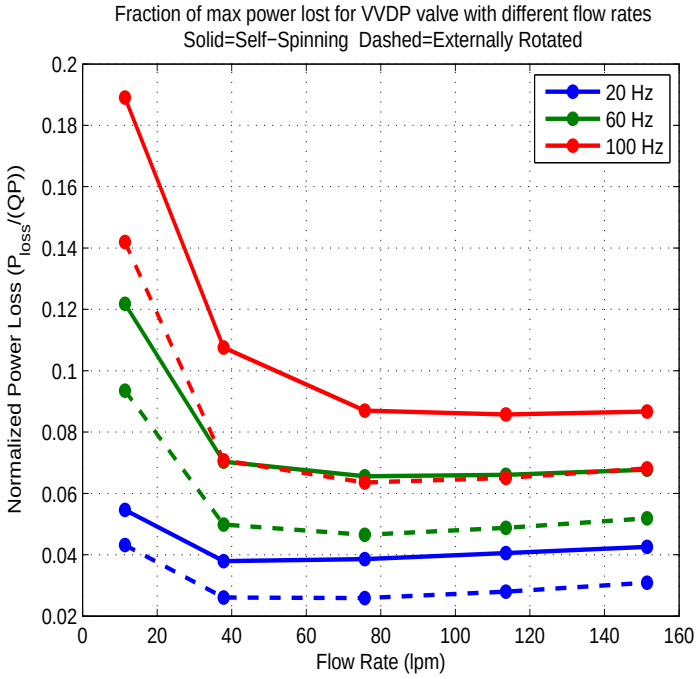

Figure 4.13: Total power losses for a self-spinning (solid lines) and an externally rotated (dashed lines) 3-way valve with different flow rates

specific application and duty cycle is presented.

4.4 Rotary Valve Enabled VVDPM

In this section, the concept of using a two degree-of-freedom on/off valve to create a variable hydraulic pump is extended to the pump/motor case. In the previous section, the 3-way valve created a Virtually Variable Displacement Pump (VVDP). Figure 4.14 shows a circuit that uses a 4-way rotary valve and two directional control valves to create a Virtually Variable Displacement Pump/Motor (VVDPM). This circuit creates a four-quadrant pump/motor, meaning it can function as a pump or a motor in either direction of rotation of the shaft. With the ability to act as a pump or a motor, this circuit can be used in more applications than a VVDP. One example application that is described in this section is a hydraulic hybrid vehicle, which requires a device that can produce or absorb hydraulic power, depending on the driving conditions and the

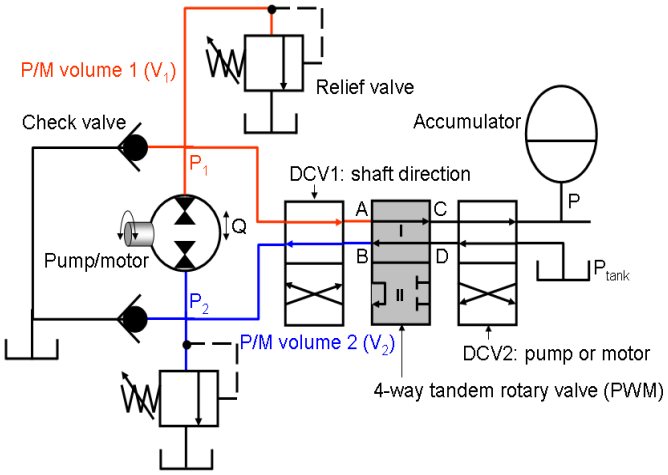

Figure 4.14: Hydraulic circuit of a Virtually Variable Displacement Pump/Motor

state of the hybrid system. This circuit uses an on/off valve to turn a fixed-displacement pump/motor into a variable displacement pump/motor by switching between two states: one port connected to pressure and the other to tank (on), or both ports connected together (off).

As shown in Fig. 4.14, Directional Control Valve (DCV) 1 controls the direction of flow through the valve. For a valve spool that is designed to be self-spinning, the turbines are only effective at capturing momentum from the fluid if it flows in one direction through the valve. Thus, if the angular velocity of the pump/motor shaft changes directions, DCV1 must be switched to maintain a consistent flow direction through the valve. This is only a requirement for a self-spinning valve; an externally rotated valve would not need DCV1. The second directional control valve, DCV2, is needed for both the self-spinning and externally rotated designs. This DCV controls which port of the pump/motor is connected to high pressure in the on state, and which is connected to tank. If the fluid out of the pump/motor is flowing toward the high-pressure accumulator, then the VVDPM is in pumping mode; otherwise it is in motoring mode.

It is clear from Fig. 4.14 that the rotary valve spool needed to create a VVDPM is different than the 3-way valve spool described in section 4.1. The VVDPM valve spool has two ports that connect to the fixed-displacement pump/motor: a pressure

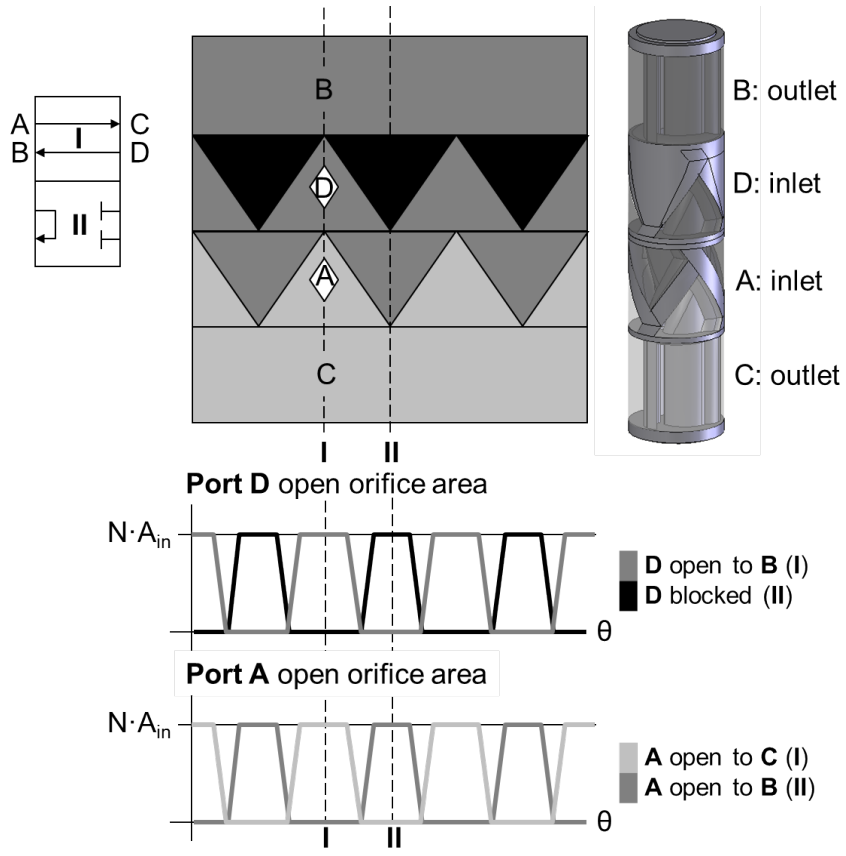

Figure 4.15: 4-way valve spool used to create a VVDPM [88]

port, and a tank port. In the on state, each pump/motor port is connected to either pressure or tank. In the off state, the two pump/motor ports are connected to each other, allowing the device to freewheel. When the pump/motor is freewheeling, the pressure and tank ports on the valve spool are blocked. Figure 4.15 depicts a valve spool that can accomplish this functionality.

The 4-way valve shown in Fig. 4.15 has four sections corresponding to the four ports on the valve. The inlet and outlet labels apply for a self-spinning valve since the flow direction must be constant in that case. The upper section of the spool (B) contains an outlet turbine, and it is connected to one of the pump/motor ports. The second section from the top (D) is either connected to high pressure or tank, depending on the state of DCV2. This section contains an inlet turbine, and it is partitioned into

two halves, a set of solid triangular sections on top to block flow, and a set of open triangular sections below that are connected to section B through the middle of the spool. The third section from the top (A) contains another inlet turbine and is also partitioned into upper and lower triangular sections. The lower triangular sections are connected through the middle of the spool to the bottom section (C). The upper triangular sections are connected through the center of the spool to the lower triangular sections of section D, which are also connected to the upper section, B. Thus, there is a connection between three sections of the spool, but due to the timing of the triangular sections, only two sections at a time are connected in either the on or off state. As shown in Fig. 4.15, in the on state, the inlets in sections D and A are over the lower triangular sections, meaning that D is connected to B and A is connected to C. As the valve rotates to the freewheeling state, both inlets transition to the upper triangular sections simultaneously, blocking the inlet over D, connecting sections A and B, and leaving C disconnected from any other section. A detailed description of this valve, along with a different configuration designed to achieve the same functionality are described in [88].

As with the three-way valve in the previous section, the design of this valve involves a number of tradeoffs and constraints that must be balanced. In order to design an optimal valve, the design problem is formulated as a constrained energy loss minimization problem.

4.5 VVDPM Design Optimization Formulation

Many of the design variables and tradeoffs that exist for the three-way valve must also be considered for the four-way valve. However, there is one significant difference in the design approach for the VVDPM. In the VVDP case, the valve was assumed to be operating with a constant flow rate and load pressure, which is a feasible application for a VVDP. However, for a device that can be either a pump or a motor, the assumption of a fixed flowrate and load pressure is much less likely to reflect a realistic application. Thus some duty cycle must be defined for the VVDPM to specify the pressure and flow demands on the valve. This duty cycle can also be specified in terms of torque and speed on the pump/motor shaft.

One possible duty cycle would be to generate a grid of torque and speed demands

that cover a specified range, and give every point in the grid an equal weight. This could be an approach for a device if there is no knowledge about the final application. However, this VVDPM was developed in conjunction with another project aimed at creating a hydraulic hybrid passenger vehicle [89]. Thus, the valve duty cycle can be specified in terms of the speed and torque demands on a pump/motor in a hydraulic hybrid vehicle that is following its own specified duty cycle.

Figure 4.16 shows a schematic for a Hydraulic Hybrid Passenger Vehicle (HHPV). The architecture shown here is known as an input-coupled power split transmission, and it uses a planetary gear to combine a mechanical and a hydraulic power path between the engine and the wheels. The hydraulic power path allows an accumulator to be used to capture braking energy to be re-used. It also provides flexibility to allow the engine to be run in a higher efficiency region than is possible when only the mechanical path is present. For more information on the design of the HHPV see [89, 90]. In this transmission architecture, there are two pump/motors that could be implemented as a VVDPM: one that is coupled to the engine output shaft (shown as 2 tandem pump/motors in Fig. 4.16), and one that is coupled to the wheels through a planetary gear set. For the example described in this chapter, an optimal design will be derived for a VVDPM that is to be used as the wheel pump/motor of the HHPV. The torque and speed requirements for the wheel motor can be determined by specifying a drive cycle for the HHPV, as well as an energy management strategy to determine the power flowing into and out of the accumulator at each point in the drive cycle [91]. In [91], an optimization procedure is described that takes into account the parameters of the HHPV, the desired drive cycle, and the efficiency of known hydraulic components. The VVDPM described in this section was designed as a replacement for a conventional variable displacement pump motor at the wheels of the HHPV. Thus, the VVDPM must operate over the same duty cycle as the conventional pump/motor when the optimization process in [91] is applied.

With a duty cycle for the VVDPM determined, an optimization problem can be formulated to minimize the total energy lost in the VVDPM as the vehicle drives through its drive cycle.

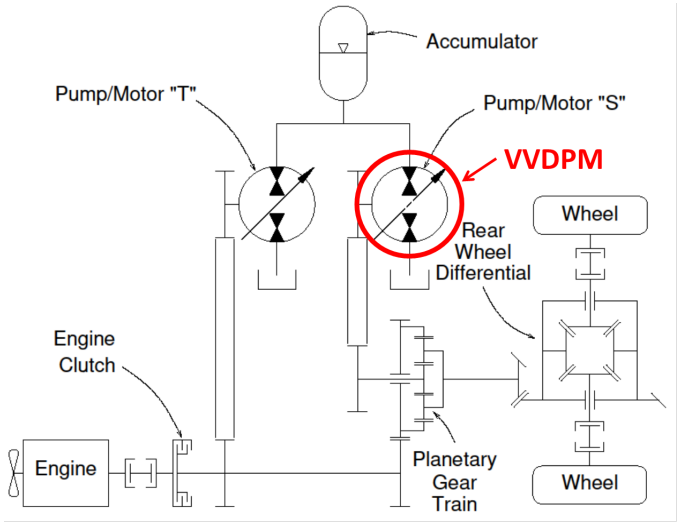

Figure 4.16: Sketch of a transmission for a Hydraulic Hybrid Passenger Vehicle with a VVDPM as a wheel pump/motor

$$\min_{\mathbf{x}} \int_{cycle} \left(L_{full-open} + L_{compress} + L_{leakage} + L_{transition} + L_{actuation}\right) dt$$

$$\begin{aligned} \text{s.t. } & c_1(\mathbf{x}) \leq 0 \\ & c_2(\mathbf{x}) \leq 0 \\ & c_3(\mathbf{x}) \leq 0 \\ & c_4(\mathbf{x}) = 0 \\ & x_{i,min} \leq x_i \leq x_{i,max} \text{ for } 1 \leq i \leq 10 \end{aligned} \tag{4.30}$$

The vector $\mathbf{x} = [R_w,\ R_h,\ D,\ l,\ c,\ N,\ A_{out},\ l_{end},\ D_d,\ r]$ contains the optimization parameters for the 4-way valve, with new optimization parameters, D_d and r. The new parameter D_d refers to the cross-sectional diameter of the inlet and outlet rails that surround the inlet and outlet sections of the valve spool. With this parameter, there is a trade off between the throttling of the fluid through the rail and the compressible loss that is associated with a larger volume on the inlet. For a VVDP with a constant flow rate, the optimal rail diameter can be easily calculated, so it was not included in the

previous section. However, with a variable flow rate through the valve, the optimal point is not as easy to find, so it is included in the optimization for the VVDPM. The variable, r, is a gear ratio between the planetary gear and the shaft of the VVDPM. Changing this ratio has a similar effect to changing the displacement of the fixed displacement pump/motor. However, for the prototype to be constructed from this design, only one displacement is available, so adding a gear reduction is the simplest way to gain the needed flexibility. If a full range of fixed pump/motor displacements are available to select from, then the gear ratio r could be replaced by the displacement value.

The design problem formulation for the VVDPM is similar to the VVDP, except that it is minimizing the entire energy loss rather than the instantaneous power loss. The first three constraint functions are similar to the VVDP example, with $c_1(\mathbf{x})$ enforcing a minimum PWM frequency, $c_2(\mathbf{x})$ ensuring that the transition fraction is ≤ 1, and $c_3(\mathbf{x})$ constraining the geometry of the inlet orifice to have the same angle and width, which ensures that there is no connection from supply to tank. The VVDPM case also has an additional inequality constraint, $c_4(\mathbf{x})$, that is related to ensuring that the VVDPM can achieve the maximum torque required by the duty cycle. This constraint places limits on the gear ratio, r, and is described in section 4.5.6.

The duty cycle from the HHPV specifies a required shaft torque, T, and speed, ω, at the planetary gear input. From these values, the flow through the valve, operating mode (pump or motor), and duty ratio setting for the valve, s, can be determined. The flow through the valve is given by:

$$Q = \left| \frac{D_0 \omega r}{2\pi} \right| \tag{4.31}$$

where D_0 is the displacement of the fixed pump/motor. The duty ratio for the valve is determined by the torque demand, and the operating mode of the VVDPM is determined from the sign of the power flowing through it:

$$s = \begin{cases} s_m = \left| \frac{2\pi T}{P D_0 r} \right| & \text{if } \omega T > 0 \\ 0 & \text{if } \omega T = 0 \\ s_p = -\left| \frac{2\pi T}{P D_0 r} \right| & \text{if } \omega T < 0 \end{cases} \tag{4.32}$$

where s_m is the duty ratio when the VVDPM is in motoring mode, and s_p is the duty

ratio when the VVDPM is in pumping mode. For the sign conventions used to define T and ω, motoring results when positive power is flowing through the VVDPM, and negative power results in pumping.

The total energy lost is comprised of the losses due to full-open throttling, compressibility, leakage, transition throttling, and actuation power, which are described in sections 4.5.1 through 4.5.5, and the constraints on the design are described in section 4.5.6.

4.5.1 Full-Open Loss

For the 4-way case, the full-open loss is given by Eq. (4.33).

$$L_{full-open} = (1 + |s|)\left((1 - \kappa)\, QP_{in} + QP_{out} + QP_{spool} + QP_{rail}\right) \tag{4.33}$$

Note that $s \in [-1, 0]$ for pump mode and $s \in [0, 1]$ for motor mode. The $(1 + |s|)$ coefficient is a result of the fact that, in the 4-way design, there can be either 1 or 2 flow paths through the spool, depending on whether the valve is off (freewheeling) or on. κ, the fraction of the rotation that the valve spends in transition is the same as for the VVDP, and is defined in Eq. (4.6). P_{in} and P_{out} are computed using the orifice equation (Eq. (4.3)), and P_{spool} is computed from Eq. (4.4), with n_{spool}, m_{spool}, and k_{spool} determined from CFD analysis of the spool geometry. The pressure drop across the inlet rail, P_{rail} is also included in this equation. The pressure drop through this rail is a function of the rail diameter, which is included as an optimization parameter for the VVDPM. The pressure drop in this rail is approximated by the orifice equation:

$$P_{rail} = \frac{\rho Q^2}{2\left(c_d \frac{\pi}{4} D_d^2\right)^2} \tag{4.34}$$

4.5.2 Compressibility Loss

Unlike the 3-way valve case, the 4-way valve does not connect pressurized fluid in the inlet volume directly to the tank when it switches. Instead, it connects the two sides of the pump/motor together for freewheeling mode. Thus, one side of the pump/motor transitions between the accumulator pressure and some mid-point pressure, P_{fw}, and the other side transitions between P_{fw} and the tank pressure. The compressibility loss

is then only a result of the pressure falling from P_{fw} to tank. The high pressure fluid in one chamber will raise the pressure of the fluid in the other chamber when the two are connected in the freewheeling mode. Thus, the freewheeling pressure can be computed by assuming the energy lost from the high pressure side is equal to the energy gained by the low pressure side.

$$V_1 \int_{P_{fw}}^{P} \frac{p_1}{\beta\left(p1\right)} dp_1 = V_2 \int_{0}^{P_{fw}} \frac{p_2}{\beta\left(p2\right)} dp_2 \tag{4.35}$$

where V_1 and V_2 are the volumes on either side of the pump/motor. This equation can be solved numerically using the equations described in section 2.3.2. However, due to the large number of function iterations required in the optimization process, an approximation using a constant bulk modulus value may be desirable to reduce computation time. With a constant bulk modulus, Eq. (4.35) reduces to:

$$P_{fw} = \frac{P}{\sqrt{1 + \frac{V_2}{V_1}}} \tag{4.36}$$

Figure 4.17 shows the freewheeling pressure computed by both numerically solving Eq. (4.35) and the approximation in Eq. (4.36). Notice that the freewheeling pressure is greater than half of the load pressure when the volumes are equal. This indicates that the rate of energy loss as a high pressure fluid is decompressed is higher than the rate that energy is gained as a low pressure fluid is compressed. This agrees with Fig. 2.5, which shows an increasing slope as the pressure is increased.

The two fluid volumes on either side of the pump/motor are different, and change depending on whether the system is in pump or motor mode. If the system is in motor mode, the volumes are given by:

$$\begin{aligned} V_1 =& \frac{\left(D + D_d\right)\pi^2 D_d^2}{4} + V_{spool} + V_{in} \\ V_2 =& \frac{\left(N-1\right)\left(D + 2l_n + D_d\right)\pi^2 D_d^2}{4N} + NV_n + V_{in} \end{aligned} \tag{4.37}$$

For the pump case, V_1 and V_2 are switched. This equation assumes that the inlet and outlet rails have the same diameter, D_d. V_{spool} is the volume inside the tandem center

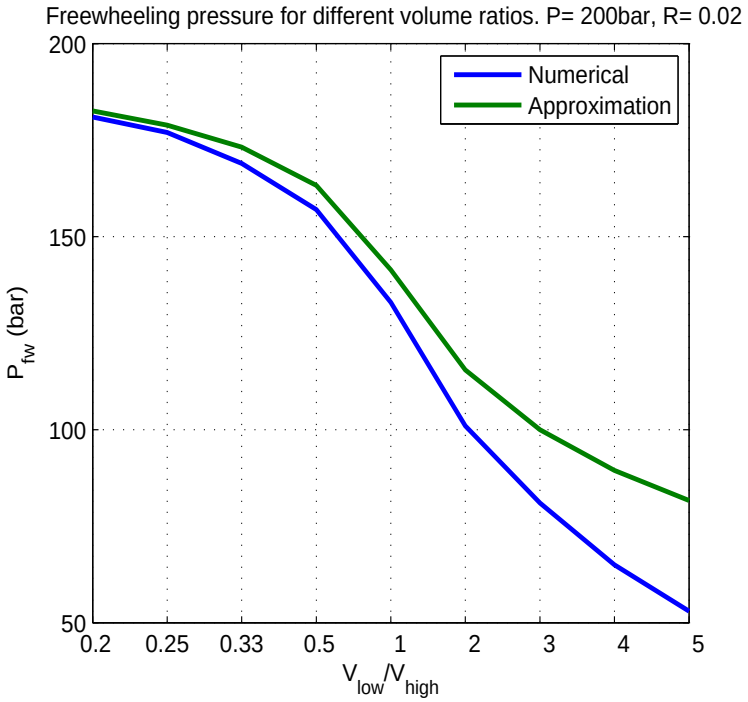

Figure 4.17: Freewheeling pressures computed from numerically solving Eq. (4.35) and by approximation in Eq. (4.36)

sections of the spool (sections B, D, and the upper half of A in Fig. 4.15). V_{in} is the volume in the lines connecting the valve to the pump/motor.

The energy lost due to compressibility is computed using the following equation:

$$L_{compress} = \frac{V_1 P_{fw}^2 N\omega}{4\beta_{eq}\pi} \tag{4.38}$$

where, similar to Eq. (4.9), the bulk modulus is represented by an equivalent bulk modulus that results from estimating the energy needed to compress oil up to P_{fw}. To be exact, β_{eq} would need to be recomputed for each P_{fw}, but a constant value can be used as an approximation. If Eq. (4.36) is used to compute the freewheeling pressure, then the compressibility loss becomes:

$$L_{compress} = \frac{V_1 V_2 P^2 N\omega}{4\beta_{eq}\pi\left(V_1 + V_2\right)} \tag{4.39}$$

4.5.3 Leakage Loss

The 4-way valve has the same 2 leakage paths that the 3-way valve has; across the helical barrier and across the high pressure end of the spool. The difference is that, rather than having constant pressures driving the leakage, the pressure alternates between P and P_{fw}. The fraction of on/off time is the duty ratio, and s can be used to determine the cycle-average leakage. Equations (4.40) and (4.41) give the leakage in the 4-way valve for the pump and motor modes.

$$\begin{aligned} L_{leak,p} = &\frac{N\left(2l_t - R_h\right)c^3\left(-s_p P^2 + (1+s_p)(P - P_{fw})^2\right)}{12\mu R_w \sin^2(\phi)} \\ &+ \frac{\pi D c^3\left(-s_p\left(P\right)^2 + \left(1+s_p\right)\left(P - P_{fw}\right)^2\right)}{12\mu l_{end}} \end{aligned} \tag{4.40}$$

$$\begin{aligned} L_{leak,m} = &\frac{N\left(2l_t - R_h\right)c^3\left(s_m P^2 + (1-s_m)P_{fw}^2\right)}{12\mu R_w \sin^2(\phi)} \\ &+ \frac{\pi D c^3\left(s_m\left(P\right)^2 + \left(1-s_m\right)\left(P_{fw}\right)^2\right)}{12\mu l_{end}} \end{aligned} \tag{4.41}$$

where the spool travel length, l_t, for the 4-way valve is given by:

$$l_t = \frac{l - 2l_{end}}{4} - R_h \tag{4.42}$$

4.5.4 Transition Loss

As the valve spool transitions between the on and off states, the inlet orifices need to close to one flow path and open to another. During this transition, the pressure drop across the valve can be significantly higher than the full-open pressure drop, which results in a higher power loss. In determining the power loss across the valve spool, it is assumed that the flow rate is constant during the transition, and that the oil is incompressible. In reality, the oil is being throttled and compressed/decompressed simultaneously, but as an approximation, the two losses are considered individually. The orifice equation (Eq. (4.3)) is used along with the linear area profiles that result from the rhombus shaped inlet orifices. In the VVDPM, the valve spool either has one or two inlet orifices open, depending on whether the device is freewheeling (off) or powered (on). This is the case for both the pump case and the motor case. In Fig. 4.14, there are check valves and relief valves that are in place to limit the pressure drop across transitioning orifices (the relief valves can also be replaced by check valves to supply). The transition loss equations must take these limiting valves into account. Note that for all transitions, since the fluid is considered incompressible and the orifice area profiles are linear and symmetric, the power loss across a closing orifice is the same as the loss across the same orifice opening. The derivation for the transition loss equations is given in Appendix A. The transition power loss for the pump and motor cases is given by:

$$\begin{aligned} L_{trans,pump} = \frac{\kappa\sqrt{P_{open}}Q}{2}\Bigg[& \frac{P_{c,high} - P_{out} - P_{spool}}{\sqrt{P_{load} + P_{c,high} - P_{spool} - P_{out}}} \\ & + \sqrt{P_{load} + P_{c,high} - P_{spool} - P_{out}} + 2\sqrt{P_{c,high} - P_{out} - P_{spool}} \\ & + 2\sqrt{P_{c,low} - P_{spool} - P_{out}} - 3\sqrt{P_{open}}\Bigg] \end{aligned} \tag{4.43}$$

$$L_{trans,motor} = \frac{\kappa Q\sqrt{P_o}}{2}\left[\sqrt{P-(P_{c,low}+P_{spool}+P_{out})}-3\sqrt{P_o}\right.$$
$$+2\sqrt{P+P_{c,high}-P_{spool}-P_{out}}+\frac{P_{c,high}-P_{spool}-P_{out}}{\sqrt{P+P_{c,high}-P_{spool}-P_{out}}} \quad (4.44)$$
$$\left.+\frac{P-2P_{spool}-2P_{out}}{2\sqrt{P-(P_{c,low}+P_{spool}+P_{out})}}\right]$$

where $P_{c,low}$, and $P_{c,high}$ are the opening pressure of the check valves to low and high pressure. Note that Fig. 4.14 shows relief valves to high pressure instead of check valves. Both configurations will work, but check valves will result in lower loss, so they are assumed in these equations.

4.5.5 Actuation Loss

Like the 3-way spool, the 4-way spool in the VVDPM can either be designed to capture momentum from the fluid and spin itself, or it can be designed to be driven by an external rotary actuator (i.e. an electric motor). If the spool is driven by scavenging power from the fluid, then there is no additional power loss due to the actuation of the spool; any power loss associated with generating the necessary fluid momentum will be taken into account through the full-open pressure drop. However, for a valve that is rotated externally, there is an additional actuation power that must be considered.

The power required to spin the valve is determined by the friction on the valve spool as it rotates. The torque on the valve spool due to friction is given in Eq. (4.20), with the effective area on the spool given by Eq. (4.21). The bearing area, $A_{bearing}$, for the 4-way spool is slightly different than it is for the 3-way spool:

$$A_{bearing} = \pi D\left(R_h + 2l_{end} + \frac{l}{8}\right) \quad (4.45)$$

where the $l/8$ term comes from the solid triangular areas in section D on the spool. The power lost due to spinning the valve against the friction torque is given by:

$$L_{actuation} = T_f\omega = \frac{A_{eff}\mu D^2\omega^2}{4c} \quad (4.46)$$

The remainder of the spool surface area also contributes to the frictional loss on the spool. This is done by multiplying the non-bearing surface area by a parameter, α,

which relates to the shear stress generated by the swirling fluid in the pockets of the valve. This parameter is estimated using CFD analysis [51].

$$A_{eff} = A_{bearing} + \alpha(\pi D l - A_{bearing}) \tag{4.47}$$

4.5.6 Constraints

The constraints on the VVDPM are similar to the VVDP, although there are several differences. The first inequality constraint, $c_1(\mathbf{x}) \leq 0$, is related to a lower bound on the speed of the spool. For a self-spinning valve, the torque generated by the inlet sections (Eq. (4.25)) and the outlet sections (Eq. (4.26)) are the same as in the VVDP case. The only difference for a self-spinning 4-way valve is that this spool can have two inlet and two outlet sections active, or only one of each, depending on whether the valve is on (2) or freewheeling (1).

$$\omega = \frac{(1+|s|)\,\rho Q^2 r_{i,off}\frac{D}{2}}{N\left(\frac{D}{2}\right)^2\left(A_{eff}\frac{\mu}{c} + r_{o,off}^2\rho Q\right)}\left(\frac{1}{A_{in}} + \frac{r_{o,off}}{r_{i,off}A_{out}}\right) \tag{4.48}$$

where Eq. (4.48) is the same as Eq. (4.27) except for the addition of the $(1+|s|)$ term in the numerator. This term accounts for the fact that there is twice as much torque generated by the inlet and outlet turbines when the valve is in the on state.

A key feature of this equation is that the valve speed is proportional to the flow rate squared. Thus, for a variable flow rate application, the valve speed can vary significantly, which results in a variation on the torque ripple applied to the output. This is a significant drawback of the self-spinning approach. It also makes setting a minimum bound on the PWM frequency impossible, unless a minimum bound can also be specified on the flow rate. For the self-spinning case the constraint on the PWM frequency must be changed from the VVDP case to set a lower bound on the average PWM frequency:

$$c_1(\mathbf{x}) = f_{min,mean} - \frac{\omega N}{2\pi} \tag{4.49}$$

where $f_{min,mean}$ is the average PWM frequency across the drive cycle. For the externally rotated case, Eq. (4.24) can be directly applied to set the minimum rotating speed on the valve spool.

The second inequality constraint, $c_2(\mathbf{x}) \leq 0$, is the same as in Eq. (4.28) for the VVDP, which states that $\kappa \leq 1$. This means that the largest fraction of the rotation that the valve can spend in transition is 1.

The third inequality constraint, given by Eq. (4.50), is unique to the VVDPM design problem. Since the valve is being optimized over a range of torque and speed demands, and the gear ratio between the VVDPM shaft and the planetary gearset is a variable, there must be a constraint that ensures that the VVDPM can meet the maximum torque requirement at the specified pressure.

$$c_3(\mathbf{x}) = T_{max} - \frac{PrD_0}{2\pi} \tag{4.50}$$

where τ_{max} is the maximum torque in the duty cycle for the valve. Note that this constraint can be achieved by either changing the gear ratio r, or the pump/motor displacement D_0. For the design example presented here, the displacement is held fixed, but that is not a requirement in all cases.

The final equality constraint, $c_4(\mathbf{x}) = 0$, is the same in the VVDPM case as it is for the VVDP case and is given by Eq. (4.29). This constraint ensures that the angle of the inlet rhombus is the same as the angle of the helical cuts on the valve spool.

With the loss and constraint equations specified, the optimal valve design can be computed. In the next section a numerical example for a VVDPM is presented.

4.6 VVDPM Optimization Results and Design Studies

The design problem formulated in the previous sections can be solved by a variety of optimization software packages. Like the VVDP optimization, the results presented in this section were obtained using the *fmincon* function included in the Matlab Optimization Toolbox. For this design example, either the SQP or Active Set solver was used, depending on which one was faster for a given operating point.

The objective and constraint equations contain a number of constants that are not included as optimization variables. The pressure in the high pressure accumulator was set at a constant $P = 200bar$. The oil density was set at $\rho = 876kg/m^3$, and the viscosity was $\mu = 0.0387m^3/s$, which match values for Mobil DTE 25 oil at $40C$. The discharge coefficient for the orifice equations was $c_d = 0.6$, the volume in the ports connecting

the rotary valve to the pump/motor was $V_{in} = 8cm^3$, the internal fluid volume of the spool was $V_{spool} = 7cm^3$, the length of each nozzle between the inlet rail and the inlet sections of the spool was $l_n = 2cm$, and the volume of each nozzle was $V_n = 0.6cm^3$. The cracking pressures for the check valves between the pump/motor ports and tank and between the motor ports and supply were set for each run to be $6.894kPa$ above the maximum pressure drop across the spool ($P_{in} + P_{spool} + P_{out}$). The factor relating the shear stress on the bearing surface to the shear stress due to oil swirling in the pockets was $\alpha = 0.2$. The CFD-determined parameters for computing the pressure drop across the spool were $k_{spool} = 2.497 \times 10^{-7}$, $m_{spool} = 2$, and $n_{spool} = 3.02$. The inlet turbine and outlet turbine offset distance fractions were $r_{i,off} = 0.79$ and $r_{o,off} = 0.57$.

In order to ensure the optimal design could be feasibly manufactured, the optimization parameters were subject to minimum and maximum limits. The spool diameter needed to be $D \geq 1.27cm$, the spool length had to be $l \leq 12cm$, the clearance between the spool and sleeve had to be $c \geq 13\mu m$, and the area on the outlet sections of the valve needed to be $A_{out} \leq 100cm^2$.

As described in section 4.5, the map of points specifying the torque and speed duty cycle on the VVDPM was generated using a separate optimization procedure for the HHPV transmission. The points are shown in Fig. 4.18.

Figure 4.19(a) shows the total energy loss over the specified duty cycle for the valve. It is clear from this plot that the self-spinning design results in much higher losses than the externally rotated design, especially at higher PWM frequencies. In Fig. 4.19(b), the drive cycle efficiency, which is defined as the total power out divided by the total loss plus the total power out, is plotted. This plot represents the average efficiency over the complete duty cycle specified in Fig. 4.18. Note that the losses used in these plots are only the valve losses described in the previous section; any losses in the fixed-displacement pump/motor that is connected with the valve are not included.

In Fig. 4.21, the overall energy loss is broken down into the individual loss components. Clearly, the throttling through the valve, both transition and full-open, is the dominant source of energy loss for the self-spinning valve. In order to satisfy the frequency constraint in Eq. (4.49), the inlet and outlet orifices must decrease to create more incoming momentum and the diameter must decrease to reduce the bearing area. The leakage is also higher in the self-spinning case because the clearance must

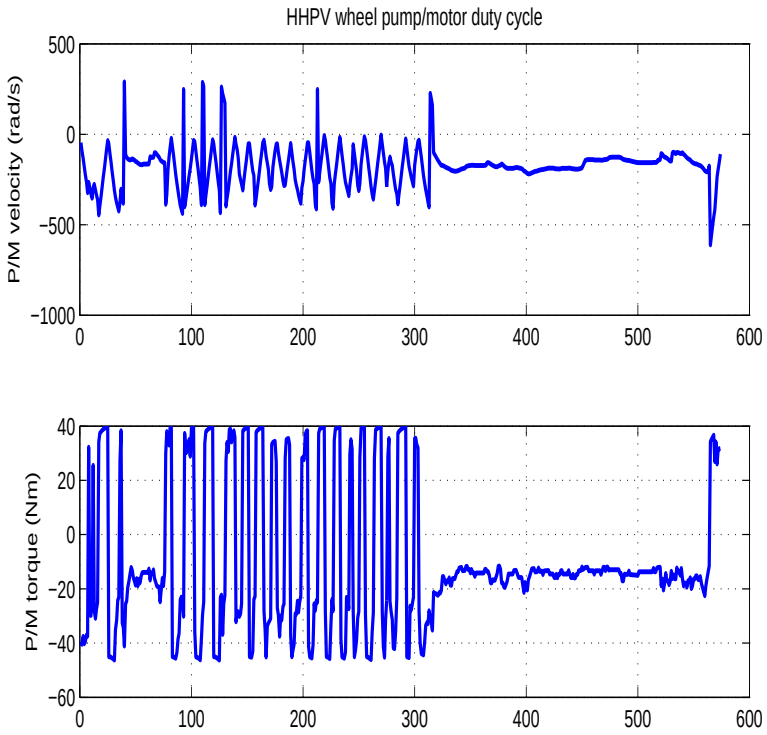

Figure 4.18: Torque and speed profile for which the VVDPM is optimized

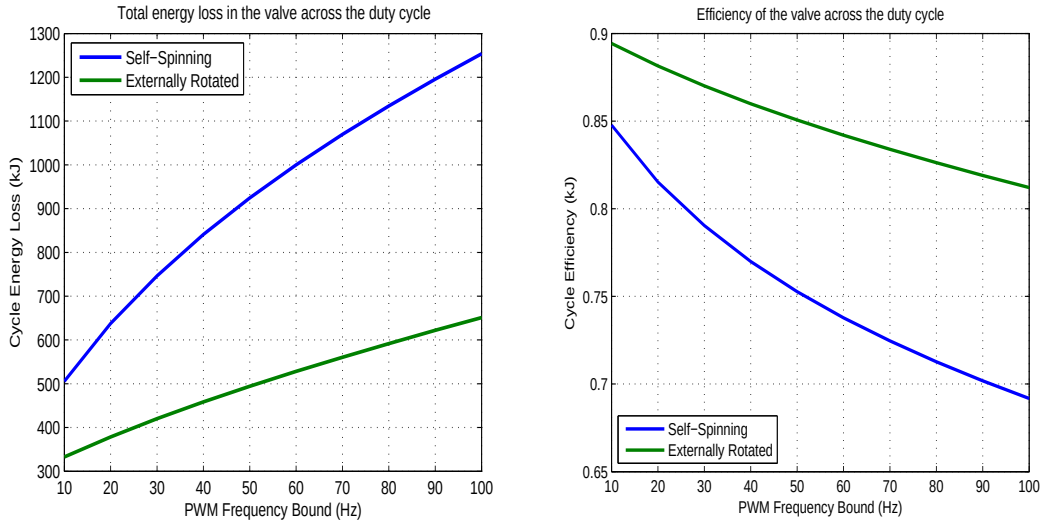

(a) Total energy loss over the drive cycle

(b) Cycle efficiency

Figure 4.19: Total energy loss and cycle efficiency for a VVDPM

increase to reduce the friction on the spool. The elimination of the actuation loss in the self-spinning case is not nearly enough to make up for the increase in the other losses.

Figure 4.20 shows the inlet turbine, outlet turbine, and viscous friction torques on the valve spool for the self-spinning and externally rotated designs. These plots were generated for a valve with a minimum frequency bound of $50Hz$. The externally rotated valve has less torque generated by the turbines, especially the outlet turbine, due to a much larger optimal value for A_{out}. However, the primary difference between the plots is that in the self-spinning case, the frictional torque is much smaller than in the externally rotated case. This highlights the fact that, despite the much larger torque on the spool, the actuation power is not a significant driver of the total power loss. This also indicates that, in order to satisfy the frequency constraint, the optimal self-spinning valve parameters are selected to bring the frictional torque down to a level that can be matched by the torque generated by the inlet and outlet turbines.

Figures 4.22, 4.23, and 4.24 show the optimal parameters for both design cases for a minimum frequency bound of 10 to 100 Hz. Many of the trends for the 4-way valve are the same as for the 3-way valve. As the PWM frequency increases, the optimal valve has a narrower spool and inlet orifice and a shorter end land. The end land decreases because

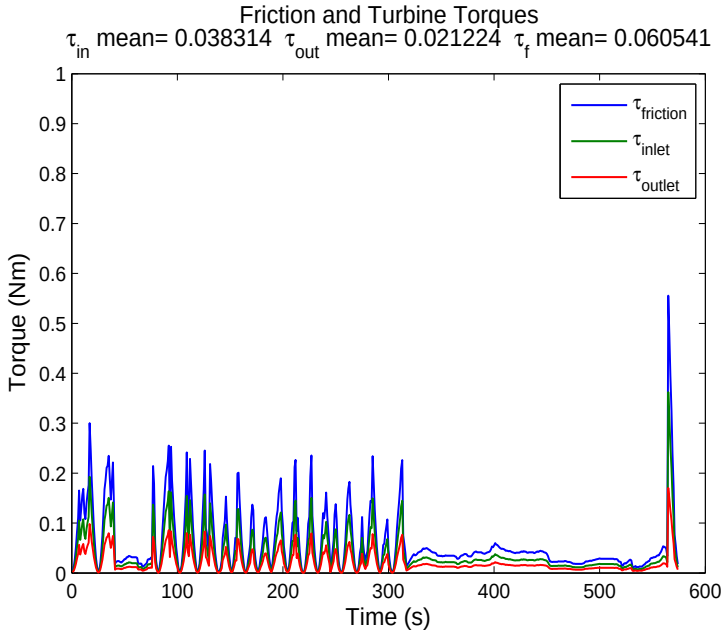

(a) Self-spinning valve

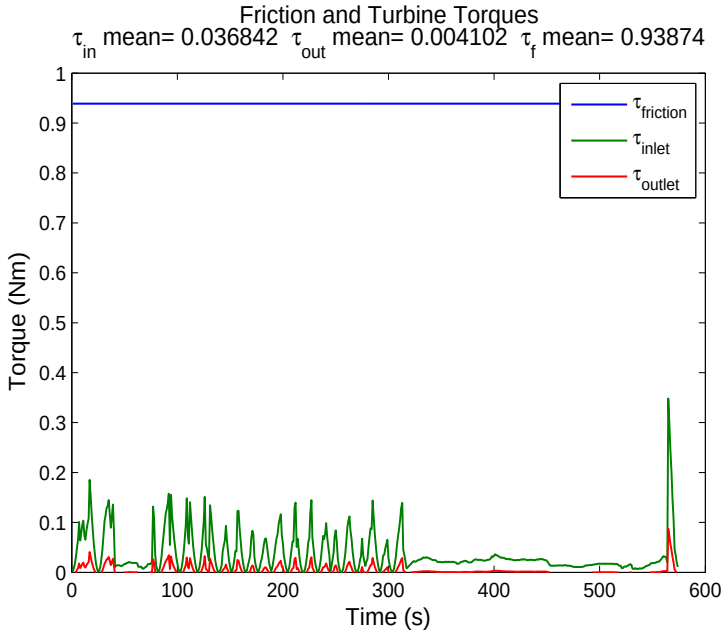

(b) Externally rotated valve

Figure 4.20: Turbine and friction torques on the valve spool

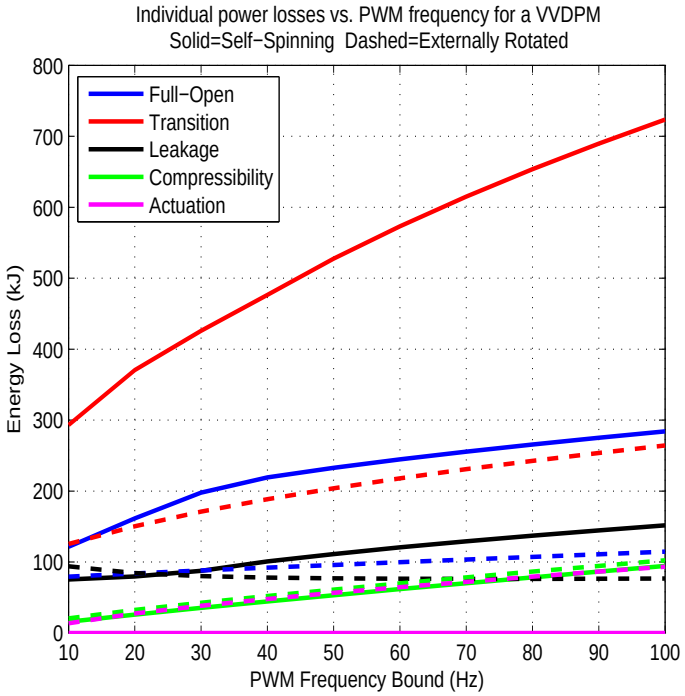

Figure 4.21: Individual energy losses over the duty cycle for a VVDPM

the increased friction on the spool becomes a larger loss in relation to the leakage. For an externally rotated design, the length and the outlet area are always maximized and the clearance is always minimized. This indicates that the effect of the clearance on reducing the friction is less significant than the effect it has on increasing the leakage. The rail diameter also decreases as the PWM frequency increases, indicating that reducing the compressibility loss becomes more important than reducing the full-open loss.

In Fig. 4.18, the largest magnitude torque demand is $T = -46.3Nm$. Using this value in Eq. (4.50), the smallest gear ratio between the VVDPM and the rest of the transmission that will satisfy the max torque constraint at $P = 200bar$ is $r = 1.4545$, which is the optimal value in both cases for all frequencies. Thus, the optimal VVDPM will have the smallest gear ratio, or equivalently the smallest displacement, that can still meet the maximum required torque demand.

The self-spinning design clearly results in significantly higher energy loss when compared with the externally rotated design, and it also has a disadvantage in the variability of the PWM frequency. The constraint equation, $c_1(\mathbf{x})$ (Eq. (4.49)), constrains the PWM frequency for the externally rotated case, but it constrains the *average* PWM frequency in the self-spinning case. Since the PWM frequency is proportional to the flow rate though the valve squared, the valve can be spinning very slowly when the VVDPM is at low speeds, and extremely fast at high speeds. This results in a large torque ripple at low speeds, and a variable noise characteristic.

Although N, the number of sections, is listed as an optimization parameter, since only integer values are valid, it is held constant for the optimization process. The previous results were all achieved with $N = 3$ PWM sections on the valve, which is attractive from a spool balancing perspective. Figure 4.25 shows the total energy loss for both the self-spinning and externally rotated designs for a valve with 2, 3, 4, 5, or 6 PWM sections. A valve with one section would be unbalanced, and more than six would be very difficult to manufacture. The plot shows that increasing the number of sections decreases the energy loss, although the effect is very small for the externally rotated case. For the self-spinning case, the effect of adding PWM sections is greater, particularly at higher frequencies. This makes intuitive sense; for the externally rotated case, increasing the PWM sections slows down the spool and decreases the actuation loss, but it also increases the leakage perimeter. As both of these losses are relatively

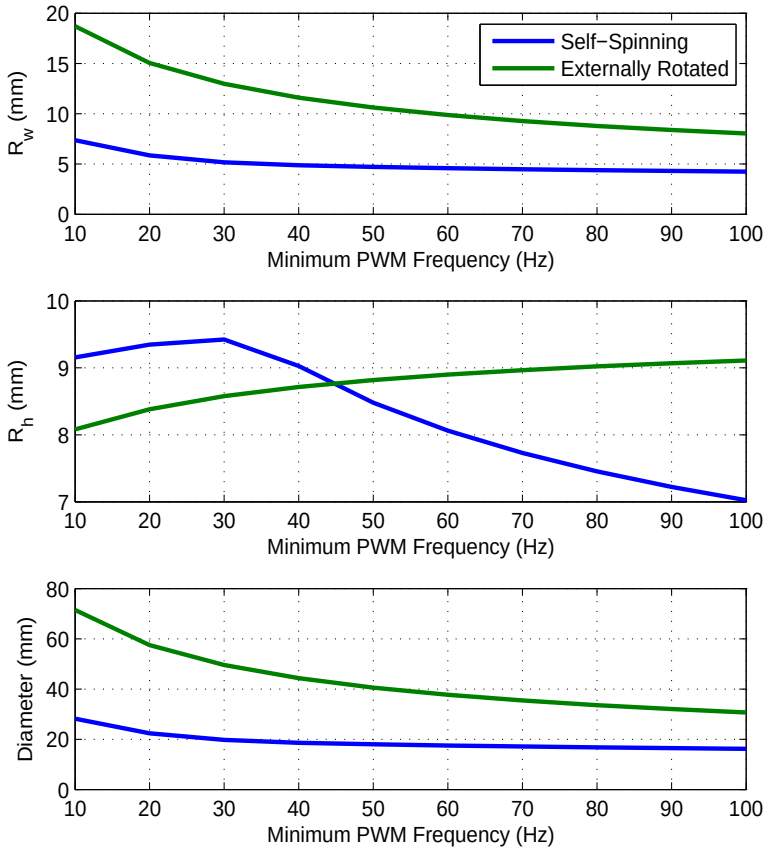

Figure 4.22: Optimal VVDPM parameters: Orifice width, orifice height, and spool diameter

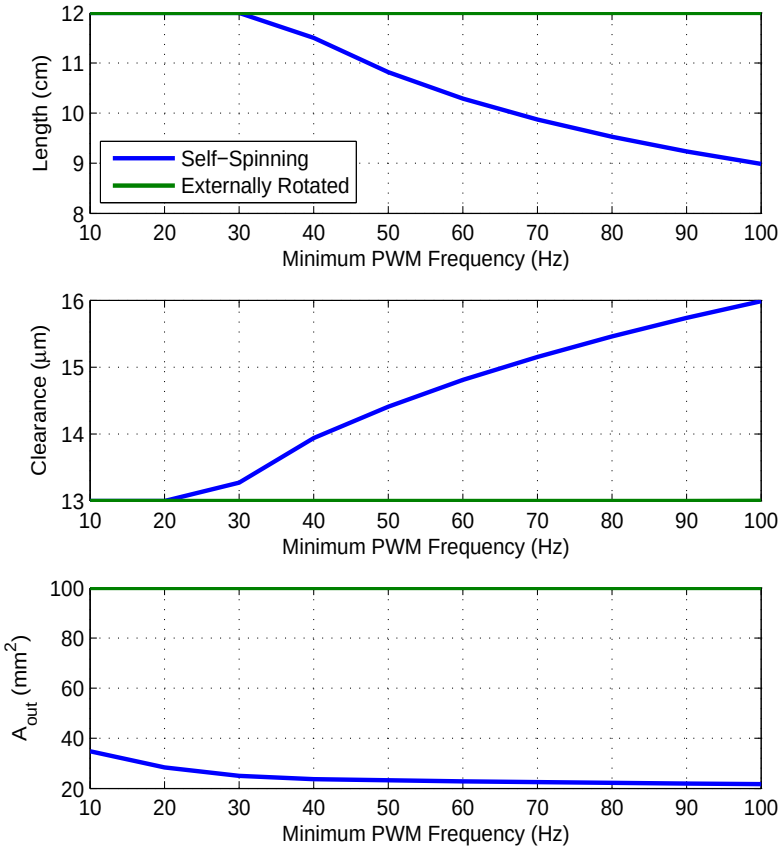

Figure 4.23: Optimal VVDPM parameters: Spool length, clearance, and outlet area

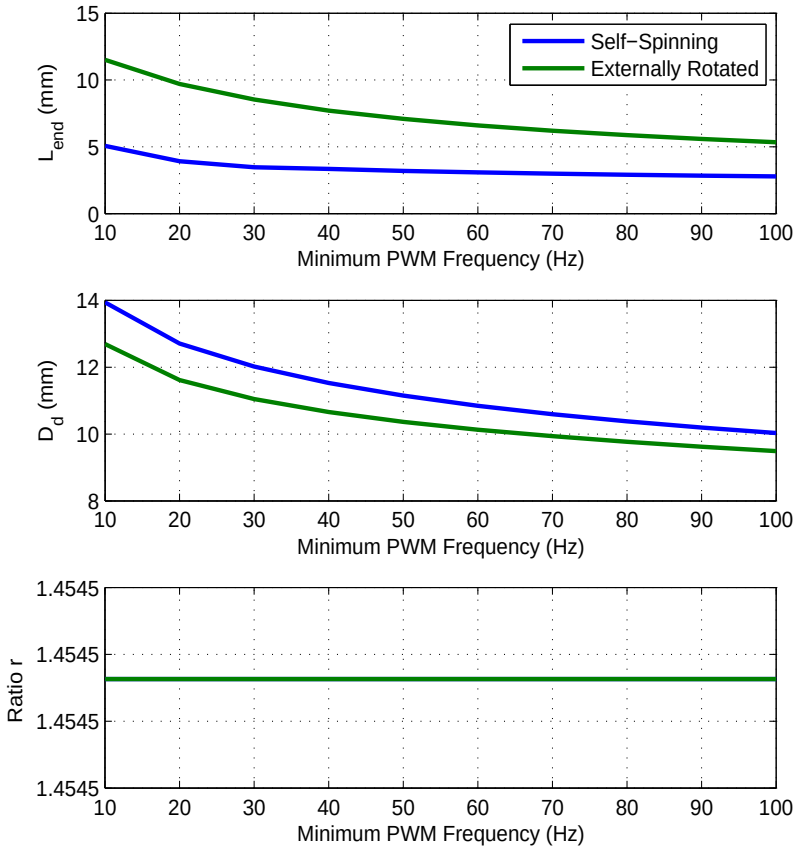

Figure 4.24: Optimal VVDPM parameters: End land length, rail diameter, and gear ratio

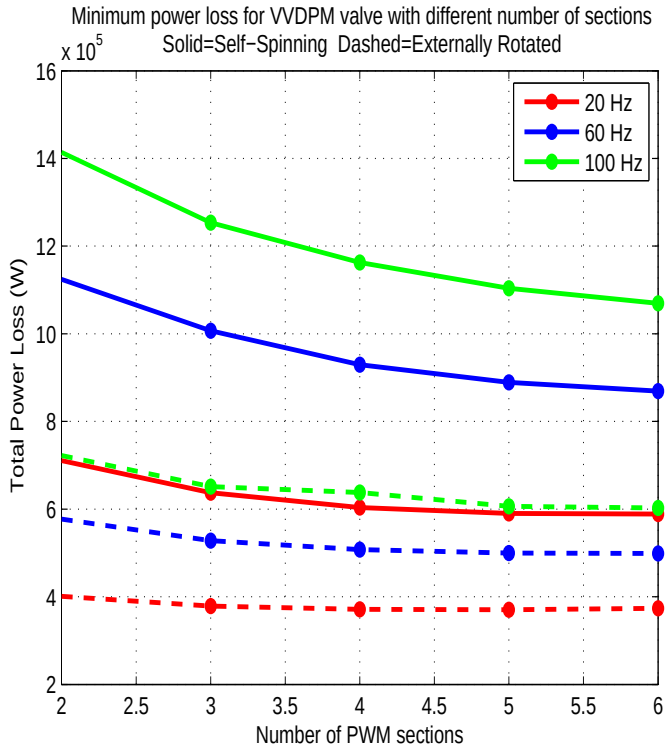

Figure 4.25: Cycle energy loss for a VVDPM with different numbers of PWM sections

small, trading off one for the other does not have a large overall effect. In the self-spinning case, the design changes that must be made to overcome the friction and satisfy Eq. (4.49) have a detrimental effect on the other, larger losses. Thus, reducing the spool speed can have more of an impact on the total loss.

The optimization results presented thus far have been generated using the duty cycle specified by the HHPV transmission design (Fig. 4.18). For a general purpose VVDPM that is not designed for a specific application, a more generic duty cycle can be specified. The duty cycle points in speed and torque can be generated from a uniform grid. In the following example, the optimization is performed over a grid from $-50 \leq \tau \leq 50Nm$ and $-5000 \leq \omega \leq 5000RPM$. Since the externally rotated design exhibited superior performance when compared with the self-spinning design, only the results from that design are shown. Figures 4.26 and 4.27 show a comparison between the optimal parameters generated with the duty cycle shown in Fig. 4.18, and those

generated with a uniform grid. The three parameters that are not shown (l,c,A_{out}) were the same in both cases. In general, the uniform grid valve is larger with larger orifices. The uniform grid places the same weight on points on the edges of the map as it does on the center points, whereas the HHPV generated duty cycle has more points that are clustered near the middle of the flow range. Thus, the uniform grid valve may be more heavily influenced by the high flow, high torque points, resulting in a larger valve. By applying weights to different regions of the operating range, this approach can be tuned for any application.

In addition to the losses in the rotary valve, there are also losses in the fixed-displacement pump/motor, and by adding the pump/motor losses to the valve losses, an estimate of the overall VVDPM efficiency map can be generated. For the design example presented in this chapter, the fixed displacement pump/motor was sized to match a Parker F11-10 pump/motor. Using efficiency data supplied for this pump/motor, an estimate of the pump/motor losses can be generated. The pump/motor efficiency data was separated into mechanical efficiency (primarily a measure of friction) and volumetric efficiency (primarily a measure of leakage) over a grid of speed and pressure. For a VVDPM, the load on the pump/motor is a constant pressure ($200bar$ in this example), but that pressure is applied over a variable duty cycle. If the assumption is made that the volumetric losses are much smaller in the unloaded case than in the fully loaded case, then the volumetric losses can be scaled by the magnitude of the PWM duty ratio, $|s|$. The mechanical losses also likely decrease in the unloaded state, since the high forces generated on the bearing surfaces are removed. However, there will still be some frictional losses in the unloaded state, and the correct scaling to apply is difficult to determine without an in-depth study of the pump/motor. Without knowing the proper scaling, the mechanical losses are conservatively assumed to be constant with s. With this scaling applied, the overall estimated VVDPM efficiency map including the valve losses, constant pump/motor mechanical losses, and scaled pump/motor volumetric losses, can be generated.

Figure 4.28 shows the VVDPM efficiency map for an externally rotated valve operating at a mid-level PWM frequency of $40Hz$. Notice that the upper-right and lower-left quadrants of the map have slightly lower efficiencies than the other two. These quadrants correspond to the VVDPM in motor mode, which is slightly less efficient than the

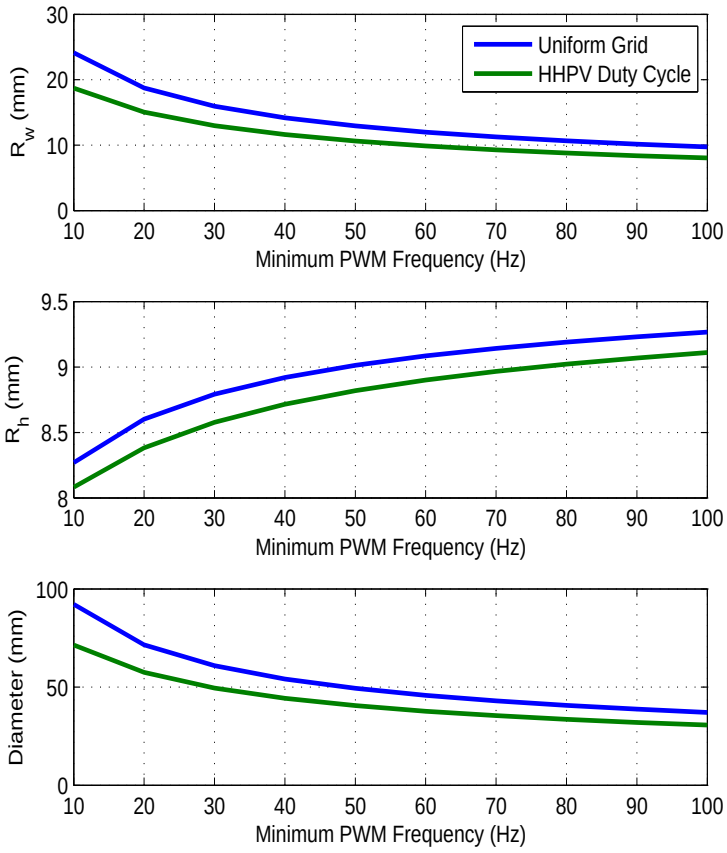

Figure 4.26: Orifice width, height, and spool diameter for a valve optimized over different duty cycles

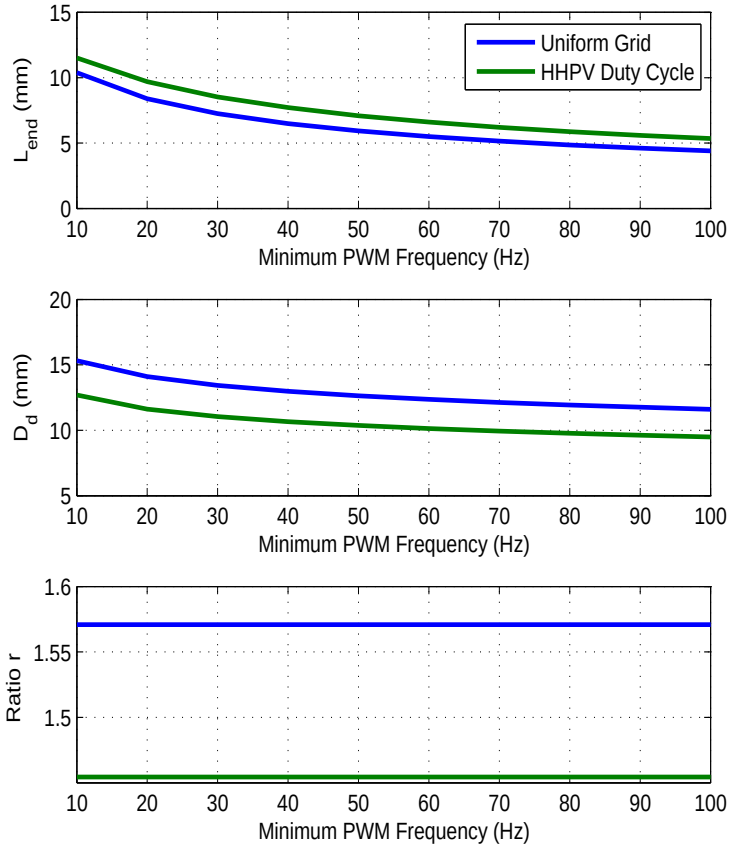

Figure 4.27: End land length, rail diameter, and gear ratio for a valve optimized over different duty cycles

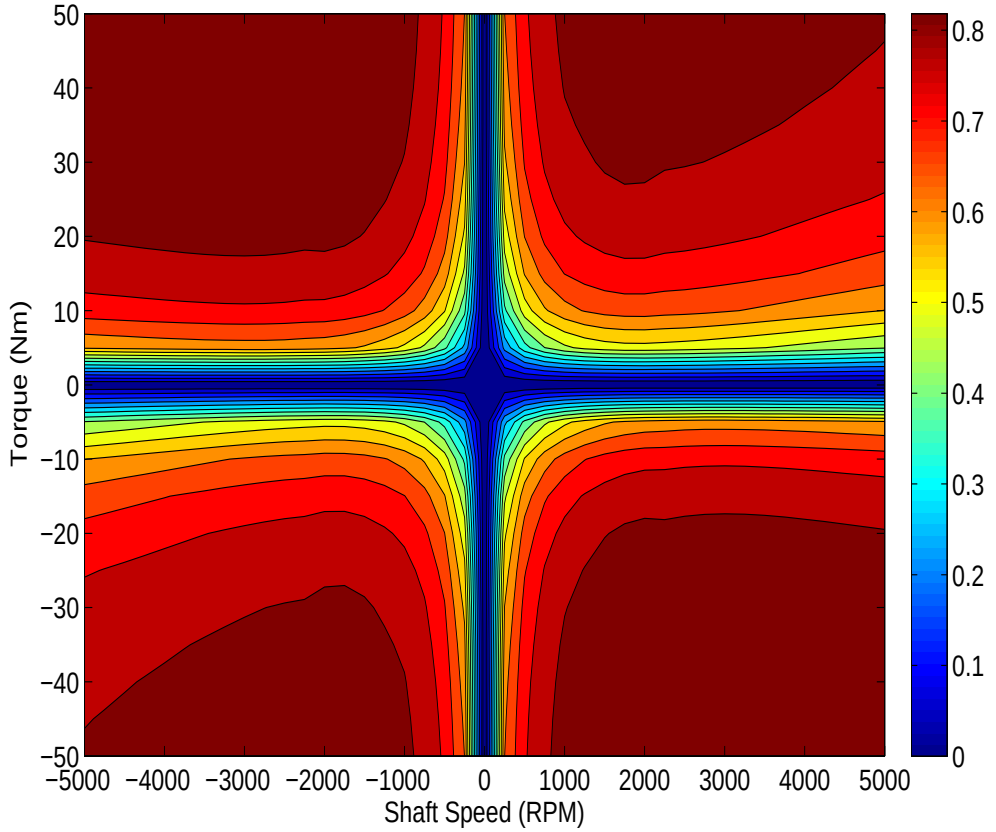

Figure 4.28: Overall efficiency map for a VVDPM optimized over a uniform grid and operating at 40 Hz

pumping mode. Figure 4.19(b) shows the trend for the average efficiency for a VVDPM with respect to frequency. While this plot is for a valve optimized over the HHPV duty cycle, the shape of the curve for the uniform grid valve matches it closely. From that plot, at $10Hz$, the average efficiency should increase by $3-4\%$ compared with the $40Hz$ case, and at $100Hz$, the average efficiency should be about 5% lower. This map is only an estimate of the VVDPM efficiency and the loss equations used to generate it contain some simplifications designed to allow for an efficient solution by the optimization algorithm. One of these assumptions is that the losses (i.e. compressibility and transition) are occurring independently of each other, when in reality, they are occurring simultaneously and affecting each other. A more detailed dynamic model could better model the losses acting together. In [88], a more detailed analysis of the VVDPM efficiency can be found that uses a dynamic model to estimate the losses.

4.7 Conclusion

In this chapter, an optimal design procedure was described for a novel type of rotary valve that can translate axially as is rotates. This two degree-of-freedom valve is useful in applications that require high-speed switches between two states, and also need the ability to adjust the ratio of time spent in those two states. Two example hydraulic circuits were described in detail: a Virtually Variable Displacement Pump and and Virtually Variable Displacement Pump Motor. The VVDP uses a three-way on/off valve to send full pump flow to either a load branch (with a smoothing accumulator) or a tank branch to unload the flow. This allows a fixed-displacement pump to provide a variable flow out to a load. The VVDPM uses a four-way tandem-center rotary valve to connect the ports of a fixed-displacement pump/motor to supply and tank or to each other in the freewheeling state.

For each valve, the design procedure was formulated as a constrained energy loss minimization problem. To accomplish this, equations for five different sources of energy loss in the valve were derived. In examining the energy loss equations, design parameters that were involved in one or more trade offs between the different losses or constraints were identified as optimization parameters. The VVDP optimization was conducted for a valve operating at a constant output pressure and input flow rate. This allowed

for a minimization of the instantaneous power lost in the valve. For the VVDPM, a constant pressure and flow rate are highly unlikely to represent reality. As a result, the optimization problem was formulated to minimize the total energy lost in the valve as the VVDPM operated through a specified duty cycle. The primary duty cycle used for optimization was generated from the design of the transmission for a Hydraulic Hybrid Passenger Vehicle. A separate duty cycle generated from a uniform grid across an operating region was also used for comparison.

Constraint equations for the valve design were also derived, most of which related to bounds on the physical parameters or other mechanical constraints. As described in chapter 2, a faster PWM frequency reduces the ripple on the output, but it also has a detrimental effect on the efficiency. In order to include both objectives of limiting the output ripple size and reducing the power loss, a lower bound was placed on the PWM frequency. Equations for two different valve designs were described: a self-spinning valve that uses fluid momentum to spin itself, and a valve that is rotated from an external actuator.

The results of the optimization showed that for both the VVDP and the VVDPM, the externally rotated valve was significantly more efficient than the self-spinning valve. Despite the fact that the self-spinning valve does not require any power to actuate it, the design trade offs that need to be made to accomplish self-spinning cause significantly more energy loss than is needed to spin the valve. A self-spinning valve tends to have a smaller diameter, inlet orifice, outlet orifice, and a larger clearance. As expected, the energy losses increase as the frequency increases, driven by the compressibility loss, the transition loss, and in the externally rotated case, the actuation loss. The largest source of energy loss in the valve is throttling when the valve is transitioning between states, although the optimization drives the inlet orifices to be so large that the valve is always in transition. The number of PWM sections on the valve was also studied. For a self-spinning valve, adding more PWM sections has a beneficial effect on the overall loss, especially at higher frequencies. For an externally rotated valve, the number of PWM sections had only a small effect on the overall loss.

By adding the estimated losses from a fixed-displacement pump/motor, an estimate of the efficiency map for an optimal VVDPM was generated. For a VVDPM operating at $40Hz$, the high efficiency regions had levels in the mid-80% range, with that

increasing to the upper 80% range for a VVDPM at $10Hz$. The pump mode efficiency remains above 70% down to about 20% displacement (note, s=T/T_{max}) at all but the low speed conditions, and the motor maintains this level down to about 30%. This is comparable to the efficiency of conventional variable displacement pump/motors, except for slightly lower at the top end. However, with this approach, lower cost or more efficient pump/motor technologies can be used as the fixed-displacement unit. In addition, there is potential to extend this approach to couple with a cylinder instead of a fixed-displacement pump/motor, which could provide a significant improvement over the efficiency of throttling valve control. The challenge in taking this step is maintaining enough inertia on the load to mitigate the torque ripple from the on/off valve. Another direction to take this rotary valve approach is to integrate it directly into a piston pump/motor to enable/disable individual pistons. This approach can use the low-power, high-speed on/off switching enabled by the rotary valve to control lower flow associated with individual pistons to control hydraulic power. In the next chapters this approach will be explored.

Chapter 5

Power Loss and Operating Principle Analysis of a Discrete Piston Controlled Hydraulic Pump/Motor

There are many ways that on/off valves can be combined with other hydraulic components to create efficient control systems. In the previous chapters, an on/off valve was placed outside of a hydraulic pump or motor to vary the power output by unloading excess flow at low pressures. This approach is more efficient than using throttling valves, and it allows the use of fixed displacement pumps and motors in applications that have a varying flow demand. However, this approach requires the full pump or motor flow to pass through the on/off valve, which can result in power losses and a large flow ripple. In addition, power losses in the on/off valve will add to the power losses in the pump or motor, reducing the total system efficiency.

In this chapter, and in chapters 6 and 7, a different approach is taken; the on/off valve is integrated into the pump/motor to create a single device that can efficiently produce a variable output flow or torque. The on/off valve enables or disables individual pistons inside of the pump/motor, rather than enabling or disabling the full output flow of the pump/motor. This approach, which is referred to as discrete piston control, has

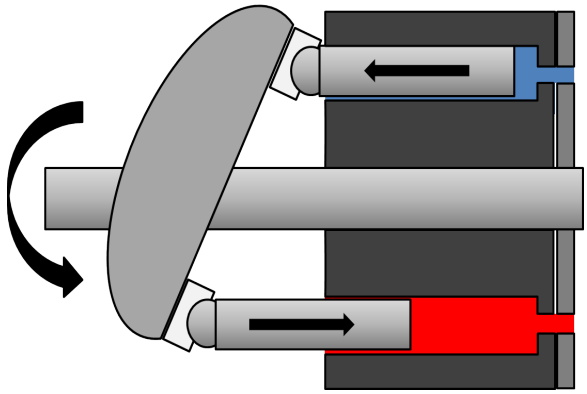

Figure 5.1: Sketch of a conventional variable displacement pump

a number of advantages and can produce a highly efficient variable power source. By only acting on one piston at a time, the flow requirements for the on/off valve, and the flow ripple resulting from on/off control, can be much lower than in the full output flow on/off strategy. Also, by changing the way the displacement of the pump/motor is varied, some of the power losses in the pump/motor itself can be reduced.

Conventional variable displacement pumps and motors are typically either swashplate or bent-axis type machines. These devices have a set of rotating pistons that push against an angled surface, the effect of which is to cause the pistons to reciprocate within their bores, as depicted in Fig. 5.1. If this reciprocating action occurs when there is high-pressure fluid in the piston chamber, energy is added to or extracted from the high pressure port. By varying the relative angle between the piston barrel and the angled surface, the distance that each piston reciprocates in one rotation is varied, which changes the volume of high pressure fluid that is produced for pumping or extracted for motoring. As less power is required from the pump or motor, the stroke of each piston is reduced. Each piston is connected to either the high pressure or low pressure port of the machine, which is accomplished by the rotating piston block passing over a stationary valve plate, which has two kidney-shaped ports. A sketch of a valve plate is shown in Fig. 5.7. Thus, half of the pistons are always at high pressure, and the other half are at low pressure.

In this chapter, an analysis of the power loss mechanisms are evaluated for both a conventional swashplate pump/motor and a discrete piston controlled device. Particular

attention is paid to how these loss mechanisms scale with the displacement setting of the pump/motor. Different piston disabling strategies are also discussed and their relative benefits and drawbacks are explained. In chapter 6, several options are compared for achieving discrete piston control using mechanical control valves. A design is selected and the detailed design of a prototype following this approach is described, including a dynamic model, mechanical design, and CFD results. Finally, in chapter 7, experimental results of the discrete piston pump/motor prototype are presented.

5.1 Introduction

Conventional variable displacement pumps and motors typically exhibit a dramatic drop-off in efficiency as their displacement is decreased. The majority of the losses in a variable displacement pump stem from the leakage and friction between parts that experience relative motion. As the displacement is decreased, the piston stroke length is decreased, but the interfaces that cause the leakage and friction losses remain at high pressure. This leads to a fairly flat power loss across the displacement range, resulting in a sharp efficiency drop at low displacements.

In contrast to conventional variable displacement devices, the approach taken in this chapter is to use on/off valves to enable/disable pistons when they are not needed, rather than changing the stroke length. With this method of control, high pressure is removed from pistons when then power demand decreases, causing many of the the leakage and friction losses to decrease as the displacement is reduced. However, by not reducing the stroke length, some losses, such as piston friction and flow throttling, may increase. A study of the losses in an example pump/motor is presented in section 5.2 which shows that the loss reduction due to removal of pressure is greater than the loss increase due to longer stroke length.

The approach of disabling individual pistons rather than varying the stroke length is relatively new, but not unique to this thesis. Other groups have investigated using on/off valves for discrete piston control, but their efforts have primarily been focused on using electrically actuated valves. A full description of other discrete piston control approaches is given in section 1.1. While electrically actuated valves can provide a high degree of control flexibility, most of the piston-by-piston control functionality can be

achieved using mechanical valves. In a similar approach to chapter 4, a two degree-of-freedom valve can be used to control both the fast on/off switching required via rotary motion, and adjustment of on/off timing via axial movement. Inside a pump/motor, the drive shaft can provide rotary actuation power for the valve, with the added benefit that the on/off switching of the valve will have fixed, reliable timing with respect to the driveshaft.

There are a number of advantages of a mechanical control solution, compared with an electrohydraulic solution. A mechanical solution is simpler to implement and control in most hydraulic applications, since the position of the rotary valve is the single control input. Power for the valve is also mechanical and hydraulic, which are both available inside the pump/motor, whereas electrical valves often need a high-current electrical supply. A mechanical or hydraulically actuated valve can be held open or closed with little or no power, in contrast to electrical actuators, which typically require a constant current to hold against a spring. Due to the lack of wires and control circuitry, the packaging of a mechanical solution can be simple and robust, and the valve timing is guaranteed to be at a consistent location in the pump rotation, independent of the pump/motor speed. This means that the control can be achieved without requiring a shaft position or speed sensor.

The disadvantages of a mechanical valving approach are primarily related to a loss of flexibility. There are a number of timing strategies that can be employed when using discrete piston control, and an electrical solution can have the flexibility to switch between them. This could allow the pump/motor to adjust the flow ripple in different operating conditions. The valve timing can also be shifted with respect to the pump rotation at different operating conditions, which can provide efficiency benefits, particularly for a motor with a wide speed range. However, adding backlash to the drive shaft can provide a mechanical timing adjustment between pumping and motoring, which will be described in section 6.2.2. A planetary gear set could also be used to restore much of the flexibility lost by using mechanical control valves. Mechanical valving strategies for a pump only are fairly straight forward, and [56, 57] have discrete piston controlled pumps that use mechanical control mechanisms. However, these designs cannot be extended to a motor. In this thesis, a mechanical solution for a piston-by-piston controlled pump/motor will be presented.

The primary drawback of the discrete piston control strategy is the flow ripple that results from turning individual pistons on and off. However, for applications that can tolerate flow/pressure ripple, or that have a smoothing element such as an inertia or accumulator, the discrete piston control approach can provide significant efficiency benefits. This is particularly true for pumps and motors that spend a substantial amount of time operating at partial displacements. In comparison to using an on/off valve to enable/disable the entire pump/motor flow, the flow ripple in the discrete piston approach is much smaller. This is shown in section 5.4.4.

In the next section, an analysis of the losses in pump/motors using conventional and discrete piston control methods is presented. In section 5.3, a quantitative comparison is done between a conventional and discrete piston design sized to match an experimental prototype. Section 5.4 outlines different strategies for accomplishing discrete piston control, and discusses the advantages and drawbacks of each. Finally, section 5.5 presents concluding remarks on the analysis of the discrete piston control approach.

5.2 Power Loss Modeling

There are a number of sources of energy loss in hydraulic pumps and motors, the largest of which result from the leakage and friction in the interfaces between parts that move with respect to each other. In this section, the losses in the piston bore, the valve plate, the swashplate, and valve throttling are analyzed to show how the losses scale with displacement. This is done for both a swashplate type machine as well as a discrete piston controlled device. In analyzing the losses in a discrete piston device, two different approaches are considered: whole piston disabling and partial stroke disabling. Whole piston disabling refers to a discrete piston approach that disables a variable number of pistons for their entire power stroke to reduce the displacement. In partial stroke disabling, each piston has a variable fraction of its power stroke disabled. The flow ripple and mechanical design implications for these two approaches are described in section 5.4. The effect of these two different strategies on a number of losses in the pump/motor is described in the following sections. The analysis of the losses show that, for a typical size pump/motor, the losses in the piston-by-piston approach decrease faster with displacement than in a conventional swashplate pump/motor.

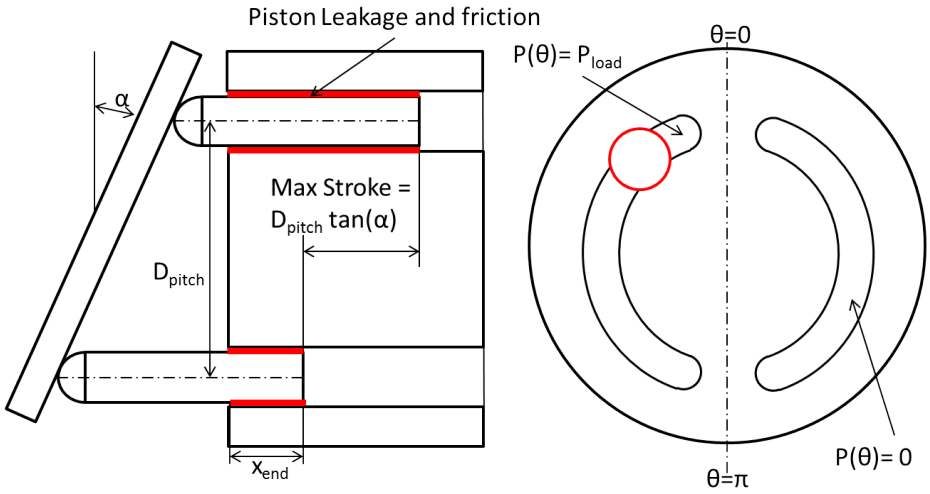

Figure 5.2: Sketch of a swashplate pump/motor

5.2.1 Piston Losses

In order to supply or extract work from the hydraulic fluid, the piston must slide relative to its bore, with a small clearance between the two parts. In this small gap, energy is lost though friction between the parts and the fluid and leakage of high pressure fluid to tank. Figure 5.2 shows a sketch of a swashplate pump/motor with the piston-bore gap highlighted. For the analysis of the leakage and friction losses between the piston and the bore, it is assumed that the fluid is Newtonian, and the flow is fully developed and steady. Since the clearance between the piston and the bore is very small, the Reynolds Number will be much less than 1, and the flow will be laminar. It is also assumed that the flow is unidirectional, and the variation of the flow velocity in the radial direction is much greater than the variation in the angular direction ($\frac{\partial^2 u}{\partial r^2} >> \frac{\partial^2 u}{\partial \theta^2}$). It can also be shown [87] that for annular flows, as the clearance between the inner cylinder and outer bore approaches zero, the annular flow equations approach the solution for flow between two parallel plates. These assumptions are similar to those made in [93, 92], and have been used to derive the following equations for the losses in the piston clearance gap.

The high pressure in the piston chamber will induce a pressure-driven, or Poiseuille, leakage flow in the clearance gap. The equation for this leakage in one piston is given

in [92, 79]:

$$Q_{poiseuille} = \frac{\pi D_p c^3 \left(1 + \frac{3}{2}e^2\right) P\left(\theta - \phi_i\right)}{12\mu x\left(\theta - \phi_i\right)} \tag{5.1}$$

where D_p is the piston diameter, c is the nominal clearance between the piston and the bore, P is the pressure in the piston chamber, μ is the dynamic viscosity of the fluid, x is the length of the piston in the bore, θ is the rotation angle of the pump/motor, and e is the eccentricity ratio of the piston. The eccentricity ratio is defined as the distance that the center of the piston is offset from the center of the bore divided by the nominal clearance, c. ϕ_i is the phase shift associated with each piston, and is equal to $\frac{2\pi(i-1)}{N_p}$ for $i = 1, 2, ..., N_p$ where N_p is the number of pistons.

To calculate the average piston leakage power loss for the swashplate and discrete piston devices, equations for $x\left(\theta\right)$ and $P\left(\theta\right)$ are applied to Eq. (5.1). The length of the piston in the bore is given by:

$$x_{sp} = cos\left(\theta - \phi_i\right)\frac{D_{pitch}}{2} tan\left(\alpha_s(t)\right) + \frac{D_{pitch}}{2} tan\left(\alpha\right) + x_{end} \tag{5.2}$$

$$x_{dp} = \left(cos\left(\theta - \phi_i\right) + 1\right)\frac{D_{pitch}}{2} tan\left(\alpha\right) + x_{end} \tag{5.3}$$

where x_{sp} and x_{dp} are the piston positions for the swashplate and discrete piston approaches respectively, D_{pitch} is the pitch diameter of the pistons, and x_{end} is the minimum length of the piston in the bore when the piston is at Bottom Dead Center (BDC). α, which is depicted in Fig. 5.2, is the maximum swashplate angle, which remains constant in both the swashplate and discrete piston cases. In the swashplate case, the displacement is varied by changing the angle of the swashplate. The variable swashplate angle, $\alpha_s(t)$ is related to the maximum swashplate angle, α, and the displacement, s, by:

$$tan\left(\alpha_s(t)\right) = tan\left(\alpha\right) s(t) \tag{5.4}$$

The parameter s is the displacement setting of the pump/motor. In the discrete piston case, the swashplate angle does not vary, and remains at the maximum angle, α. Notice that, for the swashplate type pump/motor, the piston position is a function of the displacement, but this is not the case for the discrete piston approach.

The piston velocities can be found by differentiating Eqs. (5.2) and (5.3):

$$\dot{x}_{sp} = -\omega sin\left(\theta - \phi_i\right) \frac{D_{pitch}}{2} tan\left(\alpha_s(t)\right) \tag{5.5}$$

$$\dot{x}_{dp} = -\omega sin\left(\theta - \phi_i\right) \frac{D_{pitch}}{2} tan\left(\alpha\right) \tag{5.6}$$

where $\omega = \dot{\theta}$ is the angular velocity of the pump/motor.

The valve plate in Fig. 5.2 shows the kidney-shaped ports that are used to connect each piston to high or low pressure as the barrel rotates with respect to the plate. For a discrete piston device, the barrel typically does not rotate, and a valve will connect each piston to high or low pressure. For the swashplate and whole piston disabling discrete piston designs, the pressure in each piston chamber, $P\left(\theta - \phi_i\right)$, is given by:

$$P\left(\theta - \phi_i\right) = \begin{cases} P_{load} & \text{if } 0 \leq \theta - \phi_i < \pi \\ 0 & \text{if } \pi \leq \theta - \phi_i < 2\pi \end{cases} \tag{5.7}$$

where P_{load} is the pressure that the pump/motor is operating at. Note that this is defined for a motor; for a pump the cases are reversed, with pressure applied for the second half of the rotation. This equation is a slight simplification, since there will be a small pressure difference between P_{load} and the pressure in the piston chamber due to throttling across the inlet of the piston chamber. For the motor case, the chamber pressure will be $P_{load} - \Delta P_{throttle}$, and for the pump case it will be $P_{load} + \Delta P_{throttle}$. Neglecting this throttling loss in the leakage analysis will give a value between the pump case and the motor case. Additionally, in most pump/motor designs, $\Delta P_{throttle} << P_{load}$ at typical hydraulic operating pressures.

Figure 5.3 depicts an example of the high pressure flow in a single piston chamber for a discrete piston motor using the partial stroke disabling strategy. With partial stroke disabling, each piston is connected to low pressure early for an adjustable part of its power stroke. In Fig. 5.3, the transition from a connection to high pressure to a connection to low pressure occurs at $\theta = \theta_{partial}$. In this case, the equation for the pressure applied to the pistons is slightly different:

$$P_{partial}\left(\theta - \phi_i\right) = \begin{cases} P_{load} & \text{if } 0 \leq \theta - \phi_i < \theta_{partial} \\ 0 & \text{if } \theta_{partial} \leq \theta - \phi_i < 2\pi \end{cases} \tag{5.8}$$

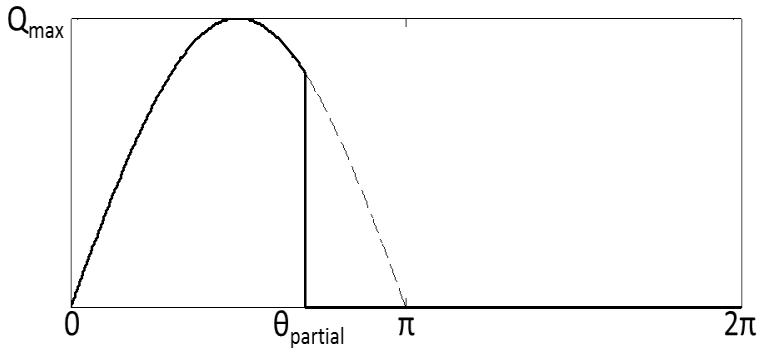

Figure 5.3: Single piston flow rate from the high pressure port in a partial stroke motor

where $\theta_{partial}$ is the angle at which the piston is disabled, as shown in Fig. 5.3. This angle can be calculated by setting s equal to the ratio of the oil volume swept by the piston between 0 and $\theta_{partial}$ to the volume swept between 0 and π:

$$s = \frac{\int_0^{\theta_{partial}} \pi D_p^2 \dot{x}_{dp} d\theta}{\int_0^{\pi} \pi D_p^2 \dot{x}_{dp} d\theta} = \frac{\cos(\theta_{partial}) - \cos(0)}{\cos(\pi) - \cos(0)} \tag{5.9}$$

$$\theta_{partial} = \cos^{-1}(1 - 2s) \tag{5.10}$$

In this equation, which is shown for the motor case, the duration of the pressure stroke is reduced by decreasing the displacement setting, s.

The power loss due to leakage from the piston chamber around the piston to the pump/motor case can be calculated by multiplying the leakage flow from Eq. (5.1) and the chamber pressure, $P(\theta)$. The average power loss over one pump rotation due to piston leakage is given by:

$$L_{poiseuille,leak,sp} = \frac{1}{2\pi} \int_0^{2\pi} \frac{N_p \pi D_p c^3 \left(1 + \frac{3}{2}e^2\right) P(\theta)^2}{12\mu x_{sp}(\theta)} d\theta \tag{5.11}$$

$$L_{poiseuille,leak,whole} = \frac{1}{2\pi} \int_0^{2\pi} \frac{N_p s \pi D_p c^3 \left(1 + \frac{3}{2}e^2\right) P(\theta)^2}{12\mu x_{dp}(\theta)} d\theta \tag{5.12}$$

$$L_{poiseuille,leak,partial} = \frac{1}{2\pi} \int_0^{2\pi} \frac{N_p \pi D_p c^3 \left(1 + \frac{3}{2}e^2\right) P_{partial}(\theta)^2}{12\mu x_{dp}(\theta)} d\theta \tag{5.13}$$

where N_p is the number of pistons in the pump/motor. In the whole piston disabling case, the displacement, s, modifies the number of pistons because the pressure is removed

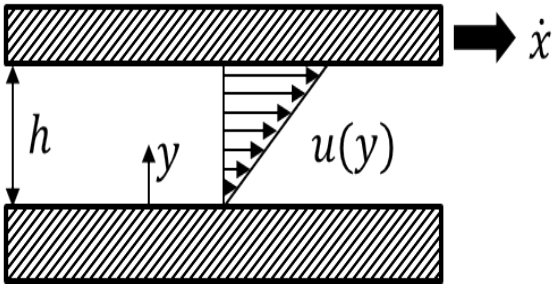

Figure 5.4: Fluid velocity profile between two parallel plates

from pistons as the displacement is decreased. For the partial stroke disabling approach, the piston leakage is also reduced by s via $P_{partial}$ by reducing the fraction of the stroke that pressure is applied.

There is also a Couette flow through the gap caused by the relative motion between the piston and the bore. With the assumptions listed at the beginning of this section, the flow through the piston gap can be computed using the equation for the fluid velocity between two parallel plates [94], which is depicted in Fig. 5.4:

$$u\left(\delta, y\right) = \dot{x}\left(1 - \frac{y}{h\left(\delta\right)}\right) \tag{5.14}$$

where u is the fluid velocity in the x (axial) direction, y is the distance from the piston surface toward the bore surface, δ is the angular coordinate around the piston, and h is the height of the gap between the piston and bore at a particular δ. Figure 5.5 depicts a cross-section of the piston in the bore. If the piston is offset by the distance $ec << D_p$ and c is the nominal clearance, then h is given by [93]:

$$h\left(\delta\right) = c\left(1 + e\cos\left(\delta\right)\right) \tag{5.15}$$

It is clear from Eq. (5.14) that the velocity profile at a given δ is linear with respect to y, and thus the average Couette flow velocity in the gap at each δ is $\dot{x}/2$. Thus, the Couette leakage flow is proportional to the piston velocity, and the power flow due to this leakage is the product of the Couette flow and the pressure in the oil that is expelled or drawn in to the clearance between the piston and bore. Without modeling the pressure build-up in the oil between the piston and the bore during a pumping stroke, a first approximation is that the piston draws in fluid from the low-pressure case

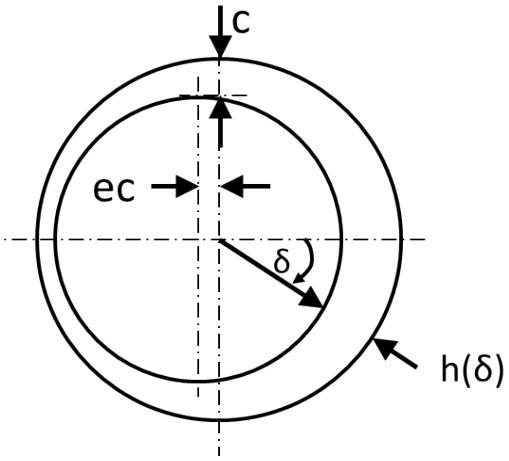

Figure 5.5: Cross-section sketch of an eccentric piston

when it is retracting into the bore, and then expels that same fluid when it is extending. Thus, the net flow of low pressure oil being pulled in and out of the bore by the piston is zero. There could be some power loss if the exhausted fluid is at a higher pressure than the intake fluid, but the pressure build-up in the piston gap is caused by high pressure fluid leaking through the gap, and attributing that loss to the couette flow would result in double-counting some of the loss computed in Eqs. (5.11), (5.12), and (5.13).

However, the friction that results from the Couette flow cannot be neglected. Using the definition of an incompressible Newtonian fluid and differentiating Eq. (5.14), the shear stress on the piston is given by [93]:

$$\tau_{couette} = \frac{\mu \dot{x}}{h\left(\delta\right)} \tag{5.16}$$

where $h\left(\delta\right)$ is given by Eq. (5.15). The average frictional power loss on the pistons over one pump rotation is given by:

$$L_{couette,fric} = \frac{N_p}{2\pi} \int_0^{2\pi} \int_0^{\pi} \frac{\mu x(\theta) \dot{x}(\theta)^2 D_p}{c\left(1 + e\cos\left(\delta\right)\right)} d\delta d\theta \tag{5.17}$$

where $\frac{xD_p d\delta}{2}$ is the differential area over which the shear stress in Eq. (5.16) is applied. The piston position, x, is defined by Eq. (5.2) or (5.3) and $\dot{x}$ is defined by Eq. (5.5) or (5.6).

There is also a shear stress due to the velocity profile of the pressure-driven flow through the piston gap. Following the derivation in [93], the shear stress at the wall can be computed from the velocity profile for pressure driven flow between two plates:

$$u_{poiseuille}\left(\delta, y\right) = \frac{1}{2\mu}\left(h\left(\delta\right) - y\right) y \frac{dp}{dx} \tag{5.18}$$

where the pressure gradient along the piston, $\frac{dp}{dx}$, is assumed to be linear. By combining this equation with the definition of a Newtonian fluid:

$$\tau = \mu \frac{du}{dy} \tag{5.19}$$

and evaluating for the shear stress at the wall ($y = 0$), the shear stress on the piston is given by:

$$\tau_{poiseuille}\left(\delta\right) = \frac{cP\left(\theta - \phi_i\right)}{2x}\left(1 + e\cos\left(\delta\right)\right) \tag{5.20}$$

The integral of the shear stress across the surface of the piston times the piston speed relative to the pump housing gives the power flow attributable to poiseuille flow induced friction. The average of this power flow over one pump rotation is given by:

$$L_{poiseuille,fric,sp} = \frac{N_p}{2\pi}\int_0^{2\pi} P\left(\theta\right)\frac{D_p}{2} c\pi \dot{x}_{sp}(\theta) d\theta \tag{5.21}$$

$$L_{poiseuille,fric,whole} = \frac{N_p s}{2\pi}\int_0^{2\pi} P\left(\theta\right)\frac{D_p}{2} c\pi \dot{x}_{dp}(\theta) d\theta \tag{5.22}$$

$$L_{poiseuille,fric,partial} = \frac{N_p}{2\pi}\int_0^{2\pi} P_{partial}\left(\theta\right)\frac{D_p}{2} c\pi \dot{x}_{dp}(\theta) d\theta \tag{5.23}$$

This power flow can be either positive or negative, depending on the direction the piston is traveling when high pressure is applied. For the motoring case, this friction force will be in the same direction as the piston velocity. Thus, in the motoring case, some of the energy from the leakage flow will be extraced to help move the piston. For the pumping case, the friction will oppose the piston motion, resulting in a positive power loss. This is the case that is simulated in the numerical example in section 5.3. As in the pressure-driven leakage equations, the magnitude of the power loss is reduced by the displacement, s, for the discrete piston case, but not directly for the swashplate case. However, the piston velocity, $\dot{x}_{sp}$, is reduced by decreasing the swashplate angle in Eq. (5.5). Note that this analysis contains a simplification in that it considers the Poiseuille flow to be fully developed and steady. The relationship between the dynamic

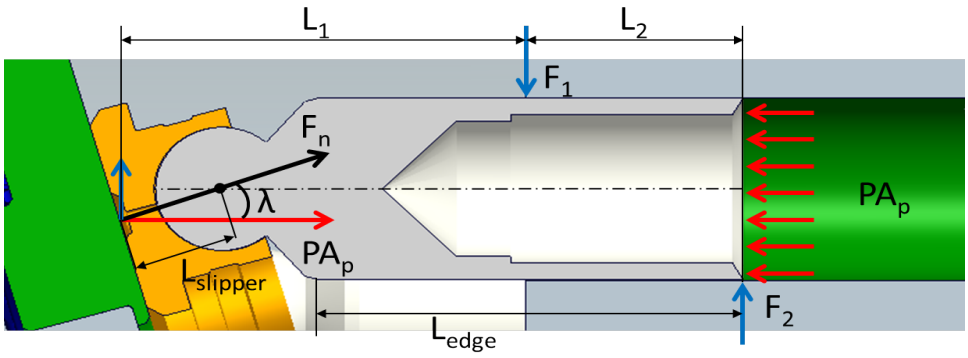

Figure 5.6: Forces applied to the piston

behavior of the velocity field and the changing piston velocity is not considered. A full numerical solution of the Navier-Stokes equations for the fluid could capture the dynamic effects of the flow field, but this would be a much more complicated analysis. The typical magnitude of the Poiseuille flow generated piston friction is much less than the Coulomb friction described next, so this approximation will not have a significant effect on the overall power loss results.

Finally, due to the side load applied to the piston by the angled swashplate, there is a coulomb friction force between the piston and the bore. The interface between the piston and bore has been studied by a number of authors [95, 96, 97, 98]. In [95], the transition to mixed lubrication is explored, and the possibility of metal to metal contact in mixed lubrication is established. In [96] and [97], detailed numerical models are used to predict piston losses. These models include the effects of the deformation and micro motion of the piston and bore, thermal effects, and variable viscosity, but they assume that there is no mixed lubrication. In [98], the friction force is modeled as a simple coulomb friction force with a constant coefficient of friction and normal forces determined by a force balance on the piston. Figure 5.6 shows the forces on the piston. Due to the angled force on the swashplate, there is a lateral force that must be balanced by a force at the end of the bore, F_1, and a force at the end of the piston, F_2. These forces can be determined from a force and moment balance on the piston:

$$F_1 = \frac{D_p^2\pi}{4} P\left(\theta - \phi_i\right) \frac{\tan\left(\lambda\right) L_1\left(x(\theta)\right) + \tan\left(\lambda\right) L_2\left(x(\theta)\right) - \sin\left(\lambda\right) L_{slipper}}{L_2\left(x(\theta)\right)} \tag{5.24}$$

$$F_2 = \frac{D_p^2\pi}{4} P\left(\theta - \phi_i\right) \frac{\tan\left(\lambda\right) L_1\left(x(\theta)\right) - \sin\left(\lambda\right) L_{slipper}}{L_2\left(x(\theta)\right)} \tag{5.25}$$

where λ is the angle of the swashplate. For the discrete piston case, $\lambda = \alpha$, for the swashplate case, $\lambda = \alpha_s = \tan^{-1}\left(\tan\left(\alpha\right) s\right)$. L_1 is the distance from the piston-swashplate interface to the pivot point, which is the end of the bore for most of the stroke, L_2 is the distance from the pivot point to the end of the piston, and $L_{slipper}$ is the distance from the center of the spherical joint on the piston to the center of the piston slipper face. L_1 and L_2 distances vary with the position of the piston:

$$L_2\left(x\right) = \begin{cases} x & \text{if } x < L_{edge} \\ L_{edge} & \text{if } x \geq L_{edge} \end{cases} \tag{5.26}$$

$$L_1\left(x\right) = L_{piston} - L_2\left(x\right) \tag{5.27}$$

where $L_{piston} = L_1 + L_2$ is the distance from the end of the piston to the slipper-swashplate interface, and L_{edge} is the length of the piston that is at diameter, D_p. The second case in Eq. (5.26) is due to the fact that the part of the piston that is at diameter D_p can fully enter the bore, at which point, the pivot point moves off the end of the bore and travels with the piston.

The friction due to these forces can be estimated by multiplying the two lateral forces, F_1 and F_2, by a coefficient of friction. The average power loss over one rotation is obtained by multiplying the friction by the piston velocities from Eq. (5.5) and (5.6).

$$L_{coulomb,sp} = \frac{N_p}{2\pi} \int_0^{2\pi} \frac{D_p^2\pi}{4} P\left(\theta\right) \tan\left(\alpha_s\right) \nu_p \dot{x}_{sp}(\theta) \frac{2L_1\left(x_{sp}(\theta)\right) + L_2\left(x_{sp}(\theta)\right) - 2\sin\left(\alpha_s\right) L_{slipper}}{L_2\left(x_{sp}(\theta)\right)} d\theta \tag{5.28}$$

$$L_{coulomb,whole} = \frac{N_p}{2\pi} \int_0^{2\pi} \frac{D_p^2\pi}{4} P\left(\theta\right) \tan\left(\alpha\right)) s \nu_p \dot{x}_{dp}(\theta) \frac{2L_1\left(x_{dp}(\theta)\right) + L_2\left(x_{dp}(\theta)\right) - 2\sin\left(\alpha\right) L_{slipper}}{L_2\left(x_{dp}(\theta)\right)} d\theta \tag{5.29}$$

$$L_{coulomb,partial} = \frac{N_p}{2\pi}\int_0^{2\pi} \frac{D_p^2\pi}{4} P_{partial}\left(\theta\right)\tan\left(\alpha\right))\nu_p\dot{x}_{dp}(\theta) \frac{2L_1\left(x_{dp}(\theta)\right) + L_2\left(x_{dp}(\theta)\right) - 2\sin\left(\alpha\right)L_{slipper}}{L_2\left(x_{dp}(\theta)\right)} d\theta \quad (5.30)$$

where ν_p is the coefficient of friction between the piston and the bore. Notice that the coulomb friction loss is a function of the piston position and velocity. In the swashplate case, the piston friction is reduced with the displacement both due to a decrease in the piston velocity and because the maximum moment on the piston is reduced with the swashplate angle. This results in a lower coulomb friction loss on the pistons for the swashplate case than in the discrete piston case as the displacement is decreased.

5.2.2 Valve Plate Losses

Another lubricating gap that causes significant losses in a conventional variable displacement pump/motor is the clearance between the rotating cylinder barrel and the stationary valve plate. The valve plate contains a low pressure port and a high pressure port, and as they rotate, the pistons are alternately connected to each. The clearance between the valve plate and the barrel must provide a seal around the high pressure port, as well as a hydrodynamic bearing between the two sliding surfaces. Since conventional variable displacement pumps and motors have rotating pistons, a valve plate is needed to make a hydraulic connection with non-rotating input and output ports. There are piston-based pump/motor designs that do not require rotating pistons, such as wobble-plate and radial piston machines, however, these machines are typically not variable displacement unless discrete piston control is used.

Studying the leakage and friction in the valve plate lubricating gap can include many details, such as hydrodynamic balancing, shaft stiffness, barrel dynamics, and mixed lubrication. It is a problem that has been studied by numerous authors, such as [99], [100], [101], [102], and [103]. A comprehensive review of existing research on the valve plate-barrel interface can be found in [103]. In that paper, a simplified approach is used to derive an analytical equation for the leakage out of the valve plate. The geometry of the valve plate is shown in Fig. 5.7. In a valve plate, there are two kidney-shaped ports, one connecting one side of the piston barrel to high pressure, the other connecting the other side of the barrel to tank. On either side of the piston inlet, there

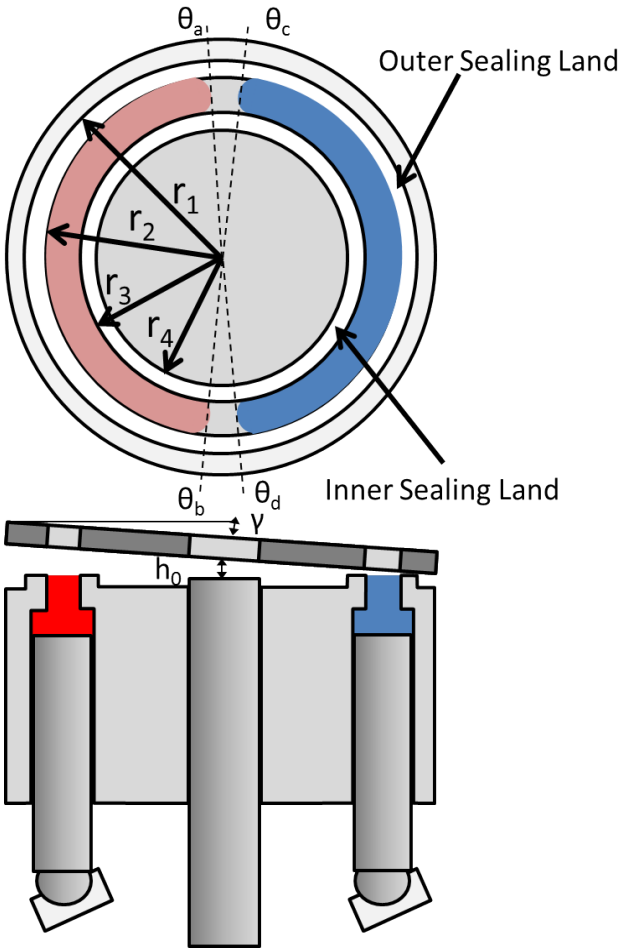

Figure 5.7: Sketch of valve plate showing the sealing land radii and tilt angle

is a land that acts as a sealing and bearing surface. The leakage and viscous friction on these two lands is considered in determining the power loss. The equations for the laminar leakage across the internal and external sealing lands given in [103] is:

$$Q_{int} = -\frac{(P_{load} - P_{case})}{12\mu \ln(r_3/r_4)} \left(h_0^3 (\theta_a - \theta_b) + 3h_0^2 \gamma \frac{(r_3 + r_4)}{2} (\sin(\theta_a) - \sin(\theta_b)) + 3h_0 \gamma^2 \frac{(r_3 + r_4)^2}{2} \left(\frac{1}{4} \sin(2\theta_a) + \frac{\theta_a}{2} - \frac{1}{4} \sin(2\theta_b) - \frac{\theta_b}{2} \right) + \gamma^3 \frac{(r_3 + r_4)^3}{2} \left(\frac{1}{12} \sin(3\theta_a) + \frac{3}{4} \sin(\theta_a) - \frac{1}{12} \sin(3\theta_b) - \frac{3}{4} \sin(\theta_b) \right) \right) \tag{5.31}$$

$$Q_{ext} = -\frac{(P_{load} - P_{case})}{12\mu \ln(r_2/r_1)} \left(h_0^3 (\theta_a - \theta_b) + 3h_0^2 \gamma \frac{(r_1 + r_2)}{2} (\sin(\theta_a) - \sin(\theta_b)) + 3h_0 \gamma^2 \frac{(r_1 + r_2)^2}{2} \left(\frac{1}{4} \sin(2\theta_a) + \frac{\theta_a}{2} - \frac{1}{4} \sin(2\theta_b) - \frac{\theta_b}{2} \right) + \gamma^3 \frac{(r_1 + r_2)^3}{2} \left(\frac{1}{12} \sin(3\theta_a) + \frac{3}{4} \sin(\theta_a) - \frac{1}{12} \sin(3\theta_b) - \frac{3}{4} \sin(\theta_b) \right) \right) \tag{5.32}$$

In this equation, P_{case} is the pressure in the pump/motor case, r_4 is the outside edge of the inner sealing land, r_3 is the inside edge of the inner sealing land, r_2 is the inside edge of the external sealing land, and r_1 is the outside edge of the external sealing land (see Fig. 5.7). Notice that the constant P_{load} pressure is used instead of the fluctuating piston pressure, $P(\theta)$, since high pressure is always applied to the valve plate. Thus, the leakage flow around the high pressure kidney port is a constant, regardless of the pressure on the pistons. Due to hydrostatic and hydrodynamic pressure forces, there is a gap between the cylinder barrel and the valve plate. The barrel can be tilted with respect to the valve plate at an angle γ. The height of the gap at the midpoint between the high and low pressure ports is h_0. The power loss due to the port plate leakage is:

$$L_{vp,leak} = (Q_{int} + Q_{ext}) P_{load} \tag{5.33}$$

Due to the viscous fluid in this gap, there is also a frictional power loss between these sealing lands. Since it is assumed that friction only occurs along the sealing lands, the other valve plate area is neglected. It is also assumed that the friction is purely due to viscous drag, and there is no mixed friction at the lowest point of the gap. Using the

equation for the velocity profile between two parallel plates, velocity of the fluid in the gap due to the relative motion of the two parts is given by:

$$u_\theta(r, y, \theta) = \frac{r\dot{\theta}y}{h_0 + \sin(\gamma)\, r\cos(\theta)} \tag{5.34}$$

where u_θ is the velocity in the circumferential direction and y is the distance from the stationary surface to the rotating surface. There will also be a pressure-driven leakage flow in the gap, but it is assumed that this flow is in the radial direction, and thus will not contribute to the friction torque. The frictional torque between the cylinder barrel and the valve plate is calculated by taking the derivative of Eq. (5.34) with respect to y, multiplying by μ to get the shear stress, multiplying by the relative velocity, and then integrating over the bearing area:

$$\begin{aligned} L_{vp,fric} = &\int_0^{2\pi}\int_{r_4}^{r_3} \frac{\mu r^3\dot{\theta}^2}{h_0 + \sin(\gamma)\, r\cos(\theta)} dr d\theta + \int_0^{2\pi}\int_{r_2}^{r_1} \frac{\mu r^3\dot{\theta}^2}{h_0 + \sin(\gamma)\, r\cos(\theta)} dr d\theta \\ &+ \int_{\theta_a}^{\theta_c}\int_{r_3}^{r_2} \frac{\mu r^3\dot{\theta}^2}{h_0 + \sin(\gamma)\, r\cos(\theta)} dr d\theta + \int_{\theta_d}^{\theta_b}\int_{r_3}^{r_2} \frac{\mu r^3\dot{\theta}^2}{h_0 + \sin(\gamma)\, r\cos(\theta)} dr d\theta \end{aligned} \tag{5.35}$$

In this equation, the area integral is split into four parts: the inner and outer sealing lands, and the two areas between the high and low pressure ports.

5.2.3 Other Losses

In typical swashplate type pumps and motors, another lubricating gap exists between the piston shoes and the swashplate. In many designs, a small hole is drilled through the piston to allow high pressure fluid to flow from the pumping chamber to the interface between the piston and the swashplate. This is done to reduce the force on the piston shoe to reduce friction and wear. Other researchers have studied the leakage losses in hydrostatic slippers in detail [104], but the predicted leakage relies heavily on specific design parameters to get an accurate balance between leakage and friction. In addition, this hydrostatic balancing is not included in all pump/motor designs, as some have the pistons either sliding directly on a swashplate or riding on a rolling element bearing. Since this feature is not a characteristic of all pumps, is heavily influenced by design details, and is not included in the piston-by-piston prototype to be described later, the

losses at this interface are modeled as simply a frictional power loss due to sliding or rolling between the piston shoes and the swashplate. In Fig. 5.6, the normal force on the piston shoe, F_n, is shown. This force is a function of the pressure force on the piston and the angle of the swashplate or wobble plate. The friction force is the normal force on the piston multiplied by a coefficient of friction, $F_{friction} = F_n \nu_s$. Multiplying the friction force by the relative sliding velocity gives the average power loss over one rotation due to slipper friction for all of the pistons:

$$L_{shoe,sp} = \frac{N_p}{2\pi} \int_0^{2\pi} \frac{\nu_s A_p P(\theta)}{\cos(\alpha_s)} \frac{D_{pitch} |\omega|}{2} d\theta \tag{5.36}$$

$$L_{shoe,whole} = \frac{N_p}{2\pi} \int_0^{2\pi} \frac{\nu_s A_p P(\theta)}{\cos(\alpha)} \frac{D_{pitch} |\omega|}{2} s d\theta \tag{5.37}$$

$$L_{shoe,partial} = \frac{N_p}{2\pi} \int_0^{2\pi} \frac{\nu_s A_p P_{partial}(\theta)}{\cos(\alpha)} \frac{D_{pitch} |\omega|}{2} d\theta \tag{5.38}$$

where N_p is the number of pistons, ν_s is the coefficient of friction between the slipper and the plate, A_p is the area of the piston exposed to high pressure, α is the maximum angle of the swashplate, D_{pitch} is the pitch diameter of the pistons in the barrel, and ω is the angular velocity of the piston block with respect to the plate. The pressure in the piston chamber is given by Eq. (5.7) and Eq. (5.8). The friction coefficient can be selected to apply to a sliding interaction, or a rolling element bearing.

Another loss that is present in all hydraulic systems is throttling through restrictions in the fluid path. The orifice equation is used to estimate the pressure drop due to the fluid flowing through the restriction in the valve plate:

$$Q_{ori} = c_d A_{ori} \sqrt{\frac{2|\Delta P|}{\rho}} sign(\Delta P) \tag{5.39}$$

where c_d is the orifice coefficient and A_{ori} is the area of the orifice. For a valve plate, the inner and outer sealing lands cover the top and bottom of the piston bore, creating an orifice that is roughly rectangular with rounded ends. The flow area is determined by the gap between r_2 and r_3 in Fig. 5.7, and the piston diameter, D_p. In the discrete piston case, the orifice area is determined by the geometry of the enabling/disabling

valves. Since $Q_{ori} = A_p\dot{x}$, the power loss due to throttling in all of the pistons is:

$$L_{throttle} = Q_{ori}\Delta P = N_p \frac{\rho \left(A_p\dot{x}\right)^3}{2c_d^2 A_{ori}^2} \tag{5.40}$$

where N_p is the number of pistons.

There are other losses present in a pump/motor, such as losses due to fluid compressibilty, throttling during valve transition, bearing friction, and fluid churning. These losses are heavily dependent on the design details of individual devices, such as valve transition timing and compressed oil volume, and will be present in both the swashplate and discrete piston cases. Equations for the losses due to fluid compressibility and valve transition throttling are considered in sections 5.2.4 and 5.2.5, and in section 6.2, the magnitude of these losses is predicted for the selected discrete piston design. Since these losses are present in both conventional and discrete piston designs, and their magnitudes depend heavily on specific design parameters, it is difficult to estimate them for generic swashplate and discrete piston devices for the purpose of comparing the two approaches.

5.2.4 Compressibility Loss

While it is often treated as incompressible, hydraulic fluid does exhibit a change in volume with a change in pressure, an effect that can be significant when air is entrained in the oil. The compressibility of the hydraulic fluid is quantified by the bulk modulus, which is defined by Eq. (2.3) in section 2.1.

The compressibility of the fluid requires that energy be added to the fluid to increase its pressure, with a lower bulk modulus resulting in more energy being stored in the fluid. The energy required to compress a unit of fluid from atmosphere to a given pressure is derived in section 2.3.2 and demonstrated in Fig. 2.5. That figure and the equation for the energy stored in the fluid are repeated here as Fig. 5.8 and Eq. (5.41).

$$E\left(P, V_0\right) = \int_{P_0}^{P} V_0 e^{-\int_{P_0}^{p} \frac{\bar{p}}{\beta(\bar{p})}\, d\bar{p}} \frac{p}{\beta\left(p\right)}\, dp \tag{5.41}$$

The fact that energy is stored in the fluid does not necessarily mean that this energy is lost. If the fluid is allowed to expand while doing useful work, then the compressed energy is not lost. For the analysis in this thesis, the energy stored in the fluid that goes out the high pressure port is not considered lost energy. Conversely, any energy in

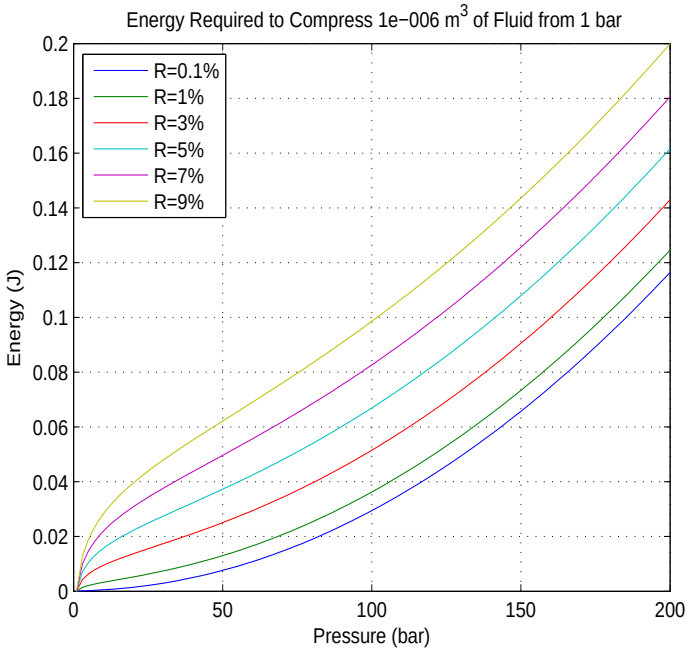

Figure 5.8: Energy required to compress $1cm^3$ of oil from atmosphere to a given pressure for different amounts of air entrained in the oil

the high pressure fluid that enters the high pressure port in the motor case is treated as energy input. However, whenever a volume of fluid at a pressure higher than atmosphere is connected to the low pressure port, the compressed energy in the fluid is considered a loss. For this reason, piston disabling strategies that connect the smallest amount of high pressure fluid to tank are preferred. In section 6.2, the compressed energy associated with each unit of high pressure oil is considered. This is included in computing the input and output power from the piston chamber.

There is another source of energy loss resulting from the compressibility of the fluid that occurs, especially in the motor case. In the motor case, the piston chamber is pressurized by connecting it to the high pressure input, rather than by compressing it with a piston. Thus, the change in volume that is required to increase the pressure in the chamber must be made up by a volume of fluid taken from the high pressure rail. Since the high pressure fluid is being used to compress a fluid chamber at a lower pressure, there is a pressure drop between the two volumes. This difference will result in a high fluid velocity between the two volumes, and, assuming none of that kinetic energy is recaptured, the pressure drop will result in an additional loss of useful energy. This throttling energy loss is given by:

$$E_{comp,throttle} = \int_0^{V_{H,f}} (P_f - P)\ dV_H \tag{5.42}$$

where V_H represents a volume of high pressure oil that is taken out of the input pressure rail, $V_{H,f}$ is the total volume take from the high pressure source during compression, and P_f is the supply pressure in the inlet rail. Once the high pressure oil is throttled down to the lower chamber pressure, it will expand so that the same mass of fluid will now take up a larger volume given by V_L:

$$V_H = V_L e^{-\int_P^{P_f} \frac{p}{\beta(p)}\ dp} \tag{5.43}$$

To solve Eq. (5.42), use Eq. (5.43) to convert the integration to be in terms of the chamber volume. Then, use Eq. (2.3) to convert the integral to be in terms of the chamber pressure:

$$E_{comp,throttle} = \int_{V_{L,0}}^{V_{L,f}} (P_f - P)\, e^{-\int_P^{P_f} \frac{p}{\beta(p)}\, dp}\, dV_L \tag{5.44}$$

$$= \int_{P_0}^{P_f} V_0 e^{-\int_{P_0}^{P} \frac{p}{\beta(p)}\, dp} e^{-\int_P^{P_f} \frac{p}{\beta(p)}\, dp}\, dP \frac{(P_f - P)}{\beta(P)} \tag{5.45}$$

$$= \int_{P_0}^{P_f} V_f \frac{(P_f - P)}{\beta(P)}\, dP \tag{5.46}$$

where V_f is the volume of the original oil in the chamber after it has been compressed up to P_f and is given by Eq. (2.29). Figure 5.9 shows the result of solving Eq. (5.46) for an initial chamber volume of $1cm^3$ being compressed up to $200bar$ using only the high pressure fluid to make up the compressed volume. Comparing Figs. 5.8 and 5.9, notice that the energy lost due to throttling in the motor case is an order of magnitude larger than the compressed energy stored in the fluid. It should be noted that if, in the pumping case, the piston chamber is connected to high pressure before the piston has compressed the oil in the chamber to high pressure, then this loss will also occur in the pumping case. In reality, the piston is moving at the same time, so the actual energy lost may be different. In section 6.2, the piston motion, the oil compression, and the valve throttling will be modeled simultaneously for the selected valving strategy.

This analysis shows that for the motor case, it is very important to minimize the initial volume of fluid to be compressed. In addition, any compression that can be done by moving the piston, rather than taking fluid from the high pressure rail, will reduce this loss.

Compressibility losses can be reduced or eliminated if the movement of the piston is used to compress and decompress the oil. If the oil volume can be brought up to high pressure by the motion of the piston before the oil volume is connected to high pressure, then there will not be any throttling of high pressure oil needed to compress the oil. In order for this precompression phase to occur, the piston chamber must be disconnected from both the high and low pressure ports, and it must occur as the piston is moving toward TDC. Conversely, if the motion of the piston can be used to decompress the oil volume, the loss of energy stored in the high pressure oil can be avoided. In this decompression state, the oil volume must again be disconnected from high and low pressure, this time with the piston moving away from TDC. This

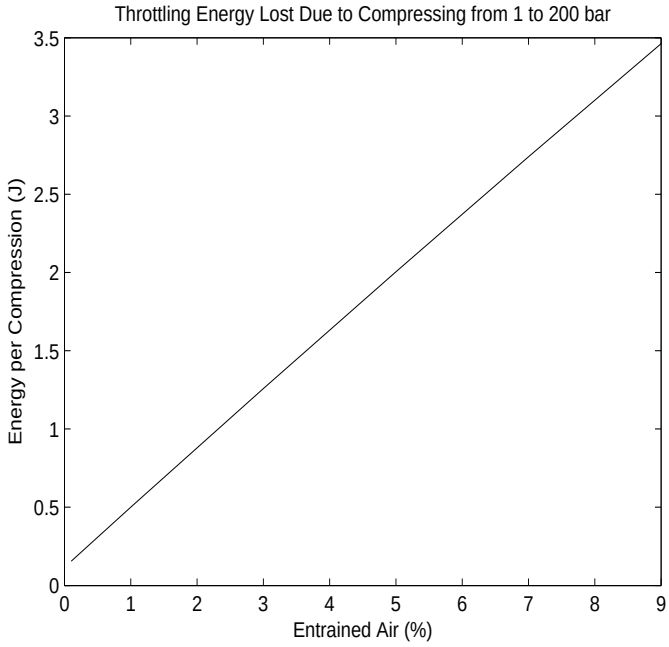

Figure 5.9: Energy lost due to throttling when compressing 1 cm^3 oil from atmosphere to 200bar in the motoring case by adding fluid at 200bar

will allow the decompressing oil to apply an aiding force to the pistons, allowing the piston to extract the energy stored in the fluid to apply useful work to the piston. Designing a valve control mechanism that allows for partial or complete precompression and decompression can reduce or eliminate the compressibility losses, but it requires a valve that can put the piston chamber into a blocked state at the correct stage of the piston travel.

5.2.5 Transition Loss

In section 5.2.3, the energy loss due to valve throttling was computed for a valve that was fully open. However, when a valve is partially open as it transitions between open and closed, the power loss due to throttling can be much higher than the nominal loss. This is particularly true for piston control strategies that transition while the piston is moving quickly and generating a lot of flow. As the pump/motor speed increases, the transition time of the control valves can become a significant fraction of the pumping/motoring stroke, so the transition loss through the valves can be significant. In general, a valve that transitions fast, and thus spends less time partially open, is preferred to one that is slow. There are many different valve configurations (i.e. disabling valve + check valve, closed-center 3-way valve, double poppet valve, etc.), and a quantitative study of each possibility is not included here. As an example, a configuration with a single valve that opens to tank and a check valve that opens to high pressure is presented for the pumping case. For simplicity, it is assumed that the fluid is incompressible. In reality, the fluid is being compressed as the valve transitions, so the transition loss and the compressibility loss are difficult to separate. All of the losses are accounted for in the dynamic model in section 6.2, but here, an approximation of the transition loss is presented. As a simple example, the area profile of the valve is assumed to vary linearly with pump rotation angle between closed and fully open. The pressure drop across the orifice can be computed from the orifice equation:

$$P_{valve} = \frac{\rho A_p^2 \dot{x}^2}{2c_d^2 A_{ori}^2 (\theta - \phi_i)} \tag{5.47}$$

where $A_{ori}(\theta)$ is the linearly varying valve open area. If P_{valve} is higher than the output pressure, then the check valve will open, and the pressure will be limited to the output

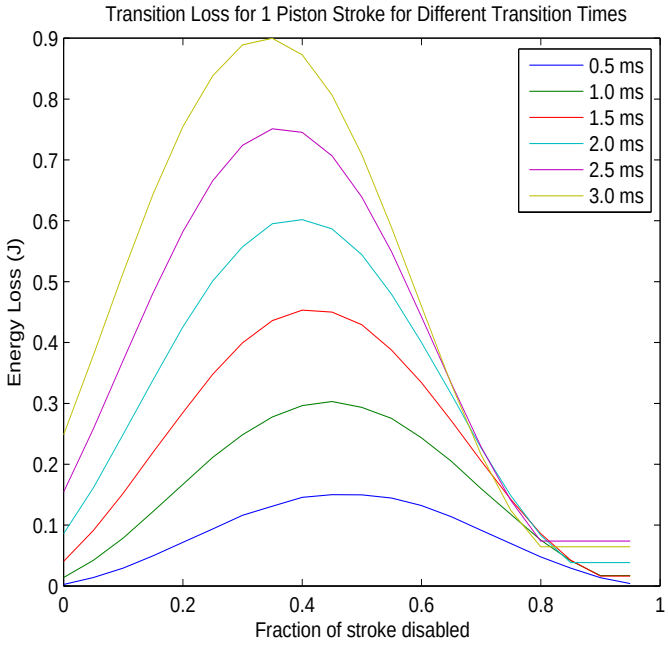

Figure 5.10: Energy lost due to throttling through a valve opening to tank

pressure. In this case, the flow through the transitioning valve can be computed by the orifice equation, Eq. (5.39). The total power loss due to transition is:

$$E_{transition} = \int_{t_0}^{t_{trans}+t_0} P_{valve} Q_{valve} \, dt \tag{5.48}$$

where t_0 is the start time for the transition, t_{trans} is the transition time for the valve, and Q_{valve} is the flow through the valve. In the current example, Q_{valve} is either $A_p \dot{x}$ or computed from Eq. (5.39), depending on whether the check valve is open. Using these equations and the numerical pump parameters used in section 5.3, the power loss through the transitioning valve is shown in Fig. 5.10.

For this example, the transition loss is computed for a number of valve transition times. Clearly, a slower valve results in a higher throttling loss. Notice also that the transition loss is highest in the middle of the pumping stroke when the most flow is passing through the transitioning valve. Ideally, the valve would only transition when the piston is near Top Dead Center (TDC) or Bottom Dead Center (BDC) when the flow is small, but that cannot be accomplished for one of the two transitions in the

partial stroke discrete piston varying approach. However, for the whole piston disabling strategy, transitions during high flow periods can be avoided, resulting in a lower average transition loss per piston. The transition loss must be taken into account when selecting the piston disabling strategy.

5.3 Numerical Comparison

The equations in the previous section can be used to estimate the total loss in a swashplate and discrete piston type pump/motor. In order to perform a numerical comparison with the preceding loss equations, the values of the physical pump/motor parameters must be selected. While the equations apply to a wide range of pump/motor sizes, in this section, the parameters are estimated from a pump/motor that is the same size as the discrete piston prototype to be described in a later section. This prototype has a full displacement of about $48cm^3$, which is a medium sized device for typical off-road equipment. The piston diameter is $D_p = 18mm$, the pitch radius is $D_{pitch} = 82mm$, the max swashplate angle is $\alpha = 16^\circ$, the piston clearance is $c = 16.5\mu m$, the length of the piston in the bore when fully extended is $x_{end} = 19.6mm$, the length of the piston that is at diameter D_p is $L_{edge} = 38.1mm$, the length from the end of the piston to the swashplate is $L_{piston} = 57.3mm$, and the number of pistons is $N_p = 8$. These physical parameters are taken from an existing wobble plate pump that was adapted to a discrete piston prototype. The fluid is assumed to be a standard hydraulic oil (DTE 25) with a density of $\rho = 876kg/m^3$ and a dynamic viscosity of $\mu = 0.0387kg/(ms)$. For all orifice calculations, the coefficient of discharge is assumed to be $c_d = 0.67$. The maximum operating pressure and speed for the prototype are $P = 200bar$ and $\omega = 1800RPM$. The coefficient of friction between the piston and the bore was selected to be $\nu_p = 0.13$, which is a typical value for lubricated steel on iron. For the slipper-swashplate interface, the original pump design, as well as the discrete piston prototype, do not use hydrostatically balanced pistons. The prototype does use a lubricated rolling element bearing to reduce friction, and a typical value of $\nu_s = 0.0035$ was used for both the discrete piston and swashplate approaches.

The eccentricity ratio, defined as the distance the piston is offset from the center divided by the radial clearance, is difficult to know without a much more detailed model.

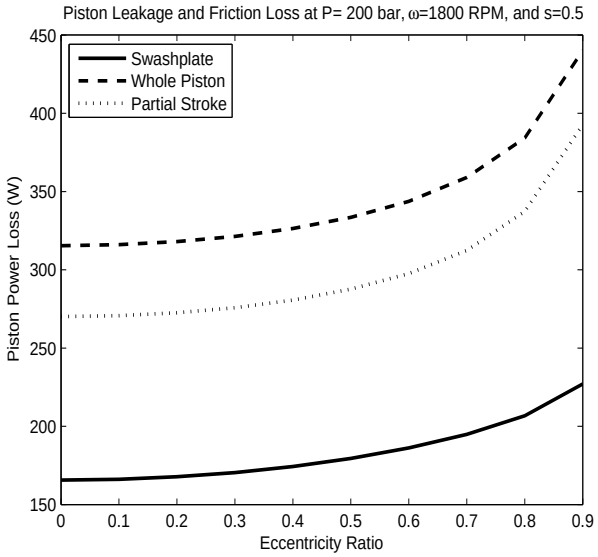

Figure 5.11: Power loss due to piston leakage and piston friction for different eccentricity ratios

However, as Fig. 5.11 shows, the percentage increase in power loss due to eccentricity is fairly small across most of the eccentricity range. Thus, for comparison purposes between the two approaches, the choice of e does not have much impact outside of all but the highest eccentricity ratios. A value of $e = 0.7$ will be used in the following results.

The geometry of the valve plate cannot be taken from the discrete piston prototype, since it does not have a valve plate. The valve plate parameters used here are estimates from measured parameters on similarly sized axial piston pumps, or values taken from published experimental results. The inner and outer sealing lands between the valve plate and the cylinder block are $r_4 - r_3 = r_2 - r_1 = 3mm$, which was a measured value from a comparably sized pump. This is similar to the pumps tested in [105], which had sealing lands of $3.5mm$ and $4.25mm$.

In [103], the barrel is described as being tilted with respect to the valve plate such that the maximum gap occurs over the middle of the high-pressure port, which is depicted in Fig. 5.7. However, in [106] experimental measurements on a number of valve plates indicate that the largest gap occurs over the low pressure port, which would

result in tilt angle $\gamma < 0$. In Eqs. (5.31) and (5.32), a negative tilt angle would seem to reduce the leakage, but experimental measurements in [106] indicate that the valve plates tilted with the largest gaps over the low pressure port also had the worst leakage. That paper also indicated that different valve plate features can significantly reduce the amount of barrel tilt. Due to the discrepancy in the location of the maximum tilt and the fact that a well-designed valve plate can have a relatively small amount of tilt, it is assumed that $\gamma = 0$. This will result in lower friction than a valve plate tilted in either direction.

In [105], values for the gap between the cylinder and the valve plate of roughly $5 - 15\mu m$ were measured. Slightly larger gaps were measured in [106], with average values around $20 - 25\mu m$. The goal the valve plate loss modeling in this chapter is to provide an estimate of the losses that can be avoided by the discrete piston approach to determine whether it has the possibility to significantly reduce the losses that occur in a conventional hydraulic pump/motor. To that end, the discrete piston approach should be compared to a well-designed conventional pump. Figure 5.12 shows the average leakage and friction losses on the valve plate for a tilt angle of $\gamma = 0$. The loss in this figure is averaged over an operating range of $35 - 200bar$ and $200 - 1800RPM$. For the numerical parameters used for this simulation, a valve plate clearance of $h_0 = 10\mu m$ produces the lowest overall loss, so that is the value that is used for the comparison.

With all of the numerical parameters defined, the magnitude of the different losses can be calculated for different displacements. Figure 5.13 shows the different losses in both approaches across the displacement range. These plots are for a pump operating at $200bar$ and $1800RPM$. Notice that, for the discrete piston case, the equations for some of these losses are not included in the preceding sections, since they rely on the valving mechanism to be selected. These losses are calculated using equations described in section 6.2, and include the valve leakage, valve throttling, valve friction, and valve actuation power.

In Fig. 5.13, the relative benefits and drawbacks of the discrete piston approach, from an efficiency perspective, are evident. The biggest advantage is clearly the elimination of the valve plate, which allows a significant reduction in the valve leakage (Q_{valve}) and friction (F_{valve}). In both the swashplate and discrete piston approaches, the valve losses are constant with displacement. The benefit in the discrete piston case arises from the

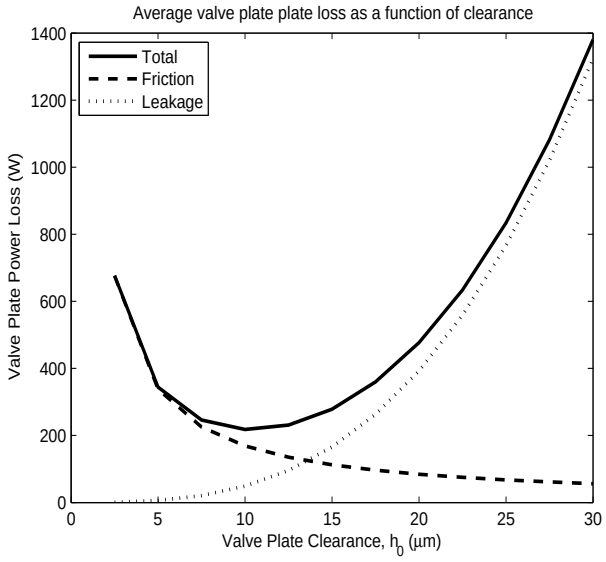

Figure 5.12: Average power loss across the operating range due to friction and leakage between the valve plate and the cylinder barrel for different clearances

fact that a single element does not need to act as both a seal and a bearing. This dual function leads to a tradeoff, illustrated in Fig. 5.12, where a larger gap is desired to reduce friction, but a smaller gap is desired to eliminate leakage. In the discrete piston approach, the pistons do not rotate with respect to the housing, so there is no need for any bearing element. This is in contrast to existing variable displacement pumps and motors, which require the pistons to rotate with respect to the high and low pressure ports to achieve commutation of the pumping/motoring chambers. The geometry of the sealing and bearing interface is also constrained in the conventional approach. The high pressure port that must be sealed is a kidney-shaped region whose size is governed by the number and pitch diameter of the pistons. The ability to have the pistons stationary with respect to the housing, while still providing variable displacement functionality, is enabled by the discrete piston approach.

Another significant benefit of the discrete piston approach is the reduction in the friction between the pistons and the swashplate with displacement. At full displacement, both the swashplate and the discrete piston approaches have the same power loss due to friction. However, in the swashplate case, each piston sees high pressure for half

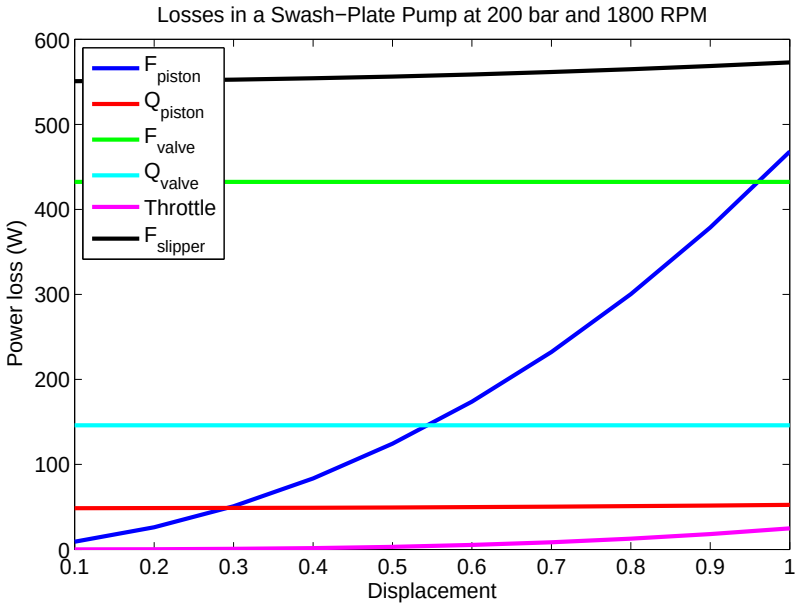

(a) Swashplate Losses

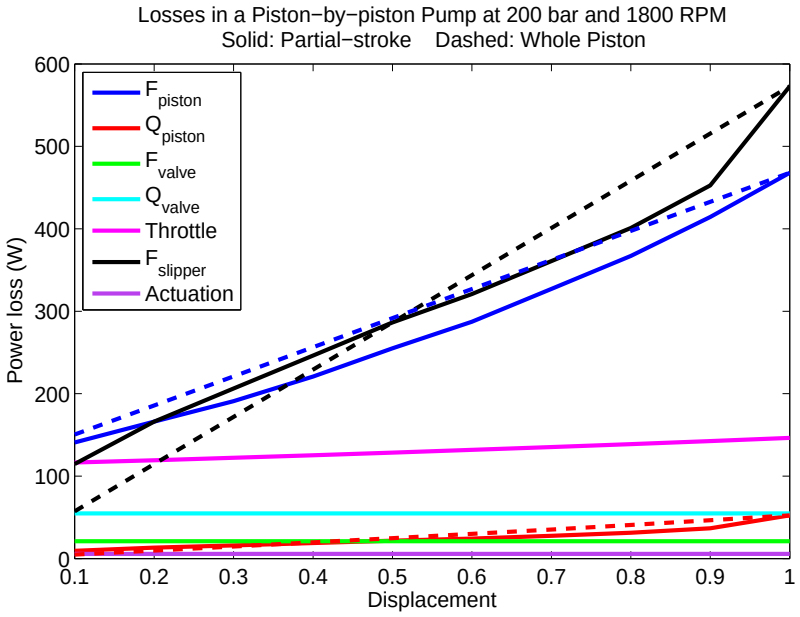

(b) Discrete Piston Losses

Figure 5.13: Losses in a Swashplate and Discrete Piston type pump for different displacements

of the pump/motor rotation, regardless of the displacement setting. In the discrete piston case, high pressure is only applied to the piston when it is doing work, so, as the displacement is reduced, the friction force due to the high contact force between the piston and swashplate is reduced correspondingly. There is a difference in this loss between the whole piston and partial stroke disabling approaches. In the whole piston approach, the frictional loss reduces linearly as the displacement is decreased since the number of pressurized pistons also decreases linearly. For the partial stroke disabling case, the frictional loss decreases faster that the whole piston approach initially, but the reduction slows down so that, at lower displacements, the frictional loss is higher than in the whole piston case. This is due to the fact that the disabling angle, $\theta_{partial}$ shown in Fig. 5.3, does not vary linearly with displacement. Since the flow from the piston follows a sinusoidal profile, near the beginning and end of the stroke, the disabling angle must be varied more to effect a change in the displacement than in the middle of the stroke. Thus, near the ends, a small change in displacement results in a relatively large change in the angle over which the pistons are pressurized, when compared with the middle of the stroke. For a pump/motor design that uses hydrostatically balanced pistons, the friction loss may be lower, but an additional leakage loss will exist. This new leakage loss would remain constant in the conventional swashplate case, and reduce linearly with displacement in the discrete piston case due to the removal of pressure from unused pistons.

The final benefit of the discrete piston approach is the reduction in the piston leakage with displacement. As with the swashplate friction loss, in the conventional case, each piston sees high pressure for half of its rotation for all displacements, but in the discrete piston case pressure is removed from pistons that are not actively pumping/motoring. Thus, the pressure driven leakage for the unused pistons is eliminated.

Figure 5.13 also demonstrates that there are several losses that are larger in the discrete piston case. The piston friction in the discrete piston case is larger than in the swashplate case since the pistons are always traveling full stroke instead of moving through a reduced stroke at lower displacements. The coulomb component of the piston friction is also higher in the discrete piston case at lower displacements. This is due to the fact that the highest side loads on the piston occur when the piston is fully extended out of the bore. In the swashplate case, as the displacement is decreased, the farthest

extension of the piston out of the bore is also decreased, which is not the case in the discrete piston case. The partial stroke disabling case can have a lower coulomb loss than the whole piston case if pressure is applied to the piston when it is further into the bore. Note that there are different ways to accomplish partial stroke disabling (i.e. start a pumping stroke late vs. end the stroke early), but, as will be discussed in following sections, the approach that results in power being applied when the piston is furthest into its bore is the preferred method.

Since the discrete piston approach requires the pistons to travel their full stroke at all displacements, the throttling losses are higher for the discrete piston case than the swashplate case with a similarly sized orifice. A consequence of reducing the piston stroke in the swashplate case is that less fluid is moved into and out of the pumping chamber at low displacements, whereas in the discrete piston case, unused pistons extract and return fluid to the low pressure port, with a loss associated with the movement of the fluid through the ports. The fact that the throttling loss can be larger highlights the need to have large, unrestrictive flow paths between the inlet/outlet ports and the piston chamber. While this is always a goal in designing efficient hydraulic systems, it is even more critical in the discrete piston case than in the swashplate case. In Fig. 5.13(b), the throttling loss is reduced slightly at lower displacements. This is due to the fact that, in the discrete piston prototype, the flow path to tank is less restrictive than the flow path to high pressure. This is strictly a consequence of the specific design, and not inherent to the discrete piston approach. A discrete piston pump/motor with equally restrictive high and low pressure paths would have a throttling loss that is constant with displacement. Another way to reduce the throttling loss in a discrete piston controlled device is the flow limiting approach described in [67, 68, 69, 70, 71, 72]. In this approach, rather than being connected to tank, disabled pistons are blocked, causing the piston to draw a vacuum. The void in the piston chamber is then filled by the piston moving in the opposite direction, allowing it to collapse in a controlled way. This avoids the throttling associated with sending and withdrawing fluid from the tank, but it may lead to challenges with air entrained in the oil. It also requires a control valve that has three states: high pressure, low pressure, and blocked.

The final drawback to the discrete piston approach is the need for actuation power. While removing the high and low pressure commutation effects of the valve plate has

significant efficiency benefits, it does create the need for valves that are actuated with another power source. This could be mechanical, electrical, or hydraulic power, depending on the design of the discrete piston control valves. In the design described in section 6.3, the actuation power is hydraulic. Achieving low power actuation for the valves is another critical design goal for creating viable discrete piston pumps and motors.

While there are both advantages and disadvantages to the discrete piston approach, the magnitude of the benefits significantly outweigh the drawbacks. That fact is emphasized by Fig. 5.14, which shows the overall efficiency of the swashplate and discrete piston devices across the displacement range. Since the total losses in the partial stroke disabling case are smaller (and that is the approach taken in the prototype to be described), the partial stroke losses were used to generate this plot. Note that the efficiency calculated here only takes the losses in Fig. 5.13 into account. There are several other losses, such as compressibility losses, valve transition throttling, bearing friction, and fluid churning losses which are not included in this result for either the swashplate or discrete piston designs. Some of these losses, such as compressibility and transition loss, may be higher in the partial stroke disabling case than in the whole piston disabling approach. Section 5.4 describes the benefits and drawbacks of these two approaches. In addition to the "Swashplate" and "Discrete Piston" efficiency curves, which represent all of the losses shown in Fig. 5.13, figure 5.14 also shows the "DP without Valve Losses" efficiency result for the discrete piston approach without the losses due to throttling, actuation, valve leakage, and valve friction. These are the losses that rely on the detailed design of the discrete piston pump/motor. The difference between the swashplate efficiency and the discrete piston efficiency without valve losses is essentially the "design space" for a discrete piston valve mechanism that will provide an efficiency benefit over conventional variable displacement pumps and motors.

Figures 5.13 and 5.14 compare the power losses between the two approaches at a high pressure ($200bar$) and speed ($1800RPM$). Figure 5.15 shows the total power losses at four different operating points. In all four cases, the discrete piston approach has a lower power loss value, especially at low displacements.

In the next section, a summary of different piston disabling strategies is presented, with benefits and drawback for each.

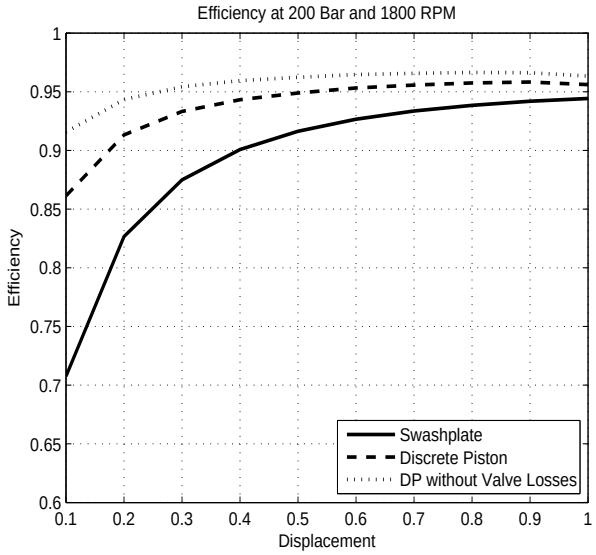

Figure 5.14: Pump Efficiency for Swashplate and Discrete Piston pumps including the losses shown in Fig. 5.13

5.4 Displacement Variation Strategies

To accomplish discrete piston control, there are several different strategies for when to disable the pistons, and which pistons to disable. The different strategies have varying effects on the performance of the pump/motor, affecting characteristics such as the compressibility loss, transition loss, piston and slipper friction, piston leakage, and output flow/torque ripple. For a system with electronically controlled valves that can open at any arbitrary rotation angle, the pump/motor could switch between the different strategies. However, the approach taken in this thesis is to use fully mechanical control, which requires a single method to be selected.

The flow ripple is a significant characteristic of the different approaches, and it will be numerically compared in section 5.4.4. However, to explain the operation of the different disabling strategies, examples are provided in the following sections that can be compared with the full displacement case shown in Fig. 5.16. In this figure, the total output flow is shown in black, and the flow out of the individual pistons is shown in a variety of colors. Note that these figures depict only high pressure flow; since each piston

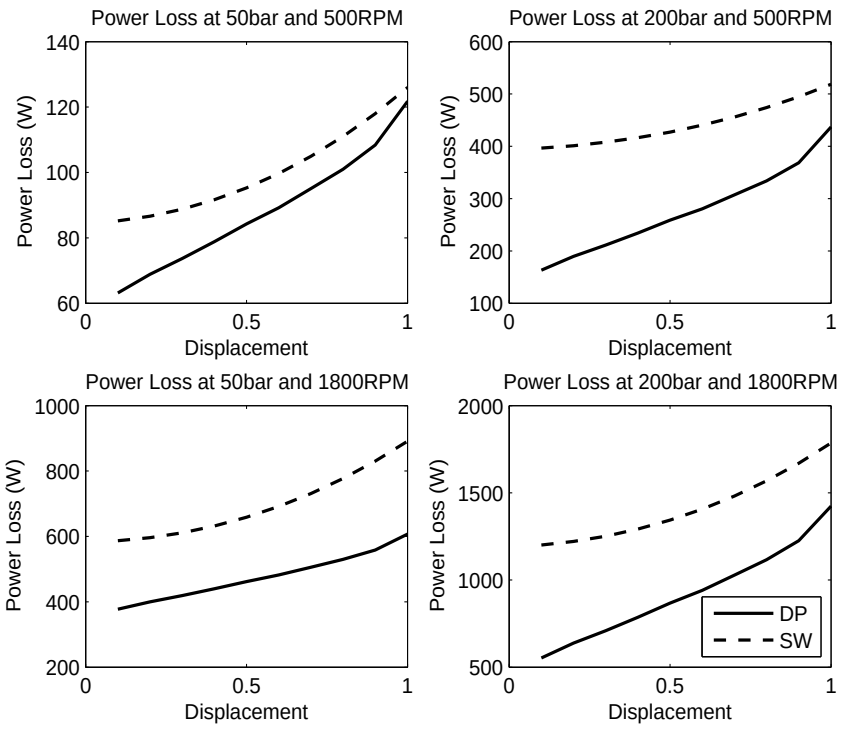

Figure 5.15: Power loss across the displacement range for a Swasplate (SW) and Discrete Piston (DP) pump at four corners of the operating range

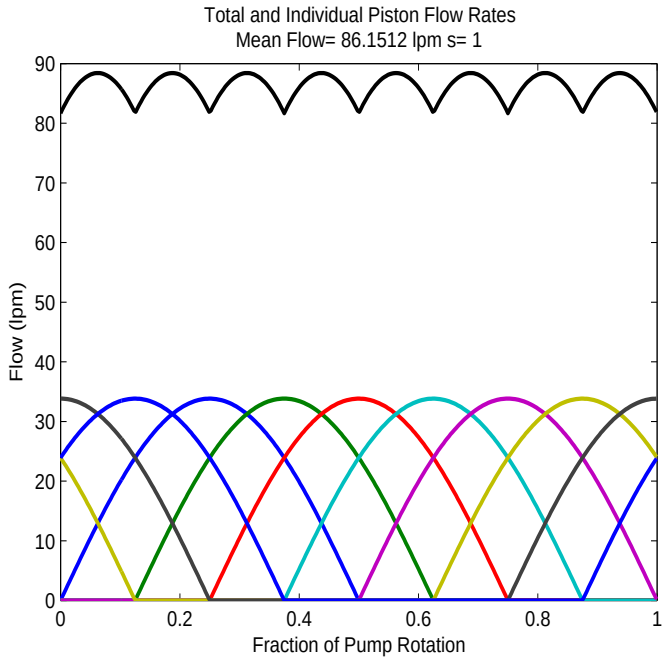

Figure 5.16: Total flow and flow through individual pistons for a pump or motor at full displacement

is always traveling through full stroke, there is always flow entering or exiting the piston chamber (except in the Partial Flow Limiting case described below). However, this flow is often low pressure flow, which is not used to do work. The flows in these figures are generated using parameters described in section 5.3, but they can easily be scaled to represent an arbitrarily sized device. These flow rates represent the ideal flow based on the velocity of the piston; compressibility and transition effects are not considered.

The strategies described in this section deal with when the piston chamber should be connected to high pressure. It is implied that when the piston chamber is not connected to high pressure, that it is connected to tank, or in transition between the two. However, there is another concept called Partial Flow Limiting, which completely blocks the piston chamber for much of the disabled portion of the stroke, rather than connecting it to tank. In this approach, a vacuum is created in the piston chamber, which is then removed in a controlled manner by the motion of the piston. The theory is that by creating and then filling the vacuum in a controlled way, the traditional problems associated with oil cavitation can be avoided. This is an active area of research by [67, 72, 71], and will not be studied further in this thesis.

5.4.1 Whole Piston Disabling

One method of reducing the pump/motor displacement is to disable a certain integer number of the pistons for each full power stroke. An example of the resulting flow from using this approach to vary the displacement is shown in Fig. 5.17. In this figure, the displacement is commanded to be 62.5% of the total displacement, which results in 3 of the 8 pistons being disabled. This figure represents the kinematic flow ripple from the pump/motor, meaning that the flow from each piston is only a result of the piston motion, $Q_{piston} = A_p\dot{x}$. Thus no compressibility or transition effects are considered. For this piston control method, only discrete displacement settings are available, with the flow resolution determined by the number of pistons. The typical equation for the flow rate:

$$Q_{average} = \frac{D\omega s}{2\pi} \tag{5.49}$$

where D is the displacement of the device. If the average is taken over more than one rotation, then the resolution of the displacement can be increased by varying the discrete displacement each rotation cycle.

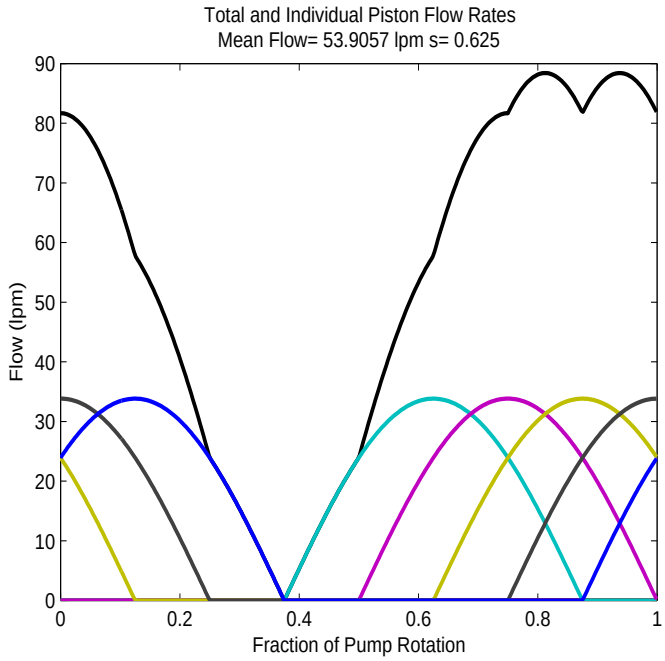

Figure 5.17: Total flow and flow through individual pistons for a pump or motor using Whole Piston Disabling

Beyond the limitation of discrete displacement settings, a significant disadvantage of the whole piston approach is evident in Fig. 5.17. There is a large flow ripple, with full flow being supplied for part of the rotation, and no flow being supplied for the rest. The application using this pump or motor would need to be tolerant of significant fluctuations in the power through the device and/or incorporate smoothing elements such as accumulators or flywheels. This disadvantage can be partially mitigated by changing the order in which pistons are disabled. In Fig. 5.17, the pistons are disabled in order. In Fig. 5.18, rather than being disabled sequentially, the pistons are disabled in an order that was selected to more evenly distribute the disabled pistons around the pump/motor. The disabling order used for the eight piston example was: $1, 5, 3, 7, 2, 6, 4, 8$ where the pistons around the pitch diameter are sequentially numbered. Notice that, in this case, the full pump flow does not drop to 0 since there is always at least 1 piston providing flow. While this approach does reduce the observed flow ripple, it may be difficult to achieve using purely mechanical control mechanisms, as the relationship between the pump rotation angle and the piston to be disabled can be very complicated.

With the whole piston disabling approach, some care must be taken in designing a control strategy for the pump/motor. The displacement setting is only valid when averaged across a full rotation. Thus, if a control algorithm calls for the displacement to vary significantly within one rotation, it might vary when all of the piston are on and extend/decrease the current rotation, or it might vary when all of the pistons are off and not take effect until the next rotation. In this case, the behavior of a control algorithm that is commanding the displacement could vary depending on when a change in command is given. As with other types of discrete control [33], this may mean that, in practice, the control bandwidth will have to be significantly slower than the pump rotation frequency. Another way of stating this is that the fundamental frequency of the flow ripple is the pump rotation frequency, and to avoid reacting to that disturbance, the control bandwidth will have to be slow enough to reject it, unless techniques are used to estimate and account for the disturbance.

If an application can accept the flow ripple from the whole piston disabling approach, there are some advantages to this approach with respect to the transition and compressibility losses. In Fig. 5.10, notice that the energy loss peaks in the middle of the power stroke, with the power loss at the beginning and end of the stroke almost

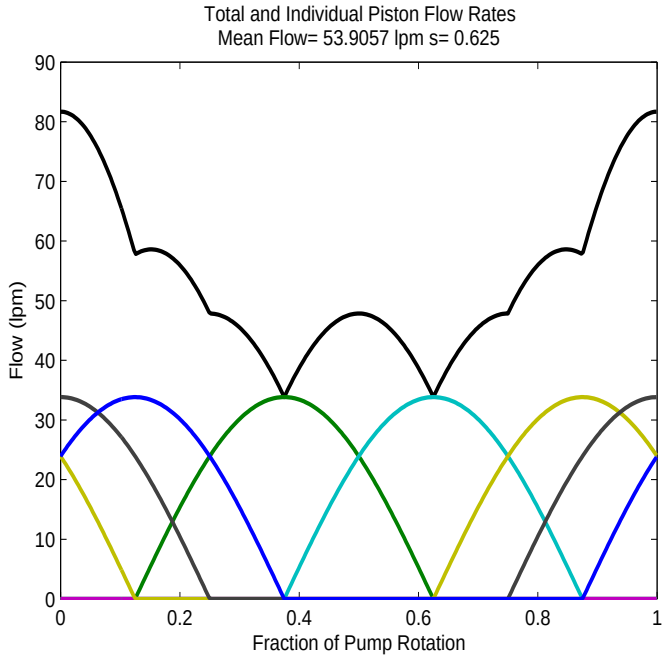

Figure 5.18: Total flow and flow through individual pistons for a pump or motor using Whole Piston Disabling with an alternating piston order

negligible. In the whole piston disabling case, the piston never transitions during the power stroke, so the loss through a transitioning valve can be very small. In addition, if the pump/motor remains at a constant displacement, then pistons that are disabled could remain disabled, and thus not have any transition loss or actuation power.

The compressibility loss in the whole piston disabling case could also be small. The disabled piston chambers never need to be charged or discharged, so the compressibility loss would only exist for the active pistons. Furthermore, since the piston is never enabled or disabled in mid stroke, the volume of fluid that must be compressed/decompressed for the active pistons can be minimized.

5.4.2 Whole Piston Plus One Partial

A slight variation on the whole piston disabling approach is to disable most of the pistons discretely, but allow one piston to be enabled/disabled mid-stroke. This would eliminate the discrete nature of the displacement variation. Figure 5.19 shows this

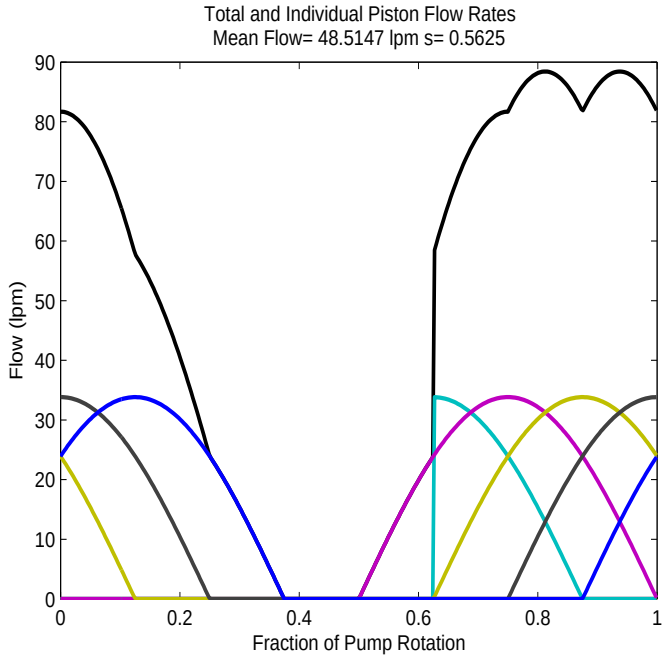

Figure 5.19: Total flow and flow through individual pistons for a pump using Whole Piston Disabling with one partial piston

case, with the displacement command reduced to 56.25% of full. This results in 3 pistons being disabled for their entire stroke, and one piston being disabled for half of its stroke. The approach could also be used with the piston disabled for the second half of the stroke, but this would have increased compressibility loss. As with the pure whole piston approach, the piston disabling order could be sequential, or it could be a different order designed to reduce the flow ripple. This may or may not be possible using mechanical methods, depending on the design of the piston disabling mechanism.

The advantage of this approach is that it allows for continuous variation of the average displacement. However, it still exhibits the large flow ripple associated with the whole piston approach, and it does come with additional transition and compressibility losses on the one piston that is disabled mid-stroke.

5.4.3 Partial Stroke Disabling

Figure 5.20 depicts a pump/motor using the partial stroke disabling method. This example also shows the device operating with a displacement setting of 62.5%, but instead of 3 whole pistons being disabled, each of the piston operates with a reduced stroke. Following Eq. (5.10), each piston is active over a rotation angle of $\theta_{partial} = cos^{-1}(1 - 2 * 0.625) = 1.82 radians$. As with the previous approach, this method allows continuous variation of the displacement, but unlike the previous approach, none of the pistons are enabled for the full power stroke. In this approach, all of the pistons are treated equally, which has advantages when designing a mechanism to control the piston enabling/disabling valves. In addition, the flow ripple for this approach is smaller than it is in the whole piston disabling case. While the ripple is still significant, the total partial-displacement flow never reaches max flow or drops to zero. In this case, the fundamental frequency of the pump ripple is the pump rotational frequency times the number of pistons. Due to this, a closed-loop controller on the displacement in this case could be significantly faster than in the whole piston case without reacting to the flow disturbance.

However, the partial piston approach does have higher transition losses and the potential for higher compressibility losses. Since the enabling/disabling valve needs to transition at any arbitrary point in the power stroke, it is not possible to avoid the high transition losses associated with high flows passing through the valve. For this approach, each piston is pressurized and de-pressurized in each rotation. Unless the valve is designed to enable completely precompressing and decompressing the dead volume using only the piston, there will be some compressibility loss associated with each piston. The magnitude of the losses due to the energy stored in the fluid depend on the volume and pressure of the fluid in the piston chamber when it is connected to tank. Thus, it is better to delay the start of the power stroke and allow it to finish normally at TDC, as shown in Fig. 5.21, rather than start the stroke normally at BDC and end it early. As shown, when the piston chamber transitions from high pressure to low pressure, the chamber will be at its minimum volume. Ideally, the valve mechanism will be designed so that the piston chamber is not connected with high pressure until it has been compressed up to high pressure. However, if that is not possible, it is still beneficial to start the pumping stroke late, when the piston volume is smaller than its

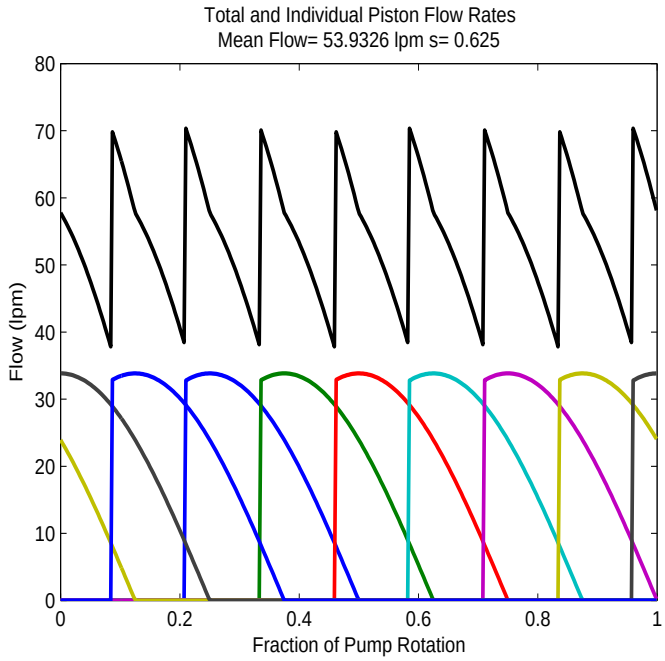

Figure 5.20: Total flow and flow through individual pistons for a pump using Partial Stroke Disabling

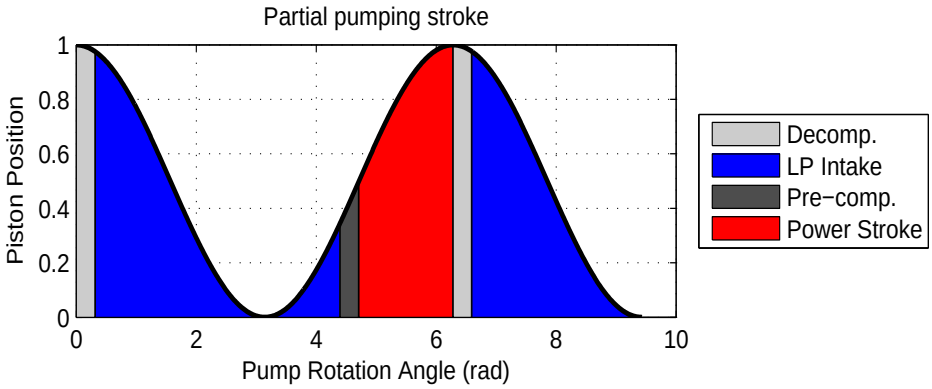

(a) Pump

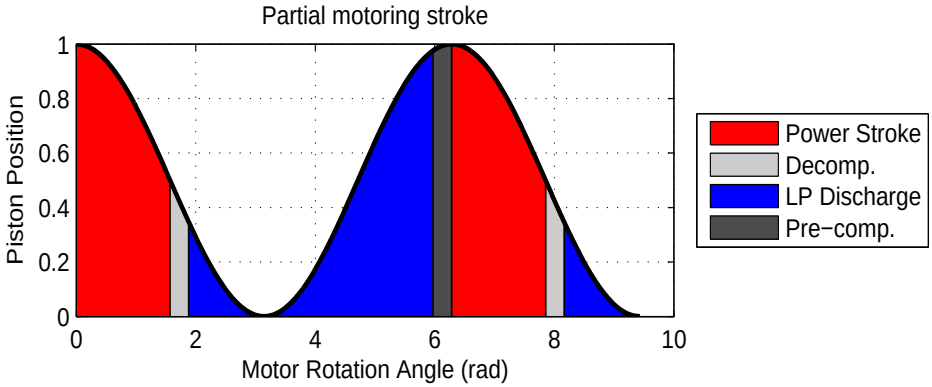

(b) Motor

Figure 5.21: Partial-displacement pumping and motoring stroke for a valve with pre-compression and decompression

maximum, than it is to do the opposite.

In Fig. 5.20, the power stroke from each piston is shortened by delaying its start, with the piston connected to tank for the beginning of the power stroke. This is the ideal configuration for the pumping case, since it always results in the power stroke ending with the piston at TDC, where the pressurized oil volume is at a minimum. This minimizes the loss of compressed energy stored in the fluid when the piston chamber is connected to low pressure. However, for the motor case, this is not the ideal situation. In the motor case, the power stroke starts with the piston at TDC, and then the oil volume expands throughout the stroke. Thus, at the normal end of the power stroke,

the high-pressure oil volume is at its maximum. By reversing the disabling strategy and ending the power stroke early, which is the opposite of the condition shown in Fig. 5.20, the volume of compressed oil in the piston chamber when it is connected to tank is reduced. In addition, Fig. 5.9 shows that energy lost due to throttling while compressing the fluid up to the motoring pressure is much higher than the compressed energy that is lost. Thus, having the oil volume being as small as possible when it is first connected to high pressure is ideal for the motor case. Starting the motoring stroke as normal when the piston is at TDC then ending it earlier than normal will minimize both the compressed energy loss and the energy lost due to throttling during compression.

The compressibility loss can be further reduced by adding precompression and decompression states to the valve timing, as shown in Fig. 5.21. In this figure, the pumping power stroke starts early, and the motoring power stroke ends early, which is the ideal order for reducing the compressibility loss. However, there is also a precompression state shown before the beginning of the power stroke and a decompression state shown at the end. In precompresion, the piston chamber is disconnected from both high and low pressure, and the motion of the piston toward TDC is used to raise the pressure until it is equal to the pressure in the high pressure rail. If the pressure can be equalized before the piston chamber is connected to high pressure, then no energy will be lost in compressing the oil. Note that energy will still need to be added to the oil by the motion of the piston, but it is not considered lost if it is forced out to the high pressure rail, or if the compressed energy is extracted in the decompression state. The decompression state at the end of the power stroke is similar to the precompression state in that it requires the valve to be disconnected from high and low pressure, and it allows the motion of the piston to achieve the required change in pressure in the oil volume. In the decompression state, the piston must be traveling away from TDC to expand the oil volume. By expanding while the piston chamber is blocked, the energy stored in the compressed oil is extracted by the piston, allowing it to be recaptured as useful work applied to the piston. In Fig. 5.21, the precompression state is shown occurring just before TDC for the motor case, and the decompression state occurs just after TDC in the pump case. The duration of the ideal precompression and decompression states will vary with operating pressure and speed of the device, and in reality, it is difficult to achieve perfect precompression and decompression. However, even achieving part of

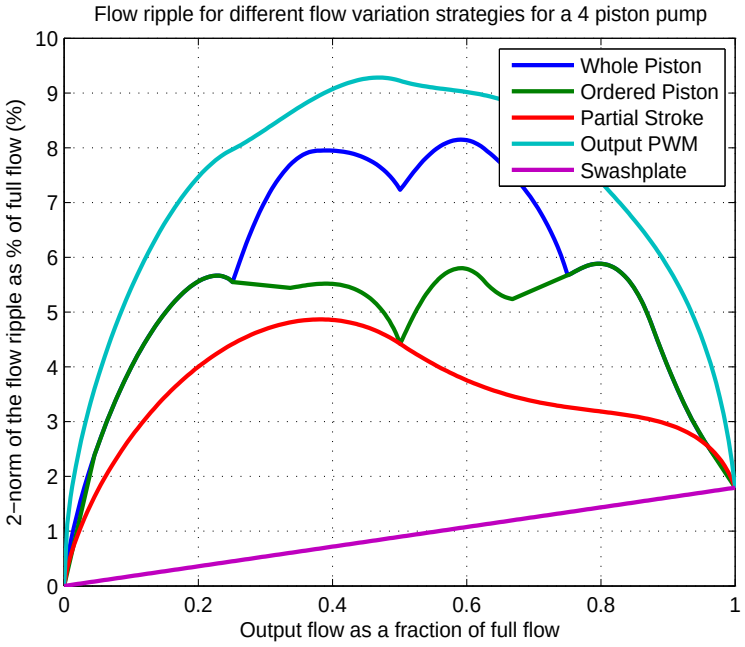

Figure 5.22: Comparison of the flow ripple for different displacement control with an 4 piston pump or motor

the compression and decompression of the oil using the piston travel will reduce the compressibility loss.

5.4.4 Flow Ripple Comparison

The different strategies described in the preceding sections exhibit different flow ripple characteristics. In this section, the magnitude of the flow ripple for each strategy is computed and compared for 4, 8, and 16 piston devices, all having the same total output flow rate of roughly $86lpm$. In this comparison, the whole piston, ordered piston, and partial stroke disabling strategies are compared, along with the flow ripple resulting from a conventional swashplate device and from a strategy using an on/off valve to pulse-width-modulate the entire output of the pump (Output PWM). Figures 5.22, 5.23, and 5.24 show the flow ripple comparisons for the 4, 8, and 16 piston devices respectively.

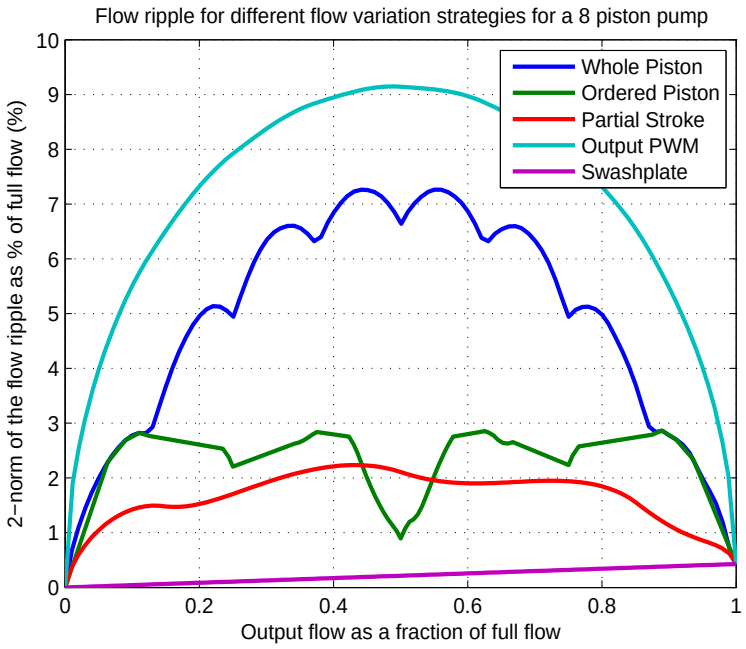

Figure 5.23: Comparison of the flow ripple for different displacement control with a 8 piston pump or motor

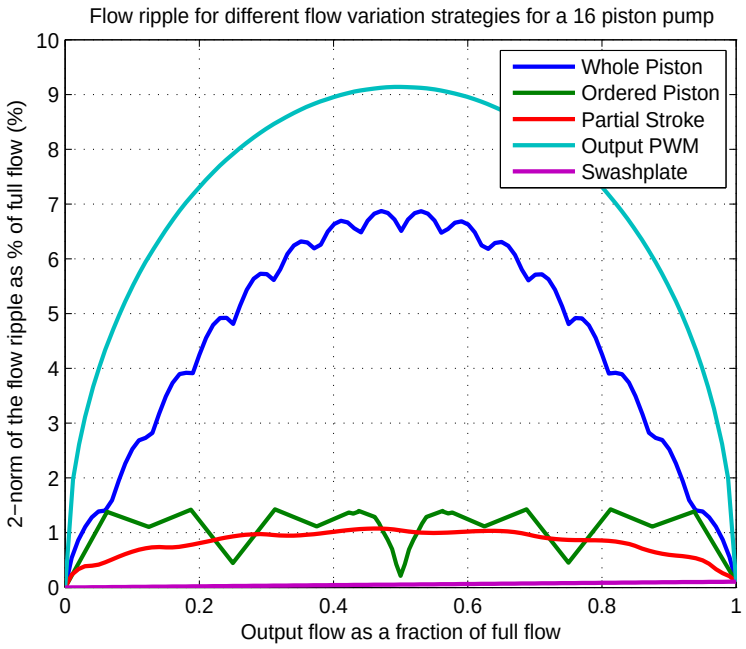

Figure 5.24: Comparison of the flow ripple for different displacement control with a 16 piston pump or motor

In these figures, the magnitude of the flow ripple is represented by the 2-norm:

$$\|Q_{ripple}\|_2 = \sqrt{\int \left(Q\left(\theta\right) - Q_{mean}\right)^2 \; d\theta} \tag{5.50}$$

These plots show that the flow ripple for a discrete piston device is greater than the ripple in a conventional pump/motor, but is significantly smaller than an approach that applies PWM to the full output flow. In addition, it is clear that the partial stroke variation displacement variation strategy has the smallest flow ripple for nearly the entire operating range. Increasing the number of pistons in the pump/motor is an effective way to reduce the flow ripple for the conventional swashplate, partial stroke variation, and ordered piston disabling approaches. However, the whole piston disabling and full output PWM approaches were not significantly improved by increasing the number of pistons.

5.5 Conclusion

In this chapter, the power loss mechanisms in a swashplate-type and a discrete piston controlled pump/motor were compared. Losses, such as the piston leakage and friction, the valve plate leakage and friction, the slipper friction, and the valve throttling were derived as a function of the pump/motor displacement. Other losses, such as the compressibility and transition throttling were defined, but they are highly dependent on the detailed design of the valve mechanism, so they were not directly compared between the swashplate and discrete piston devices. A numerical example based on an 8-piston wobble-plate type prototype was presented for both types of pump/motor. The results of the numerical example indicated a distinct efficiency advantage for the discrete piston approach, particularly at lower displacements. While some losses, such as the piston friction and throttling, were slightly higher in the discrete piston case, large reductions in the slipper friction, valve friction, and valve leakage make the overall efficiency of discrete piston control higher than the conventional approach.

Within the concept of discrete piston control, there are several options for how the pistons are enabled and disabled. The primary split is between whole piston disabling, which disables a variable number of pistons for their entire power stroke, and partial

stroke disabling, which disables each piston for a variable fraction of its stroke. In this chapter, the relative benefits and drawbacks of the different approaches, such as efficiency, flow ripple, and controllability were discussed. The whole piston disabling strategy has the potential to be more efficient since it can avoid transition losses and compressibility losses on the pistons that are fully disabled. However, the partial stroke approach has a smaller overall flow ripple. It also has the advantage of being simpler to implement using mechanical valves. Several concepts for achieving both whole piston and partial stroke disabling using mechanical control strategies are described in the next chapter. One design is selected and the detailed design of a prototype is described.

Chapter 6

Design of a Discrete Piston Controlled Hydraulic Pump/Motor Using a Mechanical Control Method

Chapter 5 established that discrete piston control can significantly improve the efficiency of a hydraulic pump/motor, particularly at low displacements. It also presented several strategies for achieving discrete piston control, such as whole piston disabling, which connects a variable number of pistons to low pressure for their entire power stroke, or partial stroke disabling, which disables each piston for a variable fraction of its power stroke. The relative advantages of each approach were described, with whole piston disabling avoiding the majority of the transition and compressibility losses, and partial stroke disabling having a smaller flow ripple.

The valve timing strategies described in the previous chapter can be achieved with a wide variety of valve actuation methods which can be driven electrically, mechanically, hydraulically, or using a combined approach. While electrically driven valves that can switch at arbitrary times offer the greatest control flexibility, mechanical and hydraulic valve actuation methods provide a number of advantages:

- Mechanical components are typically quite robust and can operate in hydraulic

oil and the harsh environments often experienced by hydraulic systems.

- Mechanical designs can be developed that only require a single control input.
- It could possibly be driven by a mechanical or hydraulic compensator, eliminating the need for control electronics.
- The control approach can be simpler and more robust than one that requires electrical control circuitry and a supervisory controller for multiple electrohydraulic valves.
- The elimination of multiple electrohydraulic valves and control electronics has the potential for significant cost reduction.
- A mechanical actuation method driven by the pump/motor shaft will have repeatable timing with respect to the pump/motor rotation angle.
- Hydraulic pumps and motors inherently contain sources of hydraulic and mechanical power available for valve actuation, eliminating the need for a supply of electrical energy.
- Hydraulic or mechanical actuators typically have a higher power density than electrical devices, allowing them to be more compact.
- Hydraulic and mechanical devices typically require minimal power to hold a valve in a particular state. This is in contrast to solenoid valves, which require a continuous current to hold a valve against an energized spring.

In this chapter, a design for creating a mechanically controlled discrete piston pump/motor is presented. There are numerous way that mechanical control of the individual pistons can be achieved, and a number of them are described in the next section. The benefits and drawbacks of the different control methods are described, and a design is selected. In section 6.2, a dynamic model of the selected control approach is developed and simulation results showing the valve timing and pump/motor efficiency are presented. Finally, the mechanical design of the full discrete piston pump/motor is presented in section 6.3.

6.1 Mechanical Control Concepts

There are a number of desirable characteristics to strive for when designing a mechanical valve control method. Since the primary purpose of the discrete piston control approach is to improve pump/motor efficiency, the valve control method should result in as little power loss as possible. Some characteristics of an ideal piston control system are:

- Low leakage
- Large flow areas to reduce pressure drop
- Fast transitions between states to avoid throttling
- Minimal actuation power
- Valve should be "closed-center," meaning no possibility of connecting supply and tank
- Durable mechanism using a small number of parts
- Compact design
- 4-quadrant operation: i.e. must operate for either shaft direction when acting as a pump or a motor
- Allow precompression and decompression of the oil volume
- Incorporate passive control elements (i.e. check valves) when possible

It is evident that some of these goals are in conflict with one another, such as the desire for large openings and fast opening speeds, while simultaneously using little actuation power. The goal of allowing pre-compression and de-compression for both pump and motor can conflict with the desire for a simple, compact solution. It is likely impossible to design an ideal valve control system that encompasses all of the design goals. This chapter describes a number of concepts that were considered in the development of this project, and discusses the relative strengths and weaknesses of each design. The selected design concept will be described as well as the reasons for its selection.

All of the concepts rely on the idea of a two degree-of-freedom device, which can use rotary motion to provide the periodic opening and closing of the valve, as well as provide

a means of adjusting the timing of the periodic valve switching. The valve described in chapter 4, for example in Fig. 4.2, operates using the two-degree-of-freedom concept, although it is not the specific design for any of the described valve control mechanisms. The valve spool can rotate as well as translate in the bore. As it rotates, it alternately connects an output port with high pressure or low pressure. The helical profile on the face of the valve spool is designed such that, as the spool translates in the bore, the timing of the high and/or low pressure connections is adjusted. This valve can either connect directly to the piston chamber and allow the piston flow to pass through it, or it can connect pilot pressure to a second-stage valve which connects to the piston chamber. A different iteration of this concept would be to use a three-dimensional cam profile to create a similar design. Instead of using a valve to hydraulically actuate a second stage valve, a three-dimensional cam design would actuate the valve through a mechanical connection to a rotating cam. While the cam approach has some advantages, such as a lack of hydraulic leakage, three-dimensional cams typically have point contact with their respective cam followers, which results in a significant challenge with mechanical wear. For this reason, the cam iteration of the rotary and translating element was not included in the following design concepts.

6.1.1 Direct Acting Whole Piston Disabling

The simplest design concept is to use the rotating and translating valve spool to directly control the flow into and out of the piston chamber. This idea can be applied in a number of different ways to create a whole piston disabling device, a whole piston plus one partial stroke device, or a partial stroke device. Figure 6.1 shows a sketch of a whole piston disabling direct acting spool.

In this figure, there is a three-section spool shown in a bore, with the three ends representing the motor end (left), the pump end (right) and the disabled section (middle). There are eight tubes leading away from the spool bore representing connections to each individual piston chamber. These connections are equally spaced around the spool bore so that the pistons in the motor case are activated at equally spaced intervals, with the transition from low pressure to high pressure timed to correspond with the piston passing through TDC. The motor end is shown as being divided into two halves, with one side being connected to high pressure, and the other connected to tank. As this

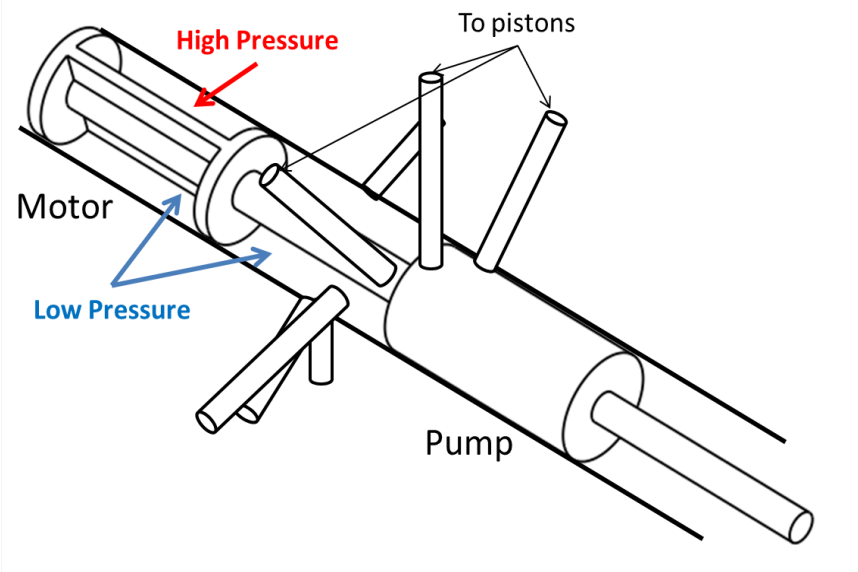

Figure 6.1: Sketch of a direct acting pump/motor spool

section rotates, it will alternately connect each piston chamber to high and low pressure. By shifting the spool axially in its bore, the number of pistons that are connected to the motor section can be adjusted, with the pistons that are not connected to the motor being connected to the disabled section. In this way, the number of active motoring pistons can be controlled. The disabled section is connected to tank pressure, so any pistons that are connected to it will remain at low pressure. The pumping end of the spool is shown as simply a solid cylinder, which blocks all connections to the piston. For this spool to enable pumping, the piston chamber must also have a check valve from low pressure and to high pressure; see Fig. 6.2 for an example circuit. Thus the only function of the spool is to connect unused pistons to tank, disabling them. For the pumping end, the spool does not even need to rotate; the ideal pumping timing is controlled by the check valves. If only a pump and not a pump/motor is required, then adding a solid cylinder to enable/disable individual pistons would be a simple way to create a variable check ball pump. As shown, the device in Fig. 6.1 has two active pump pistons, with the remaining six pistons disabled.

As this sketch is simply to convey the concept, some details, such as the connection to high pressure through the spool, are not shown. One issue with the design of the

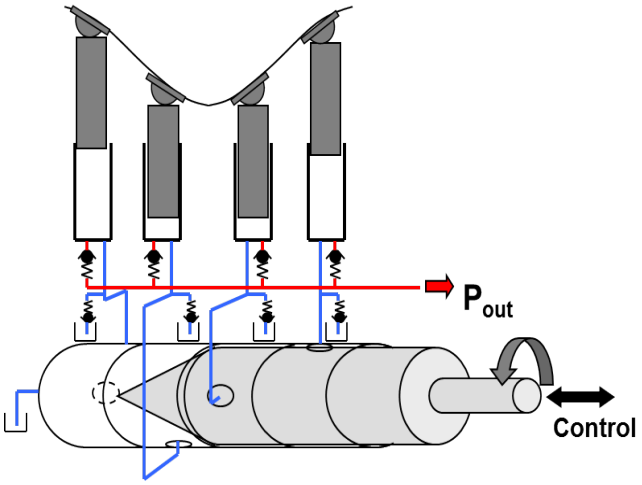

Figure 6.2: Sketch of a direct acting pump with 1 partial stroke piston

motor end as shown is that there would be a large pressure imbalance on the spool due to the high pressure being only on one side, which would likely cause the spool to seize. There are a number of ways to address this issue, such as creating some opposing regions of high pressure, or by cutting the rotational frequency in half and then doubling the high and low pressure regions so that the two high-pressure regions oppose each other. This would require a gear reduction between the drive shaft and the rotating spool. Another detail that is not described is how to couple the rotation of the drive shaft and the spool, while still allowing the spool to translate. One concept for achieving this will be described in section 6.3.

As described, this spool is for whole piston disabling, with only discrete displacements available, and the resolution of the displacement options set by the number of pistons. If the spool could be controlled sufficiently fast, this design could be used to achieve whole piston plus one partial stroke piston by commanding the spool to change the number of enabled/disabled pistons by one when that particular piston is in mid-stroke. In this manner, whichever piston was between the fully disabled and the fully enabled pistons would be moved to a different spool section during its power stroke. However, this would require fast axial control of the spool, and would remove some of the determinism gained by coupling the on/off timing to the drive shaft.

A different way to achieve whole piston plus one partial stroke piston is shown in

Fig. 6.2. For simplicity, this figure only show the pumping end of the spool, but it can easily be applied to the motoring end also. In this figure, instead of having a straight edge dividing the enabled and disabled sections of the spool, there is a shaped profile which results in the enabled section being connected to an individual piston for only part of the stroke. This shaped profile is designed such that, as the spool moves axially in the bore, the amount of the rotation that the partial stroke piston is enabled is varied. In this way, the piston that is between the fully enabled and fully disabled pistons will only be active for part of the stroke. For this method, the spool will need to rotate with the pump shaft, even for the pump only case. This approach will allow for any arbitrary average displacement between full on and full off.

The primary advantage of the direct acting whole piston disabling approach is simplicity. This is essentially a checkball pump with only the additional rotating and translating spool required to turn it into a variable displacement pump/motor. As described in the previous section, the whole piston approach results in a relatively large flow ripple. This can be reduced by changing the order in which the pistons are disabled, however, it should be evident that this could result in convoluted flow paths, as an individual connection to the spool could correspond to a piston that is on the opposite side of the device. This, along with measures to address the pressure imbalance on the spool, could reduce the simplicity of the concept. The fact that passive check valves can be used for the pumping case is an attractive feature of this design, particularly if only pumping is required. The only actuation power required for this approach is the mechanical power required to overcome the friction of the rotating spool, which should be low.

There are a number of disadvantages of this design, but possibly the most significant drawback is the size of the spool required. Figure 6.1 shows a three section spool, with each of the sections individually capable of covering the connections to all of the pistons in the device. Each piston connection must be at a distinct axial position, so each section is, at a minimum, the width of the piston connection times the number of pistons. Since this is a direct acting spool, the full flow from each piston must pass through the rotating spool (except in the pump case), and in order to avoid significant losses, the connections to each piston must be large. In addition, the spool must be able to translate in each direction so that the pistons can be completely connected to each

end of the spool. Thus, there must be space for the unused two spool sections on each end of the spool, resulting in a spool bore that is five times the width of a single active section. The approach shown in Fig. 6.2 only exacerbates this problem by requiring enough space between each piston connection to have an adjustable stroke width. It may be possibly to split the pumping and motoring sections into two separate spools that are both driven by the drive shaft, which would reduce the length requirement. However, it would require a more complicated driving mechanism and two independent control inputs, one for each spool.

In addition to the long length requirement and the need for pressure balancing, this approach presents a number of other design challenges. Since the rotating spool will see the full pump/motor pressure, tight clearances are required to create a seal between high and low pressure. With a long spool and bore, this is difficult to achieve from a manufacturing perspective, and the long length of the spool will result in a large leakage perimeter. The full flow through the spool also requires large, high-pressure flow paths connecting the spool with each piston chamber, which can be difficult from a packaging perspective.

6.1.2 Direct Acting Partial Stroke Disabling

For the partial stroke disabling case, rather than having a connection to each piston in series, all of the pistons connect to the spool bore at the same axial location, as shown in Fig. 6.3. In this sketch, eight pistons are connected to the rotating and translating spool, evenly spaced around the spool bore. The rotating spool has a helical profile on its face, which divides high and low pressure sections of the spool. In Fig. 6.3, there are two pockets of high pressure, which are the pockets on each end of the spool, with each pocket having a hole in it. As the spool rotates, each piston connection will either be over a high pressure pocket or the low pressure area outside of the pockets, and the pocket width varies as a function of axial position. This is what allows adjustment of the length of the power stroke for each piston. Since each piston is at the same axial position on the spool, each piston will be disabled for the same fraction of the stroke. Notice that the high pressure pockets at each end are on opposite sides of the spool. This means that, for a given rotation direction, one high pressure pocket corresponds to the pistons that are extending (motoring), and the other pocket corresponds to the pistons that are

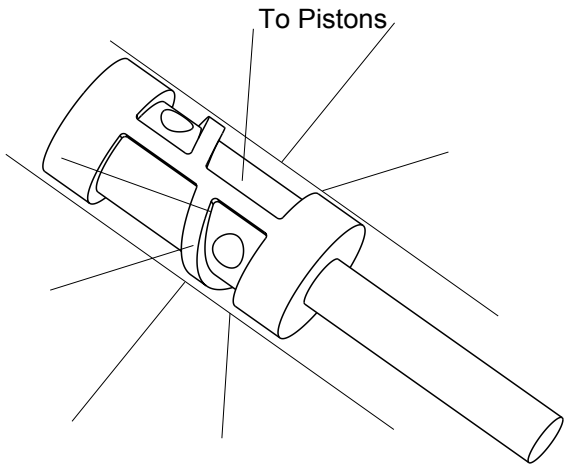

Figure 6.3: Sketch of a partial stroke pump/motor spool

retracting into their bores (pumping). Thus, one end of the spool is the motoring end, and the other is the pumping end, with a small area in between where the pistons are fully disabled. The end of the spool that is motoring, and the end that is pumping, are determined by the direction of rotation of the spool and drive-shaft. As drawn, if the spool is rotating clockwise and the upper left end is the pumping end, then to operate at less than the maximum displacement, the spool will delay the start of pumping and end the motoring stroke early. This is the configuration described in section 5.4.3 as being the best method for reducing compressibility loss. If the pump/motor changes directions, then the motor and pump ends will switch, with the start late/end early features preserved as desired. While they could be added in parallel, this design does not require the use of passive check valves for the pumping case.

One major advantage of this approach over the whole piston approach is the dramatic reduction in the spool length. The direct acting approach utilizes few parts and results in a simple control mechanism. While this spool is also not pressure balanced, the total size of the unbalanced pressure area is much smaller than in the whole piston disabling case, resulting in simpler mitigation strategies. The relative advantages and disadvantages of whole piston and partial stroke variation are described in section 5.4. However, it should be pointed out that the efficiency benefits gained by eliminating most of the transition loss in the whole piston case could easily be canceled out by the

leakage generated by a long spool, such as the one shown in Fig. 6.1. The actuation power for this approach is minimal, with the spool requiring only enough power to overcome friction.

While the direct acting spool results in a relatively simple design, it also has a number of drawbacks. These are primarily related to the fact that full flow and full pressure need to pass through an element that also needs to translate and rotate at high speeds. The design trade offs involved in achieving this present a significant challenge. In order to seal high pressure oil, the tolerances on the spool must be very tight, which presents a difficult mechanical design problem. The flow paths into, out of, and through the spool also much be large enough to handle the full hydraulic power of the pump/motor. One way to mitigate some of these challenges is to only use the rotary spool as a pilot valve to drive additional control valves. This dramatically reduces the power flowing through the valve at the expense of additional complexity.

6.1.3 Pilot Operated Three-way Spool

Figure 6.4 shows a cross-sectional sketch of a partial stroke disabling spool being used as a pilot valve to drive a three-way mainstage valve associated with each piston. In this figure, only four mainstage valves are shown, but it can be extended to any number of valves/pistons. The three-way valves are acted on by pilot or tank pressure on one end, and a spring on the other. The three-way valves can either be spring biased to high pressure and open to tank when pilot pressure is applied (as shown) or vice versa.

Although this additional valve stage introduces a number of additional parts, it does accomplish many of the design goals listed at the beginning of this section. While they are not as good as poppet valves, spool valves are routinely made with tight tolerances, which can keep leakage low. Since the mainstage spools can be fairly short and not coupled to a rotating shaft, the tight tolerances are not as difficult to achieve as they are on the rotating spool. Each valve only needs to handle the full power of one piston, as opposed to the combined power of all of the pistons. The three-way valve can be designed to be closed-center, meaning there is a deadband between opening to pressure and opening to tank. This ensures that there is no cross-port leakage. The hydraulic coupling between the pilot and main stages allows for flexibility in packaging the valves into the pump/motor housing, with the large-opening mainstage valves not needing to

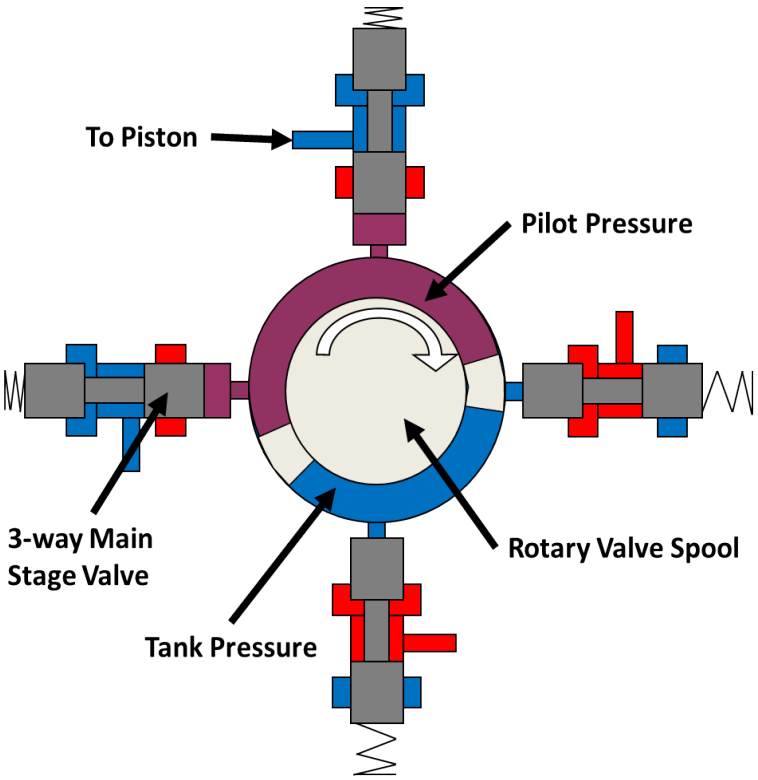

Figure 6.4: Sketch of a pilot spool driving 3-way main stage valves

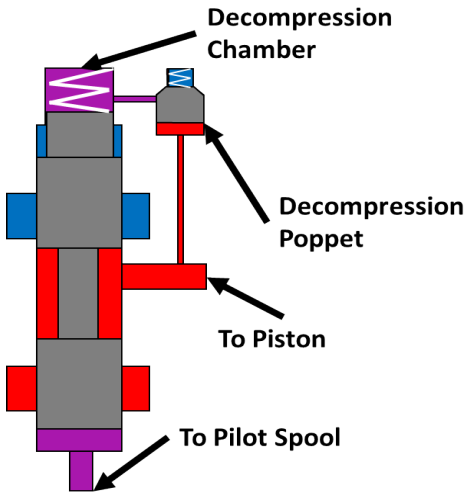

Figure 6.5: Sketch of 3-way spool with pressure based decompression

be centrally located. This has the potential to reduce the compressible volume between the piston and the valve.

In addition to the increased complexity, there are a couple of disadvantages to this design. While the spool valves do have low leakage, they are not as good as poppet valves. The three-way valves also only have two stable states: fully open and fully closed. There is not a blocked state that could allow passive check valves to achieve the ideal pumping timing. In Fig. 5.21, the ideal pumping and motoring strokes are depicted with precompression and decompression stages shown. In the precompression state, the piston is disconnected from high and low pressure, and the piston travel is used to compress the oil without generating any compressibility losses. The decompression state is similar; the high and low pressure connections are blocked and the piston is used to expand the oil volume and extract the compressed energy. For the three-way spool valve, there is no defined state with both ports blocked, and thus, the precompression and decompression only happen while the valve is transitioning through its deadband, which is not a controlled state.

One way to mitigate the lack of a decompression state is to add a decompression chamber as shown in Fig. 6.5. In the ideal timing sequence shown in Fig. 5.21, the decompression state is shown after the power stroke and before the valve opens to tank.

If the valve can be held in this state long enough for the piston to expand the oil volume and extract the compressed energy from the fluid, then the compressibility loss can be reduced or eliminated. In Fig. 6.5, the chamber at one end of the spool is blocked by a decompression poppet. This poppet is normally open with a spring, but it is closed by high pressure in the piston chamber. The blocked chamber at the end of the spool travel will hold the valve spool in the deadband and prevent the spool from opening to tank until the piston chamber pressure is low. Thus, it relies on the motion of the piston to lower the pressure in the blocked piston chamber. This provides ideal decompression, reducing the compressibility loss for the transition from high to low pressure. This design will work for a pump or a motor, however, in order for this approach to work, the piston must be extending out of its bore when the valve switch occurs, meaning that, for the motor case, the valve must be switched to low pressure before the piston reaches BDC. If the valve has not opened to tank before the piston starts to move up, the valve spool will get stuck in the deadband, and the pressure in the piston chamber will rise until a relief/check valve is triggered or there is a mechanical failure. This approach will provide ideal decompression, but at the penalty of increased mechanical complexity and the risk of a mis-timed valve switch. The decompression poppet will help recover energy that is stored in the fluid as it decompresses, but it will not reduce the potential throttling losses associated with compressing the oil volume up to high pressure in the motor case.

In addition, the added dynamics of the decompression poppet can slow down the opening of the valve spool to tank, increasing the throttling loss during transition. Dynamic modeling of the system can determine whether the decompression energy to be saved by staying in the deadband longer is greater than the additional throttling loss due to a slower opening valve.

6.1.4 Two Poppets

Figure 6.6 depicts a different mechanism for controlling the pressure applied to the pistons. Like the previous design, this valve arrangement has closed-center operation and it can achieve ideal decompression, meaning that it can be held in a blocked state until the piston motion has extracted the compressed energy in the fluid. This design

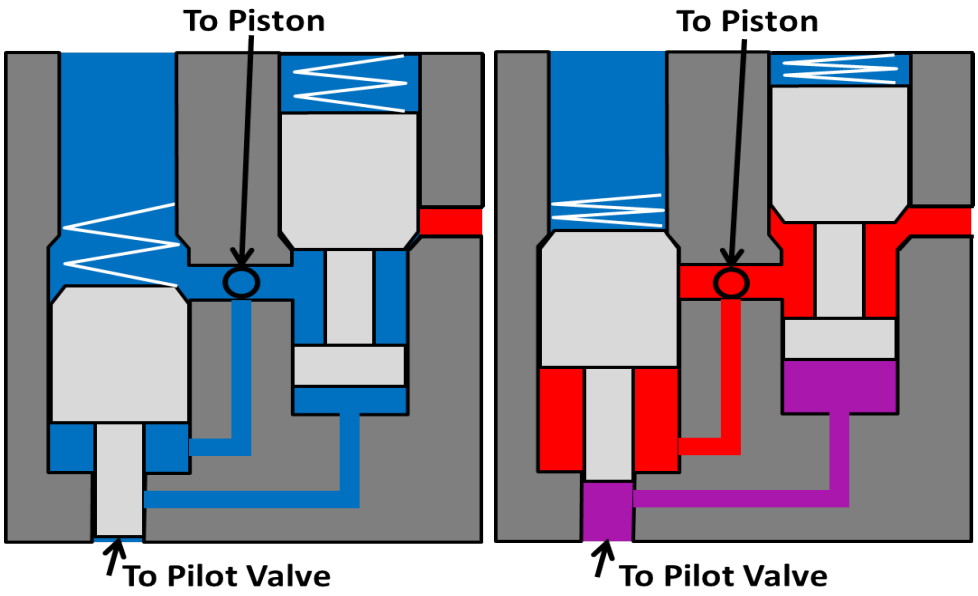

(a) Open to Low Pressure (b) Open to High Pressure

Figure 6.6: Sketch of a pilot driven 2-poppet valve arrangement in high and low pressure configurations

also has the additional benefit of poppet sealing to reduce leakage. In Fig. 6.6, a pilot-driven two-poppet approach is shown that has one poppet that is normally-open to tank and another that is normally-closed to high pressure. The two-poppet arrangement is shown in both the fully open to tank (Fig. 6.6(a)) and fully open to pressure (Fig. 6.6(b)) states. The circle in the center of each figure represents a connection to the piston chamber, and the opening at the bottom left of each figure is the connection to the rotating pilot spool.

The connections between the two poppets are designed to ensure that there is no cross-port leakage and that there is ideal decompression. Since there is no mechanical link between the connections to tank and pressure, the closed-center feature must be enforced through other means. For closed-center operation, whichever valve is open must fully close before the other valve starts to open. In transitioning from Fig. 6.6(a) to Fig. 6.6(b), the first event that occurs is pilot pressure is applied to the back of the tank poppet, which closes the tank poppet. The connection between the pilot

pressure and the bottom of the high-pressure poppet is initially blocked by the tank poppet. Only when the tank poppet is sufficiently closed will pilot pressure be applied to the high-pressure poppet, forcing it to open. Thus, the correct timing is enforced for the opening-to-pressure direction. Once pilot pressure is removed, the springs will immediately try to close the high-pressure poppet and open the tank poppet. However, there is a connection between the piston chamber and the back of the tank poppet. Thus, as long as there is pressure in the piston chamber, the tank poppet will not open. Since the piston chamber pressure cannot lower until after the high-pressure poppet is closed, this feature has the effect of both ensuring proper timing and allowing ideal decompression.

The two-poppet approach can be designed in different configurations, for example, a two-stage poppet based on a Valvistor [107] design, which uses a pilot flow path through the main poppet to generate a pressure difference to actuate the valve, could be used to reduce actuation power at the expense of additional components and leakage. It is also possible to design a configuration that has the tank poppet normally closed and the pressure poppet normally open. However, the basic principle of one normally open poppet and one normally closed poppet that use timed connections and pressure-based decompression is the same.

The two-poppet approach has a number of advantages; it has poppet sealing to reduce leakage, it provides for closed-center operation and achieves ideal decompression. The advantages of using the rotary valve as a pilot device also apply to this design. The primary disadvantage of this approach is complexity. There are two moving elements with connections between them that could prove a challenge to fit into a compact package. As with the decompression chamber on the three-way spool, in the motor case, the valve must be open to tank before the piston reaches BDC, otherwise there is a risk of missing a motoring stroke and generating high pressures in the piston chamber.

6.1.5 Stacked Poppets

Figure 6.7 shows a different mechanical configuration that has the same features as the two-poppet design. The stacked poppet design is pilot driven, closed-center, has poppet sealing, and has ideal decompression. In this figure, the pilot pressure is applied to the piston at the bottom of the figure. On the right side of the figure are two ports: the

bottom port is a connection to tank, and the upper port is a connection to the piston chamber. As the valve transitions from open to low pressure (Fig. 6.7(a)) to open to high pressure (Fig. 6.7(b)), the grey valve element on the bottom moves up first. Note that springs are not shown for clarity, but they are used to hold the valve in the low pressure state when pilot pressure is absent. After moving a set distance, the bottom valve element will contact the middle valve element. This contact will close the connection between piston and tank, and it will also cause the middle valve element to move up along with the bottom element. The two moving valve elements will then contact the upper poppet, which opens the connection to high pressure. Note that the back of this poppet could be referenced to tank to allow easier opening. Once pilot pressure is removed, the three valve elements will move down together until the top poppet contacts its seat, closing the high pressure connection. The bottom two elements will continue to move down until the middle element contacts its seat (which may be a snap ring for manufacturing purposes). At this point, there is still high pressure in the piston chamber, which will hold the bottom two elements together since the piston pressure is connected to the back of the bottom element. Once the piston extends enough to lower the pressure, the bottom element will separate from the middle element and return to its seat, opening the connection to tank.

The advantages and disadvantages of this design are nearly identical to the two-poppet design. This approach could likely be more compact, but it may also be more difficult to manufacture. There are a number of leakage paths in this design as well, but without a detailed design, it is difficult to say which design would have more leakage.

6.1.6 Design Selection

The decision on which design to pursue for prototyping must weigh the costs and benefits of each design. While it offers smaller transition and compressibility losses, the drawbacks of the mechanically controlled whole piston disabling strategy, such as excessive spool length, high leakage, and large flow ripple, outweigh the benefits. For the prototype design pursued in this thesis, the drawbacks stemming from the need to have full power flowing through the rotary spool in the direct acting case are significant enough to warrant the additional complexity of a pilot-driven approach. However, the additional complexity and design risk associated with the two-poppet or stacked

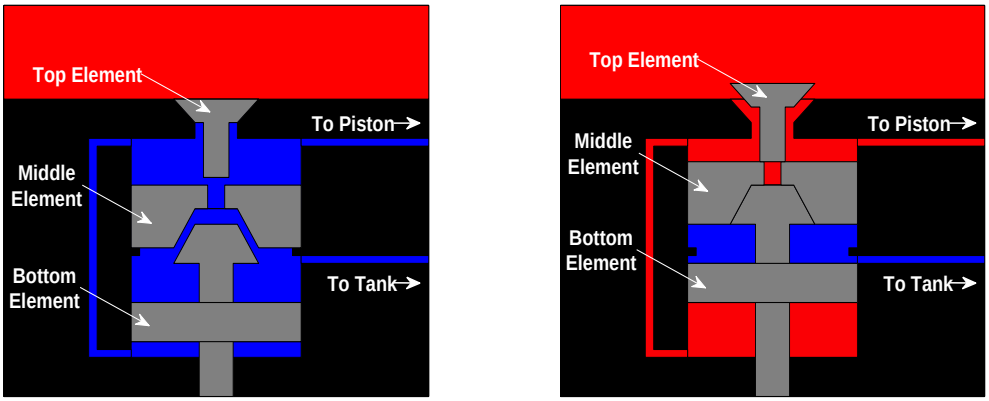

(a) Open to Low Pressure

(b) Open to High Pressure

Figure 6.7: Sketch of a pilot driven stacked poppet valve arrangement in high and low pressure configurations

poppet designs are not justified by their benefits. The primary advantage of these two approaches is the fact that they have poppet sealing to reduce leakage. However, both designs have additional non-poppet leak paths that need to be considered. Also, with typical tolerances on hydraulic spool valves being less than $10\mu m$, the power loss due to leakage around the valve spools should not be a significant source of energy loss. The fact that a three-way valve spool is a common design in the hydraulic industry is also attractive from a design risk mitigation stand point. It is also the most compact of the pilot driven options. Additionally, the fact that the two-poppet and stacked poppet designs rely on full decompression of the piston chamber in order to function properly presents a risk in that, if there is significant variation in the oil compressibility or excessive internal leakage in the prototype parts, the device may not function properly. In the motor case, if the oil volume is not able to be fully decompressed before reaching BDC, the piston chamber will switch from a motoring chamber to a pumping chamber. The three-way spool can have the ideal decompression feature added by adding a decompression chamber, but it is not a required element of the design. Dynamic modeling of the decompression chamber approach indicated that it would not provide measurable

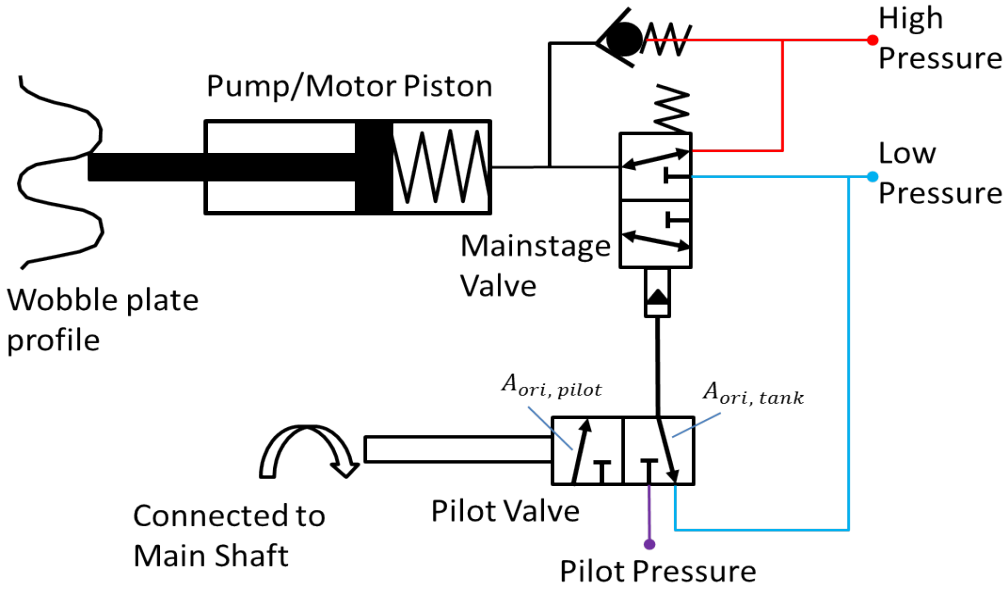

Figure 6.8: Circuit diagram of one piston and mainstage valve driven by the rotary pilot valve

energy savings, and it would significantly increase the mechanical complexity. Finally, in the three-way spool and stacked poppet designs, closed-center operation is mechanically enforced, and does not rely on precise timing. This guarantees that there will be no cross-port leakage. For these reasons, the pilot-driven three-way spool design was chosen for the prototype. In the next section, a dynamic model of the three-way spool design is described.

6.2 Dynamic Model of a Piston Chamber and a Rotary Pilot Driven 3-Way Spool Valve

Figure 6.8 shows a system schematic of the two-stage valve control design described in the previous section. The rotary pilot valve is connected to the pump/motor shaft, and as it rotates it connects the end of the mainstage spool to either tank or pilot pressure. This forces the three-way mainstage spool to be connected to either tank or supply pressure. With a mechanical design selected, a detailed dynamic model of the valve

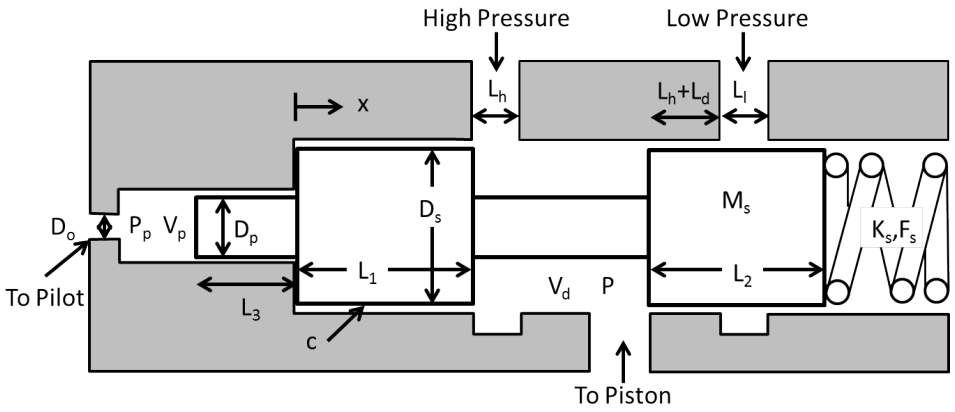

Figure 6.9: 3-way spool with features labeled

mechanism can be derived to study the power losses affected by the system dynamics, such as the transition loss and the compressibility loss. The model is also used as a tool for the mechanical design by simulating the effects on the overall power loss attributed to different design decisions. In this section, a model of the rotary pilot valve, mainstage spool valve, pump/motor piston, and the oil volumes between the elements is developed. Simulations of a single-piston device operating as a pump and a motor are presented, and transition speed and overall loss of the system are predicted.

Figures 6.9 and 6.10 depict the details of the mainstage valve and the piston chamber. Figure 6.9 shows the three-way mainstage spool, which is acted on by pilot pressure on the left end, and a spring force on the right end. The spool is shown at the position $x = 0$, which corresponds to the spool being fully open to pressure. The equation of motion for the spool is given by:

$$M_s\ddot{x} = \frac{\pi}{4}D_p^2\left(P_p - P_{tank}\right) - F_s - K_s x - b\dot{x} \tag{6.1}$$

where M_s is the spool mass, and x is the spool position. x is limited to be between 0 and $x_{max} = L_h + L_d + L_l$, which are the length of the high pressure opening, the length of the deadband, and the length of the low pressure opening respectively. D_s is the main spool diameter, and D_p is the diameter of the end of the piston that is in contact with P_p, which is the pressure in the oil volume on the end of the spool that switches between P_{pilot} and P_{tank}. Note that in the mechanical design described in section 6.3.3,

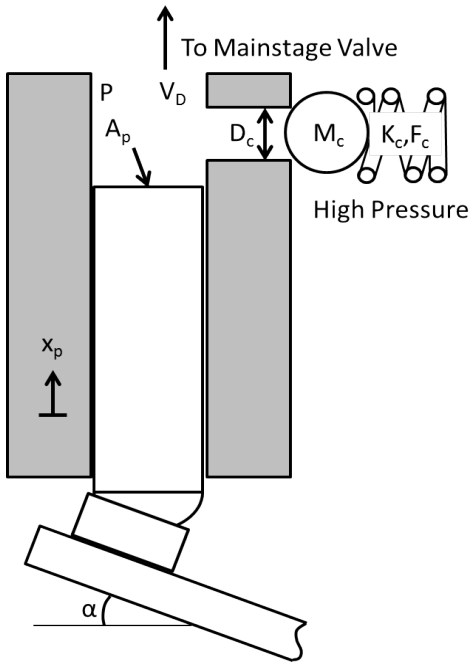

Figure 6.10: Pump/motor piston with features labeled

the end of the spool that is at diameter D_p and the rest of the spool are made from two separate pieces for ease of manufacturing. F_s and K_s are the spring preload force and spring rate respectively. b is the coefficient of viscous friction that can be estimated from the following equation, which assumes a uniform, laminar, Newtonian fluid film between the spool and the bore:

$$b = \frac{D_s \pi \left(L_1 + L_2\right) + D_p \pi L_3}{c} \mu \tag{6.2}$$

where L_1 and L_2 are the lengths of the two lands of the spool that have diameter D_s, and L_3 is the length of the spool that is at diameter D_p. c is the radial clearance between the spool and the bore. It is assumed that the clearance around D_s and D_p are the same. The spring chamber on the right end of the spool is referenced to tank, as is the annulus on the left end of the spool between D_s and D_p.

The mainstage spool orifices are circumferential about the spool, with the edge of the spool opening up to the full annulus created by undercuts in the bore. This allows for the highest possible flow gain, which minimizes the transition time. The open orifice areas

to pressure and tank are related to the spool position through the following equations:

$$A_{pres}(x) = \begin{cases} D_s\pi(L_h - x) & \text{if } x < L_h \\ 0 & \text{if } x \geq L_h \end{cases} \tag{6.3}$$

$$A_{tank}(x) = \begin{cases} D_s\pi(x - L_h - L_d) & \text{if } x > L_h + L_d \\ 0 & \text{if } x \leq L_h + L_d \end{cases} \tag{6.4}$$

The flow rates into (Q_{high}) and out of (Q_{tank}) the piston and valve volume, V_d, are given by the orifice equation, with the open areas defined by Eqs. (6.3) and (6.4).

$$Q_{high} = c_d A_{pres}(x)\sqrt{\frac{2|P_{high} - P|}{\rho}} sign(P_{high} - P) \tag{6.5}$$

$$Q_{tank} = c_d A_{tank}(x)\sqrt{\frac{2|P - P_{tank}|}{\rho}} sign(P - P_{tank}) \tag{6.6}$$

The discharge coefficient, c_d, can be used to match the orifice flow rates to computational fluid dynamics (CFD) results, as described in section 6.3.4. P_{high} and P_{tank} are set as inputs to the simulation, but the pressure, P, in the piston volume is computed as a state:

$$\dot{P} = \frac{\beta(P)}{V_d + A_p(D_{pitch}\tan(\alpha) - x_p)}(Q_{high} - Q_{tank} + A_p\dot{x}_p) \tag{6.7}$$

where $\beta(P)$ is the pressure dependent bulk modulus given by Eq. (2.4), V_d is the dead volume of oil in the piston chamber and mainstage valve, A_p is the area of the end of the piston, α is the angle of the wobble plate, and x_p and $\dot{x}_p$ are the piston position and velocity given by Eqs. (5.3) and (5.6). Figure 6.10 shows the piston chamber with the important variables labeled.

The pressure in the oil volume on the end of the spool, V_p, is also computed as a state:

$$\dot{P}_p = \frac{\beta(P_p)}{V_p + D_p^2\frac{\pi}{4}x}\left(Q_{pilot} + D_p^2\frac{\pi}{4}\dot{x}\right) \tag{6.8}$$

where the flow into the oil volume from the pilot valve is given by:

$$Q_{pilot} = \begin{cases} c_d A_{ori,pilot}(\theta)\sqrt{\frac{2(P_{pilot} - P_p)}{\rho}} & \text{if } A_{ori,pilot}(\theta) > 0 \\ -c_d A_{ori,tank}(\theta)\sqrt{\frac{2(P_p - P_{tank})}{\rho}} & \text{if } A_{ori,tank}(\theta) > 0 \end{cases} \tag{6.9}$$

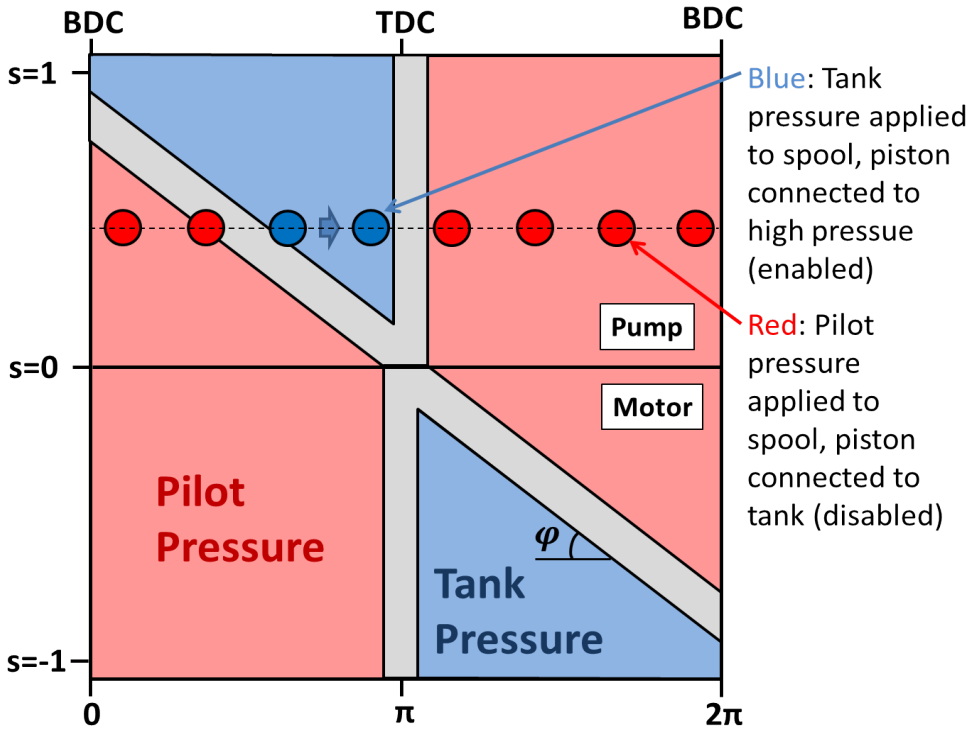

Figure 6.11: Diagram of an unwrapped pilot spool

where $A_{ori,pilot}$ and $A_{ori,tank}$ are the orifice areas on the pilot valve spool that are open to pilot pressure and tank respectively. As the pilot valve rotates, it will connect the end of the mainstage spool to either pilot pressure or tank by opening either $A_{ori,pilot}$ or $A_{ori,tank}$. The open areas of the pilot are a function of the pilot spool geometry, the diameter of the orifice connecting the pilot spool with oil volume V_p, and the rotation angle of the pilot spool.

Figure 6.11 depicts the profile of the spool shown in Fig. 6.3 unwrapped to a plane. The surface of the spool is divided into regions of pilot (red) and tank (blue) pressure. Since the mainstage spools are spring biased to high pressure, applying tank pressure to the end of the spool will result in high pressure being applied to the piston. Conversely, when pilot pressure is applied to the end of the mainstage spool, tank pressure will be applied to the piston. Thus, the red area in Fig. 6.11 corresponds to a disabled piston, and the blue area corresponds to an enabled (pressurized) piston. Figure 6.11

also shows eight circles representing connections to eight different three-way spools. These connections are all at the same axial position on the spool (vertical position in the figure), and are evenly spaced around the circumference of the spool. As the pilot valve rotates, it will move relative to the eight connections to the mainstage spools. This can be visualized as the circles in Fig. 6.11 moving horizontally with respect to the rest of the figure, although in reality, the eight holes are fixed and the spool is moving. Note that the pilot spool is fixed to the main shaft, which also rotates the wobble plate. Thus, TDC of the wobble plate, with corresponds the center of Fig. 6.11, will remain fixed in relation to the area profiles on the pilot spool.

As shown, a circle moving from left to right on the upper half of the figure will result in a pumping piston, while a circle on the bottom half will connect to a motoring piston. If the circles are instead moving from right to left, representing the opposite direction of pump/motor rotation, then the pump and motor sections will switch places. To vary the displacement of the device, the eight connections to the mainstage spools are moved vertically with respect to the metering lands on the pilot spool. For a pump operating at full displacement, the circles would be at the top Fig. 6.11. As the connections to the spool move down, the pump displacement is decreased until the pump is fully disabled with the circles in the center. If the circles move from the center toward the bottom of the figure, the device becomes a motor with increasing displacement, until it reaches full displacement with the spool connections at the bottom of the figure. In the pumping case, the fraction of the rotation over which the pump is enabled is reduced from the full displacement case by delaying the connection of tank pressure to the end of the spool, and thus delaying the application of high pressure to the piston. In the motor case, it is decreased by ending the region of tank pressure earlier than in the full displacement case.

For an individual piston, an example of the area profiles is shown in Fig. 6.12, with a displacement of 35%. This is similar to the example shown in Fig. 6.11. As designed, the pilot spool is critically lapped, meaning that the width of the land on the pilot spool is equal to the diameter of the connection between the pilot spool to the end of the mainstage spool. However, the derivation of the pilot areas can easily be adjusted to take overlap into account. To compute the pilot areas, the first step is to find the transition rotation angles where the pilot spool blocks both the connection to supply

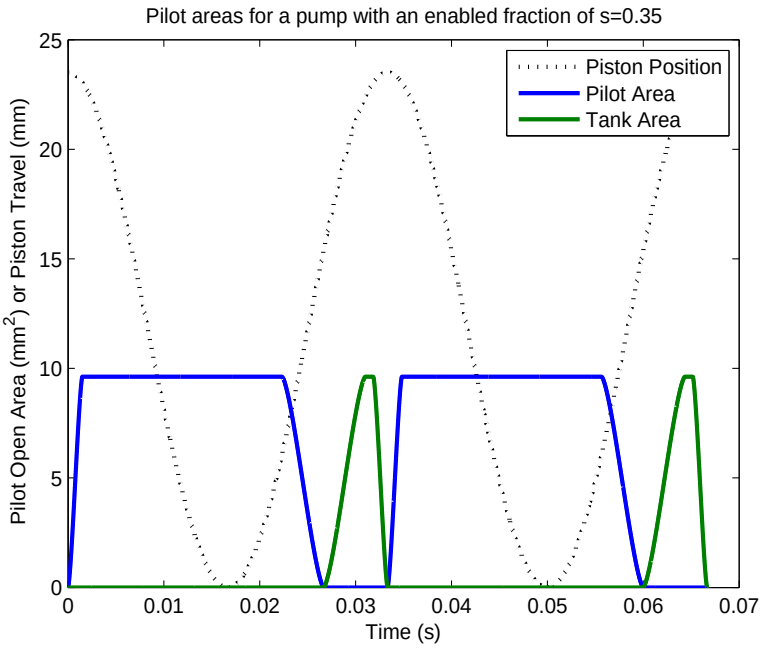

Figure 6.12: Area profiles the pilot spool in a partial pumping mode with the pump enabled for 35% of its power stroke

and the connection to tank. One of the points is associated with the piston at TDC, which is defined as 0 or 2π. The other point can be found by computing the rotation angle over which the piston is enabled, $\theta_{partial}$, which was defined in Eq. (5.10):

$$\theta_{partial} = \cos^{-1}(1 - 2s) \tag{6.10}$$

where s is the displacement of the pump/motor. This equation can be used to find the other transition point where the pilot blocks the orifices to both pilot and tank pressures:

$$\theta_{switch,pump} = 2\pi - \theta_{partial} \tag{6.11}$$

$$\theta_{switch,motor} = \theta_{partial} \tag{6.12}$$

where $\theta_{partial}$ the rotation angle for which the piston is enabled. For the pump case, the tank orifice area can be found as follows. First we compute the variables h_{open} and h_{close} which represent the instantaneous amount of overlap between the pilot spool land and the orifice with diameter, D_0:

$$h_{open,pump,tank} = (\theta - \theta_{switch,pump}) \frac{D_{pilot}}{2} \sin(\varphi) \tag{6.13}$$

$$h_{close,pump,tank} = (2\pi - \theta) \frac{D_{pilot}}{2} \tag{6.14}$$

where D_{pilot} is the diameter of the pilot spool, and φ is the angle from horizontal of the angled land shown in Fig. 6.11. Note that φ is the angle of a helix when wrapped around a spool. h_{open} is the distance, normal to the helical land, from the edge of the helical land to the leading edge of the orifice. The $\sin(\varphi)$ term is used to ensure that h_{open} is normal to the helical land. Figure 6.13 depicts the orifice in various stages of transition for the motor case, with the h_{open} and h_{close} parameters shown. With this parameter, the open area can easily be computed from the equation for the area of a circular segment:

$$A_{open} = \frac{D_0^2}{8}\left(2\cos^{-1}\left(\frac{h_{open} - \frac{D_0}{2}}{\frac{D_0}{2}}\right) - \sin\left(2\cos^{-1}\left(\frac{h_{open} - \frac{D_0}{2}}{\frac{D_0}{2}}\right)\right)\right) \tag{6.15}$$

h_{close} is the distance, normal to the vertical land, from the edge of the vertical land to the trailing edge of the orifice. This parameter can be used to compute the amount of

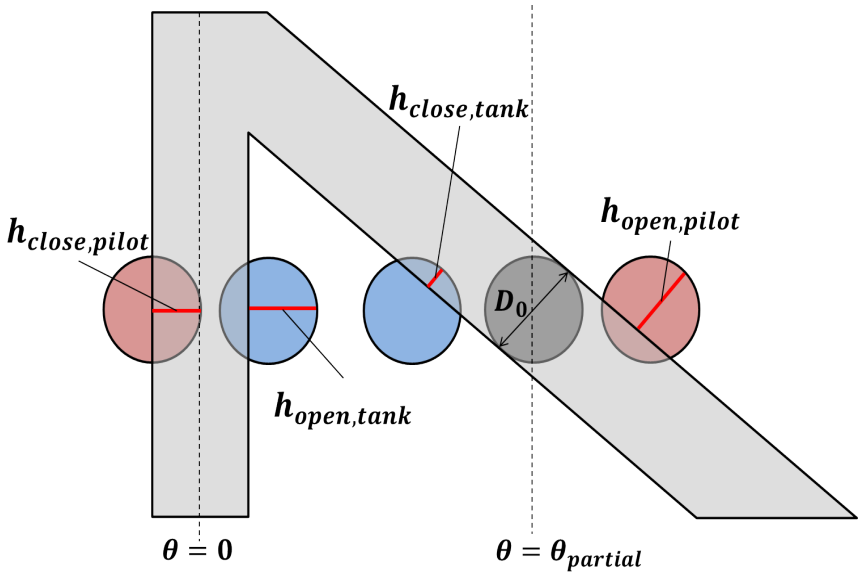

Figure 6.13: Examples of partially covered pilot orifices for the motor case

the orifice that is blocked by the vertical land on the pilot spool:

$$A_{close} = \frac{D_0^2}{8}\left(2\cos^{-1}\left(\frac{(D_0 - h_{close}) - \frac{D_0}{2}}{\frac{D_0}{2}}\right) - \sin\left(2\cos^{-1}\left(\frac{(D_0 - h_{close}) - \frac{D_0}{2}}{\frac{D_0}{2}}\right)\right)\right) \tag{6.16}$$

The total orifice area can then be computed by subtracting the blocked area from the open area. This will allow computation of the orifice area even when one side of the orifice starts to close before the other side is fully uncovered. For very small values of s, this is an approximation. When the width of the tank area is smaller than the orifice diameter, D_0, the orifice will be partially covered by both the vertical and the angled lands. In this condition, some of the area that is computed as blocked by one land may not have been uncovered yet by the other land due to the lands being at different angles. However, it provides a good estimate for most of the operating range.

$$A_{tank} = A_{open} - A_{close} \tag{6.17}$$

Equation (6.17) was used to calculate the tank area in Fig. 6.12. A similar process can be used to compute the pilot area for the pump case, and both areas for the motor case. The differences are in Eqs. (6.13) and (6.14); for the pumping pilot area and the

motoring tank area, the $\sin(\varphi)$ will be applied to h_{close} instead of h_{open}, as the helical land represents the closing side of that orifice. For the pump case, the orifice area open to pilot is:

$$h_{open,pump,pilot} = \theta \frac{D_{pilot}}{2} \tag{6.18}$$

$$h_{close,pump,pilot} = (\theta_{switch,pump} - \theta) \frac{D_{pilot}}{2} \sin(\varphi) \tag{6.19}$$

For the motor case, h_{open} and h_{close} are computed from:

$$h_{open,motor,tank} = \theta \frac{D_{pilot}}{2} \tag{6.20}$$

$$h_{close,motor,tank} = (\theta_{switch,motor} - \theta) \frac{D_{pilot}}{2} \sin(\varphi) \tag{6.21}$$

$$h_{open,motor,pilot} = (\theta - \theta_{switch,motor}) \frac{D_{pilot}}{2} \sin(\varphi) \tag{6.22}$$

$$h_{close,motor,pilot} = (2\pi - \theta) \frac{D_{pilot}}{2} \tag{6.23}$$

In Fig. 6.12, the effect of the helical land angle is evident in the different shapes of opening and closing area profiles. In the pumping case, the closing of the pilot area and the opening of the tank area occur across the helical land, and it is clear in the figure that these transitions are slower than the transition across the vertical land. As the helix angle, φ, is increased, the transition profile across the helical land will become sharper to approach the profile across the vertical land. Ideally the valve would switch as fast as possible, but in order to make the pilot spool compact with a reasonable axial stroke, the angle of the helical land must be limited.

In addition to the three-way mainstage valve, there is a check valve between the piston chamber and the high pressure port. This is included primarily for safety, as it prevents damaging pressures from building up in the case of a mis-timed three-way valve. However, it can also improve the efficiency if the opening pressure of the check valve is lower than the full-flow pressure drop through the mainstage valve. The equations for the check valve are:

$$M_c \ddot{x}_c = \frac{\pi}{4} D_c^2 (P - P_{high}) - F_c - K_c x_c \tag{6.24}$$

$$Q_c = c_d \pi D_c x_c \sqrt{\frac{2|P - P_{high}|}{\rho}} sign(P - P_{high}) \tag{6.25}$$

where M_c is the mass of the check ball, and x_c is the position of the check ball, limited between 0 when fully closed and a mechanical limit, $x_{c,max}$. The diameter of the check ball is D_c, and the spring preload and rate are F_c and K_c. It is assumed that the damping force on the check ball is negligible.

The dynamic equations of the system can be used to predict the power lost in the system due to compressibility and throttling through the valve. These losses are difficult to compute individually since they are occurring simultaneously and have an effect on each other. For example, the power lost due to throttling when the valve is in transition is affected by how much oil is going into/out of the oil volume to compress the oil. For this reason, the throttling and compressibility losses are calculated together by comparing the average hydraulic and mechanical power flows over one full rotation:

$$L_{comp,throttle} = \frac{\omega N_p}{2\pi} \int_0^{2\pi} \left[\mp \underbrace{\dot{x}_p A_p \left(P - P_{tank}\right)}_{mech} \pm \underbrace{\left(P_{high} - P_{tank} + E_{oil}\right)\left(Q_{high} + Q_c\right)}_{hyd} \right] dt \tag{6.26}$$

where the signs of the two terms depend on whether the mechanical power is the input (pump) or the hydraulic power is the input (motor). The E_{oil} term represents the energy stored in each unit of compressed oil, given by Eq. (2.30).

With this model, it is also relatively simple to calculate the actuation power required to drive the mainstage valves:

$$L_{pilot,actuation} = N_p \frac{\pi}{4} D_p x_{max} \frac{\omega}{2\pi} P_{pilot} \tag{6.27}$$

Using two different diameters, D_p and D_s, allows flexibility in designing a main diameter and travel that is large enough to minimize throttling, and still only use as much actuation power as is needed. This equation highlights the fact that, for a hydraulic valve, the only power needed is to move the valve; there is no holding power as is typical in electrically powered valves. The pilot valve also exhibits leakage and friction losses, which can be estimated from the clearance and the land design on the pilot spool. An estimate of those losses are included in the numerical simulations below.

The leakage in the mainstage spool flow primarily through two leakage paths: there is leakage from volume V_d in the middle of the spool across $L_d + L_h$ to the tank port, as shown in Fig. 6.9, and also across L_1 from high pressure to tank at the end of the

spool. If $L_h = L_l$, then the leakage path across the deadband is constant, except when the valve is in transition. The leakage path across L_1 will differ in length depending on whether the spool is at 0 or x_{max}.

$$L_{leak} = \frac{\pi D_s c^3 \left(P_{high} - P_{tank}\right)^2}{12\mu \left(L_d + L_h\right)} + \frac{\pi D_s c^3 \left(P_{high} - P_{tank}\right)^2}{12\mu} \left(\frac{\left(1 - \frac{s}{2}\right)}{L_{1,min}} + \frac{\frac{s}{2}}{L_{1,max}} \right) \quad (6.28)$$

where $L_{1,min}$ and $L_{1,max}$ are the lengths of the sealing land between high pressure and tank when the spool is at x_{max} and 0. It is assumed that pressure balancing grooves are used, minimizing the eccentricity.

The losses derived in this section give an estimate of the magnitude of the power loss in the valve mechanism. In order to compute the overall system efficiency, these losses need to be combined with results in section 5.2. The equations derived in the previous chapter relate to losses in the overall pump/motor, excluding the valve-specific losses. The relevant equations, which will be included in the numerical analysis in the following section and shown in Fig. 6.21, relate to the piston and slipper losses, Eqs. (5.13), (5.17), (5.23), (5.30), and (5.38). In the next section, numerical values are provided for the valve parameters, and simulation results predicting the dynamic response and efficiency of the valve mechanism are presented.

6.2.1 Simulation Results

The model equations in the previous section were simulated using physical parameters from the mechanical design, which is described in section 6.3. Throughout the design phase some of these parameters, such as the spool diameter, spring force, and spool travel, went through several iterations as efficiency results from the numerical simulation were balanced with physical design constraints. The simulation was solved numerically using first-order integration of the differential equations. Different time steps were tested for numerical stability, and a sample time of $0.2\mu s$ was found to produce reliable results. While the equations are valid for any load pressure, pilot, pressure, and pump speed with a typical pump operating range, the design point for the prototype was $P_{high} = 200bar$, $P_{pilot} = 20bar$, and $\omega = 1800RPM$.

The main spool had a diameter of $D_s = 13mm$, a mass of $M_s = 28g$, a spring rate of $K_s = 4.13N/mm$, a spring preload of $F_s = 28N$, and a radial clearance of $10\mu m$. The

diameter of the spool end in contact with the pilot pressure was $D_p = 7.5mm$, and the initial volume of the pilot chamber was $V_p = 1cm^3$. The pressure and tank orifice lengths were $L_h = L_l = 3mm$, and the deadband length was $L_d = 2mm$. The $N_p = 8$ pump pistons had an area of $A_p = 254mm^2$, a dead volume of $V_d = 4.5cm^3$, and they were on a pitch diameter of $D_{pitch} = 82mm$. The wobble plate had an angle of $\alpha = 16°$. The leakage lengths on the end of the main spool were $L_{1,min} = 8mm$ and $L_{1,max} = 12.5mm$. Using CFD results to include both orifice and connecting passage effects, the discharge coefficients on the main spool orifices were $c_{d,high} = 0.33$ and $c_{d,tank} = 0.44$. The orifice to the pilot spool had a diameter of $D_0 = 3.5mm$ and a discharge coefficient estimated to be $c_d = 0.67$. The pilot spool had a diameter of $D_{pilot} = 25mm$, and the angle on the helical land was $\varphi = 20°$. The check valve had a diameter of $D_c = 7.5mm$, a mass of $M_c = 1g$, a spring rate of $K_c = 0.1N/mm$, a spring preload of $F_c = 1N$, and a max travel of $x_{c,max} = 2.5mm$. The hydraulic oil was assumed to have a density of $\rho = 876kg/m^3$, a viscosity of $\mu = 0.0387Ns/m^2$, and an entrained air percentage of $r = 3\%$.

Using these parameters, the simulation was used to predict the spool position, chamber pressures, and valve flow rates, as shown for a pump with a displacement of $s = 0.8$ in Fig. 6.14.

From this figure, which shows the simulation results over two pump rotations, the speed of the valve mechanism can be estimated. While the pilot valve takes roughly $4.5ms$ to open fully, the pressure in the pilot chamber falls almost immediately, and the mainstage spool starts to move $0.45ms$ after the pilot spool starts to open to tank, with the full spring return stroke being completed $3.5ms$ after the pilot switch. The mainstage spool completes its travel in the reverse direction roughly $3.75ms$ after the pilot valve switches. The pressure rise occurs in about $4ms$, with some overshoot due to the fact that the pumping piston is supplying oil to a valve that is passing through its deadband. The check valve opens to relieve the spike once it occurs. As the mainstage valve is opening and when the piston is supplying significant flow, much of the high pressure flow passes through the check valve. Once the flow from the piston starts to decrease, the pressure drop across the mainstage orifice is no longer large enough to keep the check valve open. The speed of the mainstage valve can be increased by raising the spring force and the pilot pressure, and thus the actuation power, or reducing the mass.

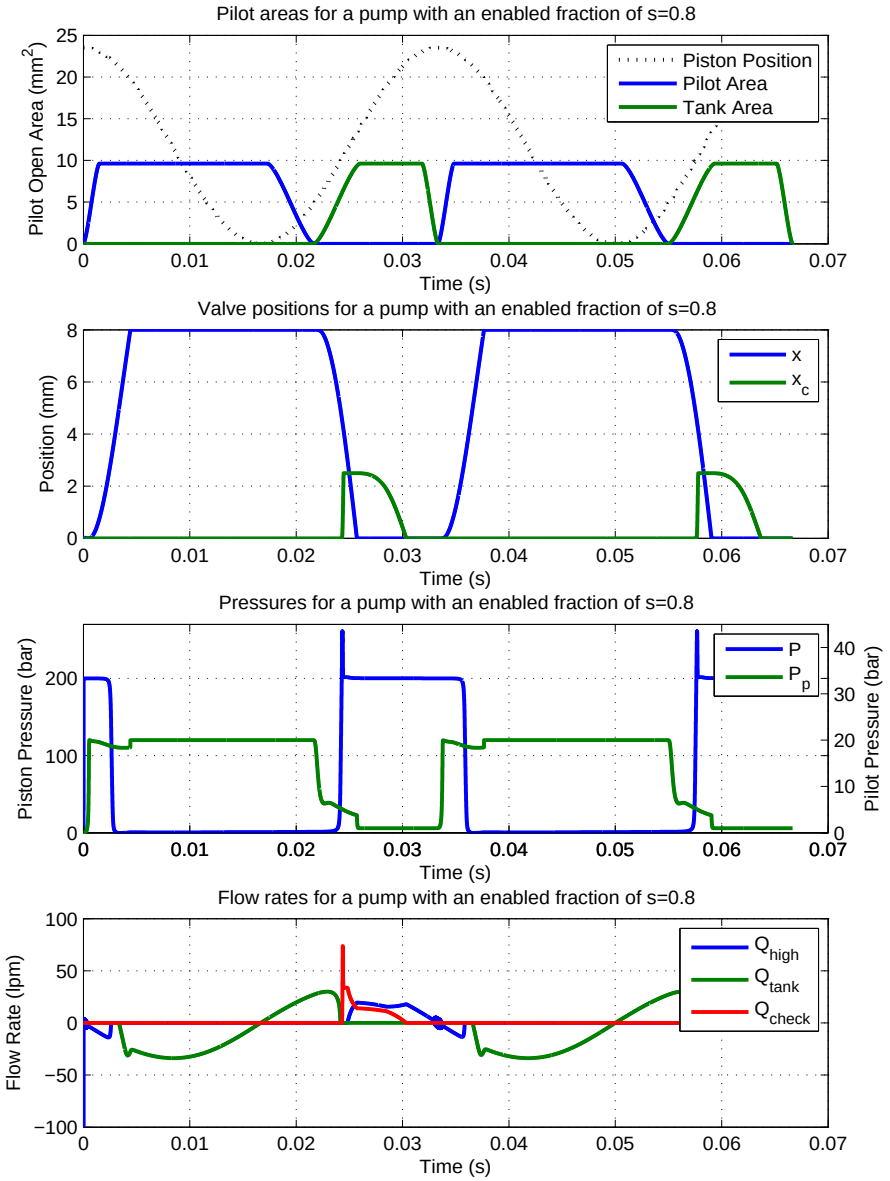

Figure 6.14: Simulation results for a pump at s=0.8 showing pilot areas, main spool (x) and check valve (x_c) positions, piston (P) and pilot (P_p) pressures, and flow rates

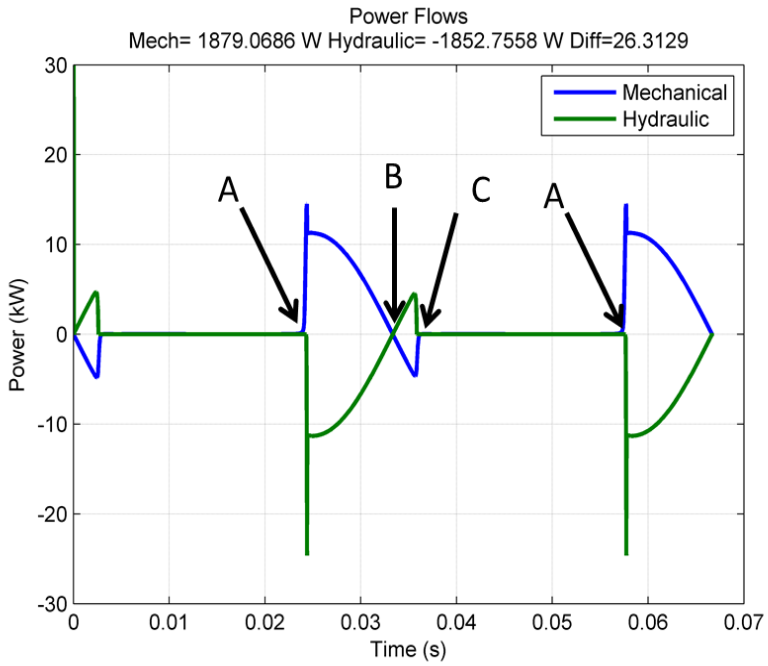

Figure 6.15: Hydraulic and mechanical power in a pump at s=0.8

Notice that, due to the time delay between the switching of the pilot valve orifices and the switching of the mainstage spool, the three-way spool remains open to high pressure for a small fraction of the piston down stroke. This means that the piston behaves as a motor for the beginning of its stroke. This does not necessarily result in much additional power loss, except for the fact that the flow rate is slightly higher during transition and there is slightly more compressed oil in the piston than there would be if the mainstage switched at TDC. However, it does reduce the effective displacement of the pump. This represents one advantage of fully independent valve control, which would allow adjustable opening times for different pump speeds. However, that is not available in a mechanically controlled device unless an additional control input is introduced to adjust the spool timing. One method that could better tune the valve timing at a particular operating speed is described in section 6.2.2. The power flowing in the device is shown in Fig. 6.15.

In this figure the hydraulic and mechanical powers are defined as:

$$Power_{hydraulic} = \left(P_{high} - P_{tank} + \frac{E\left(P_{high}, V_0\right)}{V_0} \right) \left(Q_{high} - Q_c \right) \tag{6.29}$$

$$Power_{mechanical} = \dot{x}_p A_p \left(P - P_{tank} \right) \tag{6.30}$$

where $E\left(P_{high}, V_0\right)$ is the energy stored in a volume of fluid specified by V_0, which is given in Eq. (5.41). Thus, the hydraulic power term accounts for the flow of compressed energy in the fluid in and out of the pump/motor. The difference in sign for Q_{high} and Q_c is due to the fact that $Q_{high} > 0$ is defined as fluid flowing into the piston chamber, and $Q_c > 0$ is defined as fluid flowing out.

In Fig. 6.15 the mechanical and hydraulic powers are roughly equivalent in magnitude and opposite in sign, indicating that the pump is transforming one type of power into another. At point A, the mainstage valve transitions to being open to high pressure, applying pressure and flow to the piston chamber and raising the magnitude of the mechanical power in and the hydraulic power out. Immediately upon opening there is a spike in both the hydraulic and mechanical powers. This is a result of the oil getting slightly over pressurized by the piston as the mainstage valve travels through its deadband. In Fig. 6.14 there is a pressure spike at the beginning of the enabled portion of the piston stroke, which corresponds to the spikes in input and output power. While there is a check valve to limit pressure spikes, it does not open immediately, and while it is opening, a spike in pressure is generated. While the peak magnitude of the spike in hydraulic power out is larger than the peak mechanical power in, the duration of the spike is longer on the mechanical side. In addition, the mechanical power starts ramping up as the piston chamber is pressurized, before any hydraulic power is output. Thus, the power input for this transition is greater than the power out. At point B, the piston has reached TDC, causing its velocity and the net flow in or out of the piston chamber to go to 0. After this point, the power flows reverse as the piston begins to move down again. The pilot valve transition coincides with the piston reaching TDC, but the transition time of the mainstage valve causes high pressure to remain applied to the piston chamber for a short duration, until the high pressure orifice closes at point C. Thus, the piston acts as a motor for the beginning of each intake stroke. This has the effect of slightly reducing the effective displacement of the piston.

In Fig. 6.15, there are some differences in magnitude, which represent losses or

storing/releasing energy in one of the system states. At the top of the figure, the mean power over one cycle is shown, and it is clear that the mechanical power input is larger than the hydraulic power output. The difference between the mean power is also shown, which quantifies the power losses associated with compressibility and throttling. Note that, while the leakage calculation uses inputs from the simulation, it is not included in the pressure state equations, so it will not show up in this power difference and must be accounted for separately.

Figure 6.16 shows the simulation results for a motor with a displacement fraction of $s = 0.5$. In this figure, the pilot valve switches to tank pressure at TDC, and then roughly $3ms$ later, the mainstage valve is fully open to pressure. While this is slightly faster than in the pump case, the return stroke of the mainstage spool takes roughly $4.5ms$ from the beginning of the pilot valve transition. This is partially due to the slower pilot switching speed across the helical land, which can be seen if the first plot in Fig. 6.16; the pilot valve transition that occurs when the piston is at TDC is faster than the one that occurs after TDC. It is also due to the balance between spring force and pilot pressure. The pressure rise occurs in $0.1ms$, which is significantly faster than in the pump case. This is due to the fact that, in the motor case, the oil volume is compressed by adding fluid from the high pressure line, not the motion of the piston. Thus, the pressure rise rate is determined by how fast high pressure oil can get through the opening mainstage valve. In the bottom graph, the momentary spike in flow through the high pressure valve corresponds with this fast pressure rise rate. Notice that, due to the valve delay, the motoring flow does not begin at TDC. In the ideal motoring case, the transition to high pressure would begin before TDC so that a small amount of the pumping stroke could be used to precompress the oil and reduce the large spike in high pressure flow. Section 6.2.2 will discuss one means of accomplishing that.

Rather than showing the mechanical and hydraulic power flows, as was done for the pump case, Fig. 6.17 shows the difference between the input hydraulic power and the output mechanical power. Note that this figure only shows the power difference for a single motor rotation. Not surprisingly, it shows two large spikes corresponding to the two switching events in the cycle, which is when there is the most potential for compressibility and throttling losses. It is interesting to note that the power spike when the motor is turning off, which occurs around $11ms$, is negative, meaning that, for this

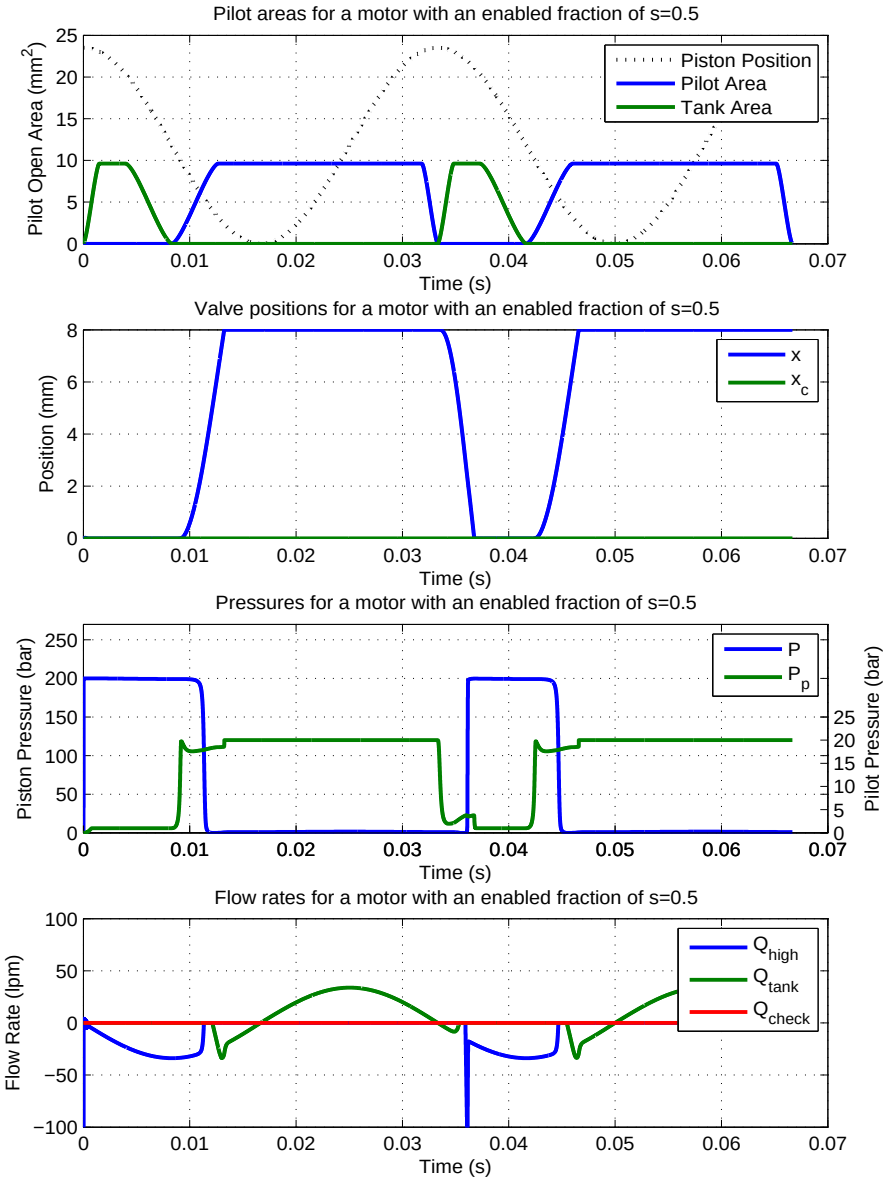

Figure 6.16: Simulation results for a motor at s=0.5 showing pilot areas, main spool (x) and check valve (x_c) positions, piston (P) and pilot (P_p) pressures, and flow rates

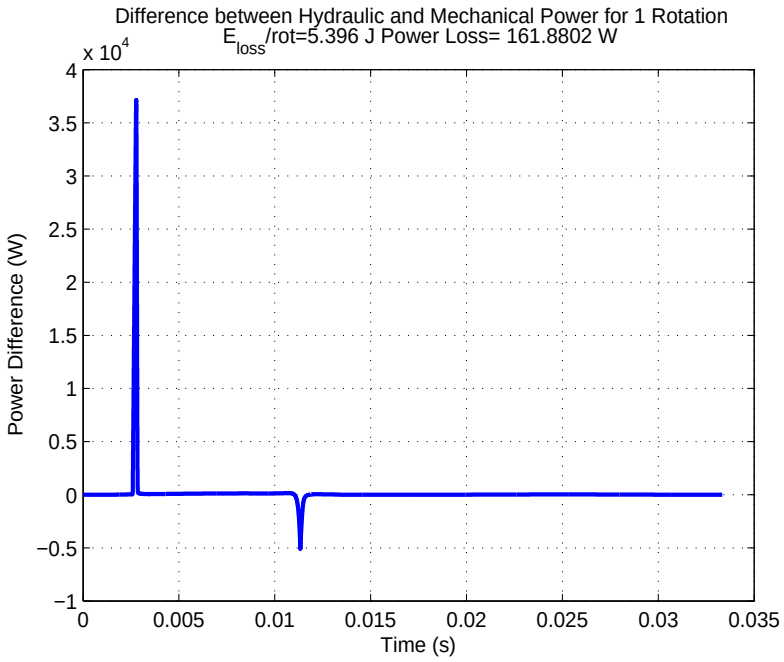

Figure 6.17: Hydraulic and mechanical power in a motor at s=0.5

event, power is being gained instead of lost. To help describe the power gain and loss in the system throughout one cycle, Fig. 6.18 shows a zoomed-in view of the difference between mechanical and hydraulic power.

In Fig. 6.18, the motor rotation is divided into five different regions. The energy loss in each of these regions is listed in Table 6.1. In region A, the piston is moving down, but, due to valve transition delay, the mainstage spool is not yet open to pressure. The power loss in this region starts low and then rises at the end. This loss rise corresponds to the transition throttling caused as the tank orifice closes. The next region contains the large power loss spike seen in Fig. 6.17. This spike occurs when the low pressure oil volume is connected with the high pressure source through the opening orifice. In order to charge the oil volume, a high flow rate, seen in Fig. 6.16, is needed for a short time. As described in section 5.2.4, this flow rate must be throttled down from high pressure to the lower oil volume pressure, which results in a lot of heat being generated. It is clear from Table 6.1 that the vast majority of the energy loss occurs during region B. In region C, the mainstage valve is open to high pressure, and oil is flowing from high

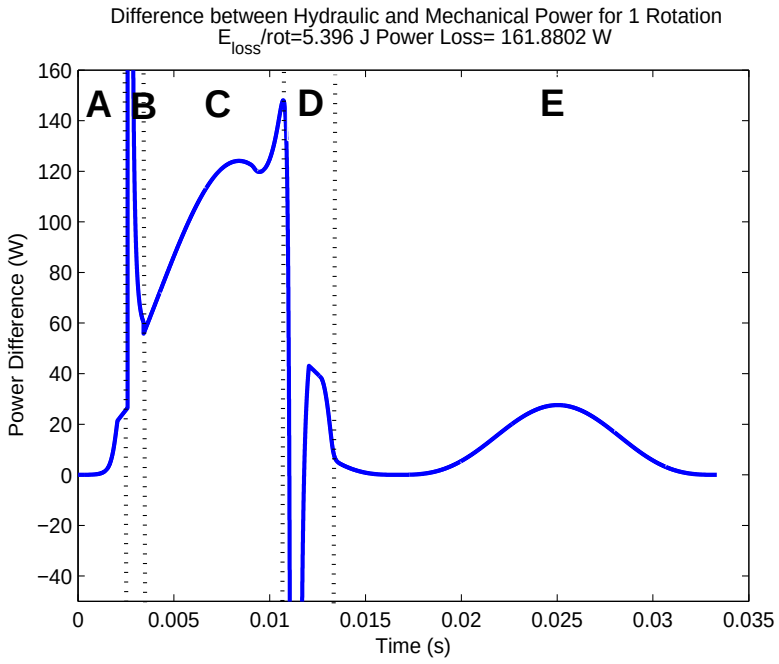

Figure 6.18: Zoom in on the difference between hydraulic and mechanical power in a motor at s=0.5

Region	Energy Loss (J)
A	0.02
B	5.17
C	0.77
D	-0.76
E	0.2

Table 6.1: Table of energy loss in regions A-E of Figure 6.18

pressure to the piston. During this region, there is power loss associated with throttling across the fully open orifice. There is also energy loss due to the flow of energy stored in the compressed high pressure oil, which is why the loss in region C is larger than the loss in region E. In region D, the mainstage valve is transitioning from high pressure back to tank. As the valve closes, there is a spike in power loss due to transition throttling, which is shown at the end of region C. Then, as the valve passes through the deadband and both orifices are blocked, the piston, which is traveling down, extracts some of the energy that is stored in the fluid. In fact, Table 6.1 shows that the amount of energy lost in region C is almost completely recovered in region D. Finally, in region E, the valve is open to tank and all of the power loss is due to throttling across the tank orifice. Initially, the tank orifice is transitioning, so there is a short spike in the loss. After that, the power loss is simply due to throttling across the full open tank orifice. Notice that the spike due to transition at the end of region D is larger than the one in region A. This is due to the fact that, for $s = 0.5$, the piston is traveling faster at the beginning of region E than it is at the end of region A.

At the beginning of region D there is $1.2J$ of energy stored in the compressed oil in the piston chamber. As the valve transitions through its deadband during region D, the moving piston extracts $0.76J$ from the fluid, or about 63% of the available compressed energy. It is possible that adding a decompression chamber could extract additional energy from the compressed oil by increasing the time spent in the deadband. However, simulations with a decompression chamber showed that, only in the worst case of a high-displacement motor, when the volume to be decompressed is at its maximum, did the decompression chamber have any effect on the length of time spent in the deadband. In

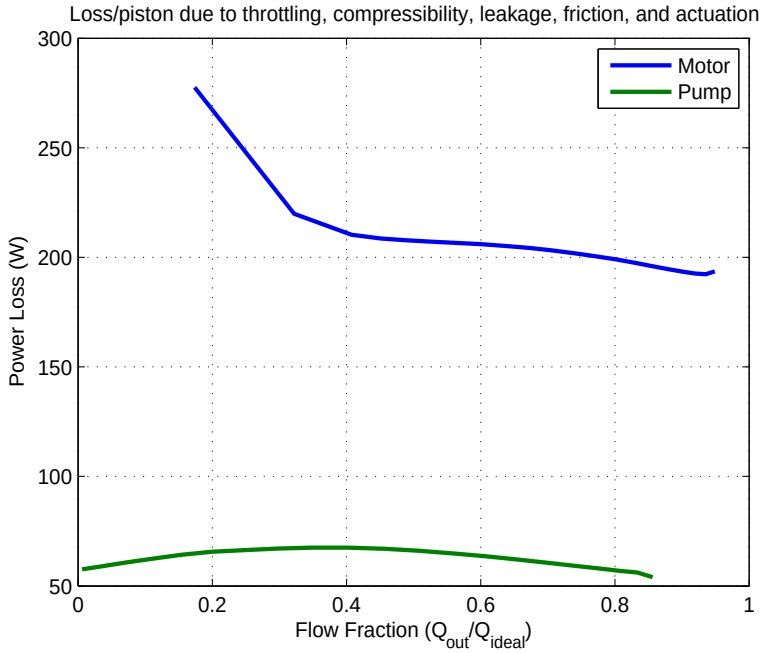

Figure 6.19: Power loss for each piston of a pump or motor due to throttling, compressibility, mainstage leakage, pilot leakage, pilot friction, and actuation power

that case, the vast majority of the compressed energy had already been extracted by the moving piston before the decompression chamber took effect. With the decompression chamber slowing the opening of the spool to tank, the throttling loss in transition was slightly higher, and the net effect of the decompression chamber was a slight increase in the power loss. The decompression chamber could possibly be useful in systems with slower moving pistons or larger compressed volumes, although for this design there was no benefit even at $450RPM$ motor speed.

Figure 6.18 only describes the power loss due to compressibility and throttling. Figure 6.19 shows the losses due to compressibility and throttling, along with the actuation power, mainstage and pilot leakage, and pilot friction across the displacement range. The mechanical displacement fraction representing the width of the enabled region on the pilot spool does not correspond directly to the pump/motor displacement due to

valve delay, pressure dynamics, and the $\cos(\theta)$ term in Eq.(5.3). Thus, in order to display a more accurate representation of the displacement, the coordinate on the horizontal axis is the high-pressure flow rate divided by the ideal flow, $Q_{ideal} = \frac{\omega D_{pitch} \tan(\alpha) A_p}{2\pi}$, which, in this simulation, is $86.15 lpm$. Also note that, due to the time delay associated with the mainstage valve, the end points for the range of s in Eqs.(6.11) and (6.12) were not 0 and 1, but were adjusted to maintain normal operation. For the pump case operating at $1800 RPM$, $s \in [.32, 1]$ was used to generate Fig. 6.19. Below this range, due to the valve closing delay, the time spent as a pump was less than the time spent as a motor, and the net flow out of the piston was negative. Note that, in Fig. 6.19, the output pump flow can still be varied from 0 to about 85% of maximum flow, even though the displacement setting is restricted to $s \in [.32, 1]$. For the motor case, $s \in [.24, .72]$ was used to generate an input flow of between about 17% and 95% of the theorectical maximum flow. For smaller values of s, the mainstage valve did not move far enough to open to high pressure before it started to close again. For higher values of s, the valve was still open to pressure, or transitioning, when the piston started to move up. Note that these limits on s will change for different values of ω, since the valve transition time is mostly independent from pump speed. For slower pump speeds, the limits on the displacement setting, s, are closer to 0 and 1.

There are a number of interesting features in Fig. 6.19. The first is that the motor case has significantly higher power loss than the pump case, which is due to the large spike in power loss that occurs when the oil volume is first pressurized (region B in Fig. 6.18). In contrast, in the pump case, the piston is moving up to pre-compress the fluid while the valve travels through the deadband, which significantly reduces the compressibility loss. For low values of s in the motor case, the power loss rises dramatically. This is due to the fact that at these low duty ratios, the mainstage valve does not get fully open before it starts to close again. Thus, the valve is decelerating and moving slowly while it is partially open to high pressure, causing a lot of throttling loss across the valve. Notice also that the motor case cannot run with less than about 17% of the total flow. One reason for this is that the flow fraction is computed from the amount of high pressure oil that flows into the piston chamber. As is evident in Fig. 6.16, as soon as the mainstage valve opens to high pressure, there is a large rush of oil into the chamber to compress the oil, which will happen for any value of s. Another reason that the flow

cannot be varied down to 0 is that, due to the valve opening delay, the piston is already moving down with some speed. Ideally, the valve will be switched at TDC when the piston isn't moving, but as designed, the transition occurs after TDC. At lower pump speeds, or faster valve switching speeds, the valve transition will be a smaller fraction of the total pump rotation, and the effects described here will be smaller. The valve transition time also affects the maximum available pump flow. Since the valve delay time causes the pumping pistons to behave as a motor for a small fraction of stroke, the maximum net flow is reduced from the ideal case.

Another interesting feature of the power loss plot is the curved shape, which peaks at around 50% of the max flow. This shape is due to the transition loss. If the transition time is fixed, then the magnitude of the transition loss is determined by the flow rate passing through the valve as it transitions. For partial stroke disabling, the fraction of flow that is output correlates to the fraction of the stroke at which transition occurs. Since the piston is following a sinusoidal velocity profile, the maximum velocity of the piston, and thus the maximum flow rate, occurs halfway through the active stroke. If the valve could transition at TDC and BDC, the transition loss would be 0. Thus, the curvature of the power loss plot gives an estimate of the max transition loss, which is roughly $12W$ in this case.

The power loss shown in Fig. 6.19 includes only the losses that can be calculated using the dynamic model equations. This does not include the piston losses or the slipper losses described in section 5.2. Those losses are added to the total loss in Fig. 6.20, which represents the total modeled power loss in the pump and motor cases. This total power loss, along with the power output, can be used to estimate the pump and motor efficiencies as shown in Fig. 6.21.

Figure 6.21 shows the overall predicted efficiency for the pump and motor cases including all of the modeled losses. There are some additional losses associated with shaft bearing friction and fluid churning, but these are expected to be small. Comparing this plot with Fig. 5.14, it is clear that the dynamic power losses not included in the earlier plot have an impact on the efficiency, particularly for the motor case. However, for the pump case, the predicted efficiency in Fig. 6.21 is higher than the efficiency that is predicted for the swashplate case in Fig. 5.14, which does not include any transition or compressibility losses. The final prediction for the discrete piston motor case is

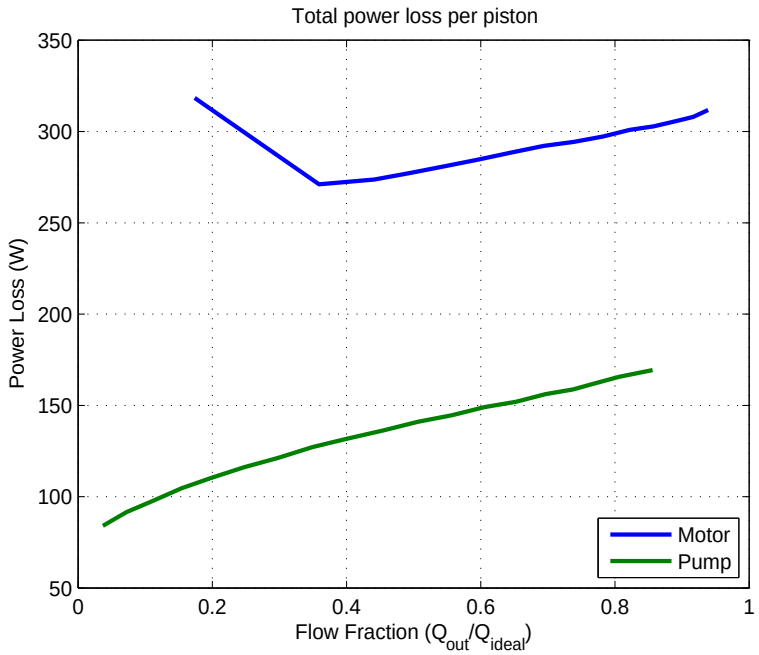

Figure 6.20: Total power loss for each piston of a pump or motor

lower than the swashplate efficiency. However, a swashplate motor will face the same challenges with fluid compressibility as the discrete piston case, but those losses are not included in Fig. 5.14. Furthermore, there are techniques for reducing the compressibility loss in the motor case, one of which is described in the next section.

6.2.2 Precompression Backlash

The dominant power loss in the motor case is the loss associated with compressing the oil volume in the piston chamber from a low pressure up to the high input pressure using oil throttled down from the high pressure line. This loss does not occur in the pump case because the oil in the piston chamber is primarily compressed using the motion of the piston as the valve transitions through its deadband instead of using high pressure oil. This same approach can be used for the motor case if the valve is switched while the piston is still moving up. In this case, the piston acts as a pump for a short period of time, and while the valve is crossing the deadband, the piston will do some compressing of the oil that will not need to be done with high pressure oil. While the piston may

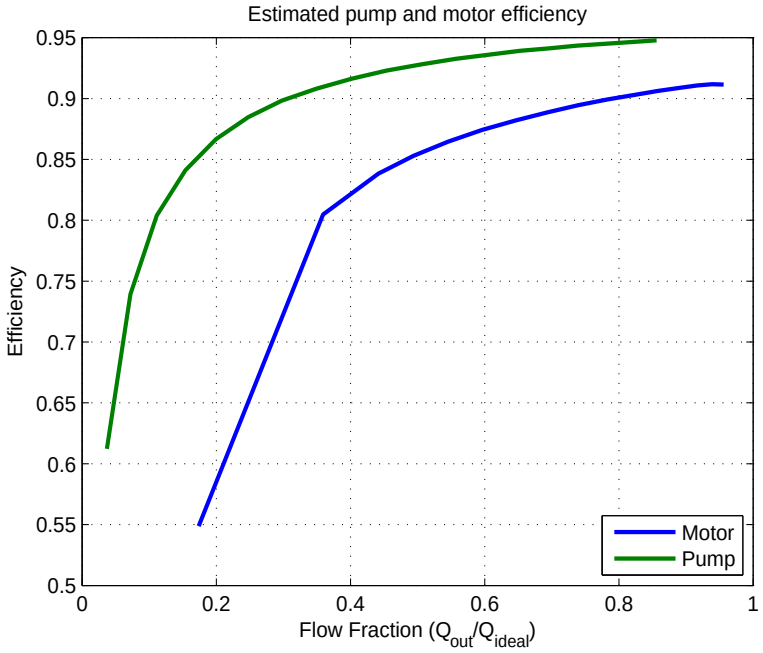

Figure 6.21: Predicted overall efficiency for a pump and motor including all modeled power losses

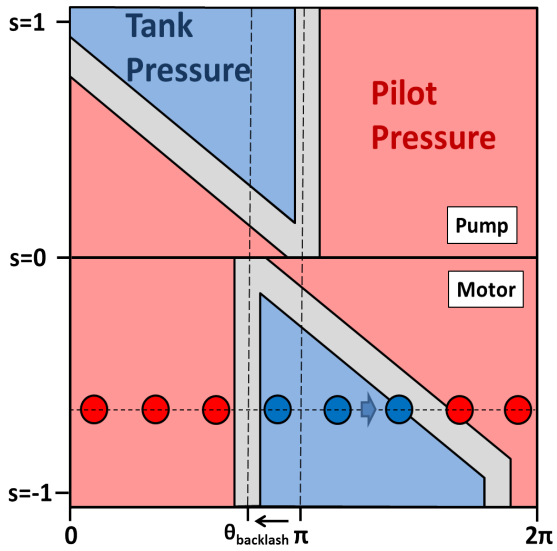

Figure 6.22: Unwrapped pilot spool with a pre-compression offset for the motor case

not completely compress the oil up to the load pressure, as Fig. 2.2 makes clear, the oil is most compressible when it is at a low pressure, so any rise in pressure that can be accomplished by the moving piston will have a large effect on the energy loss.

Figure 6.22 shows the unwrapped pilot spool areas for a spool that allows precompression for the motor case. Notice that the blue piston-enabled area on the motor side is shifted to the left by an angle $\theta_{backlash}$. On the pump side, the enabled area remains in the normal position between 0 (BDC) and π (TDC). This allows the mainstage spool to start transitioning to high pressure while the piston is still traveling up. Figure 6.23 shows the dynamic model results for a motor with an offset angle of $\theta_{backlash} = 0.67 rad$. In the first plot, it is clear that the transition from pilot area to tank area occurs before TDC, which is in contrast to Fig. 6.16. Notice that Q_{high} is very slightly positive at the beginning of the power stroke, and that the spike in flow caused by fluid rushing in to charge the oil volume is significantly smaller than in Fig. 6.16. This near elimination of the flow spike corresponds to a dramatic reduction in the power loss for the motor case, bringing it much closer to the power loss from the pump case, as shown in Fig. 6.24. Figure 6.25 shows that this reduction in the power loss results in a nearly identical pump and motor efficiency.

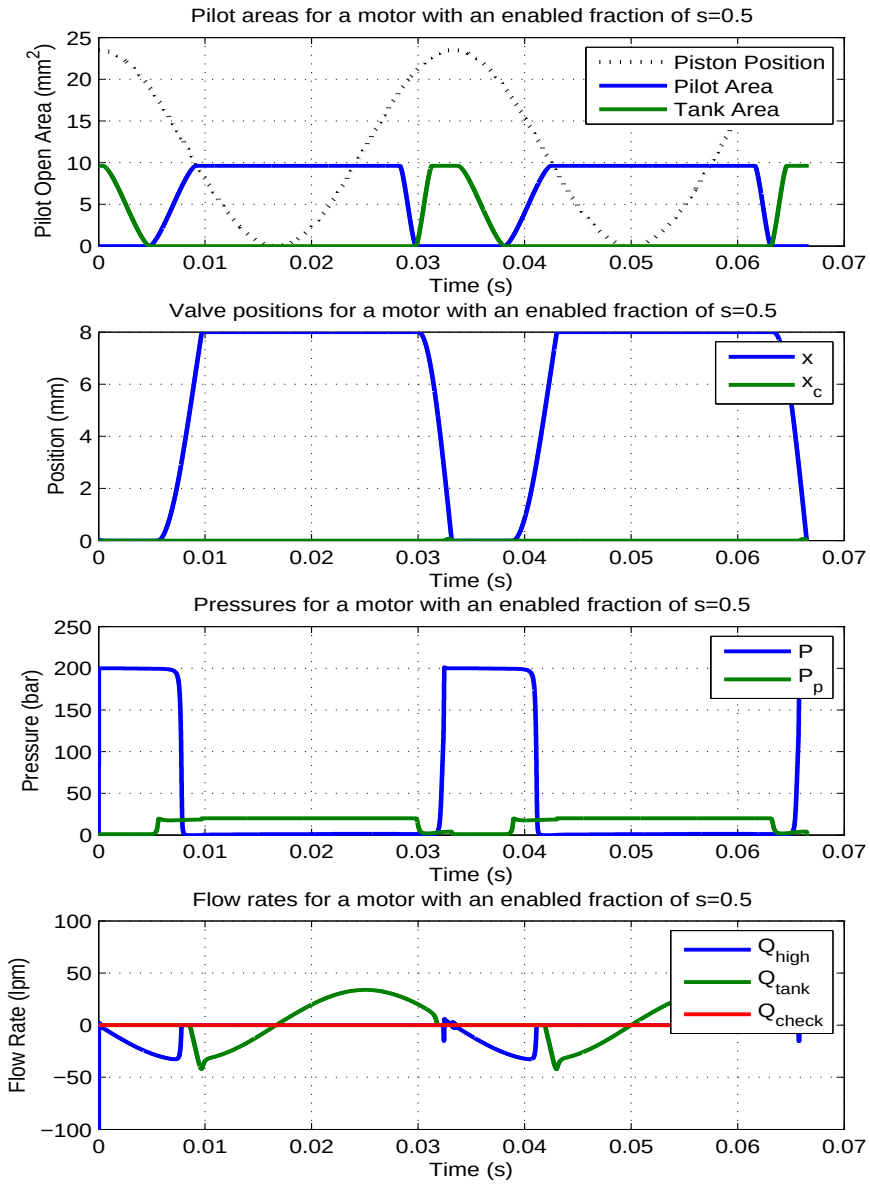

Figure 6.23: Simulation results for a motor at s=0.5 with a pre-compression angle of $0.67rad$

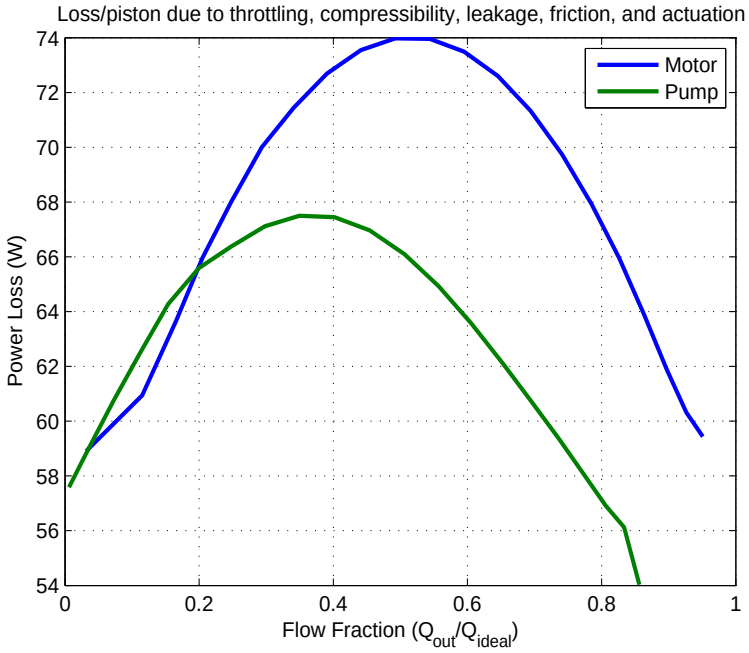

Figure 6.24: Single-piston power loss due to compressibility, throttling, leakage, friction, and actuation power for motor with a precompression angle of $0.67 rad$

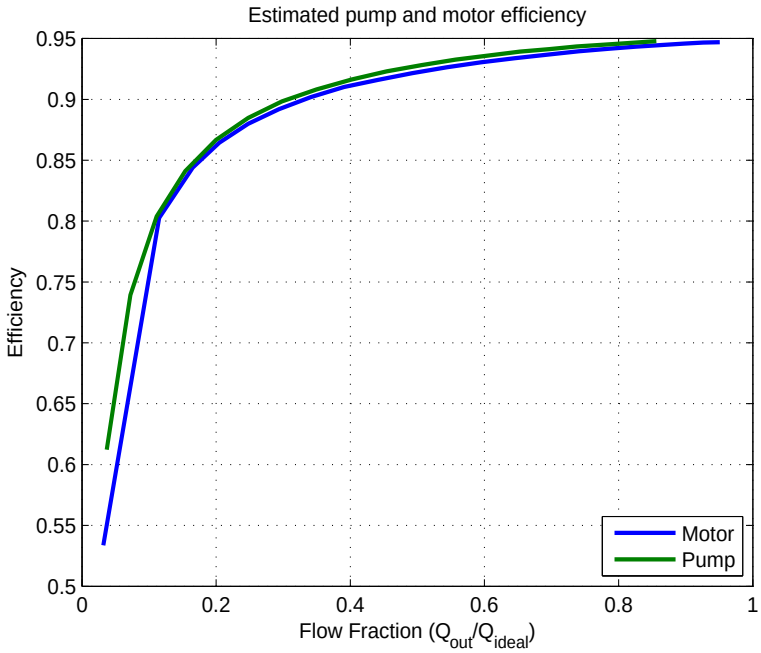

Figure 6.25: Predicted efficiency for a pump and a motor with a precompression angle of $0.67 rad$

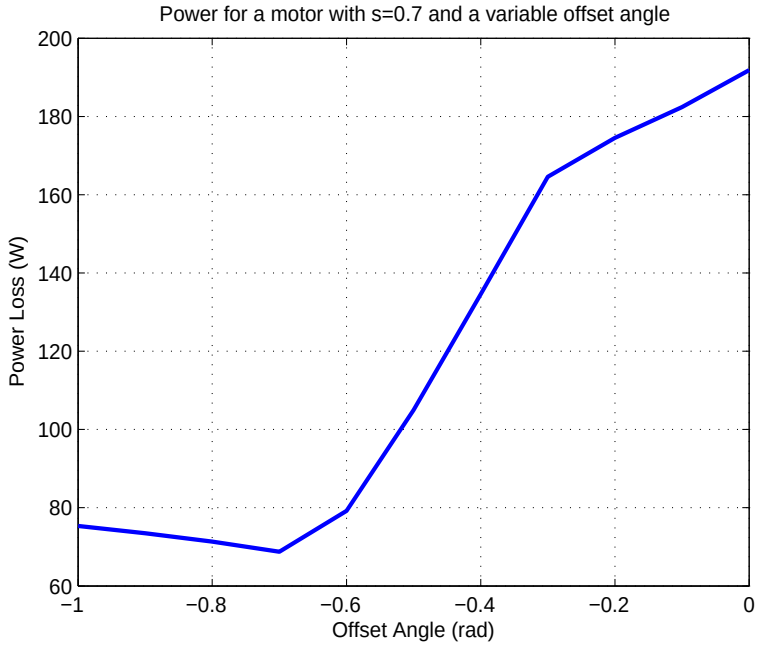

Figure 6.26: Power loss in one piston with a varying offset angle

In Fig. 6.23, the pilot spool transition occurs well before TDC, however, the mainstage delay causes it to transition very close to TDC. For this simulation, the backlash angle was tuned so that the mainstage would transition near the ideal point. At a different speed or pilot pressure, this would not be the case. This highlights one of the restrictions of mechanical valve control, as opposed to independent valve control using electrohydraulic valves. However, even when the offset angle is not ideal, it can still provide a substantial efficiency benefit, as shown in Fig. 6.26. When the backlash angle is smaller than the ideal, which in this case is roughly $0.7rad$, the mainstage valve transitions after TDC. This would also occur when the motor is rotating faster than the speed for which $\theta_{backlash}$ is tuned. While the power loss is larger than in the ideal case, it is still less than the no-offset case. When the motor is rotating slower, the mainstage will transition before TDC, which will result in some pumping action of the piston before motoring begins. While this will lower the effective maximum power output, Fig. 6.26 shows that the power loss will still be reduced from the no-offset case.

Figure 6.22 shows how the offset angle can be achieved when the pilot spool is

moving in one direction. However, the spool is designed so that each end of the spool can be either the pump end or the motor end, depending on the direction of rotation. In Fig. 6.22, the circles representing the connections to the mainstage spools are shown moving to the right with respect to the pilot areas. If the direction is reversed, then it is clear that the top half, which has switched from the pump end to the motor end, will not have an offset angle, and the bottom half, which is now the pump end, will have its turn-off point occur at an offset angle after TDC. This will exacerbate the problem of the pumping pistons acting as a motor and reduce the effective pump displacement. However, in the case where the circles are moving to the left, if both pilot areas are shifted to the right by $\theta_{backlash}$, then the bottom half (pump) will be lined up with TDC, and the top half (motor) will have the desired offset angle. Thus, the pilot areas must move with respect to the piston travel profile depending on which direction the pump/motor is rotating. This can be accomplished by adding backlash to the pump/motor drive mechanism. The backlash that is required must be between the drive shaft and the pump/motor element that generates the piston motion profile. In the prototype described in this thesis, the piston motion profile is sinusoidal and is generated by an angled wobble plate. When the device is switched to the motor case, the vertical land on the pilot spool must move from being even with TDC to leading it by $\theta_{backlash}$. When switching to the pump case, the vertical land must move from being behind TDC to being even with it. In both cases, the spool must move forward with respect to TDC. Thus, the pilot spool, which is coupled to the drive shaft, must move through $\theta_{backlash}$ before the drive shaft engages the wobble plate.

A more flexible solution to this problem would be to couple the drive shaft to the pilot spool through a planetary gear set. The planetary gear, which would have a $1:1$ ratio between the drive shaft and the pilot spool, would have another input that could be used to adjust the relative angle between the two parts. Connecting a small motor to this additional input would allow full flexibility on the timing of the pilot spool, allowing the offset angle to be adjusted as desired at different pressures and flow rates. While this would add complexity to the design, it would also provide nearly all of the flexibility of independent electrical valves to the mechanical control approach.

For the prototype design described in section 6.3, the pre-compression backlash is not included. However, the drive mechanism is designed to be adjustable so that the

pilot spool timing can be modified, and the efficiency benefits of adding backlash can be quantified. The mechanical design of the pump/motor prototype is described in the following section.

6.3 Mechanical Design

The valve design concept described in the previous sections can be incorporated into a pump/motor prototype to demonstrate the discrete piston concept. The prototype pump/motor design for this thesis is based on a wobble-plate type device, which is similar to a swashplate pump/motor, except that the pistons are stationary and the angled wobble plate is rotated. The proposed discrete piston control approach is not limited to the wobble-plate architecture; it was selected due to availability of parts and a design supplied by Sauer-Danfoss, a company that manufactures pumps and motors. This discrete piston approach can be applied to any pump/motor architecture that has stationary piston chambers, such as wobble-plate, inline pump/motors, or radial piston pump/motors. The radial piston approach may have some added efficiency benefits due to the fact that the piston shoes are sliding on a central cam, which may allow the relative sliding speed between the piston and the cam to be low, reducing the friction loss. This approach could conceivably be applied to a design with a rotating barrel of pistons, but if the pistons rotate, some form of valve plate is needed to connect the rotating pistons to the stationary pressure and tank hoses. This would eliminate much of the efficiency benefit of the discrete piston design.

The prototype was designed to accomplish a number of goals. First, the design must minimize the power losses, meaning that fluid passages must be large, compressed volumes should be small, and friction and leakage should be kept to a minimum. The design should also be compact, simple to manufacture, and allow for sensors to test its operation. The piston chambers should have check valves between them and the high pressure line to prevent against excessively high pressures from building up if a valve does not operate as planned.

In order to keep the compressed volume small, each three-way mainstage valve should be located close to its associated piston. Since the pilot valve drives all of the mainstage valves and is driven by the pump/motor drive shaft, it should be located in the center

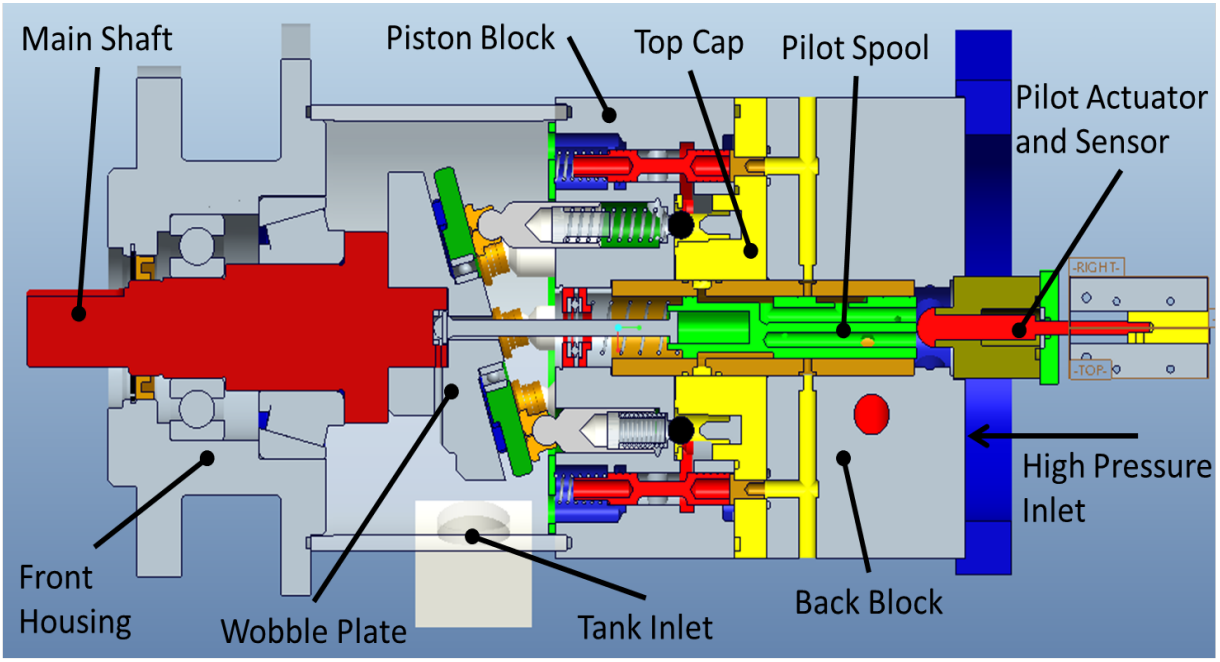

Figure 6.27: Cross sectional view of prototype pump/motor assembly

of the pump/motor. Given the size of the pistons, wobble plate, and mainstage valves, the mainstage valves do not fit within the circle of pistons. To keep them close to the pistons, the mainstage valves can either be arrayed outside of the piston circle and parallel to the pistons, or they can be behind the piston chambers perpendicular to the pistons. The latter arrangement would result in the mainstage valves traveling in the radial direction from the center. For compactness, the mainstage valves were placed parallel to the pistons at a larger pitch diameter, which slightly increases the outer diameter of the pump housing, but not as much as if the valves were arranged radially.

Figure 6.27 shows a cross section of the pump/motor assembly. The housing of the pump/motor is made up of several different pieces. The Front Housing contains the Main Shaft and the bearings that support it. Attached to the Main Shaft is the Wobble Plate, which drives the pistons in their reciprocating motion. The wobble plate rotates in a low pressure volume of oil that is contained within the Front Housing, the Piston Block, and a tube that connects them. In the side of the tube is the low pressure connection to the pump/motor. The Piston Block, Top Cap, and Back Block pieces make up the rest

of the housing. These three parts contain the pistons, mainstage valves, pilot spool, and fluid passageways connecting the different parts. The high pressure and pilot pressure connections to the pump/motor are at the back of the Back Block part. The axial position sensing and actuation mechanism for the pilot spool is also located at the back of the Back Block part. The entire assembly is held together with tie rods (not shown) which provide a clamping force between the Front Housing and the blue plate behind the Back Block shown in Fig. 6.27.

The component that is at the center of the design and is the key to enabling this discrete piston design is the pilot valve spool. It is described in detail in the next section.

6.3.1 Pilot Spool Design

The role of the pilot spool is to direct either tank or pilot pressure to one end of each of the eight mainstage valves for a defined portion of the pump/motor rotation. It must be able to be rotated by the pump/motor shaft and translate with respect to the hydraulic connections to the mainstage valves. Figure 6.28 shows a view of the pilot spool. The spool has two main sections: the control section on the upper left which contains the pilot and tank pressure pockets, and the pilot inlet section on the lower right. The section on the left is essentially Fig. 6.11 wrapped around a spool, with two pockets of tank pressure surrounded by an area of pilot pressure. The control section of the spool will hydraulically connect to the end of each mainstage spool and control whether it is open to high pressure or tank. The diameter of the spool is $25mm$, and the length of the control section is $32.5mm$, which allows for $29mm$ of travel and $3.5mm$ for the diameter of the connecting orifices. The pockets in the control section are connected to pilot and tank pressure through two rails running down the center of the pilot spool, as shown in Fig. 6.29. The tank rail is open to the end of the spool, allowing oil to exit the spool. The pilot pressure rail connects pilot pressure area of the control section with the pilot inlet section. The pilot inlet section is connected to pilot pressure through the pilot sleeve shown in Fig. 6.31. The pilot inlet section is the same length as the control section so that it will always be in contact with the pilot inlet on the sleeve, no matter where the spool is in its travel.

The three lands on the spool that bound the control and inlet sections have balance grooves to promote centering of the spool in the sleeve. The end of the pilot spool that

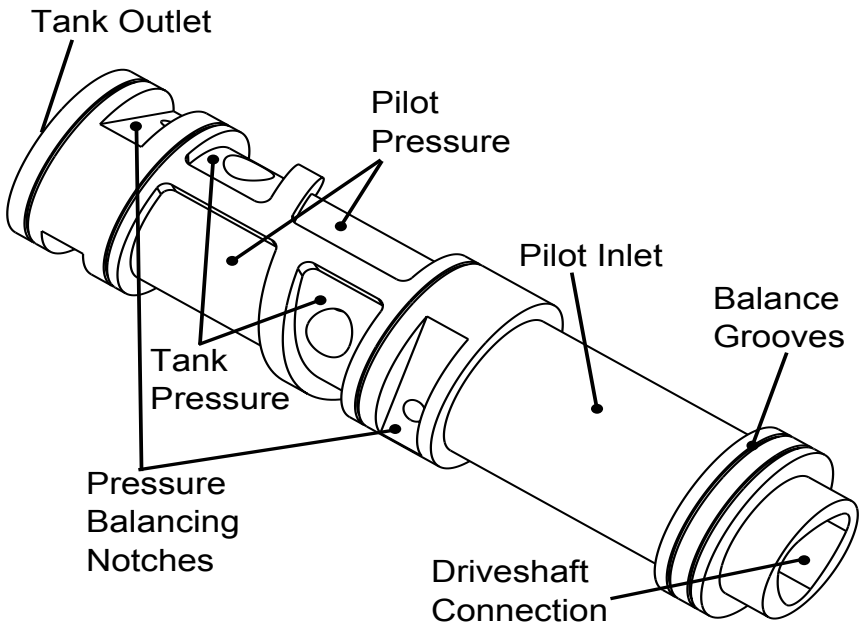

Figure 6.28: Pilot spool with features labeled

does not have the tank outlet contains the connection to the pilot spool drive shaft. The pilot spool must translate as well as rotate, with the rotational torque provided by a drive shaft connected to the main pump/motor shaft. The end of the drive shaft can translate within the end of the spool to allow the required axial travel.

The pilot spool also contains features to pressure balance the spool, which are labeled as pressure balancing notches in Fig. 6.28. The two pockets of tank pressure in the control section do not balance each other, and thus the pilot pressure on the opposite side of the spool will generate a force on the spool. In order to counter act this force, the pressure balancing notches shown in Fig. 6.28 are connected with pilot pressure. There are also notches on the opposite side of the spool from the labeled notches which are connected with tank pressure. These tank notches are included to maintain a pressure balance in a system with a pressurized tank line.

The pressure balancing notches must be located and sized to correctly compensate for the pressure imbalance generated by the pockets in the control section. Figure 6.30 shows a sketch of a cross section of the pilot spool with the x and z axes labeled (the

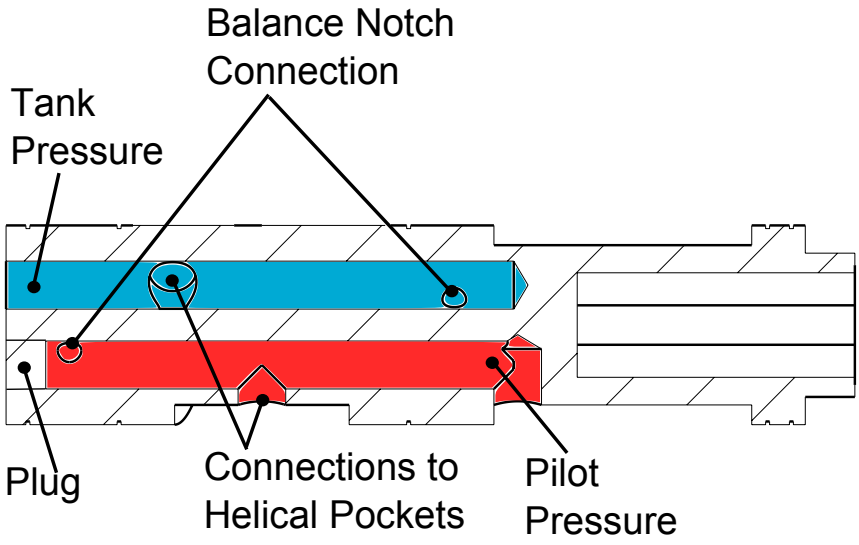

Figure 6.29: Cross section of pilot spool

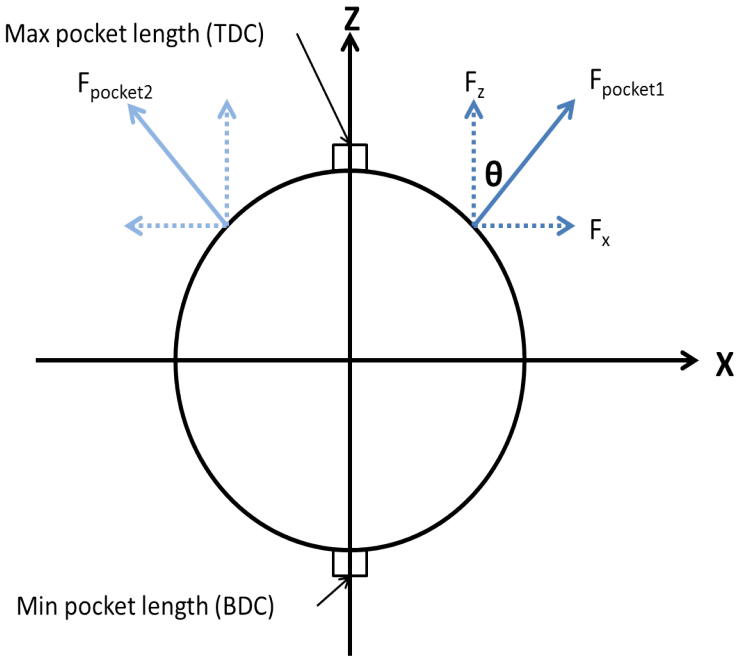

Figure 6.30: Pressure force acting on a cross-section of the spool

y-axis is along the axis of the spool). It also shows the resultant pressure force from the two unbalanced tank pockets in the control section. Since the force is generated by the unopposed pilot pressure on the opposite side of the spool, the force vectors are shown as pointing away from the spool from the centroid of the two pockets. Note that, while the forces from both pockets are shown, those forces are actually occurring at different positions along the y-axis. It should be clear from this figure that the forces in the x-direction are balanced, but the forces in the z-direction are not. Also, due to the different y-positions of the forces, there is a moment about the z-axis caused by the F_x components of the force. Since the F_z components are in the same direction, there is no moment generated by these forces. Thus, the pressure balancing notches must be located and sized to balance the forces in the z-direction and moment about the z-axis.

The component of the pressure force in the z-direction for one pocket is computed by finding the area of the low pressure pocket and multiplying by the pilot pressure on the opposing side:

$$F_z = \int_0^{\frac{D_{pilot}\pi}{2}} \int_0^{Y(s)} P_{pilot} \cos\left(\frac{2s}{D_{pilot}}\right) dyds \tag{6.31}$$

where s is a distance along the face of the spool. The height of the helix is simply a linear function of s:

$$Y(s) = y_{max}\left(1 - \frac{2s}{\pi D_{pilot}}\right) + D_{ori} \tag{6.32}$$

where y_{max} is the maximum axial length of the pocket, which is $11mm$ in the prototype. D_{ori} is the diameter of the orifice in the sleeve connecting the pilot to the mainstage spools, which in this design is $3.5mm$. The minimum height of the helix is D_{ori} to allow the orifice to be fully uncovered when the pump/motor is at full displacement. The moment about the z-axis can be computed from:

$$M_z = \int_0^{\frac{D_{pilot}\pi}{2}} \int_0^{Y(s)} P_{pilot} \sin\left(\frac{2s}{D_{pilot}}\right) (y_{center} - y)\, dyds \tag{6.33}$$

where y_{center} is the location of the center of the control section. The resultant force from the pilot pressure in the pilot balancing notch must balance F_z and M_z. In order to balance the moment about the z-axis, the balancing notch must apply a force component in the x-direction, with a magnitude depending on how far the notch is located from the center. The magnitude and angle of the pressure balancing force must be:

$$F_{balance} = \sqrt{F_z^2 + \left(\frac{M_z}{y_{offset}}\right)^2} \tag{6.34}$$

$$\theta_{balance} = \tan^{-1}\left(\frac{M_z}{F_z y_{offset}}\right) \tag{6.35}$$

where y_{offset} is the distance from the center of the control section to the center of the pressure balancing notch. This is a design parameter that must take into account space and leakage considerations. In the prototype design, $y_{offset} = 24.25mm$, which was $8mm$ below the bottom of the pocket. The area of the pocket can be computed from $F_{balance}$. There is flexibility in selecting the width and depth of the pocket to achieve that area. Note that this calculation is an approximation; there is likely to be a pressure gradient across the helical land which is not taken into account. This can easily be included, however, for the prototype parts, the strategy was to neglect this because it is easier to make the notches larger if need be rather than smaller.

The pilot spool will be spinning inside a pilot sleeve, shown in Fig. 6.31. The sleeve part was made separately from the pump housing to provide design flexibility; it allowed the housing to be built in several pieces, and it allowed for a different material and hardening selection on the sleeve than on the rest of the housing. A design made for production could do away with the sleeve part to save space and cost. As shown, the sleeve has a pilot pressure rail that connects pilot pressure to the inlet section of the spool, and it has eight $3.5mm$ orifices to connect the pilot spool to each of the mainstage spools. All of these features have o-rings around them to seal against the pump/motor housing, which contains the sleeve. The radial clearance between the pilot spool and the sleeve was chosen to be a nominal value of $7.5\mu m$, and was specified to be within $+12.5\mu m$ and $-5\mu m$. The nominal value may be a bit tighter than needed, but it allowed for some tolerance on the machining and heat treatment without getting excessive leakage. If the spool proves to be too tight in testing, it is easier to remove material than to add it.

The drive shaft that connects to the end of the pilot spool provides the rotary actuation, but not the axial actuation. Figure 6.32 shows the mechanism that controls the axial position of the pilot spool within the sleeve. The pilot spool is acted on by a spring on the driveshaft end. On the other end of the spool, the Pilot Push part

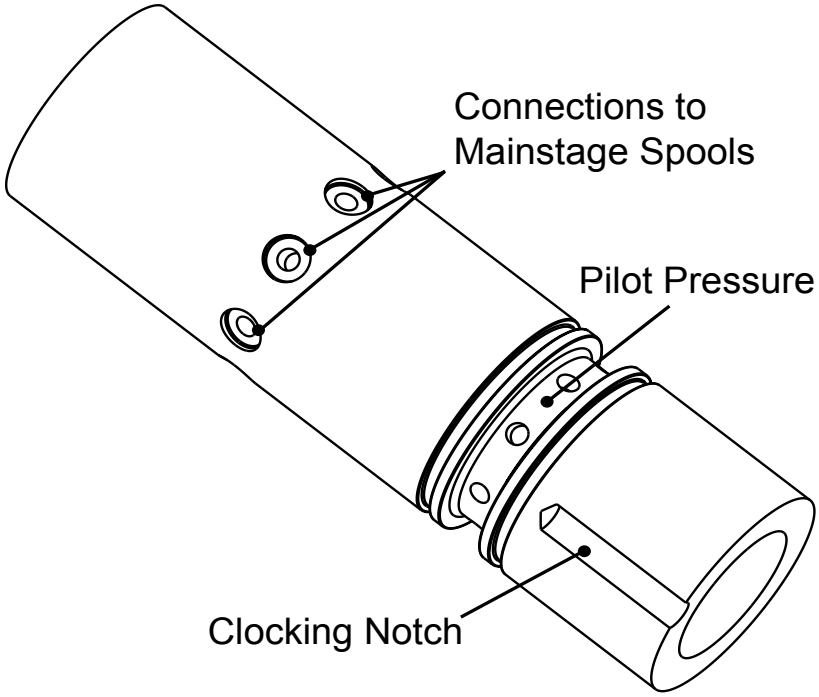

Figure 6.31: Pilot sleeve

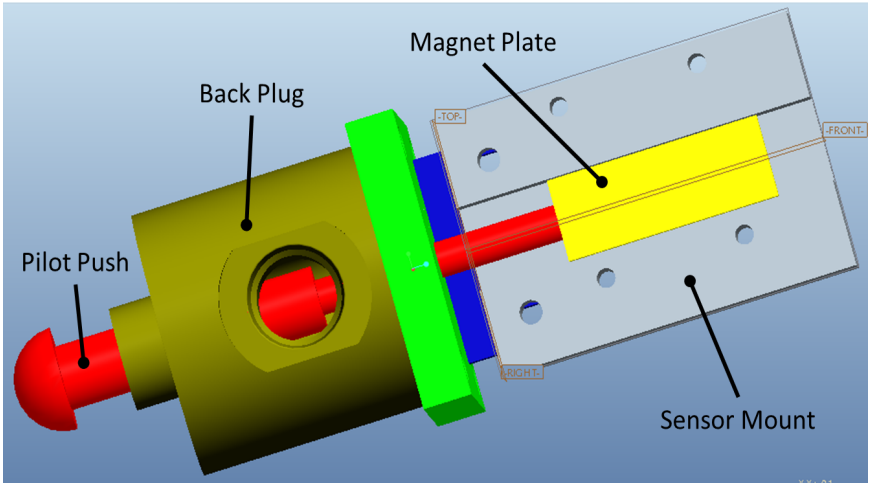

Figure 6.32: Pilot spool actuation and sensing assembly

will contact the spool to push against the spring. The Pilot Push part is essentially a small hydraulic cylinder with a rounded tip on one end, and an extension for a position sensor on the other end. The rounded end of the Pilot Push rod will be in contact with the rotating pilot spool. Since the rod does not rotate, there will be relative motion between these parts, so the rounded end is intended to provide as small of a contact area as possible. To control the position of the pilot spool, oil is added to or removed from the port in the Back Plug part from an external control valve. The opposing spring is designed to accommodate a pressure of $20bar$ pushing on the rod, although the device should still be able to reach full stroke at $10bar$. With the selected spring rate ($1.06N/mm$), spool mass ($0.25kg$), and $20bar$ pilot pressure, the pilot spool should fully compress the spring in $15ms$ and fully return to its neutral position in $30ms$. The ends of the pilot spool are both referenced to tank pressure, and large flow paths between the ends of the spool and tank should ensure minimal fluid restriction on the motion of the pilot spool. The Pilot Push rod extends out the back of the Back Plug part so that the axial position of the pilot spool can be sensed. For this prototype, a magnetic linear encoder was selected as the sensing device, although this could be replaced by a different type of position sensor. For precise control, the position of the pilot spool should be sensed and controlled. However, the pilot position is similar to the swashplate angle on a typical variable displacement pump. In many cases, swashplate pumps do not have closed-loop control of the swashplate angle, and instead rely on pressure feedback to control the pump/motor, using either electrical or mechanical compensators. Such an approach would also be possible for the discrete piston pump/motor, which could reduce cost and complexity.

The drive shaft must transmit sufficient torque to the spool to overcome the friction on the spool, as well as translate with respect to the spool. There are many different profiles of splined shafts that can accomplish this. The profile selected for this prototype, as shown in Fig. 6.33, is a roughly triangular shaped profile with three rounded corners and a larger radius arc between the corners. This profile was selected primarily for manufacturability; it can be machined into the spool using an end mill, as opposed to more complex operations for designs with more pronounced teeth. The design of the mechanical drive system that connects to this profile is discussed in the next section.

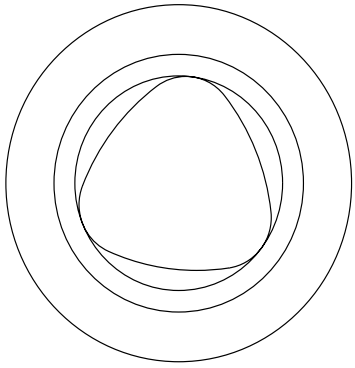

Figure 6.33: End of the pilot spool showing drive shaft profile

6.3.2 Driveshaft Design

Figure 6.34 shows a cross sectional view of the mechanical drive line[1] for the pump/ motor. The Main Shaft is the mechanical connection to the power source/sink, and it will transmit the torque from the wobble plate to the application it is connected to. The Main Shaft is supported by two bearings; a tapered roller bearing to support axial and radial loads, and a ball bearing to support the moment on the shaft. All components are sized to withstand forces generated by a $200bar$ pressure on the pistons. There is a shaft seal to prevent oil leakage. The Wobble Plate is connected to the Main Shaft via two pins, and the Drive Shaft is connected via an adjustable clocking mechanism. The connection between the two shafts is designed to allow misalignment between the Main Shaft and the Pilot Spool by only transmitting torque through a small pin that runs transversely through the end of the Drive Shaft. The pin is held in place by a small ring with notches in it, which is secured to the Main Shaft with a set screw. This arrangement allows the angle between the Main Shaft and the Drive Shaft to be adjusted. As mentioned in section 6.2.2, in the motor case, it is desirable to have an offset between TDC and the start of the motoring stroke. In order to truly realize this benefit for motoring while not degrading pump performance, backlash would need to be added between the Main Shaft and the Wobble Plate. If backlash is added between the mainshaft and the wobble plate, then when switching directions, the mainshaft and the

[1] C. Larish [109] did a significant amount of the design work for the drive line parts.

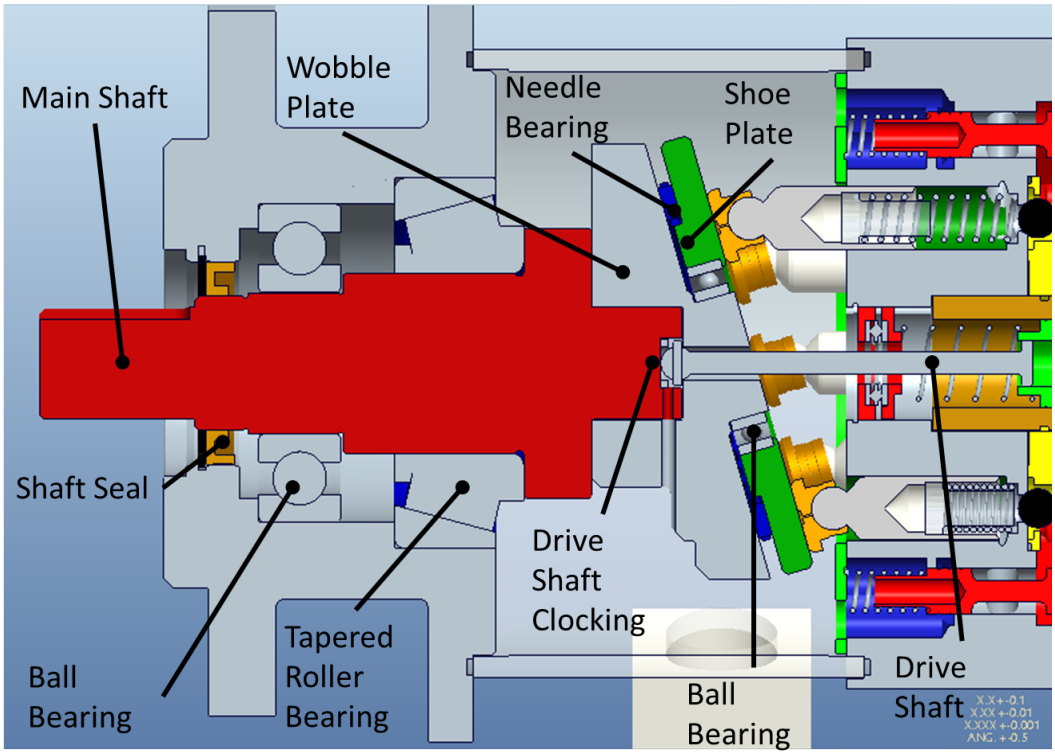

Figure 6.34: Cross section of the mechanical drive line for the pump/motor

pilot spool will move while the wobble plate stays in place across the backlash angle. This will make the pilot spool lead TDC on the wobble plate as described in section 6.2.2. While this is possible to achieve, the high forces/torques involved at this junction made adding backlash a significant design risk in the prototype. In place of the backlash, which would automatically adjust the offset for pump and motor modes, this adjustable clocking mechanism was designed. Thus, the offset angle can be manually adjusted in pump and motor modes to test the effect of a variable offset.

The Wobble Plate in the prototype has an angle of 16°, which was taken from the design of a donated pump prototype. As shown in Fig. 6.34, the Wobble Plate has a radial ball bearing and a thrust bearing attached to it, and riding on those bearings is the Shoe Plate. The pistons interface with the Shoe Plate, which can rotate with respect to the Wobble Plate. This design allows for the friction force generated by the pressure force acting on the pistons to be primarily rolling friction instead of sliding friction. As shown in Fig. 5.13, which assumes a rolling friction coefficient, the friction between the slipper and the swashplate is one of the largest sources of energy loss in the pump/motor, and anything that can reduce it will have a significant effect on the overall efficiency. Using a plate that does not rotate with the Wobble Plate to interface with the piston slippers also reduces the risk associated with non-hydrostatically balanced pistons. Designs that have rolling friction on the wobble plate exist in the hydraulic industry, but they are not as common as designs with hydrostatically balanced pistons. With the mechanism for generating the piston motion profile described, the next section details the design of the mainstage valves to control the flow in and out of the piston chamber.

6.3.3 Piston and Valve Design

In order to reduce the compressed volume of oil and create a compact design, the mainstage valve should be located as close to the piston chamber as possible. Figure 6.35 shows a cross section of one piston and valve pair. The piston has a diameter of roughly $18mm$ and was taken from a donated prototype check ball pump. There is no connection from the piston chamber to the face of the slipper as this design does not use hydrostatically balanced pistons. The piston was designed to house a check valve that could draw fluid from the low pressure chamber on the intake stroke. Since the discrete

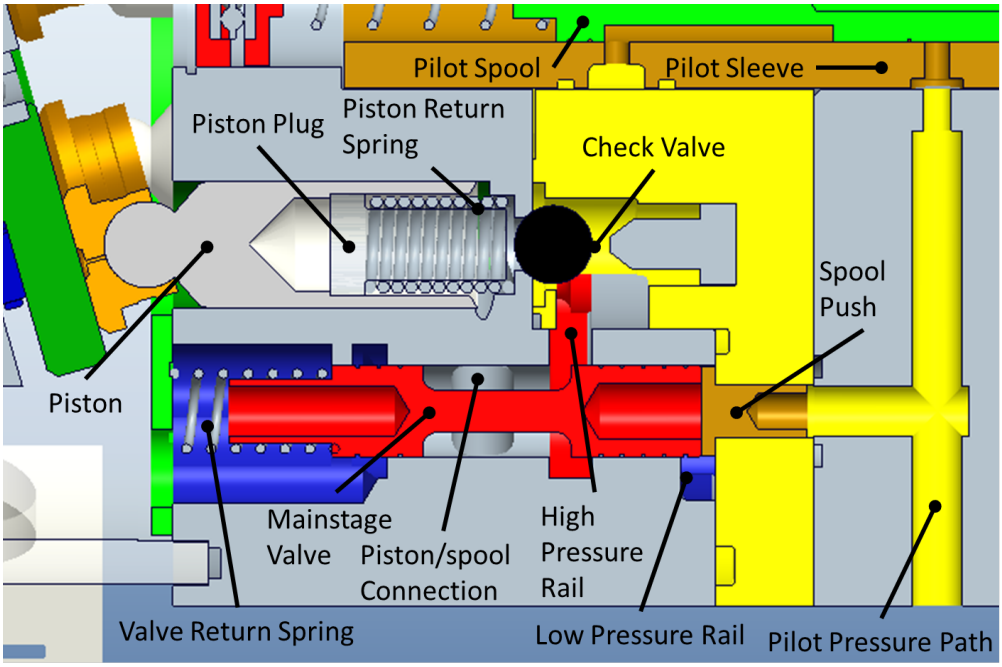

Figure 6.35: Pump/motor piston and mainstage valve

piston design includes a connection to low pressure through the mainstage valve, this check valve is not needed. To take up the added compressed volume in the center of the piston, a Piston Plug part was designed. The Piston Plug removes roughly $3cm^3$ of unnecessary compressed volume from the piston chamber and acts as the seat for the piston return spring. The return spring was sized to match the force on the donated pump/motor prototype. At the end of the piston chamber, there is a check valve that can connect the piston chamber to high pressure. While this flow path is redundant with the connection through the mainstage valve, it is included as a safety valve to ensure that the pressure in the piston chambers does not get excessively high in the case of a mis-timed mainstage valve. In the pumping case, this check valve can act as a parallel flow path and reduce the throttling loss through the mainstage valve. The prototype uses a check ball made out of polycarbonate instead of steel to reduce the mass and response time of the check valve.

The connection between the piston and the mainstage valve is not in the plane of the cross section shown in Fig. 6.35, but it can be seen as a drilled hole intersecting the back

of the spool bore, and there is another drilled hole on the other side of the spool bore that has been removed by the cross sectional view. The original design had only a single connection hole that was in the cross sectional plane, but CFD analysis, described in section 6.3.4, showed that the throttling loss could be substantially reduced by adding a second drilled hole. The cost of the second flow path is additional compressed volume, but simulations indicated that the reduction in throttling losses was larger than the increase in compressibility losses.

The mainstage spool is shown in its bore, which contains undercuts for connecting to high pressure (red) and tank (blue). In this design, the mainstage spools are designed to be spring biased open to pressure. This was chosen because the control of the pilot spool is accomplished using pilot pressure, which may only be available if the pump is able to build pressure. In order to ensure that pressure would be available to control the pilot spool, the mainstage spools are in the default position to allow pressure. There are some downsides to defaulting to high pressure, especially in the motor configuration, and the design can easily be adapted to be normally open to tank.

The mainstage spool is acted on by a spring on the tank side, and by the Spool Push part on the pressure side. In designing the mainstage valve to operate at a nominal $20bar$ pilot pressure, it was beneficial to have flexibility in selecting the mainstage diameter, which determines the main flow area, and the area acted on by pilot pressure, which determines the actuation power. The Spool Push part allows that flexibility without requiring a tight concentricity tolerance on two different diameter bores. The Spool Push part is connected to the pilot spool through the pilot pressure flow path. Both the mainstage spool and the Pilot Push parts have holes drilled in them to reduce the mass and response time of the valve.

The return spring on the mainstage spool was designed to provide roughly the same transition time in either direction when using a pilot pressure of $20bar$. The radial clearance between the spool and bore was designed to be nominally $9\mu m$ and with tolerances allowed to be between $13.5\mu m$ and $-2.5\mu m$. This is a wider tolerance than could be achieved using typical hydraulic component manufacturing practices, so leakage could likely be reduced in a production design.

Figure 6.35 shows the three parts of the main pump/motor block, with two gray parts of the housing separated by a yellow part in the middle. The piston and mainstage valve

are housed in the Piston Block part of the housing, the yellow part is called the Top Cap part, and the gray housing piece on the right of the figure is the Back Block. The housing was designed in three pieces to allow all of the fluid passages and component housings to be created using machining operations, rather than requiring a casting to be designed. This was done primarily for ease of prototyping, and a production design could easily make use of a casting to create a more compact design. The next section discusses the design of the housing and the fluid passages contained within it.

6.3.4 Fluid Passage Design

The main pump/motor housing block needs to direct high pressure, tank pressure, and pilot pressure to different components within it. Of these, the high pressure and the tank flow paths must be large enough to allow large flow rates to pass through them with minimal pressure drop. As a rule of thumb, all high pressure passages are designed to have at least $5mm$ of material surrounding them. In this section the Piston Block end of the housing which faces the wobble plate is referred to as the front, and the Back Block end of the housing that contains the high pressure and pilot pressure connections is referred to as the back.

In front of the Piston block is an open chamber containing the wobble plate, which is bounded by a steel tube. In the side of tube is the connection to tank pressure, and the chamber surrounding the wobble plate is intended to be filled with low pressure oil. While this does lead to some fluid churning losses, it also provides lubrication for the piston/swashplate interface and the shaft bearings. It also provides a simple connection to tank pressure from the Piston Block. In Fig. 6.35, the right side of the mainstage valve is shown as connecting to tank pressure through a large opening in the face of the Piston Block. This creates a large, short flow path between the piston chamber and tank, which is critical to reducing throttling losses, particularly at low displacements. CFD analysis described in section 6.3.4 confirms that this flow path achieves low throttling losses.

The Piston Block also contains the pistons and mainstage valves as shown in Fig. 6.35. The mainstage spool is connected to all three of the different pressures in the housing, with orifices opening to high pressure and tank, and pilot pressure pushing on its end. The high pressure connects to the middle of the mainstage spool. This is

accomplished through a high pressure rail that surrounds the central pilot sleeve and connects to each of the eight mainstage valves. This pilot rail is partially contained in the Piston Block part, and partially contained in the Top Cap part. The fact that the pressure rail exists at the junction of the two parts is what allows it to be machined on the interior of the pump/motor housing. In addition to connecting the eight mainstage valves, the high pressure rail also surrounds the check valves at the end of the piston chambers, creating a simple connection between the check valves and high pressure. The high pressure oil is brought to the back of the housing through three drilled passages connecting the pressure rail with the Back Block part of the housing. Within the Back Block, the three high pressure passages are brought together at the high pressure port.

There is also a low pressure rail between the Top Cap and Piston Block parts as shown in Fig. 6.35. While this low pressure rail does not contain the main flow through the pistons, it is important for allowing oil to fill in behind the mainstage valves as they transition from pressure to tank. Without this connection to tank, a vacuum would be drawn behind the valves, slowing down their transition. In order to reduce the fluid damping effect on the piston speed, this connection to tank should be large. Similarly, low pressure oil should be routed to the back of the pilot spool to allow it to transition without significant fluid damping. There are four tank pressure passages that bring tank pressure from the wobble plate chamber to the back of the pump/motor. These four passages run through the low pressure rail, connecting it to tank. They run into the Back Block part where perpendicular channels connect them in the center of the pump/motor, behind the pilot spool.

Figure 6.36 shows a view of the fluid passages in the Back Block part. The four blue tank pressure passages can be seen connecting behind the pilot spool, and the three high pressure passages which bring oil from the high pressure rail to the high pressure port are also shown connecting in the Back Block. The eight yellow passages connecting the Pilot Sleeve with the ends of the mainstage valves can be seen extending radially from the center, the ends of which are to be blocked by plugs (except for one, which will be blocked by a pressure sensor). The yellow pilot pressure inlet passage can be seen running parallel to the four tank passages through the center of the part. In order to maintain $5mm$ of material between the passages as the pilot inlet line passes through the eight radial pilot passages and still connect to the Pilot Sleeve through the Top

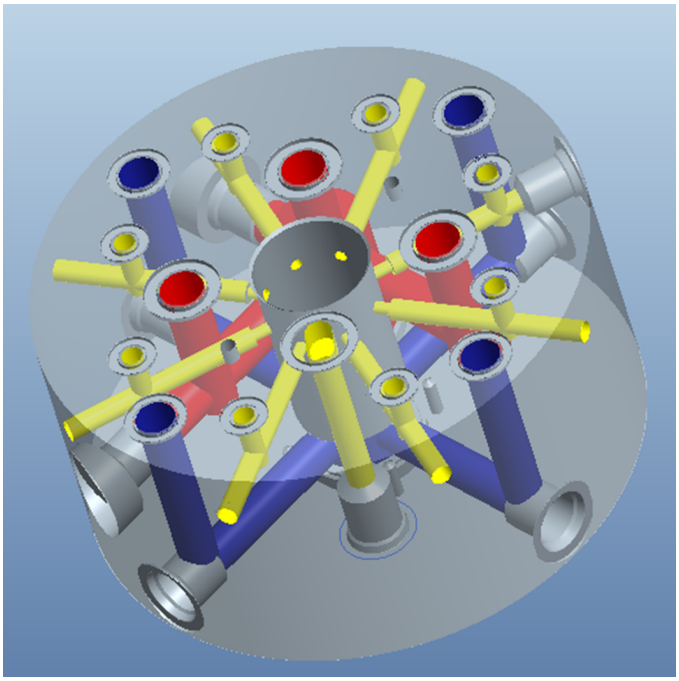

Figure 6.36: Transparent view of the Back Block part

Cap, the pilot inlet line has an offset, as shown on the front face of the Back Block part. All of the passages are surrounded by o-ring grooves at the interface between the Back Block and Top Cap parts.

Figure 6.37 shows the front face of the Top Cap part, which mates against the Piston Block part. In this figure, the four outer most holes are part of the tank pressure passages, and the eight holes just inside of those contain the Spool Push parts shown in Fig. 6.35. Inside of those holes is the nose that forms part of the high pressure rail. Inside that nose are the eight holes that contain the check valves. In the middle of the Top Cap part is a star-shaped pattern, which is included as a pressure relieving mechanism. While all passages are sealed with o-rings, if high pressure were to leak out of the high pressure rail or around the check valves and pressurize the entire face between the Top Cap and the Piston Block, the tie rods might not be strong enough to hold the pump/motor together. The star-shaped pressure relieving area is a shallow $0.5mm$ cut into the face of the Top Cap which connects to a small passage to tank around the outside of the Pilot Sleeve. This is included as a safety device, but could

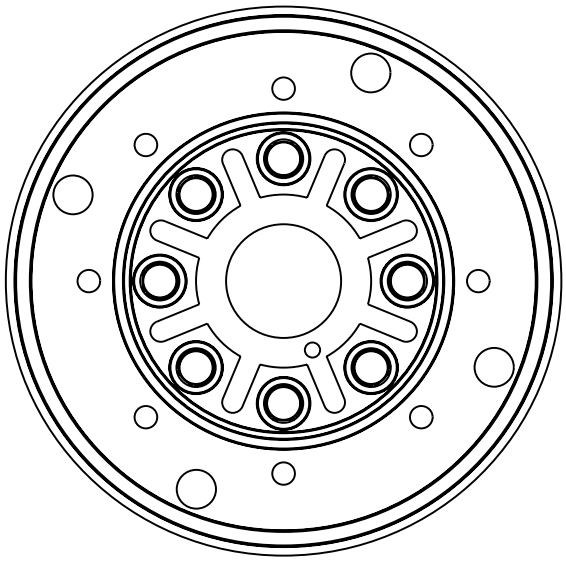

Figure 6.37: Front face of the Top Cap part

likely be excluded from a production design.

The fluid passages that direct the main pump/motor flow between the pistons, tank, and high pressure need to be large enough to minimize throttling losses. The next section details the CFD analysis and design iterations done to create an efficient design.

CFD analysis

In section 6.2, the orifice area in the mainstage spool between high pressure or tank was described as the cylindrical open area defined by the mainstage spool circumference times its max opening distance of $3mm$. However, these simple orifices do not account for all of the throttling losses experienced by the flow as it passes between the pistons and the high pressure or tank ports. Fluid friction and head loss due to changes in direction account for a significant portion of the throttling loss. To accurately analyze these losses, the simple orifice equation (Eq. (5.39)) is not sufficient. Computational Fluid Dynamics (CFD) software was used[2] to predict the throttling losses, and the feedback from this analysis was used through several design iterations to reduce the overall throttling loss. Note that, while section 6.2 uses simple orifice equations, the

[2] M. Wang set up, executed, and processed the CFD data.

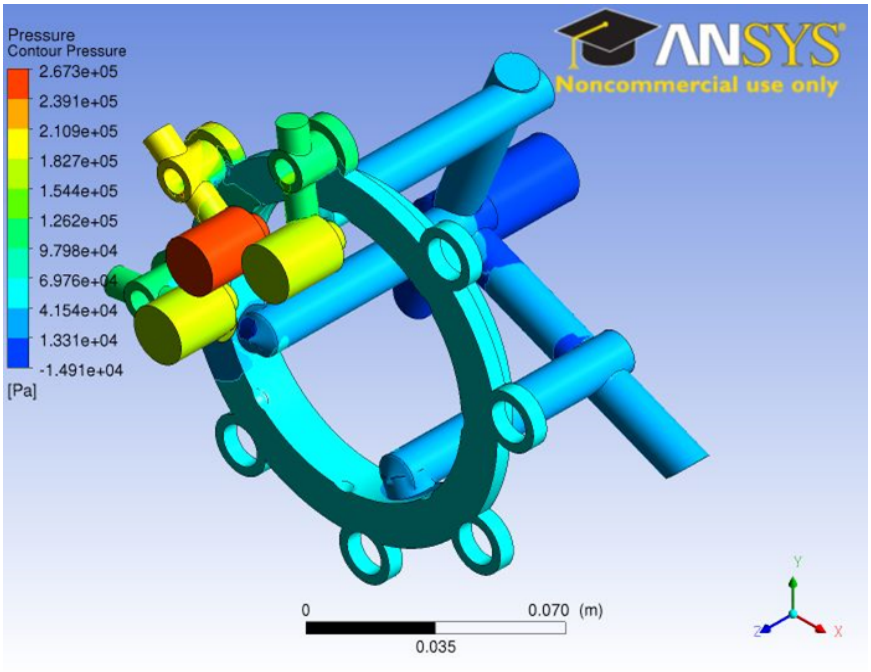

Figure 6.38: Initial design iteration of high pressure fluid domain with static pressure contours

results of this CFD analysis are included in the simulation results by adjusting the discharge coefficient (c_d) values to approximate the full path throttling losses. The CFD analysis was performed using Ansys CFD software to solve the incompressible Navier-Stokes equations. The settings used to compute the solution are identical to those used in [86], which describes the details of the numerical solver used.

Figure 6.38 shows the high pressure fluid domain colored by the static pressure at the walls. This is the initial design of the high pressure flow path, which includes the passage through the mainstage valves, the high pressure rail, and the three high pressure connections that are brought together in the Back Block. The model only includes three pistons connected to high pressure since the maximum individual piston flow occurs when three pistons are active, which can be seen in Fig. 5.16. For the CFD analysis, the pressure drop was computed for the pumping case with three flow input boundary conditions at the three pistons and an outlet pressure condition at the high pressure outlet. The input flow rates were 23.925lpm at two of the pistons, and

33.84lpm at the center piston, for a total of 81.69lpm through the high pressure path.

The average pressure drops at the three pistons were 1.62bar at the lower flow pistons, and 2.66bar at the high flow piston. This was significantly higher than the throttling loss through just the valve orifice, and higher than desired to demonstrate the efficiency of the discrete piston approach. In Fig. 6.38, there are several step changes in pressure that indicate flow restrictions. The first is from the piston chamber to the passage connecting the piston to the mainstage valve. In this initial design, there was only a single flow path, which caused a roughly 0.5bar pressure drop. The second large pressure drop is between the mainstage valve chamber and the high pressure rail. This transition includes the mainstage orifice area, but the pressure drop was significantly larger than predicted by the orifice equation. The CFD analysis showed that the flow was not evenly distributed around the annular mainstage orifice, with most of the flow passing through the valve near the opening to the high pressure rail. This indicated that the flow path from the back of the high pressure annulus around the spool to the high pressure rail was too restrictive. Finally, the long flow paths from the high pressure rail to the pump outlet had a gradual pressure drop along them, especially after the three flow paths were joined together.

The CFD analysis of the pressure drop indicated several opportunities for improvement in the design of the high pressure flow path. The first was to increase the flow area between the pistons and the mainstage valves. Initially, the diameter of the passage was increased, but it could not be increased enough without causing the mainstage spool to increase in length. So, instead of a single, large passage, a second passage was added, with the two connections evenly spaced on either side of the mainstage spool. In addition to increasing the flow area, this had the effect of helping to spread out the flow through the mainstage orifice. Since the flow was now entering the valve chamber on either side, rather than in the middle, the flow was more evenly distributed around the circumference of the mainstage spool, lowering the pressure drop across the orifice. This was further improved by increasing the size and depth of the pressure rail. In the initial design, the high pressure annulus around the valve spool intersected the pressure rail near its edge, creating a restrictive rectangular opening between the annulus and the pressure rail. By increasing the depth of the high pressure rail so that its outer diameter was roughly in line with the center of the mainstage valve, the restriction

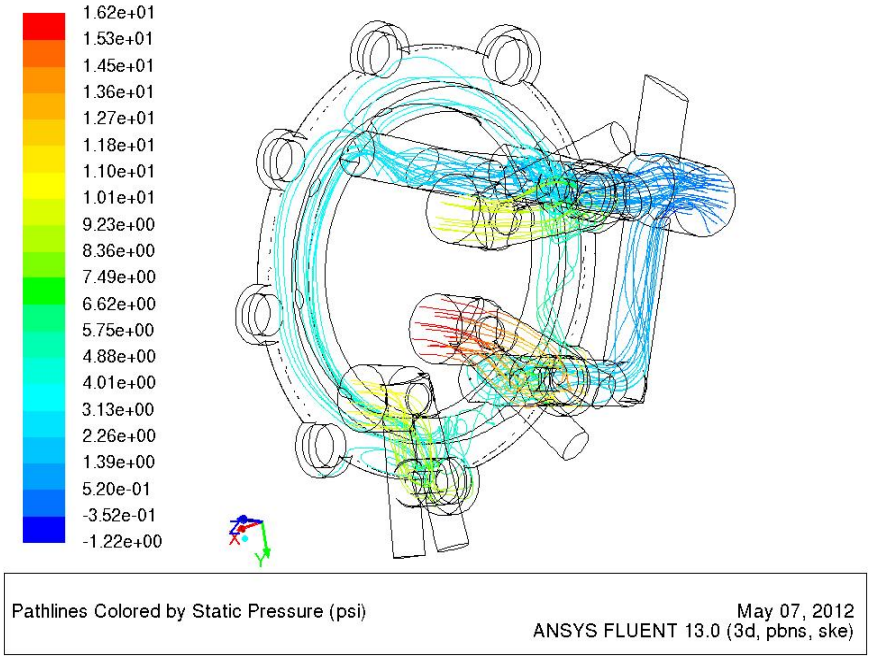

Figure 6.39: Final design of the high pressure fluid path with pressure colored pathlines

between the annulus and the pressure rail was removed. Finally, the three flow paths connecting the high pressure rail to the common exit port, and the common exit port, were increased in diameter. With these improvements, the average pressure drops were reduced to $0.7bar$ on the lower flow pistons, and $1.06bar$ on the high flow piston. The pressure colored pathlines for the improved design are shown in Fig. 6.39, which shows the reduction in pressure drop. Note that this analysis assumes that all of the flow from the piston is passing through the mainstage valve, and not across the parallel check valve. For the pumping case, once the pressure drop across the mainstage valve rises above the check valve cracking pressure, the flow will be split between the two paths, lowering the pressure drop.

The flow path between the piston chamber and the tank outlet is much simpler than the high pressure path. When the mainstage valve is connected to tank, the fluid flows from the piston chamber, through the cylindrical mainstage valve orifice, and around the end of the valve spool into the chamber enclosing the wobble plate. For the CFD analysis, it was assumed that the pressure drop through the large wobble plate

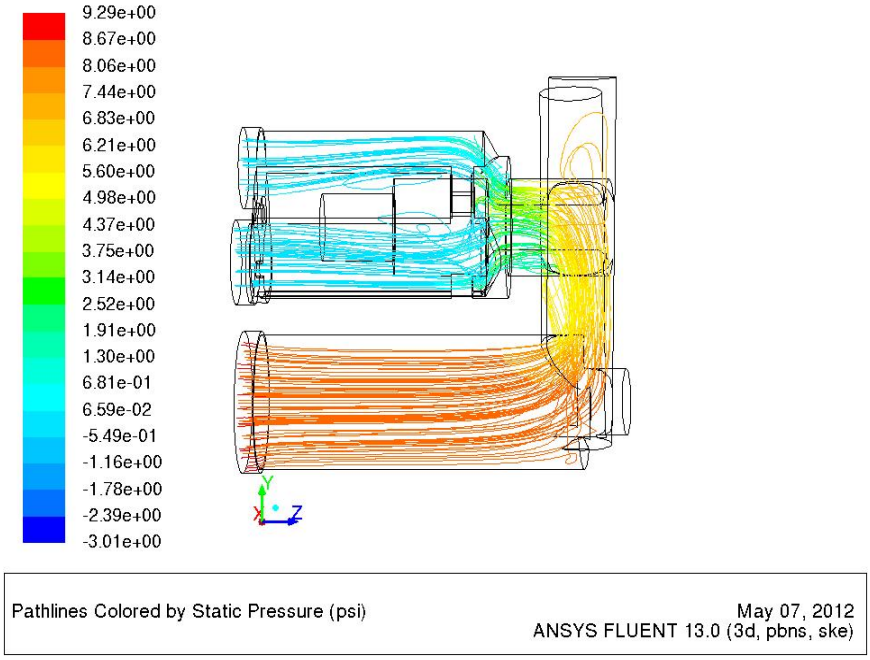

Figure 6.40: Low pressure fluid path with static pressure contours

chamber was negligible, so only the path between the piston chamber and the wobble plate chamber was modeled. Since the tank flow path for each piston is independent of the other pistons, only one piston needed to be analyzed. Figure 6.40 shows colored pathlines through one path from the piston to tank. This flow path is much shorter and more direct than the high pressure paths, which accounts for the significantly lower pressure drop of $0.60bar$ at $33.84lpm$. The values of $1.06bar$ and $0.60bar$ for the high and low pressure flow path pressure drops at max flow were used along with the fully open orifice area on the mainstage valve to estimate the discharge coefficient, c_d, in section 6.2. This is an approximate way of including the full flow path pressure drop in the simulation model, which relies on the orifice equation.

The mechanical design was completed in conjunction with the dynamic modeling to ensure that the prototype would have a design that demonstrates the expected efficiency benefit of the discrete piston approach and is also mechanically feasible to construct.

6.4 Conclusion

In this chapter, a design for a mechanically controlled discrete piston pump/motor was presented. The use of a mechanical control strategy has a number of advantages, such as a simpler, lower cost, and more robust control mechanism, a single control input that only requires hydraulic or mechanical power, repeatable valve timing, a more compact design, and minimal holding power. Several valve concepts were discussed, and a design based on a two degree of freedom pilot valve that drives three-way spool valves to control the individual pistons was selected. A dynamic model of the selected design was created, which showed that the valve could operate at the target speed of $1800RPM$, and predicted the overall efficiency of the device. Due to compressibility effects, the motor case was predicted to have significantly higher power loss, but a solution to this problem involving adding mechanical backlash to the drive train was described. This additional backlash was added to shift the valve timing in the motor case so that the mainstage valve would be crossing through its deadband as the piston is approaching TDC, allowing for some degree of precompression of the oil volume. Finally, the complete mechanical design of the discrete piston pump/motor was presented. The proposed design is capable of operating as a pump or a motor for either direction of rotation of the shaft, allowing it to be a full four-quadrant device. In the next chapter, the experimental tests performed on the prototype and their results are discussed.

Chapter 7

Experimental Results of a Discrete Piston Controlled Hydraulic Pump-Motor

In the previous chapter, a detailed design of a discrete piston controlled pump/motor based on the concept of a two degree of freedom control valve was described. Chapter 5 indicated that discrete piston control has the potential to significantly improve the efficiency of variable displacement pumps and motors, particularly at low displacements. The dynamic model presented in section 6.2 indicated that the proposed design should be capable of operating up to the design point of $1800RPM$, and it should demonstrate an efficiency of $> 90\%$ down to a displacement setting of about $s = 0.3$ for the pump case. While the baseline motor case was predicted to have a lower efficiency due to compressibility, with the use of a timing shift mechanism to achieve precompression (such as adding backlash), similar efficiency characteristics can be achieved in the motor case.

In this chapter, the experimental results of the prototype design described in the previous chapter are presented. The device was tested as both a pump and a motor, and the dynamic behavior and efficiency of the pump/motor were recorded.

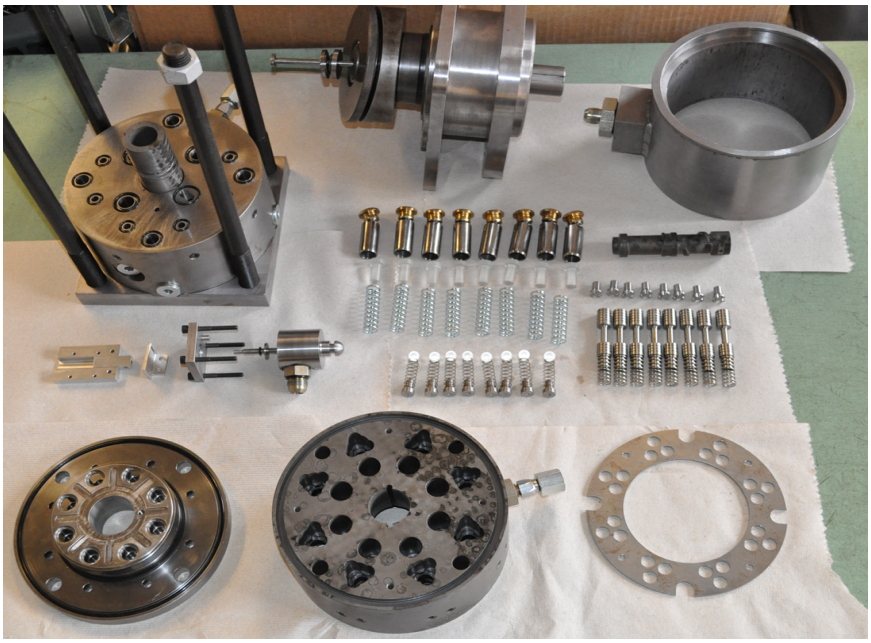

Figure 7.1: Manufactured parts used to build the discrete piston pump/motor

7.1 Experimental Results

The discrete piston pump/motor was manufactured according to the design described in the previous section. Figure 7.1 shows the individual components of the design prior to assembly. All manufactured parts were machined (not cast), and several of the parts were hardened using a nitrocarburizing process: the pilot spool, pilot sleeve, piston block, wobble plate, and shoe plate. Most of the housing components (i.e. piston block, top cap, back block, piston sleeve) were made from ductile iron, and the spools were made from mild steel. The front housing is shown at the top center of the picture, with the drive shaft, wobble plate, shoe plate, and bearings pressed together into an assembly. The design of this part of the pump/motor is described in [109].

The pump/motor was assembled and mounted on a test stand, as shown in Fig. 7.2. The test stand, which used many components from the design described in [108], has a $28cm^3$ closed-loop pump/motor that can be driven in either direction to drive or brake the Unit Under Test (UUT). In this case, the test stand pump/motor was smaller than the $48cm^3$ device being tested. This placed some restrictions on the pressure level

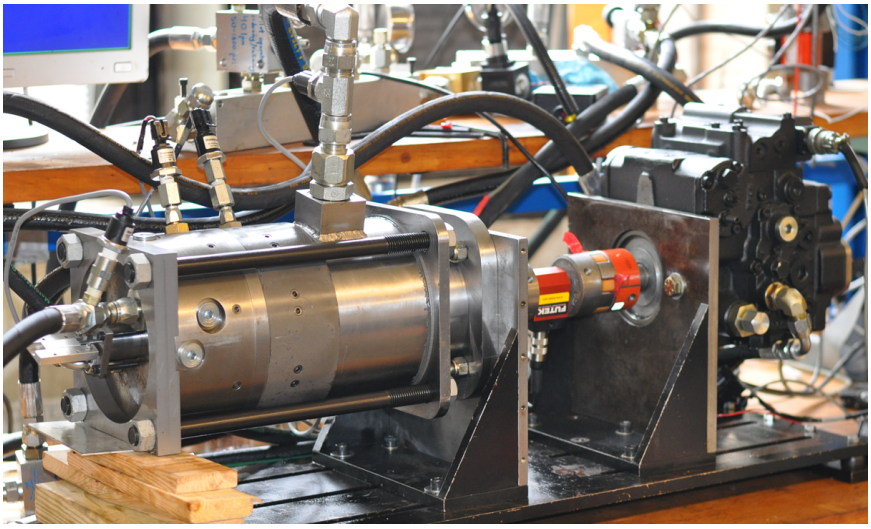

Figure 7.2: Discrete piston pump/motor installed on the test bench

that could be achieved during testing. Hydraulic power to the UUT and the drive pump/motor was supplied by a $20GPM$ power unit. The test stand was equipped with pressure, speed, torque, and flow meters which were sampled at a $1ms$ rate through a computer running Matlab XPC Target. The original design for the test stand called for the drive pump/motor and the UUT to be connected in a regenerative configuration, with the high-pressure pump output being used to help drive the motor, and the hydraulic power unit only needed to make up for the power losses in the system. However, the fact that the displacement of the UUT was larger than the drive pump/motor meant that this configuration would limit testing of the UUT to only about half of its total displacement. Thus, the stand had to be configured differently, with individual circuits for testing the motor and pump configurations of the device.

7.1.1 Motor Testing

The circuit used for testing the discrete piston motor is shown in Fig. 7.3. In this circuit, the hydraulic power unit is used to supply energy to drive the discrete piston motor, with a Pressure Reducing Valve (PRV) upstream of the motor used to set the desired test pressure. The exhaust flow from the motor was connected to the inlet of the test stand pump, which was used to brake the motor by pumping high pressure oil

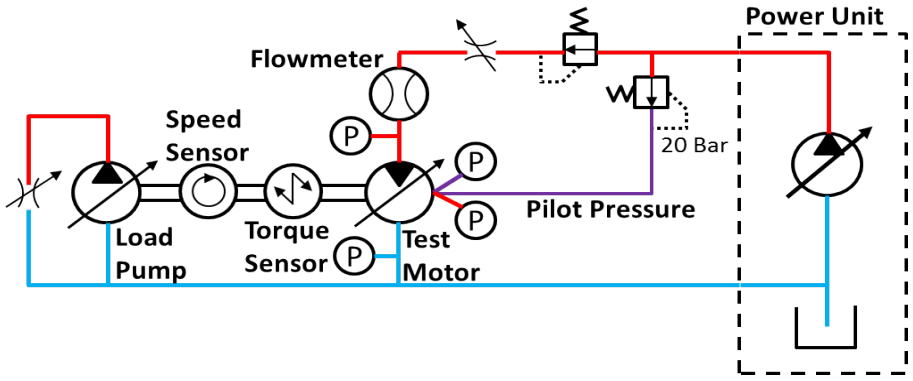

Figure 7.3: Schematic of hydraulic circuit for testing the discrete piston motor

across a needle valve. Since the displacement of the motor (UUT) was larger than the displacement of the pump, the outlet of the motor also needed to be connected to the return on the power unit. The hoses were connected in a way that the oil from the motor would primarily flow into the pump and then back to the power unit, as opposed to most of the motor flow returning to the power unit and oil circulating in a closed circuit through the pump. This was done to keep the temperature of the oil in the pump circuit at a reasonable level. The pilot pressure needed to drive the mainstage valves was also supplied via a PRV from the power unit supply, with a pressure setting of $20bar$. There were pressure sensors on the high pressure port and the low pressure port. There were also pressure sensors connected to one piston chamber and one pilot line associated with that piston. There was a flow meter on the motor input flow and a torque sensor and speed sensor on the shaft between the pump and motor. With these sensors, the hydraulic input power and the mechanical output power could be recorded.

The displacement of the motor was designed to be controlled via a hydraulic control valve that would supply fluid to push on the pilot push rod (see Fig. 6.32) and close the loop using a magnetic encoder mounted on the sensor mount plate. However, the seal used around the pilot push rod to seal the control pressure chamber added so much friction that the pilot spool could only spring return at a very slow speed. However, for efficiency mapping and pump/motor characterization, a displacement adjustment mechanism was not necessary (or desired). For the testing described in this chapter, the pilot push rod was positioned manually and then clamped.

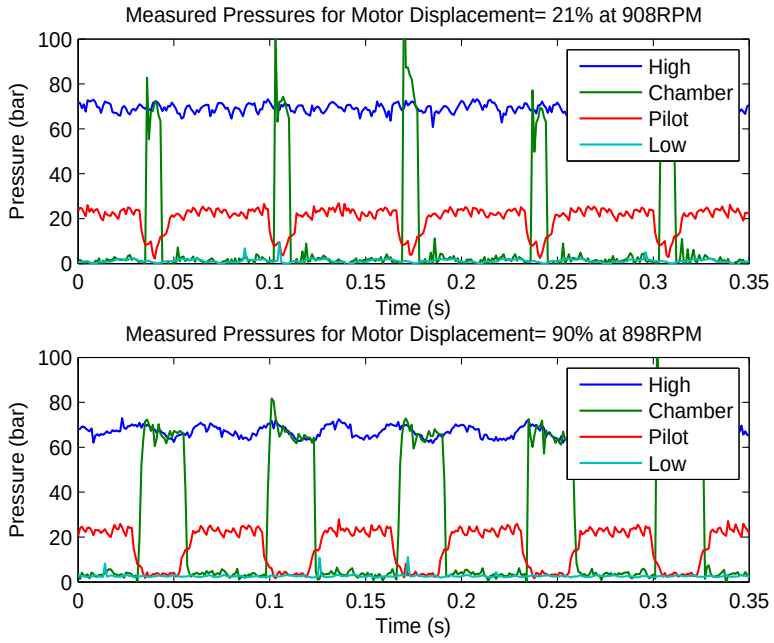

Figure 7.4: Pressure traces from a motor operating at two displacements

Figure 7.4 shows traces from the four pressure sensors with the motor operating at two different displacements and roughly $900RPM$. The operating principle of the motor is clearly shown, with the pressure in the pilot line between the pilot spool and the mainstage spool dropping, and then a short time later, the pressure in the chamber rising up to high pressure. The chamber pressure then falls after the pilot pressure starts to rise again, forcing the mainstage spool back to the low pressure position. The two displacement settings show the piston connected to high pressure for a varying fraction of the motor rotation, demonstrating the partial stroke disabling control.

The delay between the decrease in pilot pressure and the increase in the chamber pressure is a result of the transition time of the mainstage spool. This delay was measured as the time between the pilot pressure dropping below $15bar$ and the chamber pressure rising half way to the high pressure. Figure 7.5 shows a histogram of the time delays calculated using this method. This data was taken for a motor running between $30bar$ and $100bar$ and over a speed range of $500RPM$ to $1300RPM$, with 60 rotations taken at each pressure and speed point. The distribution appears roughly normal, with

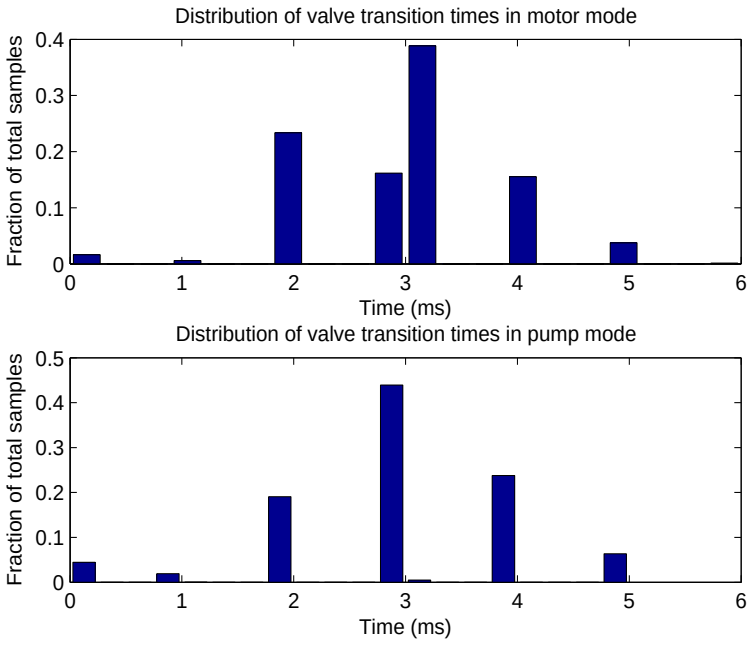

Figure 7.5: Histogram of mainstage spool transition times estimated from pressure traces

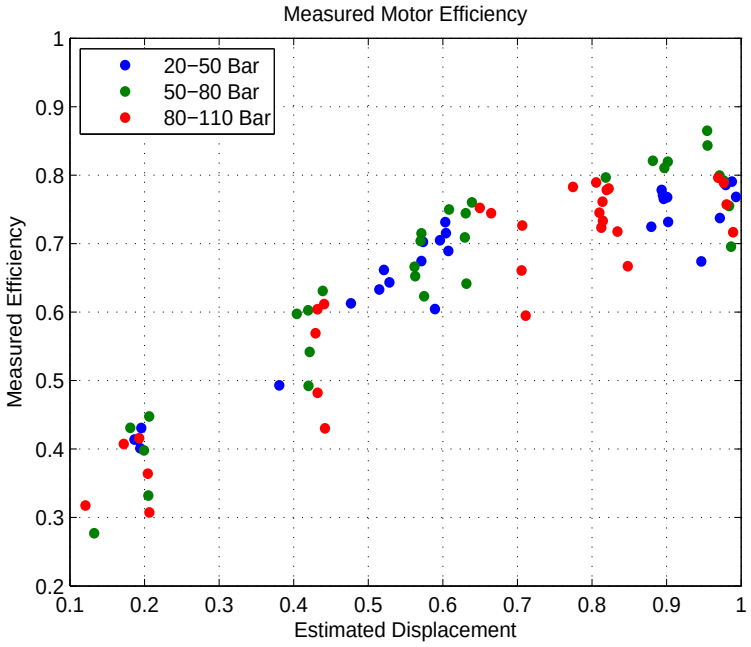

Figure 7.6: Measured efficiency of the discrete piston motor

a mean around $3ms$. This agrees with the transition time predicted by the dynamic model in Fig. 6.16 for the motor and Fig. 6.14 for the pump. Note that the actual transition time likely varied less than is shown in this figure since the method of using threshold crossings to estimate transition time introduced some variation into the data. This transition time should be sufficient to allow the pump/motor to operate effectively up to at least $1800RPM$, as was simulated in section 6.2.

With the input hydraulic power measured by the pressure sensor and flow meter, and the output mechanical power measured using the shaft speed and torque sensors, the overall efficiency of the device was computed. The result is shown in Fig. 7.6. This plot shows the efficiency as a function of estimated displacement fraction, which is computed from the width of the piston chamber pressure pulse and the mainstage valve transition delay:

$$D_{est} = \frac{1}{2}\left(\cos\left(t_{delay}\omega\right) - \cos\left(t_{high}\omega + t_{delay}\omega\right)\right) \tag{7.1}$$

where t_{high} is the time that the chamber pressure is at high pressure, ω is the motor shaft angular velocity, and $t_{delay} = 0.003s$ is the estimated time delay to open or close

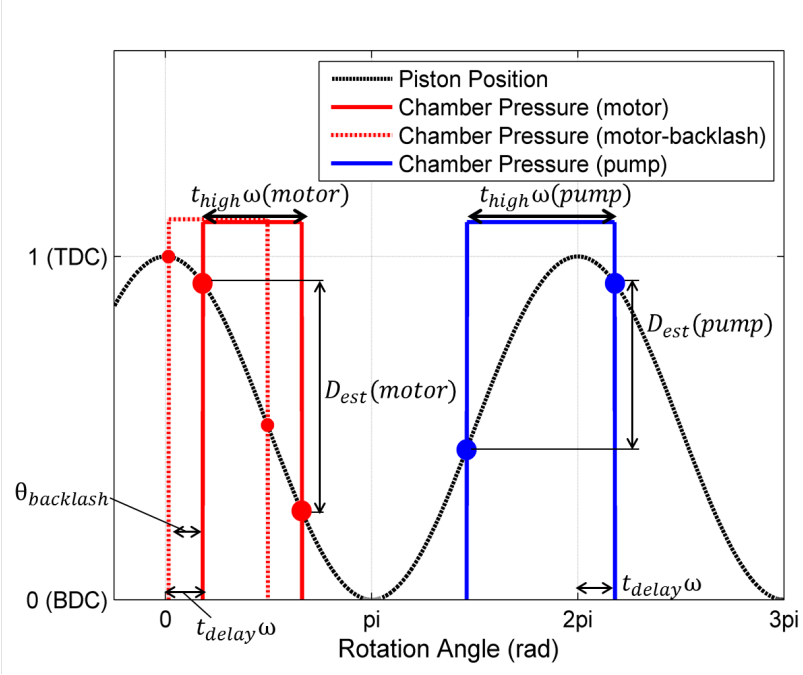

Figure 7.7: Displacement estimation method for the motor, motor with backlash timing adjustment, and pump cases

the mainstage spool. The time delay due to the mainstage valve transition needs to be included because, due to the sinusoidal trajectory of the piston, the distance the piston travels in a given time, t_{high}, will vary depending on where in the trajectory the high pressure period falls. t_{high} is determined by measuring the time that the pressure is above a threshold value during each pump rotation. Figure 7.7 depicts the displacement estimation method for the motor (Eq. (7.1)), motor with backlash (Eq. (7.2)), and the pump (Eq. (7.3)).

For each data point in Fig. 7.6, the measured values are averaged over 60 pump rotations. This method of estimating the motor displacement was used instead of measuring the position of the pilot push rod for two reasons. The first was that, despite being clamped in place, in a few of the tests, the pilot push rod appeared to move over time as a result of vibrations on the motor. Second, the delay time of $3ms$ resulted in a delay angle that varied with the rotational speed, which changed the effective displacement. This variation with motor speed could easily be compensated for with closed loop

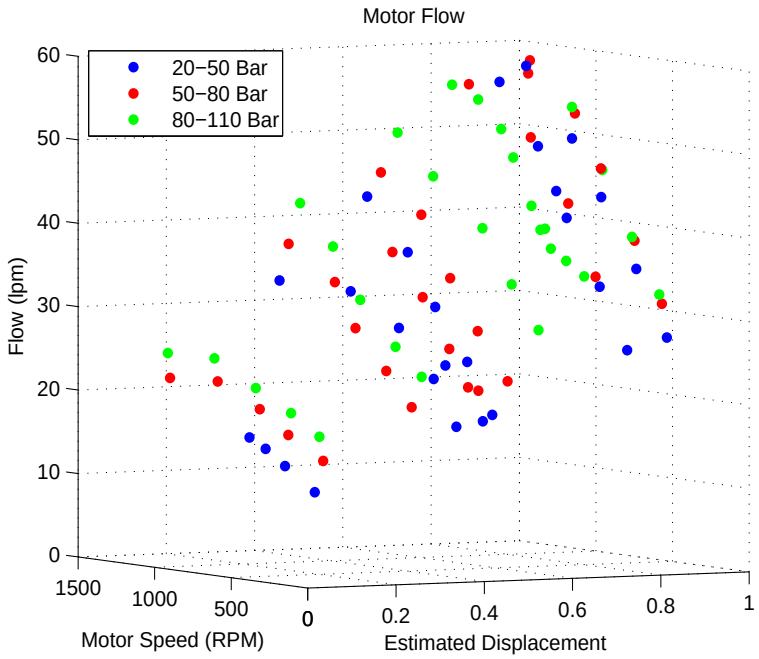

Figure 7.8: Measured motor flow as a function of speed and displacement

control of the pilot spool position.

The efficiency measurements were taken with the motor operating at 5 different nominal pilot spool positions, speeds of 500, 700, 900, 1100, and 1300RPM, and pressures of about 35, 70, and 100bar. The measured efficiency reached a maximum of about 80% at full displacement, and then dropped down to around 40% at 20% displacement. While not terrible, this efficiency is considerably lower than was predicted in section 6.2. The primary reason for this is much higher than expected leakage.

Figure 7.8 shows the overall motor flow as a function of speed and estimated displacement, with the data separated into three groups by inlet pressure. As expected, the flow through the motor increases as both the displacement and speed increase. However, less expected was the fact that the flow into the motor also noticeably increases with the inlet pressure. While this is difficult to see in the two dimensional figure, the effect is clear in the group of points at the lower left of Fig. 7.8. These fourteen points were all taken at the same displacement, and it is clear that there is an increase in flow with increasing supply pressure. This indicates a significant amount of internal leakage

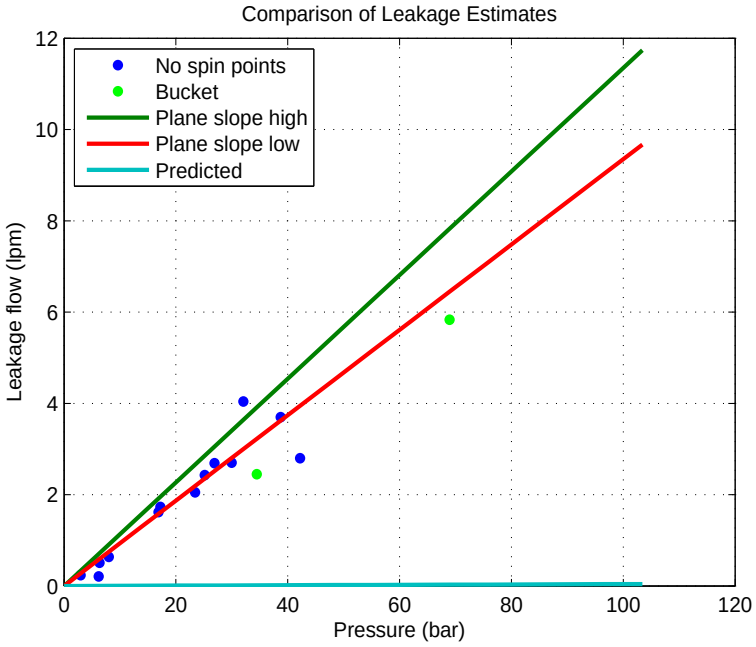

Figure 7.9: Estimated motor leakage using several methods

through the motor.

The amount of leakage was estimated in several ways. One method was to fit the flow data shown in Fig. 7.8 to a plane in pressure and speed for each nominal setting of the pilot spool position. As mentioned above, in several of the tests, the pilot spool seemed to move through the test, so the quality of the plane fit for those tests was low. However, for two of the pilot spool settings, the data fit well to the plane. The slope of these planes with respect to pressure was used to estimate the leakage. The slopes for the two data sets were $0.0935 lpm/bar$ and $0.1135 lpm/bar$. Figure 7.9 shows these two slopes as lines labeled Plane Slope High and Plane Slope Low. This plot also shows leakage estimated by directly measuring the flow when the motor was not spinning. By setting the pilot spool in the middle of its travel, the mainstage valves were all held open to low pressure, and the motor did not spin, which should have resulted in zero flow. However, significant flow was measured in this case. The last method for estimating the leakage, labeled Bucket in Fig. 7.9, was to allow the tank line to flow into a bucket and measure the volume of oil over time. One thing to note with this

Figure 7.10: Picture of two mainstage spools after testing

last method is that it was done when the oil was cool, relative to the other leakage tests. This may explain why the bucket method estimated slightly lower leakage than the other tests. The No Spin data points seemed to agree well with the Plane Slope Low estimate, with both tests run at typical testing temperature. The Plane Slope Low method was used to estimate the leakage flow. Note that the figure also shows the amount of leakage that was estimated around the mainstage valves by the leakage equation and the best case designed clearance between the spools and bores of $8\mu m$. Note that for the prototype manufacturing, the clearance was allowed to be larger than that, but in a proper production environment, the clearance could probably be even tighter.

There are several possible leak paths through the pump motor, with around the mainstage spools, around the pistons, and through the check valve seat being the most likely. Of these, leakage around the mainstage spools was likely to be the largest. Figure 7.11 depicts some of the possible leakage paths around the pistons and valves. The pistons were made by a hydraulic pump manufacturer, and were measured to be within the specified dimensions. The nominal diametral clearance on the pistons was $15.5 \pm 10\mu m$, with a relatively long sealing length. The pistons ran smoothly in their bores, but they did not feel like they had much clearance. The polycarbonate check

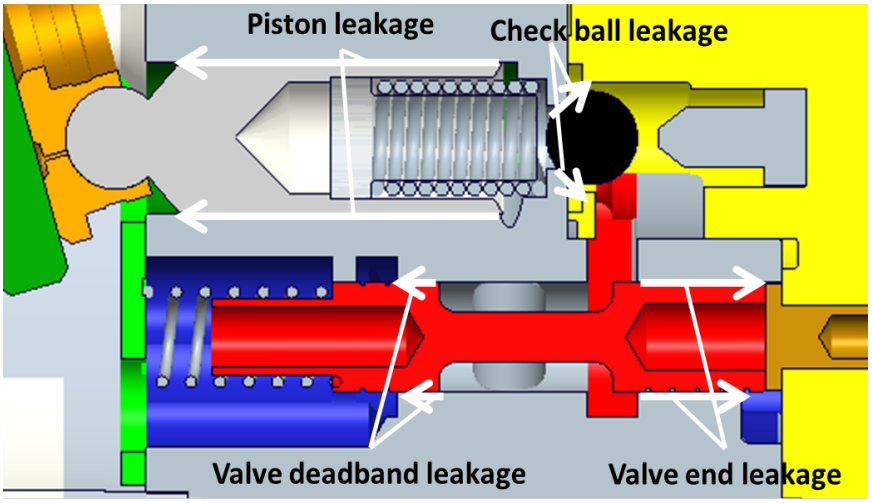

Figure 7.11: Potential leakage paths around the piston, mainstage valve, and check valve

balls, while they did show some marks after the pump/motor was disassembled, were also not likely to be a significant source of leakage in the motor case, as they should have remained pressed against their seats by high pressure. On the other hand, the mainstage spools showed evidence of being significantly undersized and a likely cause of the high leakage. On the drawing, the clearance on the mainstage spools/bores was $28 - 50\mu m$. However, the nitrocarburizing process used to harden the piston block was expected to contribute $5 - 10\mu m$ of growth to the bores, resulting in a clearance of $8 - 40\mu m$. While this amount of variation was not ideal, it was considered an acceptable range for prototype parts. Unfortunately, the hardening process did not appear to add any thickness to the parts, resulting in an additional $10 - 20\mu m$ clearance over the design. This also affected the pistons bores. In addition, the mainstage spools were measured to be at the very bottom of the drawing specification, resulting in a clearance of $50\mu m$ on the spools before they were run. Finally, the spools appeared to experience significant wear in use. Figure 7.10 shows two of the spools after the testing was complete. In this picture, there is clear evidence of wear on the land on the left side, which is the land that seals off the high pressure rail. This wear region was about $5mm$ wide, which is the amount that the land travels into the bore in operation. The measured diameter in this

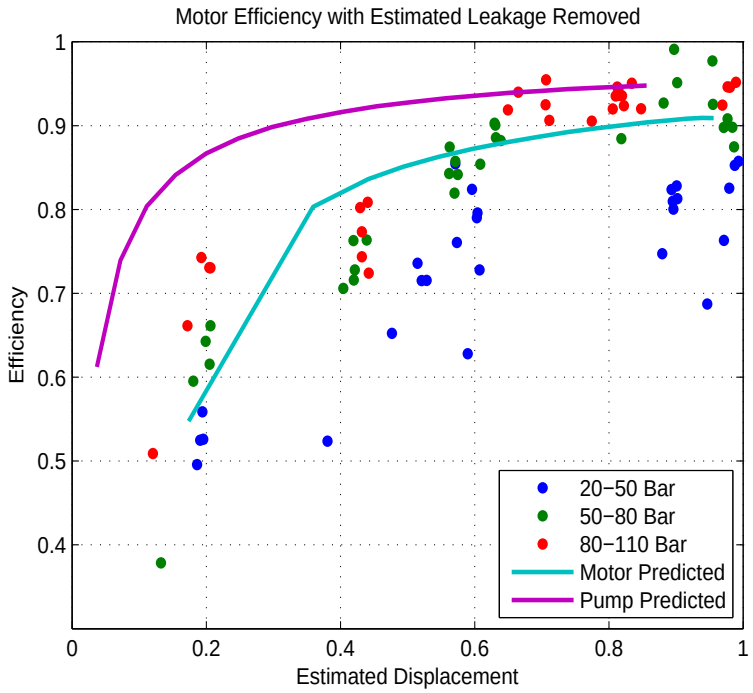

Figure 7.12: Efficiency of the discrete piston motor when the estimated leakage is removed. Estimated pump and motor efficiencies at $200bar$ are also shown.

region was $20 - 30\mu m$ smaller than the non-worn parts. Thus, the clearance on some of the spools could have been as high as $80\mu m$. Since the leakage equation (Eq. (6.28)) shows that the leakage flow is proportional to the clearance cubed, an increase from $8\mu m$ to $80\mu m$ should result in a 1000-fold increase in leakage. It should be noted that the two spools shown in Fig. 7.10 had the most obvious evidence of wear; other spools had wear marks, but not nearly as significant. The spools were not hardened, and it is likely that burrs in the bores on the edge of the high pressure rail wore some of the spools in operation.

Using the Plane Slope Low method shown in Fig. 7.9, the leakage could be estimated for a given pressure. If that leakage flow is subtracted from the measured input flow, then the efficiency of the motor without leakage can be estimated, which is shown in Fig. 7.12. This plot also includes estimates of the power lost to pilot spool leakage, about $5W$, and the mainstage actuation power, about $0.7J$ per switch. In this figure,

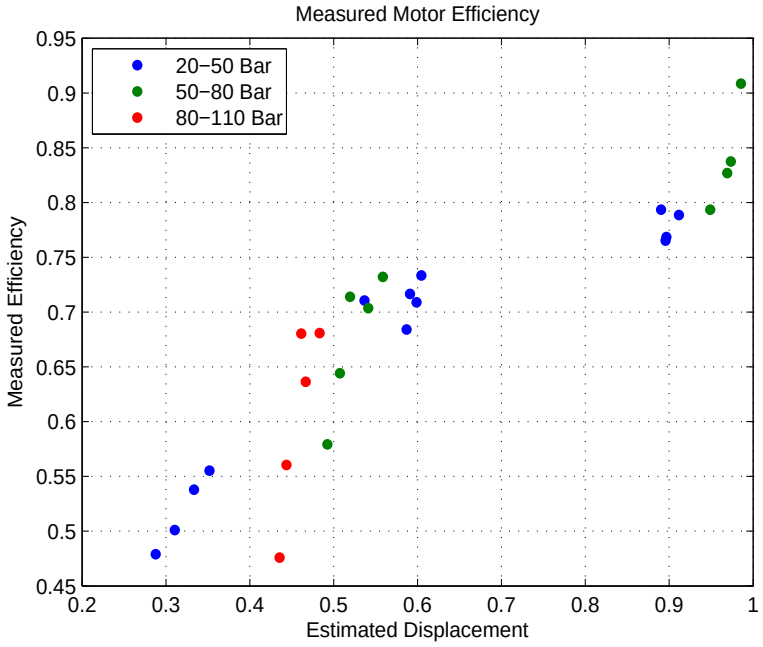

Figure 7.13: Measured efficiency of the discrete piston motor with a timing adjustment on the pilot spool

the efficiency is above 90% down to about 60% displacement, and then drops down to about 60% efficiency at 20% displacement.

Figure 7.12 also includes the pump and motor efficiency predicted in section 6.2.1 and shown in Fig. 6.21, which shows the predicted efficiency for the pump and motor without backlash cases. Since the simulations were run at $200bar$, the highest pressure experimental data points, shown in red, are the best points for comparison. The estimated experimental efficiency with the leakage removed is similar to the predicted motor efficiency, with the high pressure points falling slightly above the prediction at high and low displacements, and slightly below the prediction for mid-range displacements. Since the uncertainty of the leakage estimation is high, it is difficult to draw firm conclusions from this data. However, the experimental data does fall in a similar range as the predicted efficiency.

Figure 7.13 shows the measured efficiency for a motor with the timing of the pilot spool adjusted to simulate the pre-compression backlash described in section 6.2.2. In

order to simulate the backlash, the shaft driving the pilot spool was rotated so that the pilot spool transition lead TDC on the wobble plate by about 30°. The method for estimating the displacement fraction takes this timing adjustment into account:

$$D_{est} = \frac{1}{2}\left(\cos\left(t_{delay}\omega - \theta_{backlash}\right) - \cos\left(t_{high}\omega + t_{delay}\omega - \theta_{backlash}\right)\right) \tag{7.2}$$

where $\theta_{backlash} = 30°$ is the motor timing adjustment.

One challenge with the pre-compression setting was that, at lower displacements, when the motor was not spinning, the pistons acted as a pump nearly as much as a motor, which made it difficult to start the rotation. In a controlled system, this could be overcome by using a high displacement to start spinning, and then backing off to a lower displacement when in motion. However, this was difficult to accomplish with a fixed pilot spool position. Thus, only higher displacements could be tested. Figure 7.13 shows the measured efficiency, which can be compared with the no-backlash measured efficiency in Fig. 7.6. The measured efficiency with the timing adjustment is slightly above the measured efficiency without the timing adjustment.

Figure 7.14 shows the efficiency of the motor with a timing adjustment with the estimated leakage removed. The internal leakage was estimated using the same method as for the motor without the timing adjustment, and also includes an estimate of the pilot leakage ($5W$) and actuation power ($0.7J$ per switch) losses. The figure also shows the pump and motor efficiencies predicted in section 6.2.2 for a motor with backlash and shown in Fig. 6.25. The highest pressure experimental points, shown in red, are the most useful for comparison with the simulation results, which were generated for a system operating at $200bar$. The high pressure points clustered around 45% displacement are slightly lower than the predicted efficiency, but when compared with Fig. 7.12, the efficiency is about 10% higher for the motor with a timing adjustment. For the lower pressure points, there is also an efficiency improvement in the timing adjusted case, although it is closer to a 5% improvement. Despite the uncertainty present in the leakage and displacement estimations, these results indicate that the timing adjustment is beneficial for improving the motor efficiency.

One difference between the simulation and the experiment is that pressure drop in the hoses between the motor outlet and the reservoir could cause the tank pressure to be slightly elevated above atmospheric pressure. Since the low pressure sensor measured

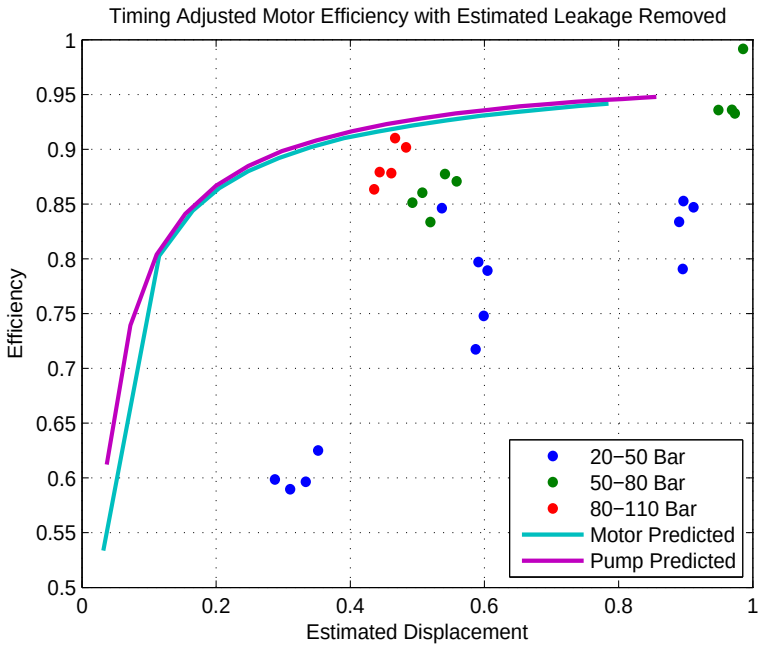

Figure 7.14: Efficiency of the discrete piston motor with a timing adjustment on the pilot spool and the estimated leakage removed

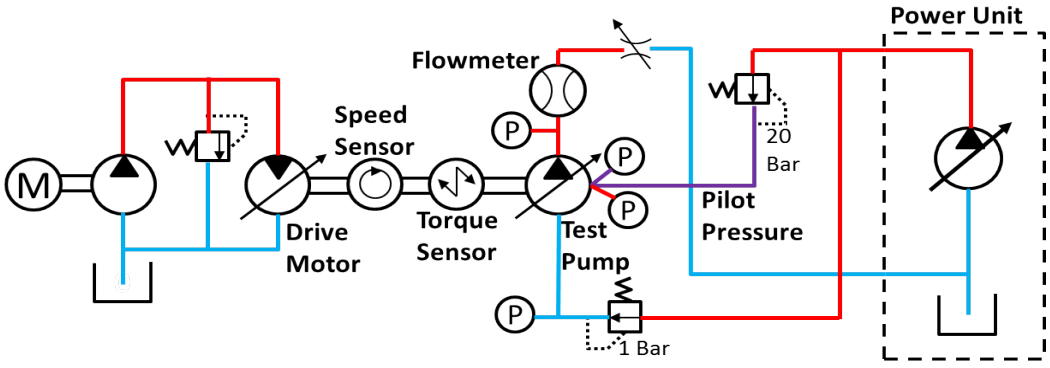

Figure 7.15: Schematic of hydraulic circuit for testing the discrete piston pump

about $2bar$ gauge pressure, this is likely. Since the oil is most compressible at low pressure, a significant amount of the energy loss in compressing the oil occurs when raising the oil volume pressure from atmospheric pressure to a slightly elevated pressure. By raising the pressure of the tank line, it is possible that some of the compressibility loss was avoided. If the inlet pressure had been kept closer to atmospheric pressure, the improvement provided by the timing adjustment may have been even more apparent.

7.1.2 Pump Testing

Figure 7.15 shows the hydraulic circuit used to test the discrete piston pump. In this configuration, the discrete piston pump and the load motor were driven by two separate hydraulic circuits. This was done because the hydraulic power unit did not have enough flow to supply both units running faster than about $1000RPM$. They could also not be connected in series because, due to the displacement mismatch, the inlet pressure to the motor needed to be higher than the outlet of the pump. The discrete piston pump also needed to have a low pressure supplied to it due to the design of the shaft seal, which limited some of the possible configurations. With this circuit, the power unit was used to supply pilot pressure and a low pressure, roughly $1bar$, inlet supply to the pump. The power unit did not have a low pressure port designed to directly supply oil to the suction inlet of a pump, so the high pressure outlet had to be reduced down to the pump inlet pressure.

The pressure traces for the discrete piston pump are shown in Fig. 7.16. This figure

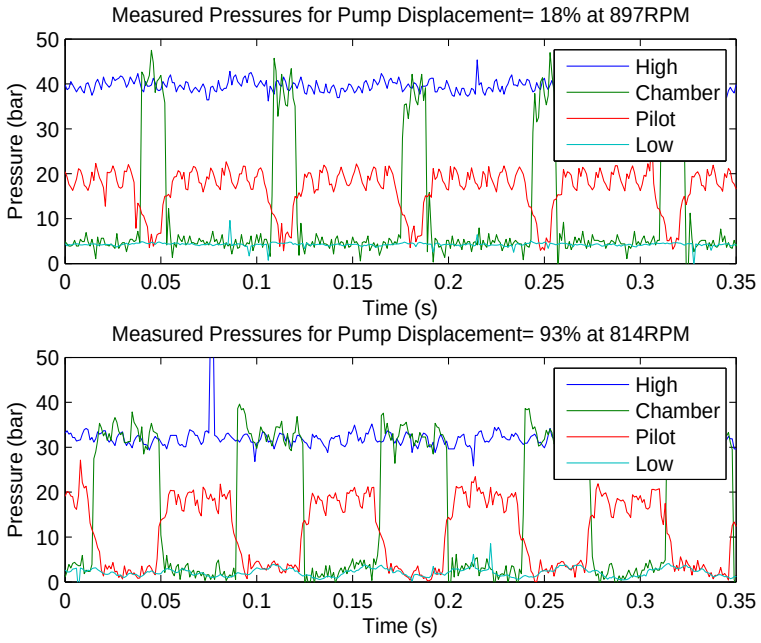

Figure 7.16: Pressure traces from a pump operating at two displacements

is nearly identical to Fig. 7.4 for the motor case, except the high pressure is at a lower level. One other subtle difference is that, in this figure, the slope of the pilot pressure decreasing appears to be slightly shallower than the slope of the pilot pressure increasing, whereas in the motor case, these slopes appear reversed. This difference in slopes can be explained by the shape of the lands on the pilot spool. As can be seen in Fig. 6.11, in the motor case, the power stroke starts at TDC with a straight land uncovering the connection to the mainstage spool, and the power stroke ends at a variable part of the rotation with an angled land covering the mainstage connection. The area profile of a circle being uncovered by an angled land is shallower than it is with a straight land. In the pump case, the power stroke starts with the angled land and ends with the straight land. Despite this difference, Fig. 7.5 shows that the mainstage transition delay is essentially identical for pump and motor.

The measured efficiency for the pump is shown in Fig. 7.17. The efficiency is shown as a function of estimated displacement fraction, which is calculated in a similar way to

the motor case:

$$D_{est} = \frac{1}{2}\left(\cos\left(2\pi + t_{delay}\omega\right) - \cos\left(2\pi - t_{high}\omega + t_{delay}\omega\right)\right) \tag{7.3}$$

Since the pilot spool was timed so that TDC corresponded with the end of the active region on the pilot valve, the t_{delay} of about $3ms$ caused the piston chamber to remain at high pressure after passing TDC. Thus, at high speeds where the time delay had the largest effect, a significant fraction of the high pressure stroke was spent as a motor. For example, the lowest effective displacement point of 0.1277 for a pump at $1140RPM$, the total angle spent at high pressure was $1.22rad$, and the delay angle was $0.36rad$, meaning that the ratio of stroke spent as a motor to the stroke spent as a pump was 0.18. Note that the pressures achieved in the pump case are lower than in the motor case; with such high leakage it was difficult to generate enough flow to build a high pressure, especially at the lower displacements. The smaller displacement of the load motor also limited the pressure range that was achievable at high displacement settings on the pump. As a result, only the mid-range displacements have test results at reasonably high pressures.

In Fig. 7.17, the measured efficiency for the pump is significantly lower than in the motor case. This could be due to higher mechanical friction, or even higher leakage than the motor case. In the pump case, the no load torque can be directly measured, unlike in the motor case. Figure 7.18 shows the power used to spin the unloaded pump, with four experimentally measured points and a best-fit curve. This loss includes the bearing friction, churning loss, and throttling loss through the valves. When compared with the input power, which ranged up to about $2.5kW$ at the higher speeds, this torque loss is fairly low. The torque loss will increase as pressure is applied, due to the increased friction on the slippers and pistons, but those losses should also exist in the motor. Note that the fact that the transition delay causes part of the pressure stroke to extend into the motoring region will add some additional frictional losses, which will also contribute to the lower efficiency in the pump case.

In theory, the leakage in the pump case should be the same as in the motor case. The no-spin points shown in Fig. 7.9 were taken with the pilot spool in the center of its travel, which is in between the pump and motor configurations. Using the method of fitting the output flow data to a plane and using the slope to estimate the leakage

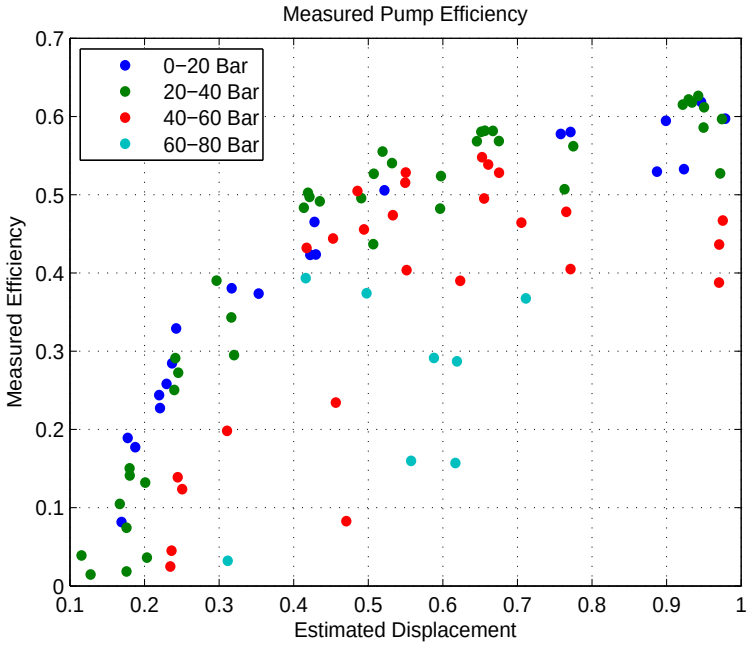

Figure 7.17: Measured efficiency of the discrete piston pump

yielded a variety of leakage estimates. A different plane was fit for each pilot spool position setting, and some of the estimates were higher than in the motor case, and some were lower. Figure 7.19 shows the estimated efficiency if the same coefficient used in the motor case ($0.0935 lpm/bar$) is used to estimate the leakage flow, which is added to the output flow in the pump case.

In this figure, the pump efficiency is increased up to about 65% for a wide range of displacements. Adding the estimated leakage did not have a large effect on the high displacement points since they are at relatively low pressures, and thus had lower estimated leakage. In the mid-range displacements, adding the estimated leakage brought efficiency of the high pressure points up above that of the low-pressure points. It is possible that some of the mismatch in efficiencies between the pump and motor case is due to the overall lower pressure level in the pump case, which makes the no-load losses more significant.

By adding the estimated leakage to the pump output flow, the majority the volumetric losses are removed from the efficiency calculation, leaving the mechanical losses.

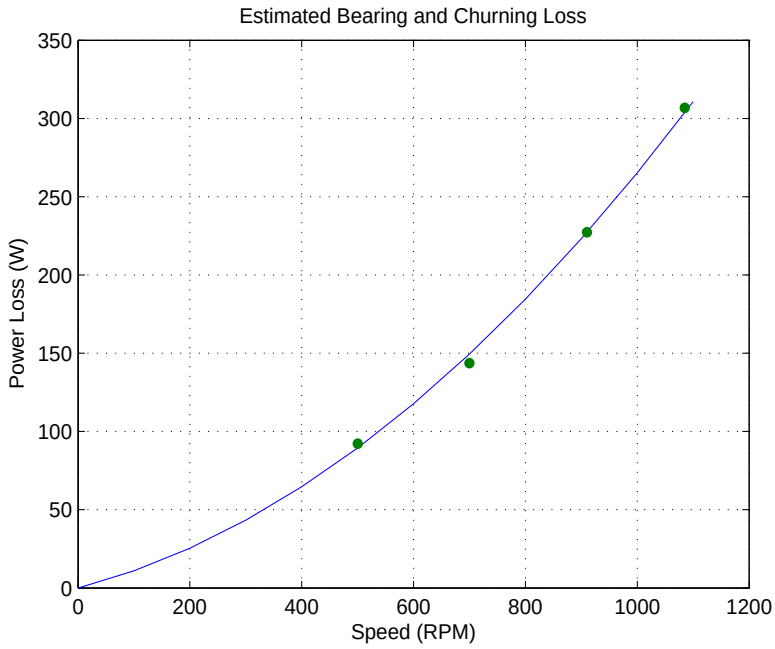

Figure 7.18: Unloaded mechanical power input in the pump case

The compressibility losses are still present in the estimate, but those should be small in the pump case. By computing the difference between the mechanical input power and the hydraulic output power with the estimated leakage added, the mechanical power loss can be estimated. This is shown in Fig. 7.20(a), along with the no-load power loss depicted in Fig. 7.18. In this figure, most of the low pressure points (blue) and many of the medium pressure points (green) have an estimated mechanical loss that is only slightly above the no-load loss. This makes sense, as the additional mechanical losses due to the loading of the pistons should be low in the low-pressure tests. The higher pressure points in Fig. 7.20(a) are scattered and significantly higher than the no-load power loss. This indicates that either the mechanical losses due to higher pressure on the piston are significant, or that the leakage was under estimated at higher pressures, resulting in some volumetric losses remaining in Fig. 7.20(a).

In Fig. 7.20(b), a similar analysis is done for the motor, with the mechanical power output compared to the hydraulic power input with the leakage removed. This figure also includes the no-load mechanical loss depicted in Fig. 7.18. When compared with

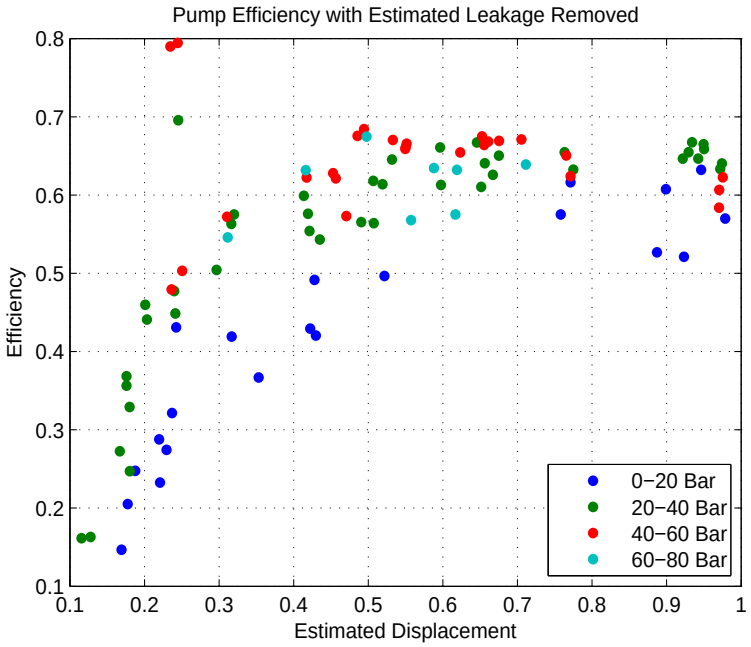

Figure 7.19: Efficiency of the discrete piston pump when the estimated leakage is removed

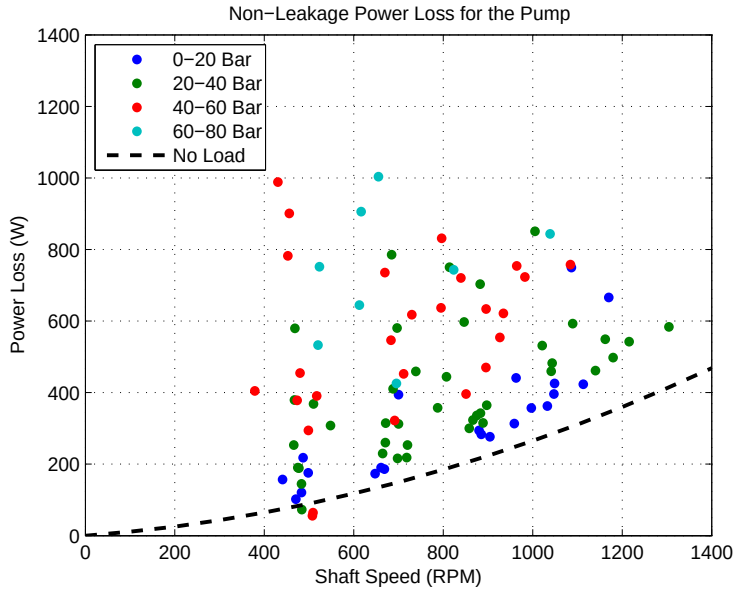

(a) Estimated mechanical loss in the pump

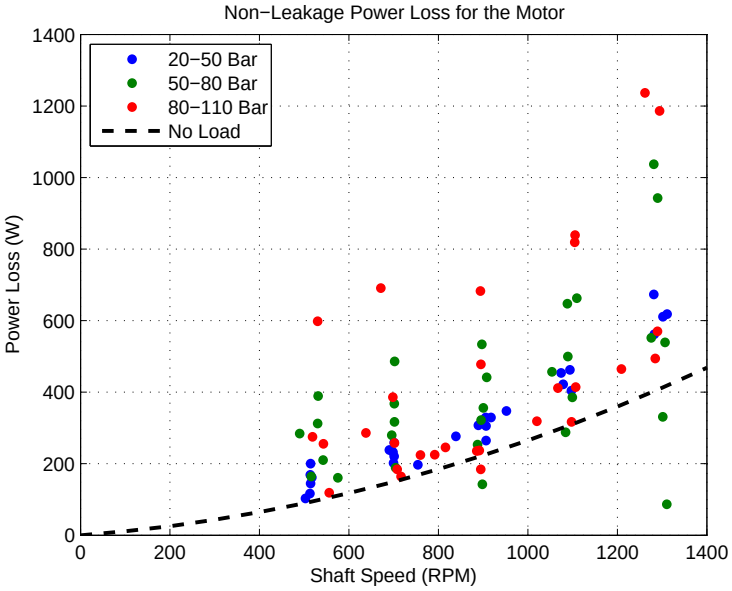

(b) Estimated mechanical loss in the motor

Figure 7.20: Non-leakage power losses estimated from the difference between the mechanical power and the hydraulic power compensated with the estimated leakage

the motor data, it is clear that many of the test points have a higher power loss that is not included in the estimated leakage. Since the mechanical friction caused by high pressure being applied to the pistons should be similar between the pump and motor cases, and many of the motor test points were run at higher pressure than the pump case, this suggests that the leakage in the pump case is higher than in the motor case.

There are several possible reasons that the leakage could be higher in the pump case than in the motor case: first, the pump testing was conducted after the motor testing. To the extent that the leakage was exacerbated by wear on the spools, it is possible that the clearances were larger for the pump testing than the motor testing. In the pump case, the check valves could open and close as pressure built in the piston chambers; it is possible that the check valves did not always seat properly or got damaged as they opened and closed. After testing, some of the check balls did show some marks on their surfaces, but it was not clear that they were damaged enough to cause additional leakage. Another possibility is that some of the additional loss occurred as the mainstage valve was transitioning through its deadband while the piston was moving at high speed. In the motor case, this transition occurs as the piston is retracting, which should tend to extract compressed energy from the fluid or draw a small vacuum in the piston chamber. In the pump case, the piston will be pumping against a blocked volume until the mainstage valve or the check valve opens. During this time, the piston chamber could experience additional leakage. However, the duration of this event is short, roughly $3ms$, so the amount of leakage would likely not be high.

The experimental results described in this section showed the operation of the discrete piston pump/motor, and demonstrated efficiencies that were fairly flat over a wide range of displacements. Unfortunately, the high amount of leakage in the prototype obscured some of the efficiency benefits of the discrete piston approach. Attempts were made to estimate the leakage, and use that to predict the efficiency in a low-leakage device, which showed good potential.

7.2 Conclusion

In this chapter, experimental results showing the operation of the discrete piston pump/motor in both pump and motor mode were described, along with measured efficiency

in both cases. While the efficiency remained fairly flat down to low displacements, the overall efficiency was degraded by high leakage in the device. The high leakage was due to larger than desired clearances in the prototype parts, and several methods were used to estimate and remove the leakage from the efficiency map. With the estimated leakage removed, the efficiency of the device was very high. However, there is some uncertainty in determining the best way to estimate the leakage in the pump case. Tests of the backlash timing indicated that adjusting the pilot spool timing to allow for some pre-compression of the piston chamber volume in the motor case resulted in a $5 - 10\%$ efficiency improvement.

After testing the prototype discrete piston pump/motor, a number of opportunities for improving the design were revealed. The first improvement is to harden the main-stage spools and reduce the clearance between the spools and bores. The leakage that occurred in the prototype due to loose clearances and worn spools resulted in much lower efficiencies than are possible with the design. Another feature that should be changed to improve the assembly of the device is the pilot spool drive shaft. In Fig. 6.34, the drive shaft is shown passing through a bearing assembly that holds the pilot spool spring and allows it to rotate with the pilot spool. However, the triangular drive on the end of the shaft was too large to fit through the bearing assembly, requiring the bearing assembly to be installed on the drive shaft prior to the wobble plate being pressed on to the main shaft. The design intent was for the front housing, shaft, and wobble plate assembly to be placed on top of the rest of the device and bolted together, but the presence of the bearing assembly around the pilot drive shaft forced a difficult installation of the bearing assembly into the piston block with very little clearance between parts. This could be remedied by a change to the pilot drive shaft or the pilot spring bearing assembly. The operation of the displacement control mechanism could also be improved. In the prototype, the seal friction was too high, and the pilot return spring was barely able to de-stroke the pilot spool. A change to the seal or the pilot spring could improve this. Alternatively, using a sensing method that could be immersed in oil, such as an lvdt, could remove the need for a dynamic seal entirely.

There are also larger changes that could be made to the design to improve the performance or efficiency. Changing the mainstage valve from a spool type to a poppet type valve could greatly reduce the leakage. Some designs for this approach are shown

in section 6.1. The trick is to achieve a design that is closed-center but also has poppet sealing. Changing from a wobble plate to a radial piston design would be a drastic change, but it should reduce the friction loss on the slippers by reducing the relative speed between the slipper and the cam. This is the approach taken in [59]. In this prototype, the oil volume around the wobble plate needed to be maintained at a low pressure to protect the seal on the main shaft from being damaged. Changing the design of the tank flow path to include a separate case drain port would allow the device to be used with an elevated tank pressure since the shaft seal could be isolated from the higher pressure. Finally, adding soft stops to the ends of the mainstage pistons could help reduce the noise caused by the spools hitting their endstops at high speeds.

Despite the list of improvements to be made, the tested design shows the potential of the discrete piston control approach for improving the efficiency of hydraulic pumps and motors at low displacements. Future development of this concept could include reducing the power loss mechanisms, such as leakage, simplifying the design by reducing parts and size, and finding ways to mitigate the flow ripple and noise associated with using on/off valves to control individual pistons.

Chapter 8

Conclusion

In this thesis, the use of on/off valves to create efficient hydraulic systems was investigated. On/off valves can be used in numerous configurations to create systems that avoid valve throttling losses or reduce hydraulic component losses, several of which were discussed in this thesis. In the first chapter, the Virtually Variable Displacement Pump (VVDP) circuit was studied, which uses an on/off valve to periodically unload excess flow from a fixed displacement pump to create a variable flow device. In contrast to conventional bleed-off circuits, the flow in a VVDP is unloaded at low pressure, minimizing the energy loss. Experimental results from a small test circuit showed that on/off control can dramatically reduce the power losses when compared with a throttling valve controlled circuit. For example, at 50% of the full flow, the throttling valve power loss of $230W$ was reduced to $110W$ in a system operating at $10Hz$, and it was further reduced to $40W$ in an on/off system at $2.5Hz$. However, the periodic switching creates a discontinuous power flow, resulting in a ripple on the output and requiring an accumulator to provide flow and pressure smoothing. The dynamics of the accumulator affect the response of the system, and a trade off exists between the size of the ripple and the responsiveness of the system. This trade off can be improved by increasing the switching frequency of the on/off valve. However, due to power losses that occur every cycle, such as transition throttling, compressibility, and actuation power, increasing the switching frequency can reduce the efficiency of the system. Experimental results from a system switching at frequencies up to $10Hz$ demonstrated that the frequency dependent losses can quickly become the dominant power loss in the system as the switching

frequency increases.

Chapter 3 presented the concept of soft switching, which can significantly reduce the frequency dependent power losses described in chapter 2. The soft switching concept uses a check valve to bypass a transitioning high pressure orifice, and a soft switch chamber to bypass a transitioning low pressure orifice. The soft switch chamber is a small chamber with a piston and a spring that can temporarily absorb oil while the valve is in transition. The stored oil is then released at low pressure once the valve is fully open. In order to eliminate losses in all four of the valve transitions, an active locking mechanism is needed that can release the soft switch piston at the correct time to enable the absorption of oil. While the final design of this locking mechanism was not defined in this thesis, several potential approaches for creating it were described. Another concept for creating the locking mechanism is discussed in [30]. In simulation results, the soft switching approach eliminated 81% of the transition losses, which reduced the overal power loss in the system studied by 64%. This enables higher efficiency systems to be created without requiring fast valves to minimize transition losses. While the softswitching concept was described in the context of a VVDP, it could be applied to other on/off valve configurations, such as a Virtually Variable Displacement Motor or a switching transformer.

One frequency dependent loss mechanism that was not quantified in chapter 2 but can cause substantial power losses, is the power needed to actuate the on/off valve. This is due to the fact that, in conventional poppet and spool valves, the valve element moves linearly and must be accelerated for every switch. As the switching frequency increases, the actuation power needed to accelerate the valve element increases with a cubic relationship. To avoid this problem, a two degree of freedom valve that can rotate and translate was designed. This valve was described in chapter 4 as the switching element in both a VVDP and a Virtually Variable Displacement Pump/Motor (VVDPM). The power loss mechanisms for the valve, such as full-open throttling, transition throttling, leakage, compressibility, and actuation power, were modeled and the design of the valve was formulated as a constrained energy loss minimization problem. Design constraints, such as limits on the physical parameters and a lower bound on the switching frequency, were applied to ensure that the valve was feasible to manufacture and could perform as desired. Two different approaches for actuating the valve were compared: one method

used the fluid momentum to spin the spool, and the other used an external actuation source. While the self-spinning approach has a number of packaging benefits, the optimization results indicated that the design constraints required to achieve self-spinning caused significantly higher power losses in the valve. The VVDP valve is a 3-section 3-way valve that was optimized at a constant pressure and flow. The VVDPM valve is a 4-section valve that either connects the two ports of a pump/motor to supply and tank, or it connects them to each other. The optimization of this valve was done over a specific duty cycle, with both a uniform grid of pressure and flow points and an application specific duty cycle applied as examples. The VVDPM application example was the wheel motor of a Hydraulic Hybrid Passenger Vehicle.

In the final three chapters, a different approach to using on/off valves to improve system efficiency was described. Rather than using an on/off valve external to the pump or motor to control the full hydraulic power flow, on/off valves were used inside the pump/motor to turn individual pistons on and off. The purpose of using discrete piston control to vary the displacement of a pump/motor, as opposed to the traditional method of varying the stroke length of the pistons, was to reduce the power losses in the pump/motor, particularly at low displacements. Most of the inefficiency of conventional variable displacement devices stems from leakage and friction between the moving parts of the pump/motor. By varying the stroke length but maintaining high pressure on all pistons regardless of the displacement, many of the power losses in a conventional pump/motor remain constant. In contrast, in a discrete piston controlled device, high pressure is removed from the pistons as the displacement is decreased, reducing the resulting leakage and friction. In chapter 5, an analysis of the power losses in a discrete piston and in a swashplate type pump/motor was described. By deriving how the different loss mechanisms scale with displacement, the potential efficiency benefit of the discrete piston approach was demonstrated. Some of the losses, such as the throttling and piston friction increased in the discrete piston approach, however other losses, such as the swashplate and valve plate friction and the valve plate leakage, decreased by a much larger amount. For the pump motor studied, which was an 8 piston device with a displacement of about $48cm^3$, the potential efficiency benefit of the discrete piston approach was about 5% at a displacement of 30%, and even larger at lower displacments.

In addition to demonstrating the potential efficiency benefits of discrete piston

control, chapter 5 described several different strategies for disabling the pistons in a pump/motor. There are two primary approaches for disabling the pistons: whole piston disabling, which involves disabling a variable number of pistons for their entire power stroke, and partial stroke disabling, which disables all of the pistons for a variable fraction of stroke. The advantage of whole piston disabling is that the disabled pistons are not enabled for any part of their stroke, which results in no transition throttling or compressibility losses. However, this approach also has a larger flow ripple than the partial stroke disabling strategy. In addition, the whole piston disabling approach is much harder to realize using a hydromechanical control mechanism, which was discussed in chapter 6.

Controlling the pistons mechanically was a focus in this thesis as mechanical control can reduce the complexity and cost of the system while ensuring reliable timing and simple, robust actuation. This is in contrast to competing designs that use either one or two electrically controlled valves for each piston. In order to achieve effective discrete piston control, a valve that switches quickly with little actuation power, can scale up its switching speed with the pump/motor speed, and has reliable timing with respect to the rotating pump/motor shaft was required. The rotary valve described in chapter 4 possessed all of these characteristics, and was well suited to being adapted to control the pistons of a pump/motor. In chapter 6, several different concepts for creating a hydromechanical discrete piston control mechanism were discussed for both the discrete piston and partial stroke disabling strategies. In order to utilize the whole piston approach, the rotary valve would need to be very long, and would be difficult to package into a compact design. The long spool would also lead to manufacturing challenges and large leakage paths, which could negate any efficiency benefit gained by avoiding transition and compressibility losses on the disabled pistons. Thus, a rotary valve design focused on creating a partial stroke disabled device was selected. Another design decision was whether the control mechanism should be single stage, with the rotary valve directly controlling the pressure at the piston, or two stage, with the rotary valve acting as a pilot stage driving a set of main stage valves. While a two stage device is more complex and has less precise timing, it also alleviates many of the design trade offs described in chapter 4 by reducing the flow and pressure flowing through the rotary valve. The selected main stage valve was a closed center 3-way valve, which was simple

to manufacture and ensured there was no cross port leakage. A dynamic model of the system was used to predict the overall efficiency of the device as well as to size some of the design parameters. Finally, the detailed mechanical design of a discrete piston pump/motor based on a wobble plate design was described.

In the final chapter, experimental measurements of the system prototype described in chapter 6 were presented. The results demonstrated the feasibility of the concept for creating a bidirectional variable displacement pump/motor based on discrete piston control. Unfortunately, due to large manufacturing tolerances and component wear, the device experienced much higher than anticipated internal leakage, which obscured the efficiency benefits of the approach. Several techniques were used to estimate the leakage, and when it was removed from the efficiency calculations, the device did appear to have a very high efficiency that was fairly flat across a wide displacement range. It is expected that manufacturing improvements to the device could demonstrate the efficiency benefits of the discrete piston approach.

8.1 Contributions

This thesis contributes to the existing body of research on hydraulic on/off valve control in a number of areas. While many researchers have studied on/off valve controlled systems, and several have examined the specific VVDP circuit, the analysis showing the trade off between the power ripple and response time, which was demonstrated through analysis and experimental results, is a new contribution. Furthermore, the positive impact of switching frequency and closed loop control on the system dynamics was demonstrated. The detailed study of the losses in the VVDP through analysis and experiments, particularly the effect of switching frequency on the system efficiency, is an important contribution. This is particularly true of the compressibility loss. While the effect of compressibility on the system efficiency has been studied in the past, other researchers have made use of a constant bulk modulus approximation. While this is often an acceptable technique for systems that operate continuously at elevated pressures, the low bulk modulus of the oil and entrained air when the pressure is low, which occurs every switching cycle in an on/off controlled system, can have a detrimental effect on the system performance and efficiency, and thus a pressure dependent bulk modulus

model should be used.

The concept of soft switching, while well established for electrical switching converters, is a novel concept in hydraulic systems. This approach, as proposed in this thesis, has the potential to drastically reduce the power loss in on/off valve controlled systems. It can also enable effective on/off valve control with conventional switching valves that may be too slow to be efficiently used without soft switching. Thus on/off valve systems could be created using cheaper or lower power valve designs.

The two degree of freedom rotary valve described in chapter 4 is a novel type of on/off valve that was developed in conjunction with other members of the research team [50, 86, 88]. This unique type of on/off valve reduces the power needed to actuate the switching valve element, enabling high PWM frequencies to be achieved efficiently. The concept of a switching valve enabled VVDPM is unique to this research group, along with the extension of the rotary valve to a four-way configuration needed to create it. This demonstrates a new potential application for on/off valve controlled hydraulic systems. This approach provides an alternative to conventional variable displacement pump/motors, which can be bulky and expensive.

One of the primary contributions to the area of discrete piston control is the analytical analysis and comparison of the power losses in the swashplate and discrete piston control techniques. While other researchers have demonstrated high efficiency in discrete piston controlled devices, the reasons for this, namely, the reduction in many of the leakage and friction losses as pistons are disabled, has not been shown in detail. The demonstration of how the losses scale with displacement can help guide the design of future devices and highlight the key motivation for selecting discrete piston control. While there have been a couple of discrete piston pumps developed that are controlled by mechanical means [55, 57], these devices cannot operate as a motor. The design proposed in chapter 6 is the first hydro-mechanically controlled discrete piston pump/motor to be demonstrated. The hydro-mechanical control approach can provide many benefits, such as lower cost and complexity, more compact packaging, simpler control, and lower electrical power consumption when compared with competing electrohydraulic designs. Furthermore the analysis of the high compressibility losses when compressing a fluid volume using high pressure oil presented in section 5.2.4 outlines an important characteristic of on/off valve or discrete piston controlled systems that must

be considered to avoid potentially detrimental effects to the system efficiency.

8.2 Future Work

There are several directions for extension of the work presented in this thesis. In chapter 2, an analysis of the system dynamics and power losses in on specific type of switching circuit, the VVDP, were studied. A similar analysis can be done for other on/off controlled circuits. Studying the characteristics of a Virtually Variable Displacement Motor or Actuator could be especially useful. While a VVDP provides efficiency benefits over the combination of a fixed displacement pump and a proportional bleed off valve to vary the flow, it is in competition with conventional variable displacement pumps, which can provide an efficient, if expensive, solution to provide a variable flow rate. In contrast, an on/off valve system that distributes power to, or absorbs power from, an actuator will be replacing a throttling valve in the vast majority of hydraulic systems. This could provide significant system energy savings. However, this approach is not without challenges. As shown in section 5.2.4, the compressibility losses when compressing a fluid volume with high pressure oil, as opposed to a mechanical pumping element, can be high. The on/off controlled actuator case also requires an inertia to smooth force or torque applied to it, which can be more difficult to incorporate than an accumulator. Finding ways to address these challenges is a possible area of future work.

The method of soft switching was proposed in chapter 3 as a way to reduce the transition losses in a VVDP. The effect of soft switching on other on/off valve architectures was not studied, but that is an potential area for future investigation. The locking mechanism that is needed to maximize the effectiveness of the soft switch is another topic that needs further development. Several concepts were presented, but a thorough analysis of different options and a detailed design have not been completed. The design of the locking mechanism could be tied to the design of new switching valves, as one effective way to trigger the unlocking of the soft switch is to use the geometry of the valve as it transitions between states.

For the rotary valve presented in chapter 4, there are several directions for further research. While the optimization results indicated that spinning the spool using an external actuator has significant efficiency benefits over the self-spinning approach, this

presents a number challenges related to packaging, sealing, and controlling the two degree of freedom valve and external rotary actuator. Another potential way to improve the rotary valve could be to incorporate the soft switching concept, as there may be ways to trigger a locking mechanism using the rotation of the valve spool. Finally, the power loss analysis of the VVDP and VVDPM did not consider the effect of the switching valve on the power losses that occur within the fixed displacement pump/motor. By studying the effect of the losses in the fixed displacement pump/motor, a better estimate of the overall VVDP or VVDPM efficiency could be generated.

The discrete piston pump/motor studied in chapters 5-7 presents a number of areas for continued research. The logical next step is to re-manufacture the main stage spools to reduce the clearance and harden them against wear. The polycarbonate check valves should also be replaced with steel balls. This should allow the high efficiency potential of the discrete piston approach to be demonstrated. Further improvements to the prototype include making it easier to assemble by changing the pilot return spring bearing, reducing the seal friction on the displacement control mechanism to allow for position control on the pilot spool, and improving the test stand to allow testing at higher pressures. A more thorough re-design of the pump/motor could investigate different valve architectures that make use of poppet sealing, which could further reduce the internal leakage. Several designs that accomplish this are described in chapter 6, but they present the challenge of ensuring that there is no simultaneous opening of the pressure and tank ports. Different pump/motor architectures could also be investigated. In particular, a radial piston design has the potential to improve the efficiency by reducing the relative speed between the piston slippers and the rotating cam. Finally, the backlash mechanism that was described in section 6.2.2 could be integrated into the design. While the concept of changing the pilot spool timing with respect to the wobble plate in the motor case was tested by manually adjusting the pilot drive shaft, a solution that could work in a real operating environment is to add backlash between the main shaft and the wobble plate. This would allow the motor to transition to high pressure as the piston is approaching Top Dead Center, which can reduce the high compressibility losses in the motor case. Further timing flexibility could also be added by placing a planetary gear set between the main shaft and the pilot spool with an additional mechanical input to vary the timing. The feasibility and potential benefits

of this approach is another area of potential research.

Another area of research that would provide significant benefits to the field of on/off control is developing ways to mitigate the noise and power ripple associated with switching valves. The flow and pressure ripple that stems from the discontinuous power flow through the switching valves is the biggest drawback on/off valve controlled systems, and finding techniques to mitigate the ripple would help to make them more attractive. Some possible areas of research could be variable energy storage elements (i.e. variable pre-charge accumulators or variable inertia flywheels) or active ripple cancellation elements. Other noise suppression techniques, such as suppressors or valve soft stops, could be used to reduce the audible noise that is often generated by switching valves.

Overall, the approach of using on/off valves to control hydraulic systems presents both challenges and opportunities for creating efficient hydraulic systems. On/off valves can be used to create hydraulic circuits that are more efficient than traditional throttling valve circuits, and they can be used to improve the efficiency of hydraulic pumps and motors. However, care must be taken when designing the system components and selecting the on/off switching frequency, as the power loss mechanisms in the valve can increase dramatically as the frequency is increased. The primary disadvantage of on/off control is the power ripple caused by the discontinuous power flow through the valve. In systems that can tolerate some power ripple or can incorporate sufficient energy smoothing accumulators or flywheels, on/off control is an attractive option for improving hydraulic efficiency.

References

[1] Love, L., Lanke, E., Alles, P., "Estimating the Impact (Energy, Emission, and Economics) of the U.S. Fluid Power Industry," Oak Ridge National Laboratory, Oak Ridge, TN, 2012.

[2] Williamson, C., Zimmerman, J. and Ivantysynova, M., "Efficiency study of an excavator hydraulic system based on displacement-controlled actuators," *Bath/ASME Symposium on Fluid Power and Motion Control*, Bath, UK, 2008, pp. 10-12.

[3] Linjama, M., "Digital Fluid Power - State of the Art," *Twelfth Scandinavian International Conference on Fluid Power*, Tampere, Finland, May 18-20, 2011.

[4] Linjama, M., and Vilenius, M., "Improved Digital Hydraulic Control of Water Hydraulic Cylinder Drive," *International Journal of Fluid Power*, 2005, pp. 29-39.

[5] Linjama, M. and Vilenius, M., "Digital Hydraulics - Towards Perfect Valve Technology," *Proceedings of the Tenth Scandinavian International Conference on Fluid Power*, 2007, pp. 181-196.

[6] Merrill, K., Holland, M., Batdorff, M., and Lumkes, J., "Comparative Study of Digital Hydraulics and Digital Electronics," *International Journal of Fluid Power*, vol. 11, no. 3, 2010, pp. 45-51.

[7] Cao, J., Gu, L., Wang, F., and Qiu, M., "Switchmode Hydraulic Power Supply Theory," *Proceedings of the 2005 ASME-IMECE*, 2005, Paper No. IMECE2005-79019.

[8] Cao, J., Gu, L., Wang, F., and Chen, Y., "Reserach on the Principle and Characteristic of Compounded Switch-Mode Hydraulic Power Supply," *Proceedings of the 2006 ASME-IMECE*, Chicago, IL, Nov. 5-10, 2006, Paper No. IMECE2006-13453.

[9] Wang, F., Gu, L., Chen, Y., "A Hydraulic Pressure-Boost System Based on High-Speed On-Off Valves," *IEEE/ASME Transactions on Mechatronics*, Vol. 18, No. 2, 2013, pp. 733-743.

[10] Johnston, N., "A Switched-Inertance Device for Efficient Control of Pressure and Flow," *Proceedings of the ASME Dynamic Systems and Control Conference*, 2009, Paper No. DSCC2009-2535.

[11] Negri, V., Wang, P., Plummer, A., and Johnston, N., "Behavioural Prediction of Hydraulic Step-up Switching Converters," *International Journal of Fluid Power*, vol. 15, no. 1, 2014, pp. 1-9.

[12] Pan, M., Johnston, N., Plummer, A., and Kudzma, S., "Theoretical and Experimental Studies on a Switched Inertance Hydraulic System Including Switching Transition Dynamics, Non-linearity, and Leakage," *Proceedings of the Institution of Mechanical Engineers, Part 1: Journal of Systems and Control Engineering*, Vol. 228, No. 10, 2014, pp. 802-815.

[13] Brown, F., Tentarelli, S., and Ramachandran, S., "A Hydraulic Rotary Switched-Inertance Servo-Transformer," *ASME Journal of Dynamic Systems Measurement and Control*, vol. 110, no. 2, 1988, pp. 144-150.

[14] Scheidl, R., Manhartsgruber, B., Kogler, H., Winkler, B., and Mairhofer, M., "The Hydraulic Buck Converter - Concept and Experimental Results," *International Fluid Power Conference*, Dresden, Germany, Apr. 1-2, 2008, pp. 501-513.

[15] Kogler, H., and Scheidl, R., "Two Basic Concepts of Hydraulic Switching Converters," *The 1st Workshop on Digital Fluid Power*, Tampere, Finland, Oct. 3, 2008, pp. 113-128.

[16] Guglielmino, E., Semini, C., Kogler, H., Scheidl, R., and Caldwell, D., "Power Hydraulics - Switched Mode Control of Hydraulic Actuation," *Proceedings of the IEEE/RSJ International Conference on Intelligent Robots and Systems*, 2010, pp. 3031-3036.

[17] Guglielmino, E., Semini, C., Yang, Y., Caldwell, D., Kogler, H. and Scheidl, R., "Energy Efficient Fluid Power in Autonomous Legged Robotics," *Proceedings of the ASME Dynamic Systems and Control Conference*, 2009, Paper No. DSCC2009-2522.

[18] Wang, F. and Gu, L., "Improving Characteristics of Switching Hydraulic System Based on High-Speed On/off Valves," *Fluid Power and Motion Control*, Bath, 2010, pp. 99-111.

[19] Wang, F., Gu, L., and Chen, Y., "A Continuously Variable Hydraulic Pressure Converter Based on High-Speed On-Off Valves," *Mechatronics*, Vol. 21, 2011, pp. 1298-1308.

[20] Zhu, K. Chen, Y., Cao, J., Li, W., and Chen, J., "Design and Research on High-Speed On/off Control Hydraulic Propeller for Underwater Vehicle Propulsion," *Proceedings of ASME Dynamic Systems and Control Conference*, 2009, Paper No. DSCC2009-2556.

[21] Jeong, H. and Kim, H., "Experimental Based Analysis of the Pressure Control Characteristics of an Oil Hydraulic Three-Way On/off Solenoid Valve Controlled by PWM Signal," *ASME Journal of Dynamic Systems Measurement and Control*, Vol. 124, 2002, pp. 196-205.

[22] Tomlinson, S., and Burrows, C., "Achieving a Variable Flow Supply by Controlled Unloading of a Fixed-Displacement Pump," *ASME Journal of Dynamic Systems Measurement and Control*, vol. 114, no. 1, 1992, pp. 166-171.

[23] Li, P., Li, C., and Chase, T., "Software Enabled Variable Displacement Pumps," *Proceedings of the 2005 ASME-IMECE*, 2005, Paper No. IMECE2005-81376.

[24] Batdorff, M. and Lumkes, J., "Virtually Variable Displacement Hydraulic Pump Including Compressibility and Switching Losses," *Proceedings of the 2006 ASME-IMECE*, Chicago, IL, 2006, Paper No. IMECE2006-14838.

[25] Lumkes J., Batdorff, M., and Marenholz, J., "Model Development and Experimental Analysis of a Virtually Variable Displacement Pump System," *International Journal of Fluid Power*, vol. 10, no. 3, 2009, pp. 17-27.

[26] Rannow, M., Tu, H., Li, P., and Chase, T.,"Software Enabled Variable Displacement Pumps - Experimental Studies," *Proceedings of the 2006 ASME-IMECE*, Chicago, IL, 2006, Paper No. IMECE2006-14973.

[27] Mansouri, G., Misovec, K., Johnson, B., Babbitt, G., and Sturman, O., "Variable Flow Supply Using Switched-Mode Control of a Fixed-Displacement Pump," *Proceedings of the Seventh Scandinavian International Conference on Fluid Power*, 2001, pp. 361-376.

[28] Seki, S. and Takahiko, I., "Application and Study on the Hydraulic Switching Power Control," *Proceedings of the 6th JFPS International Symposium on Fluid Power*, Nov. 7-10, 2005, pp. 239-244.

[29] Rannow, M., and Li, P., "Soft Switching Approach to Reducing Transition Losses in an On/off Hydraulic Valve," *Journal of Dynamic Systems Measurement and Control*, vol. 134, no. 6, 2012.

[30] Van de Ven, J., "Soft Switch Lock-Release Mechanism for a Switch-Mode Hydraulic Pump Circuit," *Journal of Dynamic Systems Measurement and Control*, Vol. 136, 2014,

[31] Lu, N., Fronczak, F., and Beachley, N., "Comparison of Analytical and Experimental Investigations of a Hydraulic Multi-Circuit Sequential Apportioning System," *Society of Automotive Engineers Transactions*, vol. 99, 1990, pp. 266-275.

[32] Lu, X., Burton, R., and Schoenau, G., "Feasibility Study of a Digital Variable Flow Divider Valve," *SAE International Off-Highway and Powerplant Congress and Exposition*, 1991, pp. 27-42.

[33] Lehman, B. and Bass, R., "Switching Frequency Dependent Averaged Models for PWM DC-DC Converters," *IEEE Transactions on Power Electronics*, vol. 11, no. 1, 1996, pp. 89-98.

[34] Taylor, D., "Pulse-Width Modulated Control of Electromechanical Systems," *IEEE Transactions on Automatic Control*, 1992, pp. 524-528.

[35] Barth, E., Zhang, J., and Goldfarb, M., "Sliding Mode Approach to PWM-Controlled Pneumatic Systems," *Proceedings of the American Controls Conference*, 2002, pp. 2362-2367.

[36] Barth, E., Zhang, J., and Goldfarb, M., "Control Design for Relative Stability in a PWM-Controlled Pneumatic System," *ASME Journal of Dynamic Systems Measurement and Control*, vol. 125, 2003, pp. 504-508.

[37] Jeronymo, C., Yamada, H., and Muto, T¿, "Application of Unified Predictive Control to On/off Control of Hydraulic System Driven by Fast-Switching Solenoid Valves," *JSME International Journal*, Series C, Vol. 39, No. 3, 1996, pp. 515-521.

[38] Royston, T., and Singh, R., "Development of a Pulse-Width Modulated Pneumatic Rotary Valve for Actuator Position Control," *ASME Journal of Dynamic Systems Measurement and Control*, Vol. 115, 1993, pp. 495-505.

[39] Rannow, M. and Li, P., "On/off Valve Based Position Control of a Hydraulic Cylinder," *Proceedings of the ASME IMECE2007*, Seattle, WA, 2007, Paper No. IMECE2007-42590.

[40] Cui, P., Burton, R., and Ukrainetz, P., "Development of a High speed On/off Valve," *SAE International Off-Highway and Powerplant Congress and Exposition*, 1991, pp. 21-25.

[41] Kajima, T. and Kawamura, Y., "Development of a High-Speed Solenoid Valve: Investigation of Solenoids," *IEEE Transactions on Industrial Electronics*, Vol. 42, No. 1, 1995.

[42] Topcu, E., Yuksel, I., and Kamis, Z., "Development of Electro-Pneumatic Fast Switching Valve and Investigation of its Characteristics," *Mechatronics*, Vol. 16, 2006, 365-378.

[43] Yamada, H., Wennmacher, G., Muto, T., and Sucmatsu, Y., "Development of a High-Speed On/off Digital Valve for Hydraulic Control Systems Using a Multilayered PZT Actuator," *International Journal of Fluid Power*, 2000, pp. 5-10.

[44] Yokota, S. and Akutu, K., " A Fast-Acting Electro-Hydraulic Digital Transducer," *JSME International Journal*, Series II, Vol. 34, No. 34, 1991, pp. 489-494.

[45] Johnson, B., Massey, S., and Sturman, O., "Sturman Digital Latching Valve," *7th Scandinavian International Conference on Fluid Power*, Linkoping, 2001, pp. 299-314.

[46] Kobata, T. and Ooiwa, A., "Square-Wave Pressure Generator Using a Novel Rotating Valve," *Metrologia*, Vol. 36, 1999, pp. 637-640.

[47] Wang, S., Tsung, T., and Han, L., "Hydraulic Square-Wave Pressure Generator With a Specific Rotating Valve," *Measurement*, Vol. 42, 2009, pp. 672-677.

[48] Van de Ven, J. and Katz, A., "Phase-Shift High-Speed Valve for Switch-Mode Control," *ASME Journal of Dynamic Systems Measurement and Control*, Vol. 133, 2011.

[49] Cyphelly, I. and Langen, J., "Ein Nues Energiesparendes Kozept der Volumenstromdosierung mit Konstantpumpen," *Aachener Fluidtechnisches Kolloquium*, 1980, pp. 44-61.

[50] Tu, H. and Rannow, M., Van de Ven, J., Wang, M., Li, P., and Chase, T., "High Speed Rotary Pulse Width Modulated On/Off Valve" *Proceedings of the 2007 ASME-IMECE*, Seattle, WA, 2007, Paper No. IMECE2007-42559.

[51] Tu, H., Rannow, M., Wang, M., Li, P., Chase, T., and Van de Ven, J., "Design, Modeling, and Validation of a High-Speed Rotary Pulse-Width-Modulation On/Off Hydraulic Valve," *ASME Journal of Dynamic Systems Measurement and Control*, Vol. 134, No. 6, 2012.

[52] Manhartsgruber, B., "A Hydraulic Control Valve for PWM Actuation at 400 Hz," *Power Transmission and Motion Control*, Bath, Sept. 13-15, 2006, pp. 373-386.

[53] Winkler, B., Ploeckinger, A., and Scheidl, R., "A Novel Piloted Fast Switching Multi-Poppet Valve," *International Journal of Fluid Power*, Vol. 11, No. 3, 2010, pp. 7-14.

[54] Uusitalo, J., Ahola, V., Soederlund, L., Linjama, M., Juhola, M., and Kettunen, L., "Novel Bistable Hammer Valve for Digital Hydraulics," *International Journal of Fluid Power*, Vol. 11, No. 3, 2010, pp. 35-44.

[55] Dynex/Rivett Inc., "Checkball Pumps Variable Delivery," Pewaukee, WI, 2011. Retrieved from http://www.dynexhydraulics.com/

[56] Stewart, P., "Variable Volume Hydraulic Pump," U.S. Patent No. US2997956A, Washington, DC: U.S. Patent and Trademark Office, 1961.

[57] Armstrong, M., Gibson, D., Pickell, M., Wear, J., and Friede, M., "Hydraulically-Actuated System Having a Variable Delivery Fixed-Displacement Pump," Patent 6216670B1, 2001.

[58] Lin, L., Gaosheng, L., Linyi, G., and Jiawang, C., "Simulation research on the variable displacement hydraulic motor with variable effective piston stroke for hydraulic propulsion system," *Oceans*, Hampton Roads, Virginia, Oct. 14-19, 2012.

[59] Artemis Intelligent Power, "Our Technology," 2015, Retrieved from http://www.artemisip.com/our-technology.

[60] Rampen, W., and Salter, S., "The Digital Displacement Hydraulic Piston Pump," *Proceedings of the 9th International Symposium on Fluid Power*, Cambridge, England, 1990.

[61] Rampen, W., Salter, S., and Fussey, A., "Constant Pressure Control of the Digital Displacement Pump," *4th Bath International Fluid Power Workshop - Fluid Power Systems and Modeling*, Bath, England, 1991, pp. 45-62.

[62] Rampen, W. and Salter, S., "Measuring and Predicting the Frequency Response of the Digital Hydraulic Pump," *5th Bath International Fluid Power Workshop - Component and Systems Design*, Bath, England, 1992.

[63] Rampen, W., Almond, J., and Salter, S., "The Digital Displacement Pump/Motor Operating Cycle: Experimental Results Demonstrating the Fundamental Characteristics," *International Fluid Power Workshop*, Bath, England, 1994, pp. 321-331.

[64] Ehsan, M., Rampen, W., and Salter, S.,"Modeling of Digital-Displacement Pump-Motors and Their Application as Hydraulic Drives for Nonuniform Loads," *ASME Journal of Dynamic Systems Measurement and Control*, Vol. 122, 2000, pp. 210-215.

[65] Payne, G., Kiprakis, A., Ehasan, M., Rampen, W., Chick, J., and Wallace, A., "Efficiency and Dynamic Performance of Digital Displacement Hydraulic Transmission in Tidal Current Energy Converters," *Proceedings of IMechE*, Vol. 221, Part A: J. Power and Energy, 2007, pp. 207-218.

[66] Wadsley, L., "Optimal System Solutions Enabled by Digital Pumps," *Proceedings of the 52nd National Conference on Fluid Power*, Las Vegas, NV, 2011.

[67] Nieling, M., Fronczak, F., and Beachley, N., "Design of a Virtually Variable Displacement Pump/Motor," *Proceedings of the 50th National Conference on Fluid Power*, Las Vegas, NV, 2005, pp. 323-335.

[68] Wilfong, G., Holland, M., and Lumkes, J., "Design and Analysis of Pilot Operated High Speed On/off Valves for Digital Pump/Motors," *Proceedings of the 52nd National Conference on Fluid Power*, Las Vegas, NV, 2011.

[69] Merrill, K., Holland, M., and Lumkes, J., "Analysis of Digital Pump/Motor Operation Strategies," *Proceedings of the 52nd National Conference on Fluid Power*, Las Vegas, NV, 2011.

[70] Holland, M., Wilfong, G., Merrill, K., Lumkes, J., "Experimental Evaluation of Digital Pump/Motor Operating Strategies with a Single-Piston Pump/Motor," *Proceedings of the 52nd National Conference on Fluid Power*, Las Vegas, NV, 2011, pp. 13-20.

[71] Merrill, K., "Modeling and Analysis of Active Valve Control of a Digital Pump/Motor," Ph.D. Thesis, Purdue University, West Lafayette, IN, 2012.

[72] Holland, M., "Design of Digital Pump/Motors and Experimental Validation of Operating Strategies," Ph.D. Thesis, Purdue University, West Lafayette, IN, 2012.

[73] Tammisto, J., Huova, M., Heikkila, M., Linjama, M., and Huhtala, K., "Measured Characteristics of an In-line Pump with Independently Controlled Pistons," *7th International Fluid Power Conference*, Aachen, Germany, 2010.

[74] Heikkila, M., Tammisto, J., Huova, M., Huhtala, M., and Linjama, M., "Experimental Evaluation of Piston-Type Digital Pump-Motor-Transformer with Two Independent Outlets," *Fluid Power and Motion Control*, Bath, England, 2010, pp. 83-98.

[75] Armstrong, B. and Yuan, Q., "Multi-Level Control of Hydraulic Geroter Motors and Pumps," *Proceedings of the American Control Conference*, Minneapolis, MN, June 14-16, 2006, pp. 4619-4626.

[76] Bishop, E., "Digital Hydraulic Transformer - Efficiency of Natural Design," *7th International Fluid Power Conference*, Aachen, Germany, 22-24 March, 2010.

[77] Yu, J., Chen, Z., and Lu, Y., "The Variation of Oil Effective Bulk Modulus with Pressure in Hydraulic Systems," *ASME Journal of Dynamic Systems Measurement and Control*, vol. 116, no. 1, 1994, pp. 146-150.

[78] Wang, J., Gong, G., and Yang, H., "Control of Bulk Modulus of Oil Hydraulic Systems," *Proceedings of the 2008 IEEE/ASME International Conference on Advanced Intelligent Mechatronics*, Xi'an, China, 2008, pp. 1390-1395.

[79] Merritt, H., *Hydraulic Control Systems,* John Wiley and Sons, New York, NY, 1967.

[80] Mohan, N., Undeland, T., and Robbins, W., *Power Electronics: Converters, Applications and Design*, 3rd Ed., John Wiley and Sons, New York, NY, 2003, pp. 172-178.

[81] Li, P., and Wang, M.,"Natural Storage Function for Passivity-Based Trajectory Control of Hydraulic Actuators," *ASME/IEEE Transactions on Mechatronics*, Vol. 19, No. 3, 2014, pp. 1057-1068.

[82] Richer, E. and Hurmuzlu, Y.,"A High Performance Pneumatic Force Actuator System: Part I - Nonlinear Mathematical Model," *ASME Journal of Dynamic Systems Measurement and Control*, vol. 122, no. 3, 2000, pp. 416-425.

[83] Mohan, N., *First Course on Power Electronics*, MNPERE, 2005, pp. 101-108.

[84] Dixon, S., *Fluid Mechanics and Thermodynamics of Turbomachinery*, 5th ed., Elsevier Butterworth-Heinemann, Burlington, MA, 2005.

[85] Wang, M. and Li, P., "Duty Ratio Control of a Rotary PWM Valve with Periodic Measurement Error," *Proceedings of the American Controls Conference*, St. Louis, MI, 2009.

[86] Wang, M., "CFD Analysis, Sensing and Control of a Rotary Pulse Width Modulating Valve," Ph. D. Thesis, University of Minnesota, Minneapolis, MN, In Preparation.

[87] Papanastasiou, T., Georgiou, G., and Alexandrou, A., "Viscous Fluid Flow," CRC Press, Boca Raton, Fl., 2000, pp. 224-229.

[88] Tu, H., "High Speed Rotary PWM On/Off Valves for Digital Control of Hydraulic Pumps and Motors," Ph. D. Thesis, University of Minnesota, Minneapolis, MN, 2014.

[89] Cheong, K.L., "Design and Analysis of Hydraulic Hybrid Passenger Vehicles," Ph. D Thesis, University of Minnesota, Minneapolis, MN, 2015.

[90] Cheong, K.L., Li, P., Sedler, S., and Chase, T., "Comparison between Input Coupled and Output Coupled Power-split Configurations in Hybrid Vehicles," *Proceedings of the 52nd National Conference on Fluid Power*, Las Vegas, NV, 2011.

[91] Cheong, K.L., Li, P., Chase, T., "Optimal Design Power-Split Transmissions for Hydraulic Hybrid Passenger Vehicles," *American Controls Conference*, San Fransisco, CA, 2011.

[92] Manring, N., *Hydraulic Control Systems,* John Wiley and Sons, New York, NY, 2005.

[93] Duan, S. and Nielsen, T., "Modeling and Analysis of Directional Control Valves with Tapered-Angle and Eccentric Clearance," *Proceedings of the ASME IMECE2007*, Seattle, WA, 2007.

[94] Young, D., Munson, B., Okiishi, T., and Huebsch, W., "A Brief Introduction to Fluid Mechanics," John Wiley and Sons, New York, NY, 2010.

[95] Fang, Y. and Shirakashi, M., "Mixed lubrication characteristics between the piston and cylinder in hydraulic piston pump-motor," *Journal of tribology*,Vol. 117, No. 1, 1995, pp. 80-85.

[96] Pelosi, M. and Ivantysynova, M., "Heat Transfer and Thermal Elastic Deformation Analysis on the Piston/Cylinder Interface of Axial Piston Machines," *Journal of Tribology*, Vol. 134, No. 4, 2012.

[97] Ivantysynova, M. and Lasaar, R., "An Investigation into Micro- and Macrogeometric Design of Piston/Cylinder Assembly of Swash Plate Machines," *International Journal of Fluid Power*, Vol. 5, No. 1, 2004.

[98] Jeong, HS., and Kim, HE., "On the instantaneous and average piston friction of swash plate type hydraulic axial piston machines." *KSME international journal*, Vol. 18, No. 10, 2004, pp. 1700-1711.

[99] Yamaguchi, A., "Tribology of Hydraulic Pumps," *ASTM Special Technical Publication No. 1310*, 1997, pp. 4961.

[100] Matsumoto, K., and Ikeya, M., "Leakage Characteristics Between the Valve Plate and Cylinder for Low Speed Conditions in a Swashplate-Type Axial Piston Motor," *Trans. Jpn. Soc. Mech. Eng., Ser. C*, 57, 1991, pp. 30083012.

[101] Manring, N. D., and Johnson, R. E., "Modeling and Designing a Variable-Displacement Open-Loop Pump," *ASME Journal of Dynamic Systems, Measurement, and Control*, 118, 1996, pp. 267271.

[102] Seeniraj, G.K. and Ivantysynova, M., "Impact of valve plate design on noise, volumetric efficiency and control effort in an axial piston pump," *ASME International Mechanical Engineering Congress and Exposition*, 2006, pp. 77-84.

[103] Bergada, J., Watton, J., and Kumar, S., "Pressure, Flow, Force, and Torque Between the Barrel and Port Plate in an Axial Piston Pump," *ASME Journal of Dynamic Systems Measurement and Control*, Vol. 130, No. 1, 2008.

[104] Koc, P. and Hooke, C., "Considerations in the Design of Partially Hydrostatic Slipper Bearings," *Tribology Internationally*, Vol. 30, No. 11, 1997, pp. 815-823.

[105] Yamaguchi, Y., Sekine, H., and Ishida, S., "Bearing/Seal Characteristics of the Film Between a Valve Plate and a Cylinder Block of Axial Piston Pumps: Effects of Fluid Types and Theoretical Discussion," *Journal of Fluid Control*, Vol. 20, No. 4, 1990, pp. 7-29.

[106] Kim, J., Kim, H., and Lee, Y., "Measurement of Fluid Film Thickness on the Valve Plate in Oil Hydraulic Axial Piston Pumps Part II: Spherical Design Effects," textitJournal of Mechanical Science and Technology, Vol. 19, No. 2, 2005, pp. 655-663.

[107] Andersson, B., "On the valvistor: a proportionally controlled seat valve. Division of Hydraulics and Pneumatics," Ph. D Thesis, Linkoping University, 1984.

[108] Grandall, D., "The Performance of Hydraulic Pumps and Motors," Masters Thesis, University of Minnesota, Minneapolis, MN, 2010.

[109] Larish, C., "Digital Hydraulic Pump Rotating Kit Design," Masters Thesis, University of Minnesota, Minneapolis, MN, 2015.

Appendix A

Derivation of VVDPM Transition Loss

The transition loss across the different inlet orifices as they transition between on and off states for the VVDPM is derived here. For this analysis, it is assumed that the oil is incompressible, and the pressure drop can be described by the orifice equation. The inlet orifice to the valve are rhombus shaped, and thus they exhibit a linear area profile with respect to the rotation angle of the valve spool. Due to the incompressibility and the linear area profiles, the throttling loss across an opening orifice is the same as the throttling loss across that same orifice closing. The area of an inlet orifice is given by:

$$A_{open} = \frac{R_h D}{4}(\theta) \quad A_{close} = \frac{R_h D}{4}(\theta_t - \theta) \tag{A.1}$$

where $\theta_t = 2R_w/D$ is the angle needed to complete one half transition (i.e. on to blocked or blocked to off). For the motor case, the energy loss for one rotation (two identical transitions) is given by:

$$E_{loss,motor} = \frac{2}{\omega}\int_0^{\theta_t} Q_v\left(\Delta P_{D-B} + \Delta P_{A-C} + \Delta P_{A-B}\right) + Q_c\left(P_{c,low} - P_{spool} - P_{out}\right) d\theta \tag{A.2}$$

where the subscripts refer to the port labels in Fig. 4.14 and Q_v is the flow though the valve. Note that there are three pressure drops to take into account: the pressure drop across the two orifices in the on state, and one orifice in the freewheeling case. The loss

from these three orifices is derived separately. Q_c is the flow through the low pressure check valve, with opening pressure $P_{c,low}$, when the inlet to the motor is closing off. The pressure drops P_{spool} and P_{out} must be subtracted from $P_{c,low}$ because Eq. (4.33) computes the full open loss as though the full flow is always passing through the valve.

$$\int_0^{\theta_t} Q_v \Delta P_{D-B} d\theta = Q \int_0^{\theta_{c1}} \Delta P_{D-B} d\theta + \int_{\theta_{c1}}^{\theta_t} Q_v \Delta P_{D-B} d\theta \tag{A.3}$$

$$= Q \int_0^{\theta_{c1}} \Delta P_{D-B} d\theta + \int_{\theta_{c1}}^{\theta_t} Q_v \left(P - (P_{c,low} + P_{spool} + P_{out})\right) d\theta \tag{A.4}$$

$$= Q \int_0^{\theta_{c1}} P_o \left(\frac{\theta_t}{\theta_t - \theta}\right)^2 d\theta + \int_{\theta_{c1}}^{\theta_t} Q_v \left(P - (P_{c,low} + P_{spool} + P_{out})\right) d\theta \tag{A.5}$$

where θ_{c1} is the angle at which the pressure drops low enough that the check valve to tank, with opening pressure $P_{c,low}$, opens. After this angle, the pressure drop across the orifice is fixed. P_o is the full-open pressure drop across the inlet orifice, and P_{spool} and P_{out} are the pressure drops across the internal spool passage and the outlet turbine. Note that when two flow paths are open through the valve, there are two P_{spool} and P_{out} pressure drops. The pressure drops across the spool and the outlet turbine are included in the full-open equation (Eq. (4.33)), so they must be excluded here. Note that for the first integral, all of the flow is passing across the closing valve orifice, but in the second integral, this is not the case since some is coming across the check valve. At the transition angle, θ_{c1},

$$P - (P_{c,low} + P_{spool} + P_{out}) = P_o \left(\frac{\theta_t}{\theta_t - \theta_{c1}}\right)^2 \tag{A.6}$$

$$\theta_{c1} = \left(1 - \frac{\sqrt{P_o}}{\sqrt{P - (P_{c,low} + P_{spool} + P_{out})}}\right) \theta_t \tag{A.7}$$

Solving the first integral in (A.5):

$$Q\int_0^{\theta_{c1}} P_o\left(\frac{\theta_t}{\theta_t-\theta}\right)^2 d\theta = QP_o\left(\frac{\theta_t^2}{\theta_t-\theta_{c1}}-\theta_t\right) \tag{A.8}$$

$$= Q\sqrt{P_o}\theta_t\left(\sqrt{P-(P_{c,low}+P_{spool}+P_{out})}-\sqrt{P_o}\right) \tag{A.9}$$

When $\theta > \theta_{c1}$, the pressure drop is constant, but the flow through the valve varies:

$$Q = c_d\sqrt{\frac{2}{\rho}\left(P-(P_{c,low}+P_{spool}+P_{out})\right)}\frac{R_h D}{4}\left(\theta_t-\theta_{c1}\right) \tag{A.10}$$

$$Q_v = c_d\sqrt{\frac{2}{\rho}\left(P-(P_{c,low}+P_{spool}+P_{out})\right)}\frac{R_h D}{4}\left(\theta_t-\theta\right) \tag{A.11}$$

$$Q_v = \frac{\theta_t-\theta}{\theta_t-\theta_{c1}}Q \tag{A.12}$$

Solving the second integral in (A.5):

$$\int_{\theta_{c1}}^{\theta_t} Q_v\left(P-(P_{c,low}+P_{spool}+P_{out})\right)d\theta \tag{A.13}$$

$$= Q\left(P-(P_{c,low}+P_{spool}+P_{out})\right)\int_{\theta_{c1}}^{\theta_t}\frac{\theta_t-\theta}{\theta_t-\theta_{c1}}d\theta \tag{A.14}$$

$$= Q\left(P-(P_{c,low}+P_{spool}+P_{out})\right)\frac{\frac{\theta_{c1}^2}{2}-\theta_{c1}\theta_t+\frac{\theta_t^2}{2}}{\theta_t-\theta_{c1}} \tag{A.15}$$

$$= Q\left(P-(P_{c,low}+P_{spool}+P_{out})\right)\frac{1}{2}\left(\theta_t-\theta_{c1}\right) \tag{A.16}$$

$$= Q\sqrt{P_o}\theta_t\left(\frac{P-(P_{c,low}+P_{spool}+P_{out})}{2\sqrt{P-(P_{c,low}+P_{spool}+P_{out})}}\right) \tag{A.17}$$

The second term in Eq. (A.2) refers to the flow through the check valve when orifice D-B is closing and is past the critical angle, θ_{c1}. This loss needs to be added to the loss in Eq. (A.17). The flow through the check valve is:

$$Q_c = Q - Qv = \frac{\theta-\theta_{c1}}{\theta_t-\theta_{c1}}Q \tag{A.18}$$

$$\int_{\theta_{c1}}^{\theta_t} Q_c \left(P_{c,low} - P_{spool} - P_{out}\right) d\theta \tag{A.19}$$

$$= Q \left(P_{c,low} - P_{spool} - P_{out}\right) \int_{\theta_{c1}}^{\theta_t} \frac{\theta - \theta_{c1}}{\theta_t - \theta_{c1}} d\theta \tag{A.20}$$

$$= Q \left(P_{c,low} - P_{spool} - P_{out}\right) \int_{\theta_{c1}}^{\theta_t} \frac{\frac{\theta_{c1}^2}{2} - \theta_{c1}\theta_t + \frac{\theta_t^2}{2}}{\theta_t - \theta_{c1}} \tag{A.21}$$

$$= Q \left(P_{c,low} - P_{spool} - P_{out}\right) \frac{1}{2} \left(\theta_t - \theta_{c1}\right) \tag{A.22}$$

$$= Q\sqrt{P_o}\theta_t \left(\frac{P_{c,low} - P_{spool} - P_{out}}{2\sqrt{P - \left(P_{c,low} + P_{spool} + P_{out}\right)}} \right) \tag{A.23}$$

The second orifice that causes transition loss is between the outlet of the motor and tank, which is represented by the second integral in Eq. (A.2). This integral can also be broken into two parts: one part for when the pressure across the orifice is not high enough to open a relief valve or a check valve to supply, and a second part when it is. Note that Fig. 4.14 depicts relief valves to limit any pressure spikes across transitioning orifices. This function can also be achieved with check valves to supply, which is a more efficient approach. The transition loss will be derived for the check valve case. At the critical angle where the relief/check valve opens, θ_{c2}, the pressure across the inlet orifice, spool and outlet turbine is equal to the supply pressure plus the drop across the check valve. Note that for a self-spinning valve, the check valve opening pressure should be higher than $P_{spool} + P_{out}$ to ensure that fluid flow through the valve when it is fully open.

$$P_{c,high} + P = P_o \left(\frac{\theta_t}{\theta_t - \theta_{c2}} \right)^2 + P_{spool} + P_{out} \tag{A.24}$$

$$\theta_{c2} = \theta_t \left(1 - \frac{\sqrt{P_o}}{\sqrt{P_{c,high} + P - P_{spool} - P_{out}}} \right) \tag{A.25}$$

With θ_{c2} defined, the energy loss across the closing tank orifice is:

$$\int_0^{\theta_t} Q_v \Delta P_{A-C} d\theta \tag{A.26}$$

$$= Q \int_0^{\theta_{c2}} P_o \left(\frac{\theta_t}{\theta_t - \theta} \right)^2 d\theta + Q \int_{\theta_{c2}}^{\theta_t} P_{c,high} - P_{spool} - P_{out} d\theta \tag{A.27}$$

$$= Q P_o \left(\frac{\theta_t^2}{\theta_t - \theta_{c2}} - \theta_t \right) + Q \left(P_{c,high} - P_{spool} - P_{out} \right) \left(\theta_t - \theta_{c2} \right) \tag{A.28}$$

$$= Q \sqrt{P_o} \theta_t \left(\sqrt{P_{c,high} + P - P_{spool} - P_{out}} - \sqrt{P_o} + \frac{P_{c,high} - P_{spool} - P_{out}}{\sqrt{P_{c,high} + P - P_{spool} - P_{out}}} \right) \tag{A.29}$$

The energy lost across the orifice that opens to the other side of the motor to enter the freewheeling state is derived in a similar manner, with a critical angle, θ_{c3} defined to determine the point at which the check valve to supply closes.

$$P_{c,high} + P = P_o \left(\frac{\theta_t}{\theta_{c3}} \right)^2 + P_{spool} + P_{out} \tag{A.30}$$

$$\theta_{c3} = \frac{\sqrt{P_o}}{\sqrt{P + P_{c,high} - P_{spool} - P_{out}}} \theta_t \tag{A.31}$$

With this critical angle defined, the energy loss across the opening orifice is:

$$\int_0^{\theta_t} Q_v \Delta P_{A-B} d\theta \tag{A.32}$$

$$= Q \int_0^{\theta_{c3}} P_{c,high} - P_{spool} - P_{out} d\theta + Q \int_{\theta_{c3}}^{\theta_t} P_o \left(\frac{\theta_t}{\theta} \right)^2 d\theta \tag{A.33}$$

$$= Q \frac{\left(P_{c,high} - P_{spool} - P_{out} \right) \sqrt{P_o}}{\sqrt{P + P_{c,high} - P_{spool} - P_{out}}} \theta_t + Q P_o \theta_t^2 \left(\frac{1}{\theta_{c3}} - \frac{1}{\theta_t} \right) \tag{A.34}$$

$$= Q \sqrt{P_o} \theta_t \left(\frac{\left(P_{c,high} - P_{spool} - P_{out} \right)}{\sqrt{P + P_{c,high} - P_{spool} - P_{out}}} + \sqrt{P + P_{c,high} - P_{spool} - P_{out}} - \sqrt{P_o} \right) \tag{A.35}$$

By combining equations (A.9), (A.17), (A.23), (A.29), and (A.35) and multiplying by two to account for the symmetric opening and closing losses, the total energy loss due to transition for one cycle is given by:

$$E_{loss,motor} = \frac{2Q\sqrt{P_o}\theta_t}{\omega}\left(\sqrt{P-(P_{c,low}+P_{spool}+P_{out})} - 3\sqrt{P_o} + 2\sqrt{P+P_{c,high}-P_{spool}-P_{out}} + \frac{P_{c,high}-P_{spool}-P_{out}}{\sqrt{P+P_{c,high}-P_{spool}-P_{out}}} + \frac{P-2P_{spool}-2P_{out}}{2\sqrt{P-(P_{c,low}+P_{spool}+P_{out})}}\right) \quad \text{(A.36)}$$

Multiplying by the PWM frequency, $f_{pwm} = \frac{N\omega}{2\pi}$, and using the definitions of $\theta_t = \frac{2R_w}{D}$ and $\kappa = \frac{4NR_w}{\pi D}$, the power loss in the valve due to transition in the motor case can be written as:

$$L_{trans,motor} = \frac{\kappa Q\sqrt{P_o}}{2}\left(\sqrt{P-(P_{c,low}+P_{spool}+P_{out})} - 3\sqrt{P_o} + 2\sqrt{P+P_{c,high}-P_{spool}-P_{out}} + \frac{P_{c,high}-P_{spool}-P_{out}}{\sqrt{P+P_{c,high}-P_{spool}-P_{out}}} + \frac{P-2P_{spool}-2P_{out}}{2\sqrt{P-(P_{c,low}+P_{spool}+P_{out})}}\right) \quad \text{(A.37)}$$

In the pumping case, there are also three orifices that cause a power loss as they transition. However, two of them are already derived for the VVDP in Eq. (4.19). The orifice closing from the pump outlet to supply and then the orifice opening from the pump outlet to the pump inlet are the same as in the VVDP case. The third orifice in the VVDPM case is the orifice between tank and that pump inlet. Note that there is a check valve in parallel with this orifice, so, depending on the setting of this check valve, the transition loss may be negligible. However, in the self-spinning case, the check valve opening pressure needs to be higher than $P_o + P_{spool} + P_{out}$ to keep oil flowing through the valve. In this case, a pressurized tank would likely need to be used to prevent cavitation. For this transition, there is a critical angle, θ_{c4}, at which the check valve opens:

$$P_{c,low} = P_o\left(\frac{\theta_t}{\theta_t-\theta_{c4}}\right)^2 + P_{spool} + P_{out} \quad \text{(A.38)}$$

$$\theta_{c4} = \left(1 - \frac{\sqrt{P_o}}{\sqrt{P_{c,low}-P_{spool}-P_{out}}}\right)\theta_t \quad \text{(A.39)}$$

The loss across the inlet orifice from tank and the tank check valve is:

$$\frac{Q}{\omega}\int_0^{\theta_{c4}} P_o\left(\frac{\theta_t}{\theta_t-\theta}\right)^2 d\theta + \frac{Q}{\omega}\int_{\theta_{c4}}^{\theta_t} P_{c,low} - P_{spool} - P_{out} d\theta \tag{A.40}$$

$$= \frac{Q\sqrt{P_o}\theta_t}{\omega}\left(2\sqrt{P_{c,low} - P_{spool} - P_{out}} - \sqrt{P_o}\right) \tag{A.41}$$

This energy loss is multiplied by two and by the PWM frequency and then added to Eq. (4.19) to get the total power loss for the VVDPM pump case.

$$\begin{aligned} L_{trans,pump} = \frac{\kappa\sqrt{P_{open}}Q}{2}\Bigg[&\frac{P_{c,high} - P_{out} - P_{spool}}{\sqrt{P_{load} + P_{c,high} - P_{spool} - P_{out}}} \\ &+\sqrt{P_{load} + P_{c,high} - P_{spool} - P_{out}} + 2\sqrt{P_{c,high} - P_{out} - P_{spool}} \\ &+2\sqrt{P_{c,low} - P_{spool} - P_{out}} - 3\sqrt{P_{open}}\Bigg] \end{aligned} \tag{A.42}$$